Novel minimally invasive labeling tools for advanced microscopy studies of voltage-gated sodium channels and associated proteins in health and disease

Dissertation

zur Erlangung des Grades eines
Doktors der Naturwissenschaften

der Mathematisch-Naturwissenschaftlichen Fakultät
und
der Medizinischen Fakultät
der Eberhard-Karls-Universität Tübingen

vorgelegt
von

Nevena Stajković
aus Kruševac, Republic of Serbia

2022

Tag der mündlichen Prüfung: .....28.09.2023.....

Dekan der Math.-Nat. Fakultät: Prof. Dr. Thilo Stehle
Dekan der Medizinischen Fakultät: Prof. Dr. Bernd Pichler

1. Berichterstatter: Dr. Ivana Nikić-Spiegel
2. Berichterstatter: Prof. Dr. Holger Lerche

Prüfungskommission: Dr. Ivana Nikić-Spiegel
Prof. Dr. Michela Deleidi
Prof. Dr. Mathias Jucker
Prof. Dr. Holger Lerche

Erklärung / Declaration:

Ich erkläre, dass ich die zur Promotion eingereichte Arbeit mit dem Titel:

„**Novel minimally invasive labeling tools for advanced microscopy studies of voltage-gated sodium channels and associated proteins in health and disease**“

selbständig verfasst, nur die angegebenen Quellen und Hilfsmittel benutzt und wörtlich oder inhaltlich übernommene Stellen als solche gekennzeichnet habe. Ich versichere an Eides statt, dass diese Angaben wahr sind und dass ich nichts verschwiegen habe. Mir ist bekannt, dass die falsche Abgabe einer Versicherung an Eides statt mit Freiheitsstrafe bis zu drei Jahren oder mit Geldstrafe bestraft wird.

*I hereby declare that I have produced the work entitled "**Novel minimally invasive labeling tools for advanced microscopy studies of voltage-gated sodium channels and associated proteins in health and disease**", submitted for the award of a doctorate, on my own (without external help), have used only the sources and aids indicated and have marked passages included from other works, whether verbatim or in content, as such. I swear upon oath that these statements are true and that I have not concealed anything. I am aware that making a false declaration under oath is punishable by a term of imprisonment of up to three years or by a fine.*

Tübingen, den .....26.10.2023..... .....

Datum / Date Unterschrift /Signature

To my parents.

Ovu doktorsku disertaciju posvećujem svojim roditeljima.

Table of Contents

Summary

The central nervous system, and in particular brain, controls how we perceive the world around us. The brain processes information collected by the receptors and generates responses in the form of electrical (action potentials) and chemical (neurotransmitters) signals. Such information processing is possible due to neurons which are basic brain units. In order to execute their complex function, neurons have a unique molecular organization emerging from interactions between various ion channels, receptors, cell adhesion molecules, adaptors, and cytoskeletal elements. Voltage-gated sodium channels (Na_V) are especially important for the generation of action potentials in neurons. Out of nine isoforms, the most abundant in the adult mammalian brain is $Na_V1.6$. The $Na_V1.6$ is clustered at high density at the axon initial segment (AIS) and the nodes of Ranvier, where it promotes the initiation and propagation of action potentials, respectively. Proper expression and maintenance of the $Na_V1.6$ clusters at the AIS and nodes of Ranvier depend on various proteins (e.g., ankyrin G and cell adhesion molecules). One particularly important cell adhesion molecule that directly interacts with $Na_V1.6$ is a 186 kDa neurofascin isoform (NF186). Since both proteins are indispensable for proper signaling in the brain, they are implicated in various neurological conditions. For example, mutations of $Na_V1.6$ have been linked to epilepsy. The altered expression and localization of $Na_V1.6$ have also been found in multiple sclerosis. The NF186 has also been linked to multiple sclerosis and other demyelinating diseases.

In order to decipher how $Na_V1.6$ and NF186 contribute to various diseases and design new therapeutic strategies, one must first understand the regulation of function, localization, and trafficking of these two proteins under physiological conditions. However, there are many open questions on the regulation of $Na_V1.6$ and NF186 in developing and mature neurons. The reason is the lack of suitable labeling approaches that would allow studying nanoscale organization and dynamics of the NF186 and $Na_V1.6$ in their native environment with advanced super-resolution (SRM) and live-cell microscopy. The current SRM and live-cell microscopy-compatible labeling approaches mainly involve labeling with antibodies conjugated to fluorescent dyes or genetically encoded fluorescent proteins (FPs). However, fluorescent antibodies are large (100–200 kDa) and can introduce artefacts in live-cell and SRM studies. Also, in most cases, they cannot be used for live labeling of transmembrane components and lack specificity when labeling closely related protein isoforms, such as Na_V. Genetically encoded FPs are smaller (~30 kDa) and provide specificity. However, they can be added only to N or C termini, potentially affecting the trafficking or localization of target proteins.

A combination of the genetic code expansion (GCE) and bioorthogonal click chemistry reactions (referred to as click labeling) has emerged as a promising tool for site-specific noninvasive fluorescent protein labeling in mammalian cells. GCE technology utilizes orthogonal translation machinery to site-specifically install unnatural amino acid (UAA) into target proteins. Subsequently, the incorporated UAA is labeled with a fluorescent dye via a bioorthogonal click reaction. Contrary to the bulky fluorescent antibodies and N- and C-terminal FP-fusions, the UAA-based tags are small (0.2–0.5 kDa) and can be introduced at any position into a protein of interest. Therefore, UAAs represent an ideal alternative for labeling of the AIS components, whose localization and function can be affected by the size of the labeling tags. Furthermore, the UAA can be labeled with various cell-permeable and cell-impermeable fluorescent dyes compatible with live-cell and SRM microscopy techniques.

The main aim of my Ph.D. was to establish highly efficient UAA-based click labeling of the axon initial segment and node of Ranvier components, $Na_V1.6$ and NF186, in living neurons that would allow quantitative, live-cell, and SRM imaging studies. By designing different plasmids encoding NF186, $Na_V1.6$, and orthogonal translational machinery and by optimizing conventional transfection and labeling conditions, I established click labeling of NF186 and $Na_V1.6$ in primary neurons without affecting their localization and function. This was the first time that the large, complex, spatially confined proteins, including ion channels, were labeled in living primary neurons with click labeling approach.

In recent years, click labeling has emerged as a promising protein labeling tool. However, due to the low to moderate UAA incorporation efficiency in mammalian cells and the complexity of the method, click labeling has not been widely used, especially in neurons. Achieving higher efficiency of the UAA incorporation in a larger number of neurons compared to conventional transfection would allow quantitative, live-cell, and SRM imaging studies of neuronal proteins. To increase click labeling efficiency of the large AIS component, $Na_V1.6$, I probed different viral-based systems for the efficient delivery of the GCE components, such as baculoviruses and adeno-associated viruses (AAVs). The usage of the AAV-based vectors that bore GCE elements led to a threefold increase in GCE efficiency and expression of $Na_V1.6$ in neurons compared to conventional transfection.

Finally, in addition to establishing a highly efficient click labeling of the $Na_V1.6$ and NF186, I demonstrated that this approach could be used for live-cell and direct stochastic optical reconstruction microscopy (dSTORM) super-resolution imaging of the AIS. Furthermore, I showed

that click labeling could be used for quantitative studies of the localization of pathogenic epilepsy-causing $Na_V1.6$ variants.

In order to optimize dSTORM imaging and allow reproducible SRM imaging of the AIS, I tested different imaging buffers, including a commonly used mounting medium Vectashield. This led to the discovery that the fluorescence of AF647 and its variant AF647 Plus are quenched in Vectashield without the effect on dSTORM imaging. These observations are important for both SRM and conventional microscopy since Vectashield is a commonly used medium for tissue mounting. Hence, these results will allow other laboratories to optimize their imaging conditions and produce reliable results.

In conclusion, I developed a new approach for the highly efficient labeling of neuronal proteins, including large and complex ion channels. This new approach is compatible with live-cell and SRM imaging. Therefore, it will allow gaining novel insight into the regulation of NF186 and $Na_V1.6$ in health and diseases at the single molecule level in their native environment. This approach will also allow studying additional pathogenic $Na_V1.6$ variants and other Na_V isoforms for which suitable labeling approaches do not exist. Furthermore, AAV-based delivery will allow efficient labeling of other complex proteins and ion channels in living and fixed neurons, as well as in more complex model systems, such as brain slices, organoids, and whole animals. Therefore, my Ph.D. work provides the basis for novel discoveries in the field of AIS and neurobiology.

1. Introduction

The nervous system coordinates and regulates essential body functions that keep us alive, such as heart rate, breathing, and metabolism[1]. The central nervous system (CNS), and in the particular brain, processes information and controls how we perceive the world around us. It ensures efficient communication with the environment and allows us to learn, think and experience emotions, solve complex problems, and create art and music[1]. The fundamental structural and functional unit of the nervous system is a highly specialized nerve cell (neuron)[1]. Neurons are excitable cells that transmit information through the nervous system via electrical and chemical signals[1]. In order to execute their functions**,** neurons are organized in three distinctive structural and functional compartments (**Scheme 1a**): a cell body (soma), short, branched processes (dendrites), and a single long process (an axon)[1]. The somatodendritic compartment receives and summarizes excitatory and inhibitory signals (synaptic inputs). If the excitatory signals reach a threshold, the action potentials are initiated in the axon initial segment (AIS), the ion channel enriched subdomain that occupies the first 10–60 µm of the proximal axon[2-4]. In most vertebrates, a discontinuous myelin sheath enwraps the distal axons, allowing fast propagation of the action potentials initiated at the AIS)[1]. The small (~1 µm) gaps in the myelin, enriched with ion channels, are termed nodes of Ranvier[5-7]. Since the myelin acts as an electrical insulator, action potentials are regenerated only at the nodes of Ranvier, resulting in fast and discontinuous (saltatory) conduction[5,6]. Upon arrival at the axonal terminals, action potentials facilitate the release of neurotransmitters that transmit signals to the surrounding neurons, muscles, or glands[1].

During my Ph.D. I was studying two AIS and the node of Ranvier constituents, the voltage-gated sodium channel isoform 1.6 ($Na_V1.6$) and its associated protein, a 186 kDa isoform of the cell adhesion molecule neurofascin (NF186). $Na_V1.6$ is the most abundant Na_V isoform in the adult mammalian brain, responsible for the action potential initiation and propagation[8]. NF186 maintains the AIS structure and has a role in the formation and maintenance of the nodes of Ranvier[9-11]. Since both proteins are indispensable for proper signaling in the nervous system, they are linked to various neurological conditions. For example, the redistribution, altered expression, and genetic mutations of $Na_V1.6$ have been implicated in multiple sclerosis, epilepsy, autism spectrum disorder, and neuronal injury[12-14]. The autoantibodies against NF186 have been found in demyelinating diseases[15].

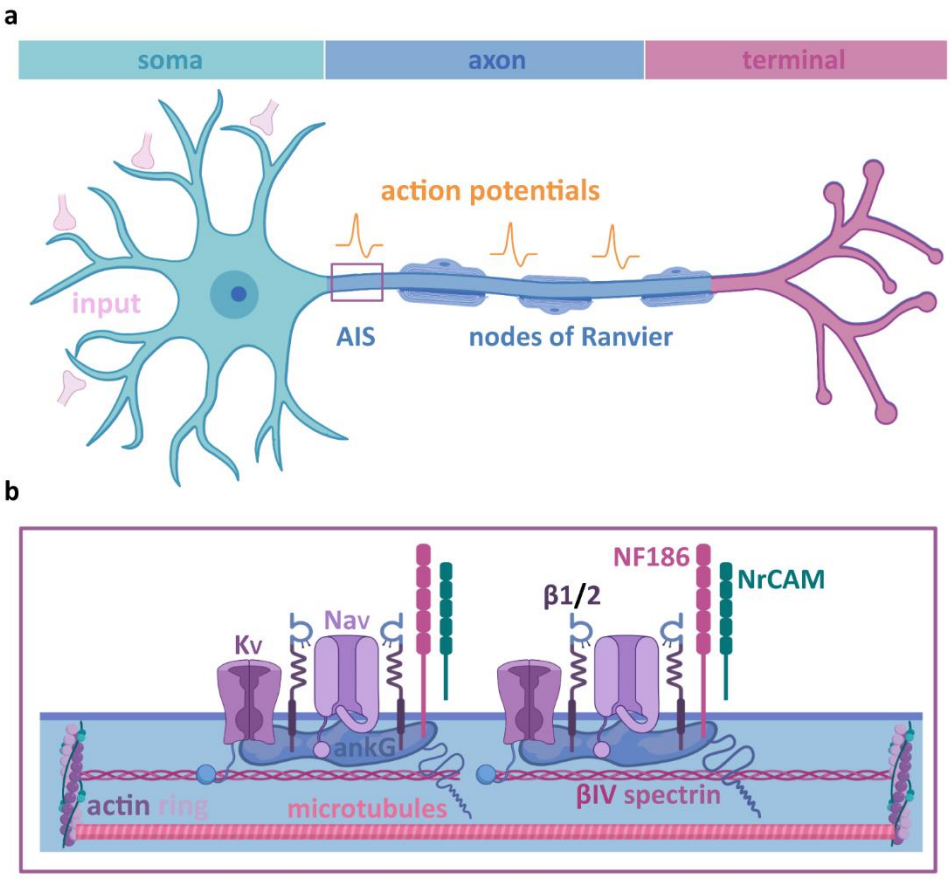

Scheme 1. Molecular organization of the axon initial segment (AIS). a: *A schematic representation of a myelinated neuron. The somatodendritic region (cyan) receives synaptic inputs (light pink). The action potentials (orange) are initiated at the AIS and propagated discontinuously along the myelinated axon. The action potentials are regenerated at the nodes of Ranvier. Upon arrival at the axon terminals (magenta), action potentials initiate the release of the neurotransmitters that pass signals to the surrounding cells.* ***b:*** *Molecular composition of the AIS. The AIS is characterized by the high-density clusters of the voltage-gated sodium channels (Na_V). The Na_V interacts with 186 kDa neurofascin isoform (NF186) via auxiliary β1 and β2 subunits. Voltage-gated potassium channels (K_V) and neuronal cell adhesion molecule (NrCAM) are also enriched at the AIS. The transmembrane AIS constituents are linked to the underlying cytoskeletal elements (βIV-spectrin) via an adaptor ankyrin G (ankG). The C terminus of ankG extends to the cytoplasm and interacts with microtubules. The βIV-spectrin interconnects 190 nm-spaced actin rings. The scheme was generated in BioRender.com according to the scheme published in[16], with permission from a publisher.*

To better understand the contributions of $Na_V1.6$ and NF186 to the pathology of neurological diseases, we need to be able to study their molecular organization and dynamics at the AIS and nodes of Ranvier with advanced microscopy. New information on the $Na_V1.6$ and NF186 neurobiology would allow the design of novel therapeutic strategies to treat diseases in which these two proteins are implicated. However, the lack of specific minimally invasive labeling tags compatible with advanced live-cell and super-resolution (SRM) microscopy has been the main obstacle in obtaining details on the dynamics and ultrastructural organization of the $Na_V1.6$

and NF186 at the AIS and the nodes of Ranvier. During my Ph.D., by combining genetic code expansion (GCE) technology with bioorthogonal click chemistry, I established a novel approach for site-specific $Na_V1.6$ and NF186 labeling in living primary neurons. I demonstrated that this approach (also termed click labeling) could be used for live-cell and SRM imaging of the AIS. Furthermore, I showed that click labeling could be utilized for the localization studies of pathogenic $Na_V1.6$ variants.

The following sections describe the molecular organization and function of the AIS and the nodes Ranvier components, focusing on $Na_V1.6$ and NF186. I also provided an overview of the current approaches for live-cell and SRM microscopy studies of the AIS and the nodes of Ranvier. Since I developed a new labeling approach based on GCE and bioorthogonal click chemistry, I introduced these two technologies in detail.

1.1. Axon initial segment

The axon initial segment provides neuronal excitability and maintains neuronal polarity[3,4,17-20]. To fulfill these important roles, the AIS has a unique molecular organization (**Scheme 1b**)[4]. One of the most distinct AIS features is the high density of the transmembrane voltage-gated sodium channels[2]. The predominant isoform is the low threshold $Na_V1.6$, localizing in the distal AIS, where it promotes action potential generation[2,21-23]. High threshold $Na_V1.2$ localizes in the proximal AIS, where it promotes action potential backpropagation[3,21]. $Na_V1.1$ is found in the proximal AIS of certain neuronal subtypes, where it controls the action potential initiation and propagation[3,22-24]. Besides the Na_V, voltage-gated potassium channels (K_V1-4, $K_V2.1$, $K_V2.2$, $K_V7.2$, $K_V7.3$) and voltage-gated calcium channels (Ca_V) are enriched at the AIS of different neuronal types. The K_V and Ca_V are essential for the action potential repolarization and the modulation of neuronal excitability[3,18,25].

The Na_V and other transmembrane AIS constituents are recruited and clustered to the AIS by interactions with a membrane domain of a multi-modular submembrane protein ankyrin G (ankG)[4,26,27]. The ankG is an adaptor that interacts with multiple transmembrane proteins (NF186, $Na_V1.6$, K_V7, neuronal cell adhesion molecule—NrCAM) and connects them to the underlying cytoskeletal elements (α2/βIV-spectrin, actin, and microtubules)[4]. The AIS structure is maintained owing to the cell adhesion molecule NF186[10].

In the last decade, advanced super-resolution microscopy such as stimulated emission depletion (STED) and direct stochastic optical reconstruction microscopy (dSTORM) provided profound insights into the ultrastructural organization of the AIS. The advanced microscopy

studies revealed that the submembrane cytoskeletal elements (α2/βIV-spectrin tetramers, adducin, and actin), adaptor ankG, the transmembrane cell adhesion molecules (CAMs), and ion channels are evenly distributed at the AIS with a spacing of ~190 nm[16,28-31]. The SRM studies also showed that the spacing of ~190 nm corresponds to the length of the α2/βIV-spectrin tetramers that interconnect submembrane actin rings. In the center of the α2/βIV-spectrin tetramer lies ankG, together with anchored membrane proteins. The C terminus of the ankG extends deeper (~32 μm) into the cytoplasm, where it interacts with underlying microtubule bundles[16].

The AIS is a dynamic structure that undergoes structural and functional changes, known as plasticity, in response to physiological (e.g., alterations of the neural activity) or pathophysiological stimuli such as injury[25,32]. The changes can happen within hours (short-term plasticity) or days (long-term plasticity). The short-term plasticity includes changes in the AIS length[33]. The long-term plasticity includes alteration of the AIS position (AIS relocation) or its length[34-36]. As an outcome, the neuronal activity gets modulated, allowing neurons to adapt to the changes in their environment[32].

1.2. The nodes of Ranvier

In vertebrates, the discontinuous multilamellar myelin sheath enwraps most axons, providing fast and saltatory propagation of the action potentials[5,7]. Oligodendrocytes produce the myelin sheath in the CNS and Schwann cells in the peripheral nervous system (PNS)[1]. The discontinuations in the myelin—nodes of Ranvier are the sites of the action potential regeneration. In order to successfully reinitiate electrical impulses**,** the nodes of Ranvier are organized into three subcompartments: nodal gap, flanking paranodes, and juxtaparanodes (**Scheme 2**)[37]. Internodes are parts of the axon between two nodes of Ranvier covered by compact myelin[5,7]. The nodes of Ranvier in the CNS and PNS differ to some extent[5-7]. This section describes the molecular architecture of the nodes of Ranvier in the CNS since its organization in the PNS was less relevant to my Ph.D. research.

Similarly to the AIS, the nodal gaps are enriched by high-density accumulations of a low threshold $Na_V1.6$ that allow the regeneration of action potentials[37-39]. In some neurons, $Na_V1.1$ and $Na_V1.6$ or $Na_V1.1$ alone accumulate at the nodal gaps[24]. Na_V, as well as voltage-gated potassium channels ($K_V7.1$ and $K_V7.2$) and cell adhesion molecule NF186, are anchored to the underlying cytoskeleton via interaction with a membrane domain of ankG[6,7,31,37,40,41]. The NF186 is an essential component since it is indispensable for the maintenance and formation of the nodes of Ranvier[7,9,11,42,43].

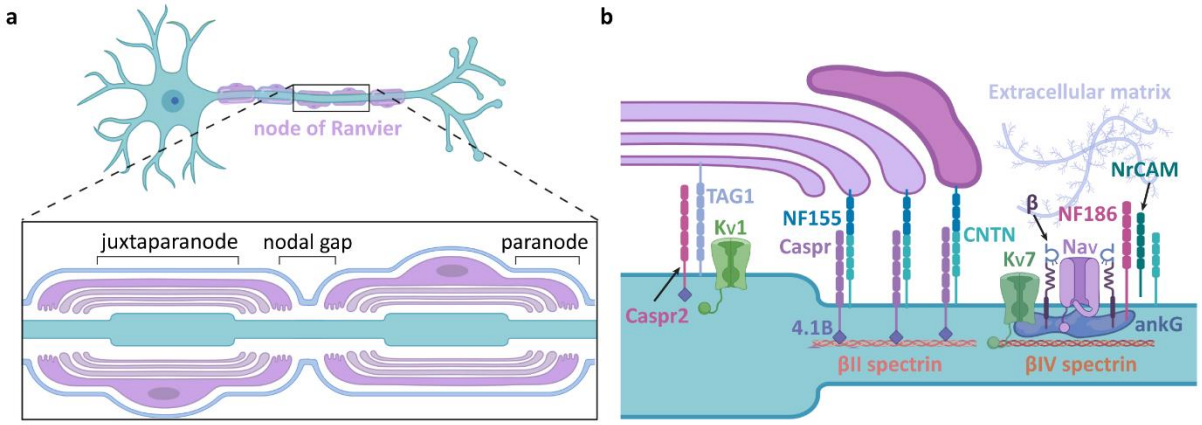

Scheme 2. Molecular organization of the node of Ranvier. a: *A schematic representation of the node of Ranvier.* ***b:*** *A molecular organization of the node of Ranvier. Similarly to the AIS, Na_V is enriched at the nodal gap. Na_V directly interacts with two auxiliary β subunits and cell adhesion molecule NF186. Likewise, K_V7 channels, secreted cell adhesion molecules NrCAM, and transmembrane contactin (CNTN) are expressed at the nodal gaps. The transmembrane nodal components interact with the extracellular matrix molecules and the submembrane ankG that anchors them to the underlying βIV-spectrin. The paranodes are characterized by a trimeric complex consisting of neuronal contactin-associated protein (Caspr), neuronal contactin, and glial 155 kDa neurofascin (NF155). The trimeric complex is anchored to the neuronal βII-spectrin via protein 4.1B. Juxtaparanodes are enriched by K_V1 interacting with neuronal Caspr2 and neuronal and glial transiently expressed axonal glycoprotein 1 (TAG-1). The scheme was generated in BioRender.com according to the scheme published in[5], with permission from RightsLink®.*

Paranodes are subdomains in which myelin tightly interacts with axolemma, forming a specific electrical barrier. This barrier restricts K_V and Na_V channels at the juxtaparanodes and the nodal gaps, respectively[6,37,42,44]. The interactions between transmembrane glial and neuronal proteins mediate the formation of this tight connection. The glial cell adhesion molecule NF155 (155 kDa neurofascin isoform) interacts with the neuronal Contactin1 and Paranodin/contactin-associated protein 1—Caspr1[6,37,40]. The trimeric complex is further stabilized by interactions of Caspr1 with a submembrane adaptor, ankyrin B (ankB), that anchors this complex to the underlying cytoskeleton[6].

Juxtaparanodes are subdomains that stabilize the saltatory conduction of action potentials. An abundance of shaker $K_V1.1$ and $K_V1.2$ channels characterizes these domains. Likewise, a dimeric complex consisting of Caspr2 and Contactin2 (TAG-1—transiently expressed axonal surface glycoprotein-1) enriches juxtaparanodes[6,37].

The ultrastructural organization of the nodes of Ranvier has been studied less extensively than the AIS[30,45]. In addition, most of these SRM studies have been carried out in peripheral myelinated neurons[30,45]. Those studies demonstrated that at the nodal gaps, all cytoskeletal elements, adaptor protein ankG, and transmembrane proteins (NF186, NrCAM, $K_V7.2$, and Na_V)

are periodically arranged with a spacing of ~190 nm[30,45,46]. The longitudinal periodic distribution of NF186 and Na_V is not always symmetrical and homogenous. In some instances, NF186 and Na_V display more complex hexagonal organization[45]. The paranodal components (βII spectrin, ankB, Caspr1, NF155) are also highly periodically arranged with ~190 nm spacing[45]. At the juxtaparanodes, only cytoskeletal elements display periodic organization, while the transmembrane $K_V1.2$ channels do not. The absence of $K_V1.2$ periodicity might be due to the compact myelin that hinders SRM imaging[45]. Finally, cytoskeletal elements exhibit periodic organization at the internodes[6,47]. In order to gain deeper insights into the ultrastructural organization of the nodes of Ranvier in CNS, detailed SRM studies of myelinated CNS neurons are needed.

1.3. The axon initial segment and the node of Ranvier components

Since the main aim of my Ph.D. was to develop new tools for voltage-gated sodium channels (Na_V) and neurofascins (NFs) labeling, I described their structure, regulation, and spatial and temporal distribution in more detail in this section.

a) Voltage-gated sodium channels

Voltage-gated sodium channels play an essential role in the electrical signaling in excitable cells by initiating and propagating action potentials[48,49]. On the membrane, Na_V forms a trimeric complex that consists of a large, highly glycosylated pore-forming α subunit (~260 kDa) and two auxiliary β subunits (30–40 kDa each)[50].

There are nine voltage-gated Na_Vα isoforms ($Na_V1.1$–$Na_V1.9$)[51,52]. Their distribution is cell and tissue-specific and developmentally regulated **(Table 1)**[53-55]. The Na_V isoforms share the general structural organization (**Scheme 3**)[51]. Briefly, the α subunit is a ~2000 amino acid-long protein organized into four homologous domains (DI–IV) interconnected by long intracellular loops (L1–L3)[50,56]. Each domain contains six highly conserved transmembrane α helixes (S1–6 segments) interconnected by short extra- and intracellular loops[50,56]. The S5 and S6 segments of each domain, together with loops between them (P loops), form a pore and selectivity filter (highly conserved DEKA sequence) that regulates Na^+ entry[48,52]. The S4 segments are enriched with positively charged amino acids, acting as voltage sensors. The voltage sensors change conformation in response to the membrane depolarization, resulting in the pore opening[48]. The fast inactivation of Na_V is regulated by the L3 loop that contains a highly conserved IFM motif (inactivation gate)[48,57] and by intracellular C-terminal tail[58]. The C terminus also represents a binding platform for interacting partners and regulators and contains multiple sites undergoing

posttranslational modification[59-63]. Likewise, the posttranslational modifications and interaction with partners occur at the N terminus and in the L1 and L2 loops[61-65].

Table 1. *Classification of the voltage-gated sodium channel isoforms based on the tetrodotoxin (TTX)-sensitivity and Na_V spatial and temporal distribution. The Na_V can be sensitive to TTX (TTXs) or resistant to TTX (TTXr). The table is generated based on the previous publication[51].*

Na_V isoform	**Resistance**	**Spatial and temporal distribution**
$Na_V1.1$	TTXs	Mature CNS: soma, proximal AIS, nodes of Ranvier; PNS
$Na_V1.2$	TTXs	Mature CNS: proximal AIS, unmyelinated axons, premature nodes of Ranvier
$Na_V1.3$	TTXs	PNS and embryonic CNS
$Na_V1.4$	TTXs	Skeletal muscles
$Na_V1.5$	Moderately TTXr	Cardiomyocytes and embryonic CNS
$Na_V1.6$	TTXs	Mature CNS: distal AIS, nodes of Ranvier, (soma), mature PNS
$Na_V1.7$	TTXs	Mostly PNS, (CNS)
$Na_V1.8$	TTXr	PNS
$Na_V1.9$	TTXr	PNS (hippocampus)

β subunits (encoded by *SCNXB* genes; X is the number of a specific β isoform) are small transmembrane proteins that belong to the CAM family[66]. The β subunits are indispensable for the full functionality of the Na_V since they modulate biophysical properties and the surface expression of the α subunits[66-68]. The β subunits also regulate *SCNXA* expression[69]. Furthermore, during brain development, they are important for cell migration, cell adhesion, and neurite outgrowth[66]. There are four transmembrane isoforms of β subunits (β1–4) and one secreted β1B isoform[67,68,70-74]. Homologous β1 and β3 interact noncovalently with Na_V via their N and C termini. The homologous β2 and β4 interact with Na_V via a covalent, disulfide bond[66]. In the adult mammalian brain, Na_V usually forms a trimeric complex with β1 and β2[67,68].

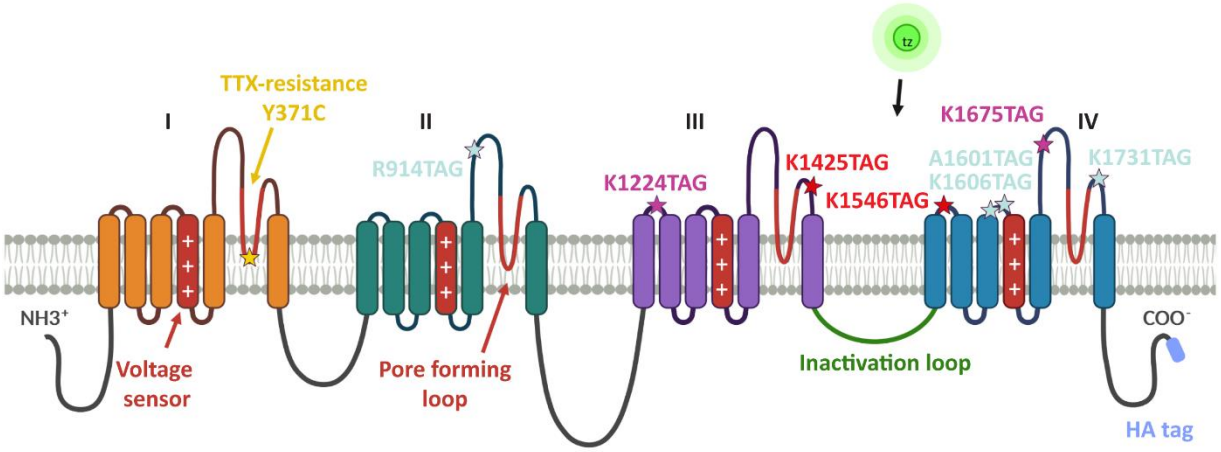

Scheme 3. Structure of an alpha $Na_V1.6$ subunit with click labeling sites*. A $Na_V1.6$ encoded by the SCN8A gene consists of four homologous domains (I–IV). Each domain contains six transmembrane α-helixes (S1–6). The S4 segment enriched with positively charged amino acids is a voltage-sensor (red) that can sense changes in the membrane potential. Domains and α-helixes are connected with intracellular and extracellular loops. The loops between S5 and S6 of each domain (red) form a pore that allows Na^+ entrance. In order to click label $Na_V1.6$, I selected eight potential labeling positions and introduced the corresponding TAG mutations into mouse SCN8A. Red stars show the most successfully click-labeled positions with ATTO488-tetrazine (tz; green). The pink stars show the additional positions tested for click labeling in neurons. The other TAG positions that have not been tested in neurons are shown as light blue stars. For the electrophysiological recordings of recombinant Na^+ currents, I introduced the Y371C mutation that rendered $Na_V1.6$ resistant to tetrodotoxin (TTX; yellow star). The hemagglutinin (HA)-tag (purple) introduced at the m$Na_V1.6$ C terminus ensured that only full-length proteins were labeled with the anti-HA antibody. The scheme was initially generated in BioRender.com and modified from[75].*

$Na_V1.6$

$Na_V1.6$ (encoded by the *SCN8A* gene) is broadly distributed through the mature nervous system (**Table 1**)[51,61,76,77]. In the adult brain, it is the major voltage-gated sodium channel isoform[3,8,76,77]. The abundance of the $Na_V1.6$ isoform is found in distal AIS and the nodes of

Ranvier, where it contributes to the generation and propagation of action potentials, respectively[8,21-23,38,39,78,79]. A low amount of individual $Na_V1.6$ molecules is also present in the somatodendritic compartment, facilitating the generation of dendritic potentials[22]. Furthermore, ankG-independent ~230 nm $Na_V1.6$ nanoclusters are present in the somatic compartment[80]. The role of the somatic $Na_V1.6$ nanoclusters is still unclear. Apart from the neurons, $Na_V1.6$ is expressed to a smaller extent in glial cells and cardiomyocytes[61,77].

Sorting and enrichment of the $Na_V1.6$ at the AIS and the nodes of Ranvier is promoted by the interaction of a highly conserved, nine amino acid-long motif (ankyrin binding domain; ABD) with ankG [65,81-84]. The interaction between ankG and Na_V is regulated by casein kinase 2 (CK2) enriched at the AIS and the nodes of Ranvier. At the AIS, the CK2 forms a tight complex with Na_V and phosphorylates ABD, modulating Na_V accumulation in this neuronal compartment[83,85,86]. The maintenance of $Na_V1.6$ on the AIS surface is promoted by microtubule-associated protein 1B (MAP1B) kinase. The MAP1B kinase binds the N terminus of the $Na_V1.6$, preventing its endocytosis[87]. The modulation of $Na_V1.6$ function and its surface expression is also regulated by posttranslational modifications (phosphorylation, ubiquitination, palmitoylation, or glycosylation) of N and C termini, L1-L2 loops, and the extracellular loops, or by interaction with various partners[60-64].

b) Neurofascins

Neurofascins (encoded by the *Nfasc* gene) belong to the L1 family of CAMs[88,89]. The NFs have important roles that involve the neurite outgrowth, formation, and stabilization of the nodes of Ranvier, AIS maintenance, and the regulation of axo-axonic synapses[9-11,89-91]. Diversity of NF is achieved by developmentally- and spatially-specific alternative splicing of a single primary transcript[89,92]. During nervous system development, neuronal 180 kDa and 140 kDa neurofascin isoforms (NF180 and NF140) control neurite outgrowth[88,89]. Likewise, NF140 promotes early nodes of Ranvier assembly[93]. To a smaller extent, NF140 is present in the healthy adult brain and demyelinated axons in multiple sclerosis (MS) patients[92,93]. The most abundant isoforms in the mature nervous system are neuronal NF186, which localizes at the AIS and nodal gaps, and glial NF155, localizing at the paranodes[40,88]. Both isoforms are essential for the formation and stabilization of the nodes of Ranvier[9].

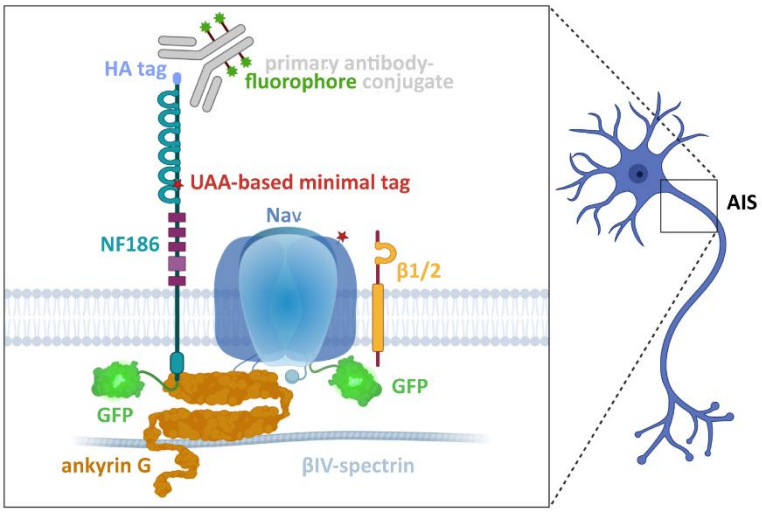

Scheme 4. Overview of the approaches for live labeling and imaging of the AIS and the nodes of Ranvier components in neurons. *AIS and node of Ranvier components such as NF186 can be labeled in living neurons with antibodies conjugated to a fluorescent dye recognizing the extracellular epitopes[33,94]. The alternative approach utilizes genetically encoded fluorescent proteins (FPs) fused to N or C termini of AIS and nodal components[26,65,83,84,95]. Such FPs fusions provide high specificity. However, due to their large size of ~30 kDa, they can perturb the localization of proteins (e.g., NF186) or change the AIS morphology[95,96]. Unnatural amino acid (UAA)-minimal tags can be placed at virtually any position while introducing changes of just a few atoms into the protein of interest[97,98]. Hence, they have emerged as a promising tool for dynamic studies of the AIS and the node of Ranvier components. The scheme was originally generated in BioRender.com and modified from[75].*

The general NF structure is shared between isoforms (**Scheme 4, Fig. 9a**). It consists of six extracellular immunoglobulin (Ig)-like domains followed by fibronectin type III (FN III) repeats, transmembrane α helix and a short intracellular tail. The number of FN III domains differs between NF isoforms[89]. Glial NF155 contains FN III domains 1, 2, 3, and 4, while NF186 contains FN III domains 1, 2, 4, 5 and the unique mucin (PAT) domain (**Scheme 4, Fig. 9a**)[89]. The cytoplasmic tail includes a highly conserved FIGQY sequence that is indispensable for the NF interaction with ankG and the NF localization at the AIS[95,99-101]. Furthermore, the C-terminal YSLA sequence is essential for NF186 sorting to the AIS[95].

NF186 is a Na_V-associated protein enriched at the AIS and nodal gaps[89]. It promotes the nodes of Ranvier formation by clustering $Na_V1.6$ and contributes to the AIS and the node of Ranvier maintenance[9-11]. NF186 also promotes the brevican-based extracellular matrix assembly at the AIS and links the extracellular matrix to the cytoskeleton via ankG[102]. Furthermore, NF186 inhibits neurite outgrowth[91].

1.4. Pathologies associated with the AIS and the node of Ranvier components

Changes or disruption of the AIS and the node of Ranvier have been associated with various neurological disorders[18,37,52,94,103-105]. The changes in the AIS length or its position have been observed in neurodegenerative diseases such as Alzheimer's disease[106] or MS[107], and the mouse and rat models of epilepsy[108]. The neuronal injury or demyelination can also cause changes (shortening) of the AIS length[32]. The redistribution of the node of Ranvier components and the elongation of the nodal gaps have been detected in MS and neonatal hyperoxia[12,37,103,105].

Since Na_V and NF186 are indispensable for the proper functioning of the AIS and nodes of Ranvier, it is not surprising that these proteins have been implicated in many diseases. The redistribution, altered expression, and genetic mutations of $Na_V\alpha$ and $Na_V\beta$ subunits have been linked to developmental and epileptic encephalopathy, epilepsy, episodic ataxia, migraine, intellectual disability, pain**,** cardiac diseases, cancer, MS, and axonal injury[8,12-14,50,66,109]. Numerous $Na_V1.6$ mutations are linked to neurological diseases such as developmental and epileptic encephalopathy, epilepsy, autism spectrum disorder, intellectual disability, or movement disorders[13,14,109]. Altered expression and redistribution of $Na_V1.6$ are implicated in MS pathology[12,105]. Moreover, overexpression of $Na_V1.6$ contributes to invasive cancer development and metastasis (e.g., breast, cervical, lung, and colorectal cancers)[110,111].

The autoantibodies against the extracellular domain of NF86 have been found in some patients with demyelinating diseases such as Guillain-Barré syndrome, chronic inflammatory demyelinating polyradiculoneuropathy, or MS[15,112-114]. The abundance of the anti-NF186 antibodies has been detected in a small number of chronic progressive MS patients, where they might contribute to axonal degeneration[15,113]. Furthermore, the altered localization of NF186 and NF155 at the nodes of Ranvier has been associated with axonal pathology in MS[103].

1.5. The labeling and imaging approaches to study the AIS and the nodes of Ranvier components

The exact mechanisms involved in the trafficking, sorting, and (re)organization of the AIS and the nodes of Ranvier components under biological and pathological conditions have remained elusive. The reason is the limited number of labeling approaches permitting dynamic and SRM studies of those two compartments. Considering the number of diseases that involve dysfunctions of the AIS and nodal components, understanding the regulation of these proteins is necessary to design new therapeutical approaches. The following sections describe the current

labeling and imaging strategies used to study the dynamic and ultrastructural organization of the AIS and nodes of Ranvier and the limitations of these approaches.

a) Live-cell labeling approaches for dynamics studies

Several live-cell labeling approaches have been used to study the dynamics of the AIS and nodal proteins (**Scheme 4**). One approach involves conventional immunostaining with antibodies conjugated to fluorescent dyes[19,33,94-96,115,116]. Since the immunostaining protocols usually involve membrane permeabilization to enable bulky antibodies to enter cells and access their epitopes, this approach is mostly used for fixed-cell labeling. The main requirement for using this approach in live-cell labeling and imaging experiments is that the epitopes recognized by the fluorescent antibodies are located in the extracellular domains of transmembrane proteins. If such epitopes do not exist, small tags (e.g., hemagglutinin—HA or V5 tags) can be introduced in the extracellular domains of the recombinant or endogenous transmembrane targets[65,101]. An example is NF186, for which live labeling and imaging fluorescent antibodies have extensively been used[19,94,95,115,117]. More recently, labeling and imaging of endogenous $Na_V1.2$ have been achieved in living neurons. To this end, the V5 tag was introduced in the extracellular loop of $Na_V1.2$ and immunostained with the corresponding fluorescent antibody[65]. One of the important advantages of fluorescent antibodies is that they can be used to label endogenous proteins. However, the antibodies are large (~150 kDa) and can be utilized only for live imaging of transmembrane proteins. Likewise, the antibodies frequently lack specificity when used for labeling closely related protein isoforms (e.g., Na_V). Finally, they proved unreliable for dynamic studies of the AIS components due to the crosslinking caused by the multivalency of primary antibodies[96]. An example is an anti-NF antibody that failed to accurately report fast changes in the AIS length upon depolarization[96].

Fluorescent protein (FPs)-based genetically encoded tags are the most widely used for live labeling and imaging studies of the AIS and node of Ranvier components[33,83,84,96,101,116,118-122]. Since genetically encoded FPs are fused directly to the protein of interest, this labeling approach is highly specific. However, FPs can be fused only to the N or C termini of the target protein. When it comes to the AIS and nodal constituents, those domains are essential for the interactions with partners or represent binding platforms for different regulators[59-63]. The N or C termini also can contain important localization sequences and posttranslational modification sites[60-63,99,100]. Therefore, adding relatively large FPs (~30 kDa) may impair some of the interactions with regulators, affect the localization of the AIS components, or interfere with posttranslational modifications. For example, the addition of a green fluorescent protein (GFP) to the C terminus

of NF186 (NF186-GFP) hides the AIS localization (FIGQY) sequence. Consequently, NF186 cannot be specifically sorted to the AIS[95,96]. On the contrary, NF186-GFP can be sorted properly to the nodes of Ranvier since FIGQY is not required to target NF186 to this compartment[95,119,120].

Due to its size and highly complex structural organization, live labeling of $Na_V1.6$ is even more challenging compared to the smaller AIS components (e.g., NF186) and other neuronal proteins and ion channels. Consequently, our knowledge about $Na_V1.6$ originates mostly from the electrophysiological recordings, biochemical, molecular, and genetic studies, and from the immunostaining of fixed samples[14,21-23,38,39,48,78,79]. This partially changed when a recombinant full-length $Na_V1.6$ fused to FPs was developed about ten years ago[83]. The FPs, such as GFP or mCherry, were fused to the C terminus of $Na_V1.6$. The imaging of living neurons that expressed such recombinant voltage-gated sodium channels provided new information about molecular mechanisms that regulate $Na_V1.6$ targeting to the AIS and nodes of Ranvier[8,80,83,84]. Moreover, the photoconvertible GFP (Dendra2) allowed super-resolution imaging of the somatic $Na_V1.6$ populations in living neurons[80]. Recently, using CRISPR/Cas9 technology, the endogenous $Na_V1.6$ was tagged with GFP to study the plasticity of this protein at the AIS[123]. Besides FPs, several other approaches have been utilized for $Na_V1.6$ live imaging. A combination of the GFP tag with an extracellular epitope that could be labeled with cell-impermeable dyes provided valuable information on $Na_V1.6$ sorting into different neuronal compartments[80,84]. The extracellular epitope consisted of 17 amino acid-long biotin acceptor domain (BAD). When biotinylated by bacterial biotin ligase, the BAD domain could be labeled with non-permeable streptavidin (SA)-conjugated dyes[84]. With this approach, it was possible to label the $Na_V1.6$ membrane populations and follow their internalization and transport. A similar approach has recently been utilized to image other Na_V isoforms ($Na_V1.7$ and $Na_V1.9$) in living sensory neurons and cell lines[121,122]. However, the SA-conjugated dyes are not ideal for live labeling due to their large size of ~53 kDa. When SA was combined with GFP (27 kDa), the total change introduced into Na_V was ~80 kDa. Recently, CRISPR/Cas9 technology was used to introduce a self-labeling HaloTag to the C terminus of endogenous $Na_V1.2$ and $Na_V1.6$[65]. The subsequent labeling of HaloTag with cell-permeable dyes allowed, for the first time, SRM and live-cell imaging of endogenous $Na_V1.2$ and $Na_V1.6$. However, since the size of HaloTag (~33 kDa) is similar to that of FPs (~27 kDa), it has the same disadvantages as described above.

b) Super-resolution microscopy for ultrastructural studies

Super-resolution microscopy is a term that refers to a collection of advanced microscopy techniques that allow the visualization of molecules below the resolution limit[124]. For SRM

imaging, proteins or cell structures of interest are typically labeled with fluorescent antibodies, dyes, or FPs[124]. The visualization of closely positioned fluorescently labeled molecules that cannot be resolved with conventional microscopy is achieved by their separate detection[125,126]. There are two main approaches for achieving separate detection of fluorescent molecules. On the one hand, SRM techniques such as STED utilize a patterned illumination to modulate the fluorescence emission of closely positioned fluorophores[127-129]. On the other hand, single-molecule localization microscopy (SMLM) techniques such as PALM, fluorescence (F)PALM, and direct (d)STORM rely on the temporal separation of the closely positioned fluorescent molecules, their subsequent localization, and reconstruction of the final SRM image[130-133]. By combining the advantages of STED and SMLM, minimal photon fluxed (MINFLUX) nanoscopy was recently developed[134]. With MINFLUX nanoscopy, the spatial resolution was improved from ~20–30 nm to ~2–5 nm, reaching the size of the individual molecules. During my Ph.D. I used mainly SMLM microscopy. Hence, I described it in detail below.

The SMLM techniques differ in the fluorophores used to label target proteins. PALM and FPALM use photoconvertible/photoactivable FPs, while (d)STORM utilizes photoswitchable organic dyes, such as Alexa Fluor (AF)647 or Cyanine 5 (Cy5)[125]. The temporal and spatial separation of the fluorescent molecules in SMLM microscopy is achieved by the specific imaging buffers that promote stochastic switching of the fluorophores between bright (ON) and dark (OFF) states when illuminated with a high-power laser[125]. This transition between the ON and OFF state is termed blinking[125]. The most commonly used imaging buffer GLOX is based on the oxygen scavenger system consisting of glucose, glucose oxidase (GO), and catalase (CAT). The GLOX buffer is usually supplemented with thiol-reducing agents such as β-mercaptoethanol (βME) or mercaptoethylamine (MEA; GLOX βME or GLOX MEA)[135]. Although GLOX, in combination with AF647 dye, is an excellent dSTORM imaging buffer, it provides efficient blinking of fluorescent dye molecules for only a few hours and needs to be replaced afterwards. Likewise, GLOX is unsuitable for mounting and long-term storage of the samples. Therefore, immunostained or click-labeled samples are usually stored in phosphate-buffered saline (PBS) before the addition of GLOX for dSTORM imaging. Keeping neurons in PBS can lead to fluorescence loss if the samples are not imaged within several days. Hence, in addition to GLOX, alternative buffers such as glycerol-based mounting medium Vectashield (VS) or oxyrase/βME (OxEA) can be used for single- and dual-color SRM[136,137].

In the last decade, advanced super-resolution microscopy (e.g., STED, PALM, and (d)STORM) has been extensively utilized to decipher the ultrastructural organization of

neurons[16,28,29,45,46,65,138]. As described above, with the help of advanced SRM microscopy, it was shown that the AIS and the nodes of Ranvier components are periodically arranged with a spacing of 190 nm[16,28,29,45,46,65]. For the SRM studies, the AIS and the nodes of Ranvier components have been typically labeled with fluorescent antibodies[16,28,29,45,46,138]. However, the bulky antibodies (100–200 kDa) place fluorophores far away from the target (~15 nm) and can potentially introduce artefacts, especially when imaging the crowded AIS and the node of Ranvier environment. Hence, new labeling approaches utilizing small tags that will reduce the distance between the target and the fluorophore are in demand. The combination of the GCE and bioorthogonal click chemistry (click labeling) has recently emerged as a promising tool for single- and dual-color SRM imaging of small synaptic proteins and cytoskeletal elements in primary neurons[97,98]. The small size of the unnatural amino acid (UAA)-based labeling tag (0.2–0.5 kDa) that can be introduced anywhere into the target protein make click labeling an ideal choice for SRM studies. In addition to the minimal size of the labeling tag, click labeling is compatible with live-cell imaging. Therefore, this approach is a promising tool for dynamic and SRM studies of the AIS and the nodes of Ranvier components.

During my Ph.D. I aimed to establish the GCE and click chemistry for labeling two large transmembrane AIS and node of Ranvier constituents, the $Na_V1.6$ and NF186, in primary neurons. The following sections describe genetic code expansion and click chemistry and their applications in neurobiology.

1.6. Click labeling for advanced microscopy studies of neuronal proteins

The genetic code is a collection of rules determining how the trinucleotide sequences (codons) encode canonical (natural) amino acids in all living organisms[139]. There are, in total, 64 codons. Three (opal, amber, and ochre) are protein synthesis termination (STOP) signals. The remaining 61 codons encode 20 canonical amino acids that represent building blocks for all existing proteins[139]. Some organisms use two additional proteinogenic amino acids—selenocysteine and pyrrolysine, encoded by opal and amber STOP codons, respectively[140,141]. The genetic code can be artificially expanded to encode unnatural (noncanonical) amino acids to introduce novel biological, chemical, or physical properties into proteins[142,143]. *In vitro* and *in vivo* UAA encoding can be achieved via metabolic UAA incorporation or genetic code expansion technology. Metabolic UAA incorporation utilizes endogenous translational machinery [aminoacyl tRNA synthetase (aaRS)/transfer ribonucleic acid (tRNA) pair] to replace one of the canonical amino acids with a noncanonical one[144]. With this technology, UAA is installed into the whole proteome in a residue-specific manner[144]. A GCE technology uses orthogonal translational

machinery that does not cross-interact with native translation to site-specifically install UAA into a protein of interest (POI)[142,143].

One of the emerging applications of GCE is protein labeling in living cells for fluorescence microscopy studies. Live-cell protein labeling is achieved through a site-specific incorporation of small UAA that can be labeled with a fluorescent dye into POI. The incorporated UAAs bear reactive groups in their side chains that can be coupled to a small organic dye via click chemistry reactions (hereafter referred to as clickable UAAs; **Scheme 5**)[145-149]. Until now, a combination of the GCE and bioorthogonal click chemistry has been used to label various membrane and cytosolic proteins in standard cell lines[145,147,148,150-158], and just recently in primary neurons and organotypic slice cultures[97,98]. The following sections describe GCE technology, different UAAs, and bioorthogonal click reactions focusing on their application for microscopy studies of neuronal proteins in mammalian cells.

a) Genetic code expansion

As mentioned above, the GCE is a protein engineering technology that utilizes orthogonal translation machinery [aminoacyl tRNA synthetase (aaRS)/tRNA pair] to site-specifically install UAAs into the POI during translation[159,160].

A prerequisite for GCE-mediated site-specific UAA incorporation is orthogonality, i.e., aaRS/tRNA should not cross-react with the endogenous translational machinery of the host cell and has to specifically recognize UAA and incorporate it in response to a unique (blank) codon[161]. These requirements are fulfilled by adopting translational machinery components from other domains of life. If necessary, aaRSs/tRNAs are further evolved[143,162]. For the GCE in mammalian cells, aaRS/tRNA pair is typically evolved in *Escherichia coli* (*E. coli*) or yeast and then transferred to mammalian cells[159,163,164]. The commonly used orthogonal pairs in mammalian cells are Tyrosil (Tyr) RS/tRNA^{Tyr} and Leucil (Leu) RS/tRNA^{Leu} pairs derived from *E. coli*[163] and Pyrrolysyl (Pyl) RS/tRNA^{Pyl} pair adopted from archaea *Methanosarcina barkeri* or *Methanosarcina* mazei[146,165-170]. The PylRS/tRNA^{Pyl} is the most widely utilized because it can recognize various UAAs and is orthogonal in both *E. coli* and eukaryotes[159].

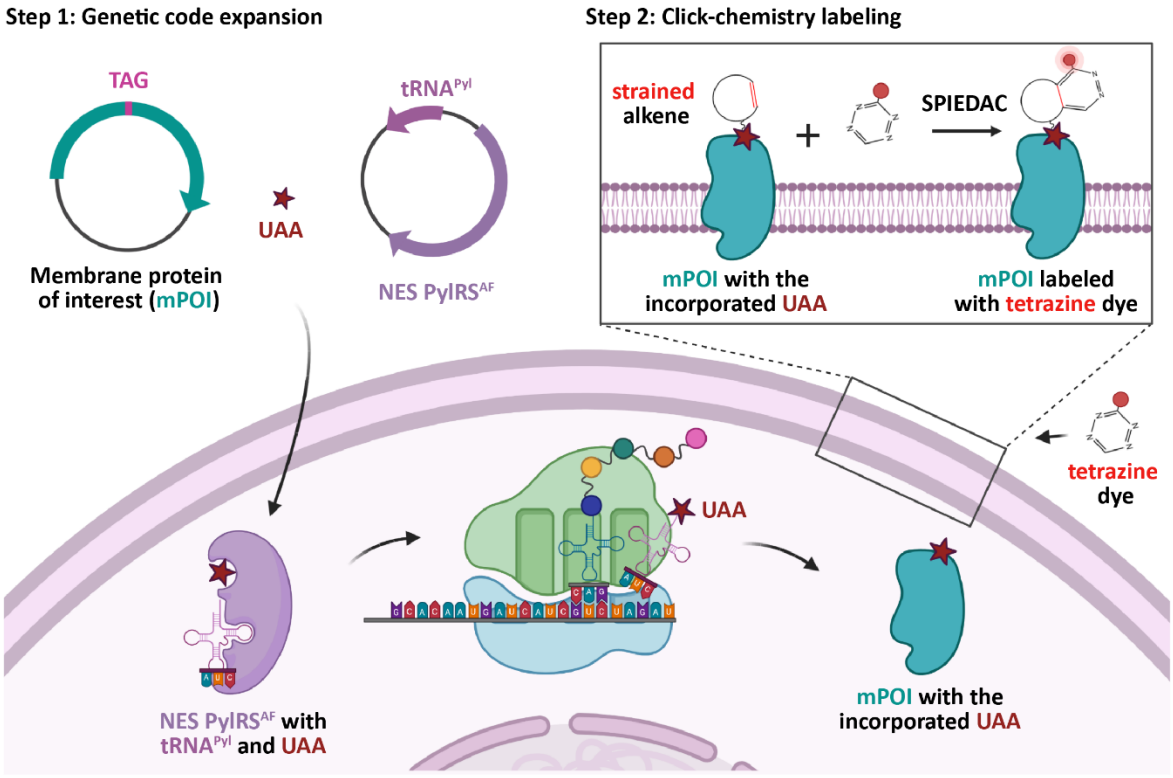

Scheme 5. Genetic code expansion (GCE) and bioorthogonal click labeling of membrane proteins. *Click labeling of membrane proteins in living cells is a two-step process. In the first step (**Step 1**), using the GCE (amber codon suppression), small UAAs, such as TCO*-Lys or endo-BCN-Lys are introduced into the recombinant membrane protein of interest (mPOI). To successfully incorporate UAA, genes that encode for mPOI bearing TAG labeling site are delivered to the cells via transfection or transduction, along with the bioorthogonal translational machinery elements—NES PylRS^{AF} and tRNA^{Pyl}. The UAA is added to the transfection/transduction or the culturing medium. During translation, with the help of the orthogonal translational machinery, UAA is incorporated in response to an amber (TAG) stop codon, resulting in the synthesis of the full-length mPOI. In the second step (**Step 2**), mPOI is labeled via ultra-fast bioorthogonal click reaction, such as strain-promoted inverse electron-demand Diels-Alder cycloaddition (SPIEDAC) between a strained alkene and the tetrazine. The scheme was initially generated in BioRender.com and modified from*[75].

To encode the UAAs, in-frame nonsense codons are typically used. The most widely used is an amber UAG (STOP) codon due to its low abundance in prokaryotic (~7%) and eukaryotic cells (~20%)[171,172]. Therefore, the subtype of the GCE technology that utilized the TAG stop codon is also referred to as amber codon suppression. The amber codon is introduced at the specific position into the gene encoding the POI (hereafter referred to as an amber mutant) by site-directed mutagenesis[161]. For the UAA incorporation**,** the genes encoding the amber mutant and the orthogonal translational machinery elements are usually delivered via transfection[161]. Alternatively, amber codon suppression elements can be delivered via transduction (typically used for animal studies)[161]. Since most UAAs are cell-permeable, they are usually added to the

growth medium for *in vitro* studies. For *in vivo* studies, the UAAs can be added to the drinking water[173,174]. Alternatively, for *in vivo* neuronal studies, UAAs can be injected directly into the ventricles of the mouse brain[175]. If all the required components are present during the translation, orthogonal translation machinery recognizes the STOP codon in the messenger (m)RNA and incorporates UAA in response to it. As a result, a full-length target protein with installed UAA is produced.

A successful UAA incorporation via GCE has been achieved in prokaryotes (*E. coli*)[176], single-cell eukaryotes (*Saccharomyces cerevisiae*)[177,178], mammalian cell lines, neuronal stem cells, primary neurons[163,179], brain organoids [180], and multi-cellular organisms (*Caenorhabditis elegans*, *Drosophila melanogaster*, *Danio rerio* and *Mus musculus*)[173-175,181-185]. More than 200 UAAs have been encoded into various proteins by the GCE[186]. These UAAs bear custom-designed functional handles that have been used to study protein interactions, protein activity, and the effect of posttranslational modification on protein function[186,187]. In addition, clickable UAAs have been used for *in vitro* and *in vivo* protein labeling via click chemistry reactions[188,189]. The following section describes the application of click chemistry for UAA-based protein labeling.

b) Bioorthogonal click chemistry reactions

Bioorthogonal click chemistry is a collection of fast, selective, and biocompatible reactions that proceed under mild, aqueous conditions between a biomolecule and a specific reporter, probe, or substrate[190,191].

Bioorthogonal click chemistry can be used for site-specific protein labeling in living cells (click labeling). The click labeling of proteins is a two-step process that involves: 1) site-specific incorporation of the clickable UAA into a protein of interest via GCE (typically amber codon suppression) technology, 2) subsequent labeling of the side chains of the clickable UAAs with small organic dyes via click chemistry reaction[170]. In order to be used for live-cell protein labeling, click reactions should be bioorthogonal, i.e., should not interfere with any native biological processes[191]. Such reactions must also be non-toxic, fast, and highly specific under physiological conditions[191].

Several bioorthogonal click reactions have been developed for live-cell protein labeling: copper(I)-catalyzed Huisgen azide-alkyne cycloaddition (CuACC), photo click reaction[192-195], and copper-free click reactions—SPAAC (strain-promoted alkyne-azide cycloaddition) and SPIEDAC (catalyst-free strain-promoted inverse-electron demand Diels-Alder cycloaddition)[145-147,149,196].

CuACC click reaction between azides and terminal alkynes is highly specific. However, this reaction requires copper as a catalyst. Since copper is toxic for most cells, the CuACC use for live-cell labeling is limited[192]. Photo click cycloadditions between tetrazoles and terminal or strained alkenes are fast and less toxic than the CuACC as they use ultra-violet (UV) light as a catalyst[192,193]. Therefore, they have also been employed for protein labeling in living cells[195]. Catalyst-free SPAAC and SPIEDAC are non-toxic, ultra-fast, and highly specific. They give a high yield and proceed under physiological conditions. Hence, these two are the most suitable for live-cell protein labeling[192]. Commonly used UAAs for SPAAC- and SPIEDAC-based protein labeling are L-lysine derivatives. Side chains of these UAAs are modified to carry strained alkynes or alkenes that react with organic dyes bearing azides or tetrazines. The examples are trans-cyclooct-2-en – L – lysine (TCO*-Lys) and its axial (A) isomer (TCO*A-Lys)[148,197], trans-cyclooct-4-en – L – lysine (TCO4en-Lys) and its equatorial isomer (TCO4en/eq-Lys)[196,198], cyclopropene – L – lysine (CpK)[199], bicyclo [6.1.0] nonyne – L – lysine (endo-BCN-Lys)[147,149], and cyclooctyne – L – lysine (SCO-Lys)[146,169].

Due to its high reaction rate, SPIEDAC click reaction has been used the most for protein labeling in living cells[192]. SPIEDAC-based click labeling happens between the UAA side chain that carries strained alkenes or alkynes and tetrazine conjugated to an organic dye[145,146,148,149]. The additional advantage of SPIEDAC click reaction, particularly for microscopy studies[152,200], is its fluorogenicity. It is known that when conjugated to free tetrazine moiety, the fluorescence of certain red dyes is quenched. Upon cycloaddition (click reaction), the fluorescence of a dye is restored or increased. As a result, only click-labeled POI is fluorescent, while the background originating from the free dye is minimal[152,192,200].

To date, click labeling has been employed for single-color, dual-color, and pulse-chase labeling of various proteins in living mammalian cell lines[145,147,148,150-158,201]. Some of the proteins that have been successfully labeled are membrane proteins and receptors such as insulin receptor (IR)[148], epidermal growth factor receptor (EGFR)[145], tumor necrosis factor 1 receptor (TNFR1)[152], G protein-coupled receptor (GPCR)[151], ligand-gated ion channels[153], and intracellular cytoskeletal elements[147,150,152,157,158]. Bioorthogonal click reactions have also been used to label small, low-abundance, or difficult-to-label proteins that could not be visualized with other labeling tags. The examples are 137 amino acid-long (~15 kDa) interferon-inducible transmembrane protein 3 (IFITM3), viral human immunodeficiency virus-1 (HIV-1) structural protein, and nuclear pore complex (NPC) components[150,156,201].

Although multi-color click labeling of POIs has remained challenging, there are some reports on successful dual-color protein labeling. SPIEDAC and its subtype, a selectively enhanced (se)SPIEDAC reactions, were combined in a pulse-chase manner to label two different UAAs incorporated into two populations of IR in a highly transfectable derivative of human embryonic kidney 293 (HEK293T) cells[148]. Click labeling of two IR populations was possible due to the mutual orthogonality of SPIEDAC and seSPIEDAC. Also, with the help of mutually orthogonal aaRS/tRNA pairs, two distinct UAAs were site-specifically incorporated into the same membrane receptor and labeled with two fluorescent dyes in HEK293T cells [202]. Two mutually orthogonal aaRS/tRNA pairs and the combination of SPIEDAC and SPAAC reactions were employed to label two different proteins in *E. coli*[203]. However, labeling two distinct proteins in the same eukaryotic cell has remained challenging.

Since various tetrazine dye derivatives can be attached to a UAA, including the photoswitchable ones, click labeling can be combined with advanced SRM microscopy. The click-labeled IR was the first protein to be imaged with SRM microscopy[148]. In this study, dual-color SRM of two IR populations was achieved using two different photoswitchable dyes[148]. Likewise, the various extra- and intracellular click-labeled proteins, as well as viral ones, have been imaged with different SRM techniques (e.g., ground state depletion microscopy—GSDIM, STORM, STED, spatial light interference microscopy—SLIM, and MINFLUX)[97,98,153,157,158,170,201,204].

By combining click labeling with DNA-PAINT (points accumulation for imaging in nanoscale topography; hereafter referred to as click-PAINT), it was possible to label the low-abundance component of the NPC, nucleoporin 153 (Nup153) and image it with super-resolution microscopy[150].

c) The advantages of genetic code expansion and click chemistry for protein labeling in living cells

Click labeling has emerged as one of the most powerful approaches for fluorescent protein labeling. Besides the compatibility with live-cell labeling and imaging, the other advantages of click labeling are the following[160,188]: the POI is modified in a minimally invasive way (only a few atoms are added to the UAA side chain), the UAA and the fluorescent dye can be introduced at virtually any position into the POI, and the UAAs with attached organic dyes are smaller (~0.5–2 kDa) than the other fluorescent labeling tags (~30 kDa; **Scheme 4**). Owing to these features, there is a minimal chance that the UAA installment will perturb function, trafficking, localization of the protein of interest, or its interactions with partners and regulators. Furthermore, the organic

dyes used for UAA labeling are typically brighter and more stable than fluorescent proteins. This feature is important for labeling the low-abundance targets, live-cell, and SRM studies. Also, the diverse commercially available tetrazine dyes covering the visible spectrum can be used for different imaging applications (e.g., live-cell or SRM microscopy[152], dual-color labeling and imaging, or quantitative studies). Finally, since the organic dye is directly attached to the POI, the distance between the fluorophore and target (a linkage error) is reduced compared to the antibodies, nanobodies, and other labeling tags[204,205]. Small linkage error is crucial for SRM microscopy methods, where the bulky antibodies or larger fluorescent tags that place fluorophore further away from the target can introduce imaging artefacts[204,205].

d) Applications of genetic code expansion and click chemistry in neuroscience

A successful site-specific incorporation of non-clickable UAAs via GCE was achieved in mammalian cells, including primary neurons, for the first time about 15 years ago[163]. Since then, GCE technology has been used in neuroscience to some extent. Apart from the proof of principle GCE of GFP^{TAG} in primary neurons[163], neural stem cells[179], induced pluripotent cells, brain organoids[180], and mouse brains[173], the diverse UAAs were successfully incorporated into various neuronal proteins. These UAAs that bore diverse functional handles allowed studying inactivation, function, activity, gating properties, and the interactions between subunits of the neuronal ion channels and receptors *in vitro* (in mammalian cells and neurons) and *in vivo* (in mouse brain). Some examples are ion channels (e.g., K_V1.4, *Ciona intestinalis* voltage-sensitive phosphatase—CiVSP, potassium inwardly rectifying 2.1 channel—Kir2.1) and receptors (e.g., N-methyl-D-aspartate—NMDA and α-amino-3-hydroxy-5-methyl-4-isoxazolepropionic acid—AMPA)[163,175,179,206-208].

In recent years, the GCE-mediated site-specific incorporation of clickable UAAs was combined with bioorthogonal click chemistry to label neuronal proteins in living mammalian cells[97,98,152,153,209]. For example, NMDA receptors have been labeled with this approach and imaged with confocal and dSTORM super-resolution microscopy in standard and neuronal (NG108-15) cell lines[153]. This study demonstrated the superiority of click labeling over conventional immunostaining. Gamma-aminobutyric acid (GABA)-A and kainite Gluk2 receptors[152,209] and Shaker B K_V channels[210] are other examples of neuronal proteins that have been click labeled in mammalian cells. Likewise, click labeling has been used to study the amyloid precursor protein (APP) processing and biogenesis and localization of its product (amyloid β peptide) in cell lines[154,155].

Although bioorthogonal click chemistry was successfully used for site-specific labeling of neuronal proteins in mammalian cells[152-155,209], click labeling in living primary neurons has remained a challenge for a long time. Recently, click labeling in primary neurons has been established for small transmembrane synaptic regulatory proteins (TARPs; 30–40 kDa) and cytoskeletal element, a neurofilament light chain (NFL; 60 kDa)[97,98]. Both neuronal proteins were successfully imaged with confocal and SRM microscopy in primary neurons. Moreover, different populations of NFL were labeled during neuronal growth or injury with two tetrazine dyes[97]. Also, by combining CRISPR/Cas9 genome editing technology with bioorthogonal click chemistry, proof-of-principle click labeling of the endogenous NFL was achieved for the first time[97]. As I will describe below, the results of my thesis have expanded the application of click chemistry for efficient labeling of large, spatially confined AIS components, NF186 and Na_V (~186 kDa and ~260 kDa, respectively) in living primary neurons[75].

In addition to the abovementioned applications, the incorporation of clickable UAAs was combined with bioorthogonal click chemistry to label neuron-specific proteome *in vivo* and follow how it changes upon stimulation, during memory formation, and in pathological conditions[211-213].

e) Challenges associated with genetic code expansion and click labeling and strategies to improve it

A combination of genetic code expansion and bioorthogonal click chemistry has emerged as a powerful tool for live-cell protein labeling. However, certain limitations prevented this approach from being widely used, especially for microscopy studies in more complex model systems (e.g., neurons, slice cultures, brain organoids, or mouse brains)[160].

The main limitation of GCE is the low UAA incorporation efficiency in eukaryotic cells[160]. The UAA incorporation in eukaryotes was achieved by importing orthogonal translational machinery from other domains of life. Since the transcription in prokaryotes and eukaryotes differs considerably, the main obstacle to a successful UAA incorporation was the expression of the orthogonal tRNA. In prokaryotes, all RNA molecules are transcribed from the same polymerase (pol), and the promoter elements are located outside the coding regions[159,160]. There are three types of RNA polymerase in eukaryotes, transcribing different RNA molecules[214]. Mammalian tRNA is transcribed by pol III. The mammalian tRNA expression is driven by type 2 pol III promoter, which has intragenic promoter elements (A and B boxes)[214]. Type 3 pol III promoters that transcribe short RNAs are similar to prokaryotic ones—they do not require any intragenic elements and, presumably, have a well-defined transcription start site[159,160,163]. Hence, these

promoters have been utilized to express the orthogonal tRNA in mammalian cells[163,168]. For the efficient expression of orthogonal tRNA, it was necessary to use type 3 pol III promoters with strong transcription activity. The H1 was the first to be used for the UAA incorporation in mammalian cells and neurons[163]. In the meantime, U6, the best-characterized type 3 pol III promoter, became widely used for UAA incorporation in mammalian cells and, recently, neurons[97,98,168,170]. In a recent study, another type 3 pol III promoter 7SK was also used to express the orthogonal tRNA in brain organoids[180].

Despite the successful expression of orthogonal tRNA in eukaryotic cells, it is required to further increase the UAA incorporation efficiency[159]. To this end, several strategies have been used. One of the strategies aimed to increase the amount of orthogonal tRNA in the cytoplasm by delivering multiple tRNA copies to the cells (3–16 copies)[173-175,179-181]. This strategy resulted in a successful UAA incorporation in neural stem cells and mouse brains[173,175,179]. Multiple tRNA copies, along with amber mutant and aaRS, were delivered by transfection[151,175] or viral-based vectors[173,179]. The virus-based delivery of the GCE components will be described later in detail. An additional strategy, described previously[150], improved the GCE efficiency by increasing the amount of orthogonal tRNA in the cytoplasm was the addition of the strong nuclear export signal (NES) signal to the N terminus of PylRS^{AF}. Since the PylRS^{AF} contained nuclear localization signal (NLS), it accumulated in the nucleus with the orthogonal tRNA^{Pyl}. The addition of the NES redirected the localization of the orthogonal translational machinery back to the cytoplasm, resulting in an increased GCE yield[170]. An alternative way to increase the tRNA amount in the cytoplasm would also be to improve the effectiveness of tRNA transcription by finding more efficient type 3 pol III promoters[159]. Apart from U6, H1, and 7SK, the other promoters, such as mitochondrial RNA processing (MRP)/7-2[159] and Y3, could potentially be used for the expression of orthogonal tRNA.

In addition to the initiation, transcription termination is indispensable for efficient orthogonal tRNA expression. The PolyT sequence (cluster of four or more T residues) is recognized as a transcription termination signal by pol III in the absence of other factors, leading to the disassembly of the elongation complex[214,215]. That is why the polyT tail is typically added to the 3' end of the orthogonal tRNA to successfully express it in mammalian cells. Recently, it has been shown that the length of the polyT signal affects the termination efficiency of small noncoding (sn)RNA[216]. T4 is a minimal signal for transcription termination. However, efficient termination is achieved for polyT consisting of at least T6[216]. Furthermore, while the termination site is always within the polyT, it is variable and mostly ranges from T3–T5. A variable transcription termination

site leads to the production of the transcript with a variable PolyU tail that could reduce snRNA stability[216]. The same may occur with orthogonal tRNA. An alternative way of increasing the tRNA amount in the cytoplasm and, subsequently, GCE efficiency would be to improve the stability of the transcripts by eliminating PolyU tail variability, as previously reported for snRNA[216,217]. Likewise, the evolution of the orthogonal tRNA could improve its stability and UAA incorporation efficiency[218-220]. Alternatively, a tRNA scaffold could be engineered to make it more stable, or chimeric tRNAs could be designed[151,221].

Apart from inefficient orthogonal tRNA expression, another important reason for the low GCE efficiency in eukaryotic cells is the competition of the endogenous translation termination factors (eukaryotic release factor 1—eRF1) with orthogonal tRNA to bind the amber STOP codon[159,188]. Interaction of the eRF1 with the amber STOP codon can result in premature translation termination and production of the truncated POIs[159,188]. The suppression of the eRF1 by expressing engineered eRF1 mutant E55D ($eRF1^{E55D}$) has been utilized to improve the GCE efficiency in mammalian cells[222]. A similar strategy has recently been used to improve the expression of NFL^{TAG} amber mutant and reduce the amount of truncated NFL^{TAG} in primary neurons[97]. However, $eRF1^{E55D}$ can potentially affect the synthesis of endogenous proteins. Although the $eRF1^{E55D}$ effect on endogenous translation in neurons did not seem to be apparent, as reported in the previous study[97], its exact effect should be studied further.

An additional obstacle to the efficient UAA incorporation represents the eukaryotic nonsense-mediated decay (NMD) surveillance pathway that recognizes premature STOP codons and fast degrades mRNAs with such in-frame STOP codons[223]. Hence, the NMD can reduce the amount of the mRNA encoding amber mutant and, subsequently, the amount of POIs[159,188]. The UAA incorporation yield in yeast[178], *C. elegans*[182], and mice has been improved by suppressing the NMD mechanism[185].

The UAA incorporation efficiency and the ratio of the full-length vs. truncated protein also depend on the TAG position in the mRNA and its surrounding nucleotide sequence[224]. That is why it is essential to test different positions for the UAA incorporation. Furthermore, since the UAA incorporation efficiency depends on the nucleotide sequence in the proximity of the TAG mutation, GCE can potentially be improved by exchanging surrounding codons with synonymous ones[224].

Strategies to improve genetic code expansion and click labeling efficiency in neurons

In terms of the GCE and click labeling efficiency in terminally differentiated primary neurons, apart from the abovementioned problems, an additional challenge is low transfection efficiency[163]. The transfection efficiency in neurons is further reduced when multiple large genes have to be delivered[225], i.e., ones encoding the orthogonal translational machinery and amber mutants (e.g., *SCN8A*). Low GCE efficiency, in combination with low transfection efficiency, results in the poor expression of the amber mutants in very few neurons. Consequently, click labeling might be absent/pale or could not be used for quantitative studies due to a low number of labeled neurons expressing POI. To achieve a high yield of the GCE in neurons, it is necessary to find a way to efficiently deliver multiple large genes encoding orthogonal translational machinery and amber mutant.

Several different approaches have been utilized for the delivery of GCE components to neural stem cells and primary neurons[97,98,163,173,175,179,180,226,227]. The most common approach is transient transfection[97,98,163]. By optimizing transfection protocols, the GCE of neuronal proteins was achieved in cell lines[153] and primary neurons[175]. The same approach has recently been used for click labeling of synaptic proteins and cytoskeletal elements in living neurons[97,98]. However, besides the low efficiency of transient transfection in neurons, the copy number of individual components delivered via transfection cannot be regulated precisely[225]. The inability to precisely regulate copy number of individual GCE components can affect GCE efficiency since it is important that the orthogonal tRNA, which is a limiting component, is expressed at a higher level compared to aaRS[227].

As an alternative to transfection, cells that stably express orthogonal translational machinery have been generated. To this aim, PiggyBac transposase has been used to integrate orthogonal translational machinery into the genome of standard cell lines, embryonic stem, human induced pluripotent stem cells (hiPSCs), and brain organoids[180,228]. Although this approach is efficient, the disadvantage is that it cannot be used to deliver GCE components into non-dividing cultured primary neurons.

The viral-based vectors (lentivirus-, AAV-, and baculovirus-based vectors) with high transduction efficiency have also been used to deliver GCE to neural stem cells, primary neurons, organotypic slice cultures, or living mice[173,179,226,227]. The lentivirus-based vectors stably integrate into the genome. Hence, in addition to the abovementioned PiggyBAC transposase, they have

been used to generate neural stem cells that stably expressed orthogonal translational elements and that were subsequently differentiated into neurons[179]. The main limitation of this system is the instability of the lentiviral genome (single RNA strand), which can lead to the recombination between multiple tRNAs and subsequent loss of these transgenes[229]. Unlike the lentiviruses, the AAVs and baculoviruses do not integrate into the genome. Therefore, they can be used for the transient expression of GCE components. The AAV-based vectors are widely used to deliver the transgenes into neurons and brains of living animals[230]. There are reports on using an AAVs-based system to deliver the orthogonal translational machinery along with amber mutant to mouse brain[173]. Although AAVs have a high transduction rate, the main limitation of this system is their limited cargo capacity[231]. Baculoviruses are nontoxic, have large cargo capacity, and have a stable DNA-based genome that tolerates repetitive sequences[231,232]. Recombinant *Autographa californica* nuclear polyhedrosis virus (AcNPV) is used the most[231]. In addition to insect cells, this virus can infect mammalian cells without the ability to replicate in those cells[231]. The commercially available AcNPV-based systems (e.g., MultiPrime and MultiBacMam systems) were designed to allow the delivery of large and multiple genes (e.g., proteins involved in the GPCR signaling pathway) to difficult-to-transfect cells such as primary neurons and iPSCs[233]. Moreover, custom-made baculovirus-based vectors have been developed to deliver GCE elements to various mammalian cells, primary neurons, and mouse brains[226,227]. These custom baculovirus-based vectors allowed efficient UAA incorporation into GFP^{TAG} expressed in primary neurons[227]. Therefore, baculoviruses, especially commercial MultiBacMam system represent a promising way to achieve efficient GCE and click labeling in primary neurons.

2. Research aim

The main aim of my Ph.D. project was to develop a novel, efficient live-cell and SRM microscopy-compatible tool for labeling of WT and pathogenic AIS and the node of Ranvier components, $Na_V1.6$ and NF186, in living primary neurons. The UAA-based labeling tags are small, minimally invasive, and can be placed at virtually any position into target proteins. Therefore, I combined GCE technology with bioorthogonal click chemistry to introduce UAA into $Na_V1.6$ and NF186 and label them in living neurons.

Within the aim, I defined the following objectives:

- Identify appropriate intermediate host cell lines for the efficient GCE of the AIS and node of Ranvier components.
- Design and probe suitable, highly efficient plasmids for the GCE of the AIS and the node of Ranvier components in the intermediate host cell line and primary neurons.
- Establish the GCE and click labeling of $Na_V1.6$ and NF186 amber mutants in intermediate host cell lines and select the most suitable clickable amber mutants.
- Establish GCE and click labeling of the clickable $Na_V1.6$ and NF186 in living primary neurons.
- Establish live-cell imaging of click-labeled neurons expressing $Na_V1.6$ or NF186.
- Demonstrate the applicability of the click labeling for studies of the pathogenic $Na_V1.6$ variants.
- Improve the efficiency of the GCE and click labeling in neurons by establishing viral vectors to deliver the orthogonal translational machinery elements and amber mutants to primary neurons.
- Establish dSTORM super-resolution imaging in primary neurons immunolabeled with the antibodies against the AIS and the node of Ranvier components.
- Establish dSTORM super-resolution imaging of click-labeled primary neurons expressing $Na_V1.6$ and NF186.

3. Materials and Methods

3.1. Plasmids, cloning, and mutagenesis

$Na_V1.6$ plasmids

In the experiments involving voltage-gated sodium channel 1.6 isoform, I used the gene encoding 1978 amino acids-long mouse $Na_V1.6$ (*mSCN8A*; transcript variant 1, NCBI Reference Sequence: NM_001077499.2). The tetrodotoxin-sensitive (TTXs; *mSCN8A*) or TTX-resistant (TTXs; $mSCN8A^{Y371S}$) variants of the WT gene were synthesized by GenScript. To generate clickable variants of the $Na_V1.6$, the *mSCN8A* was modified by mutating Lysine (K) to TAG amber stop codon at the following positions: K1224TAG, K1425TAG, K1546TAG, or K1606TAG. Likewise, $mSCN8A^{Y371S}$ was modified by replacing Lysine (K), Arginine (R), or Alanine (A) with TAG amber stop codons at the following positions: R914TAG, K1425TAG, K1546TAG, A1601TAG, K1675TAG, K1731TAG. The genes encoding WT or TAG $Na_V1.6$ were cloned into a commercially available pcDNA3.1-P2A-EGFP vector. The *mSCN8A* was inserted upstream of the P2A-EGFP using EcoRI and Xbal restriction enzymes. The final plasmids contained *mSCN8A* under the control of the enhanced (e)CMV promoter followed by 22 amino acids-long P2A sequence and EGFP ($Na_V1.6$-P2A-EGFP). Importantly, in these plasmids, TAA was used as a stop codon. GenScript performed the TAG mutagenesis and clonings. I later modified these commercially generated plasmids by introducing alternative TTXr mutations (Y371C or S371C)[109,234] into $SCN8A^{WT/TAG}$ genes via polymerase chain reaction (PCR)-mediated site-directed mutagenesis (details are provided later in the text).

For the initial optimization of the $Na_V1.6$ genetic code expansion in cell lines, I used plasmids in which monomeric (m)GFP was fused to the C terminus of $Na_V1.6^{WT/TAG}$ ($Na_V1.6^{WT/TAG}$-mGFP). To generate these constructs, *mSCN8A* was PCR amplified from $Na_V1.6$-P2A-EGFP. Subsequently, *mSCN8A* was inserted into the mGFP-N1 plasmid (a gift from Michael Davidson, Addgene plasmid #54767; http://n2t.net/addgene:54767; RRID: Addgene_54767) by using HindIII and ApaI enzymes. As I also explained in the Result section, these plasmids were propagated in One Shot™ TOP10 Electrocompetent™ *E. coli* since I was still establishing protocols for NaV1.6 propagation in bacterial cells at the time.

For the GCE and click labeling $Na_V1.6$ in primary neurons, I used plasmids in which the *Human influenza* hemagglutinin (HA) tag was added to the C terminus of $Na_V1.6^{WT/TAG}$. The TTXs and TTXr (Y371C) versions of the $Na_V1.6^{WT/TAG}$-HA were generated by replacing P2A-EGFP with an HA tag (using XbaII and ApaI restriction enzymes) in the following plasmids:

$Na_V1.6^{WT}$-P2A-EGFP, $Na_V1.6^{WT, Y371C}$-P2A-EGFP, $Na_V1.6^{K1224TAG}$-P2A-EGFP, $Na_V1.6^{1425TAG}$-P2A-EGFP, $Na_V1.6^{K1425TAG, Y371C}$-P2A-EGFP, $Na_V1.6^{K1546TAGTAG}$-P2A-EGFP, $Na_V1.6^{K1546TAG, Y371C}$-P2A-EGFP, and $Na_V1.6^{K1675TAG, Y371C}$-P2A-EGFP. The HA tag was obtained from Sigma Aldrich in the form of two complementary single-stranded oligonucleotides that were annealed before ligation into the vector (**Appendix Table 1**).

The $Na_V1.6^{Y371C}$-HA constructs that bore pathogenic LOF mutations were generated by introducing I1652N or T1785P mutations[13] *into mSCN8A^{WT,Y371C}-HA, mSCN8A^{K1425TAG,Y371C}-HA*, and *mSCN8A^{K1546TAG,Y371C}-HA* genes via PCR-mediated site-directed mutagenesis (details are provided later in the text).

All mutations were introduced into *mSCN8A* genes using the Quick Change II XL site-directed mutagenesis kit, following previously published protocols[235] and manufacturer's recommendations (Agilent). In all experiments involving modifications or amplification of the $Na_V1.6$ plasmids, I used chemically competent XL 10-Gold Ultracompetent *E. coli*, except for the $Na_V1.6$-mGFP. The XL 10-Gold Ultracompetent *E. coli* were grown between 27–28°C at all propagation steps to prevent undesired changes in the *mSCN8A* genes[236]. As previously suggested[235,236], only small colonies were selected from the agar plates. After the isolation of plasmid DNA from bacterial cells, restriction digestion was performed, and the DNA patterns were analyzed on the agarose gel to check for rearrangements. Before the experiments were carried out in mammalian cells, *mSCN8A* open reading frames (ORFs) were fully sequenced to check if the additional undesired mutations were introduced.

In addition to the XL-10 Gold cells, I probed chemically competent MAX Efficiency Stbl2™ cells to propagate $Na_V1.6$ plasmids[236]. Alternatively, I grew One Shot™ TOP10 Electrocompetent™ *E. coli between* 27–28°C. However, all the constructs described in the thesis (except for the initial $Na_V1.6$-mGFP plasmids) were propagated in the XL 10-Gold Ultracompetent cells to avoid inconsistency between experiments.

β1 and β1 plasmids

Mouse (m)β1 and mβ2 plasmids were obtained from GenScript. The mβ1 (654 base par-long *mSCN1B*, Clone ID: OMu07915D ORF clone, accession no. NM:011322.2) and mβ2 (558 base pair-long *mSCN2B*, clone ID: Omu42415D ORF clone, accession no. XM:006510629.3 ORF sequence) ORFs were cloned by GenScript into commercially available pcDNA3.1+/C-(k)-DYK vectors. To generate stable neuronal cell lines, mβ1 and mβ2 were cloned into vectors provided with a PiggyBac Transposase kit using the NheI and NotI restriction

enzymes (the details are provided in The generation of stable cell subsection). To generate a multigene plasmid containing mβ1, mβ2, and mGFP, I used a MultiBacMam™ kit. To this end, mGFP was PCR amplified from commercially available mGFP-N1 plasmid (a gift from Michael Davidson, Addgene plasmid #54767; http://n2t.net/addgene:54767; RRID: Addgene_54767) and cloned using BamHI and Xbal into pMDC donor vector. The *mSCN1B* and *mSCN2B* were PCR amplified from the abovementioned plasmids obtained from GenScript. Using the NheI and NotI, mβ1 and mβ2 were cloned into the pACEMam2 acceptor and pMDS donor vector, respectively. Donor and acceptor vectors were provided with the MultiBacMam™ kit. These vectors contained locus of X over P1 (LoxP) sites that facilitated the generation of a multigene plasmid via Cre-Lox recombination. Following the manufacturer's recommendations, I combined genes of interest into the pACEMAM2-mβ1-mβ2-mGFP multigene construct. The amplification of pMDC and pMDS donor vectors was carried out in pirHC^{+} cells supplied with a MultiBacMam™ kit. All other plasmids were propagated in One Shot™ TOP10 Electrocompetent™ *E. coli*.

NF186 plasmids

In the experiments that involved NF186, I used a commercially available plasmid that contained rat *Nfasc* expressed from CMV promoter and fused to HA tag at its N terminus (HA-NF186^{WT}; a gift from Vann Bennett, Addgene plasmid # 31061; http://n2t.net/addgene:31061; RRID: Addgene_31061)[101]. I further modified this plasmid by introducing K534TAG or K680TAG amber mutations into the *Nfasc* by PCR-mediated site-directed mutagenesis (HA-NF186^{TAG}). Afterwards, I moved the HA tag from N to the C terminus of NF186. I used the Quick change II XL mutagenesis kit to remove nine amino acid-long HA from HA-NF186$^{WT/TAG}$, following the manufacturer's protocols. In the resulting plasmids, the HA tag was cloned to the C terminus of NF186. To this end, I used the ApaI restriction site in the ORF of *Nfasc* and the NotI restriction site at the end of the *Nfasc* to excise ~277 base pairs-long fragments from NF186$^{WT/TAG}$. The missing fragments were replaced with ones in which the HA tag was added by PCR amplification (CMV-NF186$^{WT/TAG}$-HA). Afterward, I generated additional NF186^{TA}-HA amber mutants (K519TAG, K571TAG, K604TAG, or K809TAG) by PCR-mediated site-directed mutagenesis of NF186^{WT}-HA. In order to lower the NF186-HA expression in primary neurons, the CMV promoter was replaced by weak human Neuron-Specific Enolase 2 promoter (hNSE). I PCR amplified latter from commercially available pGL3 NSE construct (a gift from Rosalyn Adam, Addgene plasmid # 11606; http://n2t.net/addgene:11606; RRID: Addgene_11606)[237], and subsequently cloned it into CMV-NF186$^{WT/TAG}$-HA using AseI and BglII restriction enzymes. In all molecular biology

experiments involving NF186, I used One Shot™ TOP10 Electrocompetent *E. coli* unless stated otherwise.

Plasmids containing genetic code expansion elements

For the genetic code expansion and click labeling in standard cell lines and primary neurons, I used a system consisting of Y306A/Y384F (AF) double mutant of the *Methanosarcina mazei*-derived orthogonal $tRNA^{Pyl}$ synthetase fused to a nuclear export signal (NES) and orthogonal $tRNA^{Pyl}$ (NES $PylRS^{AF}$/$tRNA^{Pyl}$ system). For the initial optimization of $Na_V1.6$ click labeling, I used the previously described codon non-optimized NES $PylRS^{AF}$/U6-$tRNA^{Pyl150}$ that was a gift from Prof. Dr. Edward Lemke (EMBL, Heidelberg, and IMB, Mainz). I generated additional plasmids that contained codon-optimized NES $PylRS^{AF}$ and its cognate suppressor $tRNA^{Pyl}$ expressed from various type 3 polymerase III promoters. The codon-optimized NES $PylRS^{AF}$ was synthesized by GenScript and cloned into the commercially available pcDNA3.1/Zeo(+) vector. In this plasmid, the NES $PylRS^{AF}$ was expressed from the CMV promoter (CMV-NES $PylRS^{AF}$). GenScript also synthesized U6-$tRNA^{Pyl}$ and U6-$tRNA^{Pyl}$-HDV (Hepatitis Delta Virus) cassettes. I cloned these cassettes upstream of CMV-NES $PylRS^{AF}$ in the reverse direction by using BgIII and MfeI restriction sites (NES $PylRS^{AF}$/U6-$tRNA^{Pyl97}$ and NES $PylRS^{AF}$/$tRNA^{Pyl}$-HDV). I also cloned a cassette containing four copies of improved $tRNA^{Pyl}$ (M15) expressed from U6 promoter (4xU6-$tRNA^{M15}$) upstream of CMV-NES $PylRS^{AF}$ in the reverse direction by using the same enzymes (NES $PylRS^{AF}$/4xU6-$tRNA^{M15}$)[97]. The 4xU6-$tRNA^{M15}$ was PCR amplified from pNEU-hMbPylRS-4xU6^{M15} plasmid (a gift from Irene Coin, Addgene plasmid #105830; http://n2t.net/addgene:105830; RRID:Addgene_105830)[151]. I designed Y3-$tRNA^{Pyl}$, Y3-$tRNA^{Pyl}$-HDV, MRP/7-2-$tRNA^{Pyl}$, MRP/7-2-$tRNA^{Pyl}$-HDV, 7SK-$tRNA^{Pyl}$, 7SK-$tRNA^{Pyl}$-HDV cassettes using sequences from the previously published literature[151,216,238-240]. These cassettes were synthesized and cloned upstream of CMV-NES $PylRS^{AF}$ (codon-optimized version) in the reverse direction by Eurofins Genomics [NES $PylRS^{AF}$/Y3-$tRNA^{Pyl}$(HDV), NES $PylRS^{AF}$/MRP/7-2-$tRNA^{Pyl}$(HDV), or NES $PylRS^{AF}$/7SK-$tRNA^{Pyl}$ (HDV)].

All the plasmids were propagated in One Shot™ TOP10 Electrocompetent *E. coli except for the* NES $PylRS^{AF}$/4xU6-$tRNA^{M15}$. This plasmid was propagated in chemically competent XL 10-Gold Ultracompetent *E. coli* grown between 27–30 °C to prevent the recombination between repetitive sequences. The 4xU6-$tRNA^{M15}$ was fully sequenced to confirm that no rearrangements had occurred between multiple tRNA copies.

The genes encoding codon non-optimized NES PylRS^{AF} and eRF1^{E55D} used for the AAV generation were gifts from Prof. Dr. Edward Lemke (EMBL, Heidelberg, and IMB, Mainz), and members of his laboratory generated them. U6-tRNA^{Pyl,} used for AAV production or transduction of HEK293T cells in combination with transfection, was also a gift from Prof. Dr. Edward Lemke. The 4xtRNA^{Pyl} used for AAV production was a gift from Jason Chin (MRC Laboratory of Molecular Biology, Cambridge, UK).

Plasmids containing fluorescent reporters

The NLS-mCherry-GFP^{Y39TAG} plasmid used for AAV generation and NLS-iRFP-GFP^{Y39TAG} plasmid used to probe type 3 pol III promoters in cell lines were gifts from Prof. Dr. Edward Lemke (EMBL, Heidelberg, and IMB, Mainz).

An iRFP-GFP^{Y39TAG} plasmid without an NLS signal was used for the experiments that involved transfections with type 3 pol III promoters tests in primary neurons. This plasmid was generated by removing the NLS sequence from NLS-iRFP-GFP^{Y39TAG} by PCR-mediated cloning using NotI and NheI restriction sites. The same plasmid was inserted in the bacmid (more details are provided in the following section).

MultiBacMam plasmids

For the baculovirus production, the genes encoding GCE elements and amber mutants were cloned into donor (pMDC) and acceptor (pACEMam1) vectors by PCR-mediated cloning. All the steps were carried out according to the manufacturer's instructions. The codon-optimized NES PylRS^{AF}/U6-tRNA^{Pyl} cassette was cloned into the pACEMam1 acceptor vector using PvuI and BstZ17I restriction sites. In contrast, the CMV-NF186^{K680TAG}-HA or iRFP-GFP^{Y39TAG} were cloned into pMDC donor vector using SalI and XbaI restriction enzymes. The donor vectors contained R6Kγ origin of replication that allowed the propagation of the donors only in the presence of *pir* gene. Therefore, the donor vectors had to be propagated in pirHC^{+} cells (Geneva biotech) provided with a MultiBacMam^{TM} kit. All acceptor plasmids were propagated in One Shot™ TOP10 Electrocompetent™ *E. coli*.

The genetic code expansion elements and amber mutants that had been cloned in donors and acceptors were combined into multigene expression plasmids (pACEMam1_NES PylRS^{AF}, U6-tRNA^{Pyl} and CMV-NF186^{K680TAG}-HA and pACEMam1_NES PylRS^{AF}, U6-tRNA^{Pyl} and iRFP-GFP^{Y39TAG}) via Cre-Lox recombination. Donors and acceptors contained genes for the resistance to specific antibiotics, allowing the selection of a multigene with the desired

combination of the genes on the agar plates. The additional selection step included the propagation of a multigene in pir$^-$ bacteria (One Shot™ TOP10 Electrocompetent™ *E. coli*).

In the final steps, the genes of interest (GOIs; NES PylRS^{AF}/U6-tRNA^{Pyl} and CMV-NF186^{K680TAG}-HA or NES PylRS^{AF} and U6-tRNA^{Pyl}_iRFP-GFP^{Y39TAG}) were inserted into bacmid following manufacturer's instructions. To this aim, a chemically competent *E. coli* carrying a single copy of the DH10EMBACVsV™ bacmid (supplied with a MultiBacMam™ kit) were transformed with multigene plasmids. A transposition acceptor site (mini-attTn7) in bacmid allowed the insertion of GOIs via Tn7 transposition. The bacmids with the inserted GOIs were identified on agar plates via blue-white selection. Blue colonies that indicated a successful transposition were amplified. Afterward, the bacmid was isolated, purified, and stored at -20 °C in isopropanol for baculovirus production. Storing bacmids in isopropanol was required to prevent their degradation.

All primers used for cloning and mutagenesis are provided in **Appendix Table 1.** The sequences of the genes, promoters, and different cassettes are also provided in Appendix.

3.2. Mammalian cells

Standard and neuronal cell lines

For the experiments described in this Ph.D. thesis, I used standard HEK293T and neuronal ND7/23 (mouse neuroblastoma x rat neuron hybrid; ECACC 92090903) and N1E-115-1 (mouse neuroblastoma; ECACC 08062511) cell lines. HEK293T cells were a gift from Prof. Dr. Edward Lemke (EMBL, Heidelberg, and IMB, Mainz), while neuronal cell lines were obtained from Sigma Aldrich. I also generated PiggyBac ND7/231$^{\beta1}$, ND7/231$^{\beta1\beta2}$, N1E-115-1$^{\beta1}$, and N1E-115-1$^{\beta1\beta2}$ stable cell lines, as will be described below.

Mammalian cell lines were grown in high-glucose Dulbecco's Modified Eagle Medium (DMEM) supplemented with 10% FBS and 1% penicillin-streptomycin (PS). HEK293T and ND7/23 culture mediums were also supplemented with 1% sodium pyruvate and 1% L-glutamine. For ND7/23 cell propagation, FBS was heat-inactivated at 56 °C for 30 min before it was used for medium preparation. The PiggyBac stable cells were grown in the presence of 3 µg/ml puromycin that was added to the medium after subculturing. Cell lines were kept in the incubator that was set at 37 °C and 5% CO_2. Cells were subcultured every 2–3 days and used from passages 3–15. HEK293T and N1E-115-1 cells were incubated with Trypsin-EDTA before splitting to help cell to detach from the bottom of the Petri dish.

Mammalian cells were seeded on six-well plates, four-well Lab-Tek II chambered cover glasses, or eight-well Lab-Tek II chambered cover glasses a day before the experiments were performed. The cells were seeded on six-well plates for patch clamp recordings and western blot expression analysis. For microscopy experiments, cells were seeded on Lab-Tek II chambered cover glasses that had been pre-coated with 10 µg/ml Poly-L-lysine (PLL) or Poly-D-lysine (PDL) solution in double-distilled water (ddH_2O). Dishes were incubated with PLL or PDL solution for at least 3 h at RT and washed 2–3 times with ddH_2O before cell seeding. The PLL was used for HEK293T cell lines, while PDL was used for neuronal cell lines.

Generation of stable cell lines

Stable cell lines ND7/231$^{\beta1}$, ND7/231$^{\beta1\beta2}$, N1E-115-1$^{\beta1}$, and N1E-115-1$^{\beta1\beta2}$ were generated using a commercially available PiggyBac Transposon system (BioCat). I first cloned *mSCN1B* or *mSCN2B* into PiggyBac-CMV-MCS-EF1-Puro cDNA/miRNA Cloning and Expression Vector (BioCat, Cat. no. PB510B-1-SBI) provided with a PiggyBac kit (PiggyBac-mβ1 or PiggyBac-mβ1β12). Next, I determined the appropriate concentration of the antibiotic for the selection of stable cell clones. To this aim, 200,000–250,000 neuronal ND7/23 or N1E-115-1 cells were seeded in a six-well plate. The following day different concentrations of puromycin (selection marker) were added (0–10 µg/ml). Puromycin was added in two wells of a six-well plate for each concentration. Cells were examined daily for cell toxicity and survival for a week. The medium was replaced every 2–3 days with the addition of a fresh puromycin. The optimal dose of the selection marker corresponded to the lowest concentration of the puromycin that killed all cells after a week of culturing. For ND7/23, the optimal dose of puromycin was 1.2 µg/ml (later increased to 3 µg/ml), while for N1E-115-1 cell line optimal dose was 3 µg/ml.

I seeded 200,000–250,000 cells in 6-well plates to generate stable cell lines. I transfected cells the following day using a JetPrime transfection reagent. To generate ND7/23$^{\beta1}$ stable cells, ND7/23 were transfected with 1.5 µg PiggyBac-mβ1 and 0.6 µg Super PiggyBac Transposase Expression Vector (BioCat, cat. no. PB210PA-1-SBI). For the Generation of ND7/23$^{\beta1\beta1}$ stable cells, ND7/23 cells were transfected with 0.75 µg PiggyBac-mβ1, 0.75 µg Super PiggyBac-mβ2, and 0.6 µg PiggyBac. For the Generation of N1E-115-1$^{\beta1}$ stable cells, N1E-115-1 cells were transfected with 1 µg of PiggyBac-mβ1 plasmid and 0.4 µg Super PiggyBac Transposase. For the Generation of N1E-115-1$^{\beta1\beta2}$ stable cells, N1E-115-1 cells were transfected with 0.5 µg of each PiggyBac-mβ plasmid and 0.4 µg Super PiggyBac Transposase. The DNA/JetPrime reagent ratio of 1 µg/0.5 µl was used for all the transfection. The transfection mix was replaced with a fresh culture medium after ~4 h. The selection was initiated the following day by adding the puromycin

(1.3 µg/ml for ND7/23 and 3 µg/ml for N1E-115-1). The puromycin concentration was later doubled for all stable cell lines to ensure that all untransfected cells were eliminated. Cells were incubated with a puromycin for 72 h. Afterward, cells were subcultured to p10 Petri dishes and propagated further. Since N1E-115-1 cells provided better expression of $Na_V1.6$, I subcultured those in p20 Petri dishes to isolate single clones. For each stable cell line and clone, sufficient amounts of cells were cryopreserved.

The final step in the generation of a stable cell line involved confirmation that *mSCN1B* and *mSCN2B* were stably incorporated into genomes of neuronal cell lines. To this aim, I isolated genomic (g)DNA from stable cell lines with the PureLink gDNA kit. Afterward, I amplified *mSCN1B* and *mSCN2B* genes from the gDNA using a polymerase chain reaction (PCR) and analyzed patterns on the agarose gel. The clones with the successfully incorporated *mSCN1B* and *mSCN2B* were used in the experiments, while the others were discarded.

Primers used for the generation of stable neuronal cell lines and isolation of the gDNA are provided in **Appendix Table 1**.

Primary neurons

In the experiments described in this thesis, I used Gibco primary cortical neurons isolated from Sprague Dawley embryonic day 18 rats (RCNs), Gibco primary cortical neurons isolated from embryonic day 17 C57BL/6 mice (MCNs), or hippocampal neurons isolated from embryonic day 18 C57BL/6NCrl mice (MHNs). Rat and mouse cortical neurons were obtained from Thermo Fisher Scientific, while mouse hippocampal neurons were prepared by the laboratory of Prof. Dr. Holger Lerche. Animal protocols for the mouse hippocampal neuron preparation were approved by the local Animal Care and Use Committee (Regierungspraesidium Tübingen, Tübingen, Germany). Details on the preparation of mouse hippocampal neurons have been published in[75]. Rat and mouse cortical neurons were thawed and maintained according to the manufacturer's instructions, as briefly described below.

Neurons obtained from Thermo Fisher Scientific were grown in the B-27™ Plus Neuronal Culture System. The medium was supplemented with 2% B27 Plus and 1% PS while the MHNs were grown in a Neurobasal culture medium. The Neurobasal medium was supplemented with B27, L-glutamine, and PS. The culture medium was replaced two times per week (usually every 3–5 days) by removing 200 µl of the old medium and adding 300 µl of the fresh, prewarmed medium.

For microscopy experiments, the neurons were seeded on eight-well or four-well Lab-Tek II chambered cover glasses that had been pre-coated with PDL solution in double-distilled water (ddH_2O). For RCNs and MCNs seeding, Lab-Tek II chambered cover glasses were incubated with 20 µg/ml PDL solution for 2 h at RT, washed three times with ddH_2O, and dried before neuron seeding. For MHNs seeding, Lab-Tek II chambered cover glasses were incubated with 0.1 mg/ml PDL solution, washed three times with ddH_2O, and dried before neuron seeding. After seeding, neurons were left in the incubator set at 37 °C and 5% CO_2. After 4–6 h, the culturing medium was replaced (for MCNs and RCNs, 250 µl of the medium was replaced with an equal amount of fresh prewarmed culturing medium).

Insect cell lines

Insect Gibco Sf21 cells in Sf-900™ III serum-free medium (SFM) cells were obtained from thermos Fisher and thawed according to the manufacturer's recommendation. Briefly, 1 ml of frozen Sf21 cells were placed drop by drop into 25 ml of the Sf-900™ III SFM complete 1x liquid medium. After three days, cells were counted and passaged if they reached a density of at least 2 million cells/ml and 90% viability. Cells were frozen at a density of 20 million cells in a 1 ml freezing medium. The freezing medium was prepared by adding 7.5% dimethyl sulfoxide (DMSO) to the mixture of fresh and conditioned culture medium (1:1 ratio).

Sf21 cells were propagated in Sf-900™ III SFM complete 1x liquid medium according to the manufacturer's instruction and instructions from Geneva Biotech. Briefly, cells were grown in suspension in sterile non-vented glass flasks that were replaced every 1–2 weeks. The suspension culture to flask volume was 1:5, which ensured proper aeration. The Sf21 suspension cultures were kept at 27–28°C (in a non-humidified, air-regulated, CO_2-free atmosphere) on the orbital shakers set at ~130 revolutions per minute (RPM). Cultures and mediums were protected from light. Cells were counted every second day and passaged when they reached a density between 2–4 million cells/ml with more than 90% viability. Cells were used for experiments from passage three and propagated for around two months.

3.3. Unnatural amino acids

For the experiments described in this Ph.D. thesis, I used the following UAAs: nonreactive N-ε-t-butyloxycarbonyl-L-lysine (BOC-Lys; Iris Biotech GMBH, cat. no. HAA1096) and reactive TCO*A-Lys (Sirius Fine Chemicals, SICHEM, cat. no. SC-8008), endo-BCN-Lys (SICHEM cat. no. SC-8014), or TCO4en/eq-Lys (a gift from Prof. Dr. Edward Lemke; can be obtained from SICHEM, cat. no. SC-8060). The 100 mM UAA stock solutions were prepared in

0.2 M NaOH/15% DMSO. For the experiments in mammalian cells and primary neurons, The UAAs stocks were diluted in 1 M HEPES buffered saline (1:4 ratio) to the final concentration of 250 µM (UAA/1 M HEPES ratio of 1:4). The diluted UAAs were added directly to the medium, or mixed with the medium and added to the cells.

3.4. Transfections

For experiments described in this thesis, I used the following transfection reagents: Cellfectin™ II and FuGene HD for the Sf21 cell line, JetPrime for neuronal cell lines, Lipofectamine 2000 and Lipofectamine 3000 for cell lines and primary neurons.

Transfections of mammalian cell lines

For the transfection of mammalian cell lines, cells were always seeded a day before transfection. JetPrime or Lipofectamine 3000 transfections were performed according to the manufacturer's recommendations. Lipofectamine 2000 transfection were performed according to previously published protocols[97,241,242]. I used a DNA/Lipofectamine 2000 reagent ratio of 1 µg/1.6 µl (**transfection protocol a**) or 1 µg/2.4 µl (**transfection protocol b**). The DNA DNA/Lipofectamine 3000 ratio was 1 µg/1.5 µl, while DNA/P3000 ratio was 1 µg/2 µl (**transfection protocol c**; I will refer to these protocols later in the text). The transfection mixes were prepared in Opti-MEM Reduced serum media unless stated otherwise. After adding the transfection mix, UAAs (TCO*A-Lys or BOC-Lys) were added to the medium. After approximately 6 h, the transfection mix was replaced with a fresh culture medium containing UAAs. In the control wells, neurons were transfected the same way as described above without adding the UAAs.

Click labeling and/or fixation and immunostainings were performed the day after transfection except for $Na_V1.6$, where cells were click labeled and/or fixed ~48 h after transfections. During and upon transfections, cells were incubated at 37 °C and 5% CO_2 unless stated otherwise.

Transfections with $Na_V1.6$ in neuronal cell lines

For pilot microscopy experiments involving transfections with $Na_V1.6$-mGFP plasmids **(**data shown in **Fig. 1)** or $Na_V1.6$-P2A-EGFP (data shown in **Fig. 2** and **3**), I used Lipofectamine 2000 (**transfection protocol a**). ND7/23$^{\beta1/\beta1\beta2}$ (25,000 cell/well) or N1E-115-1$^{\beta1/\beta1\beta2}$ (~19,000 cells/well) cells were seeded on eight-well Lab Tek II chambered cover glasses. Cells were transfected with the total DNA amount of 0.4 µg/well for single transfections or 0.8 µg/well (0.4 µg WT/TAG plasmid, 0.4 µg NES PylRS^{AF}/tRNA^{Pyl}) for double transfection. For

transfection in four-well Lab Tek II chambered cover glasses, the number of seeded cells, amounts of DNA, reagents, and mediums were doubled to correspond to the size of this dish. ND7/23 stable cells transfected with $Na_V1.6^{WT}$-mGFP were moved to 30 °C, 5% CO_2, after replacing the transfection mix with the culture medium[242]. Neuronal cells expressing $Na_V1.6^{WT}$-mGFP were fixed with 4% paraformaldehyde (PFA) in 0.1 M phosphate buffer (PB) for 15 min and analyzed afterward.

For experiments involving transfections with $Na_V1.6$-P2A-EGFP (data shown in **Fig. 4a**–**7**), Lipofectamine 3000 transfection reagent was used (**transfection protocol c**). ND7/23^{WT} (40,000 cells/well), N1E-115-1^{WT} (30,000 cells/well), or N1E-115-$1^{\beta1/\beta1\beta2}$ (30,000 cells/well) cells were seeded on four-well Lab Tek II chambered cover glasses. Cells were transfected with a total DNA amount of 1 µg/well (0.5 µg WT/TAG plasmid, 0.5 µg NES PylRS^{AF}/tRNA^{Pyl}) for double transfection and 0.5 µg/well for single transfection.

For experiments involving transfections with $Na_V1.6$-HA (data shown in **Fig. 17**), Lipofectamine 3000 (**transfection protocol c**) was used as well. However, for these experiments, ND7/23^{WT} cells were seeded at a density of 100,000 cells/well while N1E-115-1^{WT} cells were seeded at a density of 60,000 cells/well cells on four-well Lab Tek II chambered cover glass. Furthermore, cells were transfected with a total amount of 1.8 µg/well (0.8 µg WT/TAG plasmid, 0.8 µg NES PylRS^{AF}/tRNA^{Pyl} plasmid, 0.1 µg pACEMam2-mβ1 and 0.1 µg pMDC-mβ2 plasmids). Details on the transfections with $Na_V1.6$-HA were also published[75].

Other transfections in cell lines

For the experiments involving transfections with NF186, HEK293T (110,000 cells/well), ND7/23 (50,000 cells/well), N1E-115-1 (50,000 cells/well) were seeded on four-well Lab Tek II chambered cover glasses. Standard and neuronal cell lines were transfected with 0.5 µg HA-$NF186^{WT}$ using Lipofectamine 2000 (**transfection protocol b**) or Lipofectamine 3000 (**transfection protocol c**). Alternatively, for click labeling of NF186, ND7/23 cells were transfected with the total amount of 1 µg/well (0.5 µg WT/TAG plasmid and 0.5 µg NES PylRS^{AF}/tRNA^{Pyl} plasmid; **transfection protocol b**). This protocol was published [75].

For experiments involving testing of type 3 pol III promoters, HEK293T, ND7/23, or N1E-115-1 were seeded on eight well Lab Tek II chambered cover glasses. Cells were transfected the same way as was described for NF186-HA. The seeding cell numbers, amount of DNA, and reagents were scaled down to correspond to the size of an eight-well Lab Tek II chambered cover glasses (reduced to ½). Cells were incubated with nonreactive

BOC-Lys/1 M HEPES. The following day, cells were fixed in 4% PFA/PB for 15 min and imaged with widefield microscopy.

Transfection of primary neurons

Primary MCNs or RCNs (90,000–110,000 neurons/well) were seeded on eight-well Lab Tek II chambered cover glasses. Neurons were transfected with Lipofectamine 2000 following a previously published protocol[97,241]. The exception was the optimization of $Na_V1.6$ click labeling (data shown in **Fig. 21**), where Lipofectamine 3000, following the manufacturer's recommendations, was used. The transfection mix was replaced after ~6 h with a warm medium containing 250 µl conditioned medium, 250 µl fresh culture medium, and UAA/1 M HEPES.

For transfections with Lipofectamine 2000, a total DNA amount of 1 µg (0.5 µg WT/TAG plasmid and 0.5 µg NES $PylRS^{AF}/tRNA^{Pyl}$ plasmid) and the DNA/Lipofectamine 2000 reagent ratio of 1 µg/2.4 µl, were used for each well of the eight-well Lab Tek II chambered cover glasses. The DNA and Lipofectamine 2000 reagents were diluted in Neurobasal Plus (NB) medium containing 1% PS. After 20 min incubation, an equal amount of NB containing 4% B27 Plus and 1% PS was added to the transfection mix to obtain the final B27 Plus concentration of 2%. After 3–5 min incubation (37 °C, 5% CO_2), 200 µl of the transfection mix was added to each well of eight-well Lab Tek II chambered cover glasses.

For transfection with Lipofectamine 3000, I followed **transfection protocol c** described above. Neurons seeded on eight-well Lab Tek II chambered cover glasses were transfected with a total DNA amount of 0.5 µg/well (0.25 µg WT/TAG plasmid and 0.25 µg codon-optimized NES PylRS/tRNA). Before adding the transfection mix to neurons, 250 µl of the medium was removed from each well and stored (37 °C and 5% CO_2) for the medium change. Afterward, 25 µl of the transfection mix was added to each well containing 250 µl of the remaining medium.

For click labeling of NF186-HA, RCNs were transfected on DIV 7 except for dSTORM of click-labeled neurons, where neurons were transfected on DIV 8 or DIV 10. Neurons were incubated with TCO*A-Lys. Click labeling, fixation, and immunostaining were performed four days after the transfection. The exceptions are experiments involving dSTORM of click-labeled neurons where click labeling, fixation, and immunostaining were performed 4 or 6 days after the transfection.

For click labeling of $Na_V1.6$, RCNs were transfected on DIV 8. Neurons were incubated with TCO*A-Lys, endo-BCN-Lys, or TCO4en/eq-Lys. Click labeling was performed four days later

except for the dSTORM imaging experiments, where neurons were click labeled, fixed, and immunostained 4 or 6 days later.

For click labeling of LOF $Na_V1.6$-HA variants, MHNs (120,000) were seeded on four-well Lab Tek II chambered cover glasses and transfected on DIV 7–8 using Lipofectamine 2000 (37 °C, 5% CO). The MCNs were transfected the same way described above[97,241], except that the amounts of DNA, reagents, and mediums were doubled to correspond to the size of the four-well Lab Tek chambered cover glasses. Neurons were incubated with TCO*A-Lys. After four days, neurons were click labeled, fixed, and immunostained.

For experiments involving type 3 pol III promoters, MCNs were transfected on DIV 8 using Lipofectamine 2000 transfection reagent as described above[97,241]. Neurons were incubated with nonreactive BOC-Lys. After four days, neurons were fixed in 4% PFA/PB for 15 min and imaged with widefield microscopy.

Note that in the control wells, neurons were transfected without adding the UAAs.

Transfection of insect cells

To produce baculoviruses, I tested different transfection reagents—Cellfectin™ II and FuGene HD. Before transfection, bacmids stored at -20 °C in isopropanol were washed in 70% ethanol and dried under the cell culture hood for ~2–3 h, as previously described[243]. Afterwards, bacmids were resuspended in 30 µl (Cellfectin™ II transfection) or 20 µl (FuGene HD transfection) sterile ddH_2O prewarmed at 65 °C.

For the transfection with Cellfectin™ II, I followed previously published protocol[243] and the protocols provided by Prof. Dr. Edward Lemke's laboratory. Sf21 cells were split a day before transfection. The following day, the cells were seeded in a six-well plate at a density of 500,000 cells/ml or 300,000 cells/ml in 3 ml of Sf-900™ III SFM medium. Sf21 cells were seeded in 2 wells of the six-well plate for each baculovirus. Cells were left in the incubator at 27 °C (around 15 min) to settle down while preparing the transfection mix. Wells seeded with 500,000 cells/ml were transfected with 10 µl bacmid and 5 µl Cellfectin™ II transfection regent in 0.2 ml of Sf-900™ III SFM medium. Wells seeded with 300,000 cells/ml were transfected with 15 µl of the bacmid and 8 µl Cellfectin™ II transfection regent in 0.2 ml of Sf-900™ III SFM medium. Transfection mixes were incubated for 15–30 min at the RT before addition to the Sf21 cells. Transfected cells were sealed with parafilm and incubated for 5 h at 27 °C. Afterward, the transfection mix from each well was replaced with 3 ml of fresh Sf-900™ III SFM medium.

For the transfection with FuGene HD transfection reagent, Sf21 cells were seeded in a six-well plate at a density of 300,000 cells/ml in 3 ml of Sf-900™ III SFM medium and transfected on the same day. Sf21 cells were seeded in 2 wells of the six-well plate for each baculovirus. Cells were left in the incubator at 27 °C (around 15 min) to settle down while preparing the transfection mix. Sf21 cells were transfected with 15 µl bacmid and 5 µl FuGene HD transfection reagent in 200 µl Sf-900™ III SFM medium. The transfection mix was incubated at RT for 15 min before addition to the cells. Transfected cells were sealed with parafilm and incubated at 27 °C.

The cells were observed daily for the mCherry signal (a transfection marker). After ~48–60 h, V0 viral stocks were harvested, filtered with 0.2 µm filters to get rid of the cell debris, and stored at +4°C, protected from the light.

3.5. Viruses

Baculovirus production

For the baculovirus production, I followed previously published protocol[243] and the protocols provided by Prof. Dr. Edward Lemke's laboratory and Geneva Biotech. I generated the V1 and V2 generations to provide larger amounts of the baculovirus. For V1 production, Sf21 cells were subcultured at a density of 0.9–1 million cells/ml in 50 ml of Sf-900™ III SFM medium (in 0.5 l flasks). After cells reached more than 2 million cells/ml, they were subcultured to 0.9–1 million cells/ml and transduced with 3–6 ml V0. Transduced Sf21 cells were counted and subcultured daily at a density below 1 million cells/ml until proliferation was arrested. Afterward, cells were incubated for ~48–60 h before the V1 stocks were harvested (cells should become large and swollen, and the cultures should turn pink as the virus amplifies). V1 stocks were spun down (500 g, 10 min) to remove Sf21 cells. The supernatants were filtered and stored at +4 °C, protected from light. Depending on the experiment, smaller amounts of V1 can be produced (e.g., 25 ml Sf21 cells can be infected with 3 ml of V0). The proliferation should be arrested after a minimum of 3 days upon transduction to a maximum of 9 days. For V2 production, Sf21 cells were split at the density of 500,000 cells/ml in 100 ml of Sf-900™ III SFM medium (in 2 l flasks). After two days (when cell density reached more than 2 million cells/ml), the medium amount was doubled (200 ml). If necessary, the cell stocks can be doubled again (400 ml). The ~4–8 ml of V1 was added to each flask. Transduced insect cells were incubated at 27 °C with shaking (130 RPM) and protected from light. The subsequent steps were the same as described for V1.

Filtered unconcentrated V2 stocks were used for the transduction of mammalian cell lines. Alternatively, before the transduction of mammalian cells, the V2 stocks were concentrated by ultracentrifugation or Amicon® Ultra-15 centrifugal filter units (100 kDa MWCO, 15 ml sample

volume)[244]. I tested two protocols for V2 ultracentrifugation. I concentrated viral stocks in a 25% sucrose cushion[233] by loading V2 into 36 ml PA thin-walled ultracentrifugation tubes with the 3 ml of 25% sucrose/5 mM NaCl/10 mM EDTA. The tubes with V2 were centrifuged at 75,000 g at 4°C for 75 min. Alternatively, 33 ml of V2 stocks were loaded into 36 ml PA thin-walled ultracentrifugation tubes and centrifuged at 39,000 g for 1 h[227]. After the centrifugation, pellets were collected, diluted in sterile 0.01 M phosphate-buffered saline (DPBS), and stored at +4°C. I followed the manufacturer's instructions to concentrate V2 using an Amicon centrifugal concentrator (50 ml of V2 was concentrated in one round of centrifugation by pouring V2 into multiple Amicon units). Titers of the V2 stocks were determined using a BacPAK^{TM} baculovirus rapid titer kit following the manufacturer's instructions.

AAVs

I used the following AAV9A2 in this thesis: CMV-NES PylRS^{AF} (AAV#1), 4xU6-tRNA^{Pyl} (AAV#2), CMV-eRF1^{E55D} (AAV#3), minimal (m)CMV-NES PylRS^{AF} and U6-tRNA^{Pyl} (AAV#4), mCMV-eRF1^{E55D} and U6-tRNA^{Pyl} (AAV#5), CMV-NLS-mCherry-GFP^{Y39TAG} (AAV#6; **Fig. 31a**). In addition, I tested AAV9A2 carrying mCMV-NLS-mCherry-GFP^{Y39TAG}, and AAV7A2 carrying NLS-mCherry-GFP^{Y39TAG} expressed from either CMV or mCMV promoter. The AAVs were generated by Ning Meng, a Ph.D. student in the laboratory of Prof. Dr. Dirk Grimm (Virology, Medical Faculty, University of Heidelberg, Cluster of Excellence CellNetworks, BioQuant, German Center for Infection Research and German Centre for Cardiovascular Research, Heidelberg, Germany). The AAVs production details have been published previously[75].

3.6. Transduction with baculoviruses

Before carrying out experiments in mammalian cells, I checked the functionality of baculoviruses by following protocols from Geneva Biotech. To this end, I split Sf21 cells at a density of 1 million cells/ml. I seeded 150,000 cells/well from the freshly split culture in 1 ml Sf-900 III SFM medium (12-well plates were used for seeding). After the cells settled down, I transduced them with different amounts of the viral stocks by directly adding V1 or V2 to the wells (0 µl, 2 µl, 4 µl, 6 µl, 12.5 µl, 25 µl, 50 µl, 100 µl, 200 µl, 300 µl, or 500 µl). Plates were wrapped by parafilm and incubated at 27°C. A day after the transduction, I estimated mCherry fluorescence and cell morphology under an epifluorescent microscope. Afterward, I fixed cells with 4% PFA/PB and imaged them with widefield microscopy.

To optimize the transduction of mammalian cells, I tested different protocols (**transduction protocol a–c**), as described below, by following Geneva Biotech's recommendations.

HEK293T and ND7/23 cells were seeded a day before transduction on four-well Lab-Tek II chambered cover glasses. Before the transduction, cells were washed in the Opti-MEM Reduced serum media (~1–1.5 h) to remove FBS that could have affected the binding of the virus. Afterward, cells were rinsed 2–3x in phosphate-buffered saline (PBS; 137 mM NaCl, 10 mM Na_2HPO_4, 1.8 mM KH_2PO_4, 2.7 mM KCl, pH 7.4). Following washing, transduction was performed. If the transfection and transduction were combined, cells were transfected cells after washing and transduced afterwards. The cells were washed twice in PBS between transfection and transduction. Cells were incubated with V2 at 37 °C or RT. After ~4–4.5 h, the V2 was replaced with a prewarmed culture medium with 3 mM sodium butyrate/ddH_2O. The BOC-Lys diluted in 1 M HEPES was added with a culture medium (**transduction protocol b–c**) or the following day (**transduction protocol a**). Cells were fixed with 4% PFA/PB for 15 min and analyzed with widefield microscopy.

Transduction protocol a *(data shown in* ***Fig. 27****):*

HEK293T cells were seeded at the following densities: 100,000, 80,000, and 60,000 cells/well. ND7/23 cells were seeded at the following densities: 60,000, 40,000, and 30,000 cells/well. The different seeding numbers allowed to follow cells for 24–72 h. Transduction was carried out by adding the V2 stock directly to the well (300 µl, 600 µl, or 1000 µl). Cells were incubated with V2 at 37 °C or RT (with shaking). Cells were fixed after 24 h (110,000 HEK293T and 60,000 ND7/23 cells/well), 48 h (80,000 HEK293T and 40,000 ND7/23 cells/well) or 72 h (60,000 HEK293T and 30,000 ND7/23 cells/well).

Transduction protocol b *(data shown in* ***Fig. 28****):*

HEK293T cells were seeded at a density of ~90,000–100,000 cells/well. Cells were transfected with orthogonal translational elements and transduced with V2 afterwards. Alternatively, cells were transduced with V2 without transfection. Transfections were carried out using Lipofectamine 2000 with a DNA amount of 0.5 µg/well (U6-tRNA^{Pyl} or codon-optimized NES PylRS^{AF}) as described for the **transfection protocol b**. The V2 stock was added directly to the well (600 µl or 1000 µl) for the transduction. Alternatively, 100 µl Amicon-concentrated V2 was mixed with 400 µl DPBS, added to the cells, and incubated for ~2 h at 37 °C. Cells were fixed 48 h after the transduction.

Transduction protocol c *(data shown in* ***Fig. 29*** *and* ***30****):*

HEK293T cells were seeded at a density of ~90,000–1000,000 cells/well. Cells were either transfected with orthogonal translational elements and transduced with (ultra)concentrated V2 or only transduced with (ultra)concentrated V2. Transfections were carried out with a 0.5 µg/well U6-tRNA^{Pyl} described in the **transfection protocol b**. Cells were transduced by adding the concentrated V2 stock directly to the well (10 µl, 30 µl, 60 µl, and 120 µl of the V2 was mixed with DPBS to the final volume of 300 µl). Cells were fixed 48 h after the transduction.

3.7. Transduction with AAVs

For the experiments involving transduction with the AAVs, neurons were seeded at a density of 100,000–110,000 on eight-well Lab Tek II chambered cover glasses.

To determine the best AAV serotype and the best promoter, I transduced neurons on DIV 5 or DIV 8. I probed AAV9A2 or AAV7A2 carrying NLS-mCherry-GFP^{Y39TAG} expressed from CMV or mCMV. AAVs were added at a multiplicity of infection (MOI) of 50,000 and analyzed on DIV 12. For the experiments involving the GCE, I transduced RCNs on DIV 8 with different combinations of the AAV9A2 (**Fig. 31a** and **b**). Each AAV was added at MOI of 15,000 together with TCO*A-Lys/1 M HEPES. Neurons were fixed in 4%PFA/PEM 3 days after the transduction and imaged with widefield microscopy.

The RCNs were transfected on DIV 8, except for dSTORM of click-labeled Na$_V$1.6, where neurons were transfected on DIV 8 or 10. RCNs were transfected with Lipofectamine 2000 following a previously published protocol[97,241] with a total DNA of 0.5 µg/well. After ~6 h transfection mix was replaced with a culture medium containing TCO*A-Lys and different combinations of the AAV9A2 (as described in the Results section, data are shown in **Fig. 32**, **33, 44,** and **45**). Each AAV was added at an MOI of 15,000 (Na$_V$1.6) or 10,000 (NF186). Neurons were click labeled, fixed, and immunostained after three (widefield and confocal) or four days (for dSTORM).

Detailed protocol on the transduction was published previously[75].

3.8. Western blot expression analysis

For western blot analysis of CMV-NF186-HA expression, 250,000 ND7/23 cells/ well were seeded into six-well plates a day before transfection. Cells were transfected with a total DNA amount of 5 µg per well (2.5 µg WT/TAG plasmid and 2.5 µg codon-optimized NES PylRS^{AF}/tRNA^{Pyl} plasmid) **following transfection protocol 2** described in the Transfection

section. The following day, ND7/23 cells were collected from six-well plates and lysed in cold RIPA buffer (pH 8): 12.5 mM Trizma hydrochloride, 37 mM sodium chloride, 3 mM sodium deoxycholate containing 1:50 protease inhibitor cocktail (PIC), 1 mM phenylmethanesulfonyl fluoride and 50 mM sodium fluoride. Lysis was performed by incubation on ice for 30 min, followed by centrifugation (15 min, 18,000 g). After centrifugation, supernatants were collected, and the total protein concentration of the lysates was measured by Bradford assay.

For Sodium dodecyl-sulfate polyacrylamide gel electrophoresis (SDS-PAGE), proteins were prepared in 4x Leammlie buffer containing βME and denatured by incubation at 95 °C for 5 min. The equal amounts of protein (10 µg per well) were separated by molecular weight on NuPAGE™ 4-12% Bis-Tris Protein Gels together with 5 µl of Precision Plus Protein™ WesternC™. Electrophoresis was performed in 1xNuPAGE™ MOPS SDS running buffer for 40 min at 200 V. The proteins were transferred onto 0.2 µm nitrocellulose membrane by semi-dry transfer using a Trans-Blot® Turbo™ Transfer System for 7 min at 25 V and 1.3 A. Total proteins were visualized by staining in Ponceau S solution [0.1% (w/v) Ponceau S in 5% (v/v) acetic acid]. The membrane was washed 3x10 min in ddH_2O. The membrane was blocked in 10% (w/v) skim milk in Tris-buffered saline (TBS) buffer (20 mM Tris, 150 mM NaCl, pH 7.6) containing 0.05% Tween 20 (TBST) for 1 h. The membrane was cut in half and incubated with rabbit anti-HA tag (SG77) polyclonal antibody (Thermo Fisher Scientific, cat. no. 71-5500) or mouse anti-β3-tubulin primary antibody ON at 4°C. The incubation with goat-anti-rabbit (Thermo Fisher Scientific, cat. no. A16104) and anti-mouse horseradish peroxidase (HRP; Thermo Fisher Scientific, cat. no. A16072) was carried out for 2 h at RT. Primary and secondary antibodies were diluted in 3% BSA/TBST**.** Membranes were washed 3x 10 min in TBST after incubation with primary and secondary antibodies and incubated with the Clarity Western ECL substrate for 5 min. Afterwards, the chemiluminescence was visualized using an Azure 600 imager (Azure Biosystems). Western blot images for the figure were prepared in ImageJ/Fiji software[245].

3.9. Click labeling

For the experiments described in this Ph.D. thesis, I used the following tetrazine dyes: Cy5-tz (Jena Bioscience), AF647-tz (a gift from Prof. Dr. Edward Lemke), ATTO488-tz (Jena Bioscience, cat. no. CLK-010-02), and AF647-Pyr-tz (Jena Bioscience, cat. no. CLK-102). The dye stock solutions were prepared in DMSO at the following concentrations: 500 µM (Cy5-tz), 500 µM (AF647-tz and ATTO488-tz), and 1250 µM (AF647-Pyr-tz). The stock solutions were diluted in a warm culture medium and added to the cells. Click labeling was performed at 37 °C degrees for 10 minutes unless stated otherwise.

Neuronal cells were washed briefly in PBS and fixed in 4% PFA/PB for 15 min at RT unless otherwise stated. Primary neurons were fixed in the same way except that 4% electron-microscopy-grade PFA diluted in a cytoskeleton-preserving buffer (PEM; 80 mM PIPES, 5 mM EGTA, 2 mM $MgCl_2$; pH 6.8) was used. After fixation, cells were washed 3x5 min in PBS. For live imaging, after click labeling, the neurons were placed in a warm Hibernate E medium supplemented with 2% B27 Plus and 1% PS.

For experiments involving NF186, ND7/23 cells were click labeled and fixed one day after transfections. For the experiments involving $Na_V1.6$, ND7/23 or N1E-115-1 cell lines were click labeled and fixed two days after the transfection. In initial click labeling experiments (data shown in **Fig. 2–4**), $Na_V1.6$-P2A-EGFP expressing cells were washed in a fresh warm culture medium without UAAs for 2 h at 37 °C, 5% CO_2. Afterwards, cells were labeled with 1.5–3 µM AF647-tz or Cy5-tz on ice or at 37 °C and washed in a warm culturing medium. In some instances, the cells were washed after click labeling for ~1 h. In experiments where I sought the cause of the click labeling-like single, I tested various conditions: 2 h vs. no washing before click labeling and washing vs.no washing after click labeling. I compared click labeling on the ice vs. 37 °C with 1.5 µM AF647-tz or Cy5-tz. Final protocols for click labeling in cells excluded washing steps before or after the labeling. For click labeling of NF186-HA and $Na_V1.6$-HA in neuronal, I used ATTO488-tz (1.5 µM and 3 µM, respectively)[75].

Click labeling of primary neurons was performed 4 days after the transfection, except for experiments involving AAVs or dSTORM. In the experiments involving AAVs, neurons were click labeled 3 or 4 days after the transfection, while in the experiments involving dSTORM, neurons were click labeled 4 or 6 days after the transfection. Usually, I removed UAAs a day before click labeling. The exceptions were the experiments involving click labeling of test $Na_V1.6^{K1546TAG}$-mGFP plasmid where TCO*A-Lys was removed 2 h before click labeling. Neurons were labeled with 5 µM ATTO488-tz, 5 µM AF647-tz or 12.5 µM AF647-Pyr-tz at 37 °C. The exception was $Na_V1.6$-mGFP, labeled for 10 min on ice. For click labeling of $Na_V1.6$-HA constructs, I introduced additional washing and blocking steps. These steps included washing in warm Tyrode's solution (100 mM NaCl, 5 mM KCl, 5 mM $MgCl_2$, 2 mM $CaCl_2$, 15 mM D-glucose, 10 mM HEPES; pH 7.4, osmolarity 243–247 mOsm), 3 times before labeling, and subsequent blocking for 3 min at 37 °C in 1% BSA/Tyrode's solution, as described in[98]. Before live imaging or fixation, neurons were washed 4 times

3.10. Immunostaining

Table 2. *Protocols for immunostaining of the recombinant NF186 and $Na_V1.6$ in cell lines. The Materials and Methods section provides the product numbers of the primary (‘) and secondary (‘‘) antibodies (ab). The protocols for NF186 and $Na_V1.6$ immunostaining were previously published[75].*

	NF186	**$Na_V1.6$-HA**
Permeabilization	30 min, 0.2% Tween 20/PBS*	10 min, 0.1% Triton X-100/PBS
Blocking	5% FBS/PBS, 1 h at RT	10% goat serum /3% BSA/PBS, 1 h at RT
‘ab solution	5% FBS/PBS	10% goat serum /3% BSA/PBS
‘ab	Mouse anti-HA (1:1000), ON at +4 °C	Rabbit anti-HA (1:1000), ON at +4 °C
‘‘ab solution	5% FBS/PBS	3%BSA/PBS
‘‘ab	Goat anti-mouse AF(+)647 (1:500), 1h at RT	Goat anti-rabbit AF555 (1:500), 1 h at RT

**For HA-NF186 immunostaining, a permeabilization step was not necessary.*

Upon fixation, cells or neurons were washed 3x5 min in PBS. Afterwards, cells were blocked for 1 h at the RT unless stated otherwise. In some instances, cells were permeabilized, or the autofluorescence was quenched (**Table 2–4**). Cells were incubated with primary antibodies ON at +4 °C, while the incubation with secondary antibodies was carried out for 1 h at the RT. Before and after incubation with secondary antibodies, cells or neurons were washed 3x5 min in PBS. Cells were fixed in 4% PFA diluted in PB or PEM buffer unless stated otherwise.

The following primary antibodies were used for the immunostainings: mouse anti-HA tag (Thermo Fisher Scientific, cat. no. 26183), rabbit anti-HA tag (C29F4) monoclonal antibody (Cell Signaling, cat. no. 3724), rabbit anti-panNF (Abcam, cat.no. ab31457), mouse anti panNa_V (Sigma Aldrich, cat. no. S8809), mouse $Na_V1.6$ Na^+ channel (Neuromab, cat. no. 75-026), mouse anti-ankG antibody (Santa Cruz, cat. no. 12719), mouse anti-β3-tubulin antibody (BioLegend, cat. no. 801202).

The following secondary antibodies were used for the immunostainings: goat anti-rabbit AF555 (Thermo Fisher Scientific, cat. no. A21429), goat anti-rabbit AF(+)647 Plus (Thermo Fisher Scientific, cat. no. A32733), goat anti-mouse AF(+)647 Plus (Thermo Fisher Scientific, cat. no. A32728), goat-anti-mouse AF647 (Thermo Fisher Scientific, cat. no. A21236), goat anti-mouse

AF633 (Thermo Fisher Scientific, cat. no. A-21052). The secondary antibodies were diluted at 1:500 in all experiments.

Dilutions of the primary antibodies and detailed protocols for immunostainings are provided in **Table 2–4**.

Table 3. *Protocols for immunostaining of the recombinant NF186 and $Na_V1.6$ in primary neurons that were imaged with conventional or dSTORM microscopy. The Materials and Methods section provides the product numbers of the primary (') and secondary ('') antibodies (ab). The protocols for NF186 and $Na_V1.6$ immunostaining were previously published[75].*

	NF186-HA (conventional microscopy)	**$Na_V1.6$-HA (conventional microscopy)**	**$Na_V1.6$-HA (dSTORM microscopy)**
Permeabilization	/	10 min, 0.1% Triton X-100/PBS	
Blocking	0.2% Triton X-100/10% goat serum/3% BSA/PBS, 1 h at RT	10% goat serum /3% BSA/PBS, 1 h at RT	
'ab solution	Blocking solution	Blocking solution	
'ab	Rabbit anti-HA (1:2000) Mouse anti-ankG (1:50), ON at +4 °C	Rabbit anti-HA (1:1000) Mouse anti-ankG (1:50)* ON at +4 °C	Rabbit anti-HA (1:250), ON at +4 °C
''ab solution	3%BSA/PBS		
''ab	Goat anti-rabbit AF555** Goat anti-mouse AF633 (1:500), 1 h at RT	Goat anti-rabbit AF555 Goat-anti-mouse AF633* (1:500), 1 h at RT	Goat anti-rabbit AF555 or goat anti-rabbit AF(+)647** (1:500), 1 h at RT

**For quantification of the AIS length of the neurons expressing $Na_V1.6$-HA, RCNs were co-immunostained (in addition to anti-HA primary and AF555 secondary antibodies) with anti-ankG primary and anti-AF633 secondary antibodies. In all other experiments, ankG antibody was not used. **For dSTORM of click labeled neurons, AF555 secondary antibody was used, while for dSTORM of immunostained neurons, AF (+)647 antibody was used.*

Table 4. *List of permeabilization solutions, blocking solutions, and antibodies used for immunostaining of the untransfected primary neurons that were imaged with dSTORM microscopy. The Materials and Methods section provides the product numbers of the primary (‘) and secondary (‘‘) antibodies (ab) and more details on the immunostaining protocols. The detailed protocols for panNa$_V$ immunostaining were previously published[246].*

	dSTORM of the AIS in untransfected neurons		
Quenching	0.1% sodium borohydride/PBS, 7min at RT (optional)		
Washing	3x10 min in PBS (after quenching step) at RT		
Blocking	0.2% Triton X-100/10% goat serum/3 %BSA/PBS, 1h at RT		
‘ ab solution	0.1% Triton X-100/5% goat serum/3 %BSA/PBS		
‘ ab	Rabbit anti-panNF (1:50), ON at +4 °C	Mouse anti-panNa$_V$* (1:50), ON at +4 °C	Mouse anti-Na$_V$1.6 (1:100), ON at +4 °C
‘‘ ab solution	5% goat serum/0.1% Triton X-100/PBS		
‘‘ ab	Goat-anti rabbit AF(+)647 (1:500),1 h at RT	Goat-anti mouse AF(+)647 or goat-anti mouse AF647** (1:500), 1 h at RT	Goat-anti mouse AF(+)647 (1:500), 1 h at RT

**The same immunostaining protocol was used for the optimization of dSTORM imaging of the AIS and the experiments involving the investigation of Vecatshield-induced fluorescence quenching. **In addition to AF(+)647, for imaging of panNa$_V$ in VS and 25% VS, the AF647 secondary antibody was used.*

3.11. Microscopy and image processing

For confocal imaging, I used LSM 710 confocal scanning microscope (Carl Zeiss, Oberkochen, Germany) controlled by ZEN Software (Carl Zeiss, Oberkochen, Germany). Fixed-cell confocal imaging was performed in PBS, while live-cell confocal imaging was performed in Hibernate E supplemented with 2% B27 and 1% PS. For widefield and 3D dSTORM imaging, I used Inverted Nikon Eclipse Ti2-E (Nikon instruments) controlled by NIS-Elements AR software (Nikon Instruments). WF imaging was performed in PBS, Vectashield (VS), or 25% VS. The 3D dSTORM imaging was performed in Glox βME, 100% VS, or 25% VS. The 25% VS and GLOX βME imaging buffers were prepared according to previously published protocols[135,136,246]. The 25% VS was prepared by mixing 100% VS with Tris-Glycerol (5% v/v glycerol and 1 M Tris,

pH 8). The GLOX solution was prepared by adding 14 mg glucose oxidase and 50 µl catalase to Buffer A (10 mM Tris, pH 8, 50 mM NaCl). GLOX βME imaging buffer was prepared before the imaging by adding 7 µl GLOX solution and 7 µl βME to 690 µl Buffer B (50 mM Tris, pH 8, 10 mM NaCl) that contained 20% w/v glucose.

Microscope setup and image acquisition

For confocal imaging, I used a Plan-Apochromat 63× objective (NA 1.4, oil). A temperature module and a heating insert (PeCon, Erbach Germany) set at 37 °C were used for live-cell confocal imaging. A fluorescent lamp was used to identify neurons that were click-labeled with ATTO488-tz (live-cell imaging) or immunolabeled with anti-HA primary and AF555 secondary antibodies (fixed-cell labeling), and ND7/23 cells click-labeled with ATTO488-tz. The fluorophores (ATTO488-tz, AF555, AF(+)647, and AF633) were excited with 488, 561, and 633 laser lines, respectively. Images were taken in one (ATTO488-tz; live-cell imaging), two (ATTO488-tz and AF(+)647 or AF555; fixed-cell imaging), or three channels (ATTO488-tz, AF555, and AF633; fixed-cell imaging). Two- or three-color images were taken sequentially. I took single planes (ND7/23 cells and primary neurons) or z-stacks (primary neurons; 0.42 µm step size). All images were acquired as 16-bit with 2x line averaging, frame size of 1024x1024 pixels, pixel dwell time of 6.30 µs, and pixel size of 0.132 µm. During acquisition, the pinhole was set at 1 Airy Unit.

For widefield and dSTORM imaging, the inverted Nikon microscope with a built-in N-STORM module, XY motorized stage, a Perfect Focus System, ORCA-Flash 4.0 sCMOS camera (Hamamatsu Photonics), fluorescent lamp (Lumencor Sola SE II), various filter cubes, and laser lines (see below) was used. For widefield imaging, I used Apo 60x (NA 1.4, oil) and HP Apo TIRF 100×H (NA 1.49, oil) objectives. A fluorescent lamp was used to excite fluorophores (AF488, ATTO488-tz, AF555, AF647, AF(+)647, AF647-tz, AF647-Pyr-tz, Cy5-tz) or fluorescent proteins (mCherry, iRFP, mGFP, EGFP). The light was filtered through 488 (AHF; EX 482/18; DM R488; BA 525/45), 561 (AHF; EX 561/14; DM R561; BA 609/54), and 647 (AHF; EX 628/40; DM660; BA 692/40) filter cubes.

The 3D dSTORM imaging was performed on the N-STORM module of the inverted Nikon microscope. For 3D dSTORM imaging, I used HP Apo TIRF 100xH (NA 1.49, oil) objective. The 405 and 647 laser lines (LU-NV Series Laser Unit; the microscope also contains 488 and 561 laser lines) were used to stimulate blinking or excite the fluorophores (AF647, AF(+)647, AF647-Pyr-tz), respectively. The light was filtered using Nikon Normal STORM cube (T660lpxr,

ET705/72 m). The 3D dSTORM imaging was possible due to a cylindrical lens that had been introduced into the light path[247].

All widefield images were taken as 16-bit, with a frame size of 1024x1024 pixels. For the image acquisition, I used Apo 60× objective (NA 1.4, oil) and the pixel size of 0.27 µm, except for the imaging of click-labeled Nav1.6^{K1546TAG}-mGFP in neurons where I used HP Apo TIRF 100×H (NA 1.49, oil) objective and the pixel size of 0.16 µm. The camera exposure time was set to 30 ms while the excitation light intensity was set at 20%–30% (the exceptions are listed in the following paragraph).

Image acquisition of HA-NF186^{WT} in cell lines: 10 ms exposure time and the excitation light of 10%. Image acquisition of hNSE-NF186 in neuronal cell lines: 20 ms exposure time. Image acquisition of the AAVs with a fluorescent reporter in neurons: 10 ms exposure time and the excitation light intensity of 10%. Image acquisition type 3 pol III promoters in cell lines: 10 ms exposure time and the excitation light intensity of 5% (EGFP).

To acquire 3D dSTORM images, I always followed the same procedure. Click or immunolabeled cells were detected with widefield microscopy, and corresponding images were acquired. Afterwards, the region of interest in the same cell/neuron was selected, and the images were first acquired with 647 laser power of 1%. In the next step, I performed 3D dSTORM of the same region of interest with a maximum (100%) 647 laser power and continuous illumination. The 405 laser (5%) was used during the acquisition to stimulate blinking. dSTORM was performed in the total internal reflection fluorescence (TIRF) or highly inclined and laminated sheet microscopy (HILO) mode. Prior to imaging, I calibrated 3D dSTORM following instructions provided by Nikon. For the calibration, I used TetraSpeck Microspheres. All 3D dSTORM images were acquired as 16-bit with a frame size of 128x128 pixels or 256x256 pixels. I acquired 15,000–30,000 frames at 25 Hz, 33 Hz, or 50 Hz. The camera exposure time was set to 20–40 ms.

The data were acquired in at least two to three experiments.

Image processing

I used ImageJ/Fiji to process all widefield and confocal images unless it was stated otherwise. Images acquired in the form of z-stacks were converted to the maximum intensity projections prior to the analysis. For multicolor images, I separated channels before converting z-stacks to maximum intensity projections. For each channel, I linearly adjusted brightness and contrast (for comparison of different conditions, the same values were set in different images).

For presentation purposes, regions of interest (ROIs) were cropped. Different channels in multicolor images were cropped in the same way and merged afterwards. Scale bars and look-up-table (LUT) intensity bars were set in ImageJ/Fiji. For presentation purposes, I converted processed images from 16-bit to 8-bit (composite images were converted to RGB Color) and exported them from ImageJ/Fiji as .tiff files. All figures were created in Adobe Illustrator. Schemes were created in BioRender.com, imported in Adobe Illustrator, and incorporated into figures.

I used Nikon-Elements AR software to process 3D dSTORM images. For the analysis, I used default settings to identify the molecules (200 nm minimum width, 700 nm maximum width, 300 nm initial fit width, 2.5 max axial ratios, 1 max displacement). The maximum height was set to 65,000, and the minimum height was set to automatic, or between 80–200 (dSTORM imaging of the AIS components). The molecule localization was carried out with the overlapping peaks algorithm. The drift correction based on the autocorrelation was performed automatically by Nikon-Elements AR software. For the reconstruction of the 3D images, the Gaussian rendering size was set to 10–15 nm. The 3D dSTORM reconstructed images were exported without z rejected molecules, with height maps containing color-coded z positions. The regions of interest in 3D dSTORM images were cropped in Nikon-Elements AR software. Scale bars of dSTORM and corresponding TIRF images were added in Nikon Elements AR and exported as .tiff files. Images were imported into Adobe Illustrator and arranged into figures.

3.12. Quantitative analyses

For the AIS length or the AIS fluorescence intensity analysis, images were acquired on LSM 710 confocal microscope. The AIS length of the neurons transfected with $Na_V1.6$-HA or NF186-HA and surrounding untransfected neurons were analyzed as previously described[34,75]. Briefly, confocal images were analyzed in ImageJ/Fiji, described in the Image processing section, and exported as 16-bit. Afterwards, the AIS lengths were measured in MATLAB using a previously published custom-written ais.m script[34,248]. The AIS lengths were measured in ankG channel. I used the data acquired in 3 experiments for the analyses. Prior to measurements, all experimental groups were blinded to avoid bias.

The AIS fluorescence intensity of the neurons transfected with clickable LOF $Na_V1.6$-HA was analyzed in ImageJ/Fiji using a previously published macro set: https://github.com/cleterrier/Measure_ROIs. Briefly, confocal images were analyzed in ImageJ/Fiji according to the instructions provided with the following macro: https://github.com/cleterrier/Process_Images. The AIS fluorescence intensity was measured in

both click and HA channels by following the instructions provided with a macro set and with the help of the NeuronJ plug-in[249]. The analysis details were previously published[75]. As the macro set instructions suggested, we used the mean intensity measured along the AIS with a subtracted background (the corrected mean) for further statistical analysis. I analyzed only neurons with a signal localizing in the AIS. I used the data acquired in 4 experiments for the analyses. Prior to measurements, all experimental groups were blinded to avoid bias.

For the quantification of the GFP^{Y39TAG}/mCherry ratio, images were acquired on the inverted Nikon microscope. In order to quantify the mCherry and GFP^{Y39TAG} fluorescence intensity in neurons transduced with AAVs, widefield images were analyzed in ImageJ/Fiji using a macro written by Aleksandra Arsić (modification of the macro published in[250]). Aleksandra Arsić also performed the analysis. The macro worked in a way that it opened NLS-mCherry and corresponding GFP^{Y39TAG} images. Afterwards, the thresholding was done in the mCherry channel (based on the Li dark algorithm), allowing the generation of the regions of interest (that corresponded to mCherry nuclear signals). The out-of-focus nuclei and non-nuclear fluorescent signals were not measured. They were excluded manually from each image. The user also checked if all the ROIs were appropriately selected in this step. In the subsequent steps, the intensity measurements were performed in mCherry and GFP^{Y39TAG} channels in the selected regions of interest (the mean fluorescent intensity, integrated density, and raw integrated density). The background fluorescence was subtracted by measuring a rectangular ROI in the area without a fluorescent cell. The results were imported in excel to calculate a corrected total cell fluorescence (CTCF) and the mCherry and GFP^{Y39TAG} ratios according to the following formulas:

$$CTFC = raw\ integrated\ density - (ROI\ area * mean\ fluorescence\ of\ a\ background)$$

$$mCherry/\ GFP^{Y39TAG}\ ratio = CTFC(mCherry)/CTFC(GFP^{Y39TAG})$$

For the mCherry and GFP^{Y39TAG} fluorescence measurements in neurons transduced with AAVs, the cells with oversaturated pixels were excluded prior to the analysis. The data were acquired in 2 experiments. For each condition, five images were analyzed per experiment (ten images in total). Prior to measurements, all experimental groups were blinded to avoid bias.

3.13. Patch clamp recordings

For the whole-cell patch clamp recordings of recombinant Na^+ currents, the TTX-resistant constructs were used (constructs were rendered TTXr by introducing Y371S or Y371C mutation into the *mSCN8A*). The N1E-115-1 (250,000 cells/well) or N1E-115-$1^{\beta1\beta2}$ (160,000–200,000) were

seeded into six-well plates. N1E-115-1 cells were transfected with a total DNA amount of 8.4 µg (4 µg $Na_V1.6$-HA plasmid, 4 µg codon-optimized NES $PylRS^{AF}$/U6-$tRNA^{Pyl,}$ and 0.4 µg pACEMam2_mβ1_mβ2_mGFP multigene plasmid). N1E-115-1 ^{β1β2} cells were transfected total DNA amount of 5 µg (2.5 µg $Na_V1.6$-P2A-EGFP plasmid and 2.5 µg codon non-optimized NES $PylRS^{AF}$/U6-$tRNA^{Pyl}$) using Lipofectamine 3000 (**transfection protocol c**). Alternatively, N1E-115-1 cells were transfected with a total DNA amount of 5 µg (4 µg $Na_V1.6$-P2A-EGFP plasmid and 4 µg codon non-optimized NES $PylRS^{AF}$/U6-$tRNA^{Pyl}$ plasmid) using Lipofectamine 2000 (**transfection protocol a**). Transfected cells were incubated with a TCO*A-Lys. After two days, cells (~180,000) were reseeded in 35 mm Petri dishes (Greiner Bio-one, cat. no. 627160), incubated for a few hours without UAAs (until cells settled down), and recorded afterwards. Details on the transfection protocols were published previously[75].

Recombinant Na^+ currents were measured in neuronal cell lines via a whole-cell patch clamp in the presence of 500 µM TTX. The measurement and the analyses were performed by Dr. Yuanyuan Liu (a postdoctoral researcher in the laboratory of Prof. Dr. Holger Lerche). The protocols and analysis details were previously published[75]. The data were acquired in at least three experiments. Prior to measurements, all experimental groups were blinded to avoid bias.

3.14. Statistics

The statistical analysis was performed in the IBM SPSS Statistics 28.01.0 (Armonk, New York, USA) except for the electrophysiological recordings analyzed in GraphPad Prism (GraphPad Software, Inc., San Diego, CA, USA). The distribution of the data was assessed using a Shapiro-Wilk normality test. The normally distributed data were tested for homogeneity of variances using Levene's test. In addition, I checked if the outliers were present in the data. If one of the assumptions was not fulfilled (normal distribution, absence of outliers, or homogeneity of the variance), data were analyzed with the nonparametric Kruskal-Wallis test and with Dunn-Bonferroni *posthoc* (if required). If all requirements were fulfilled, ANOVA with Tukey posthoc was performed. The AIS length and the fluorescence intensity statistical analysis results were previously published[75]. The results of the electrophysiological recordings were analyzed by Dr. Yuanyuan Liu (a postdoctoral researcher in the laboratory of Prof. Dr. Holger Lerche). A detailed analysis description has been published[75]. The graphs were generated in IgorPro (Wavemetrics, Portland, OR, USA). All the graphs were imported in Adobe Illustrator and incorporated/arranged in the figures.

4. Results

4.1. Genetic code expansion and click labeling of $Na_V1.6$

The electrophysiological recordings described in section 4.1c were performed in collaboration with the laboratory of Prof. Dr. Holger Lerche. My contribution includes the $Na_V1.6$ mutagenesis, transfection, and cell preparation for the electrophysiological recordings. Whole-cell patch clamp recordings of cells expressing recombinant $Na_V1.6$ and the data analysis were performed by Dr. Yuanyuan Liu, a member of the laboratory of Prof. Dr. Holger Lerche. This section briefly summarizes the results of the electrophysiological recordings of the $Na_V1.6^{K1425TAG}$-P2A-EGFP (published in Stajković et al. "Direct fluorescent labeling of NF186 and $Na_V1.6$ in living primary neurons using bioorthogonal click chemistry." bioRxiv (2022)[75]) and $Na_V1.6^{K1546TAG}$-P2A-EGFP (unpublished data).

a) Generation of WT and clickable $Na_V1.6$ constructs

The mammalian recombinant $Na_V1.6$ plasmids are highly unstable when propagated in bacteria[236,251]. As a result, the undesired point mutations or rearrangements are introduced into the *SCN8A* gene during propagation in commonly used *E. coli* strains, such as electrocompetent TOP10. Therefore, special protocols must be followed when handling recombinant $Na_V1.6$ plasmids. These protocols include using the *E. coli* strains designed for cloning large unstable inserts (e.g., Stbl2, Stbl4, or XL-II gold)[235,236,242]. Furthermore, bacteria should be propagated at a lower temperature (27–29 °C), and a complete *SCN8A* open reading frame needs to be sequenced to confirm that the gene sequence is not compromised[236]. To identify the most suitable protocol for $Na_V1.6$ propagation, I probed chemically competent XL-II gold[235] and Stbl2 *E. coli* strains since both had been used for the *SCN8A* propagation[83,236,242]. Both strains allowed the $Na_V1.6$ propagation without introducing undesired mutations and gene rearrangements. To avoid inconsistencies, I used the XL-II gold in all molecular biology experiments that involved $Na_V1.6$ unless it was stated otherwise.

A mouse (*m*)$SCN8A^{WT}$ gene was synthesized commercially by GenScript. A self-cleaving P2A sequence[252] was introduced at the C terminus of $SCN8A^{WT}$, followed by enhanced (E)GFP and TAA stop codon (**Scheme 6a**). EGFP allowed the identification of the transfected cells expressing $Na_V1.6$. Posttranslational self-cleaving of the P2A sequence provided separation and equal expression of $Na_V1.6$ and EGFP. Furthermore, it minimalized the possibility that $Na_V1.6$ localization or function would be affected by EGFP.

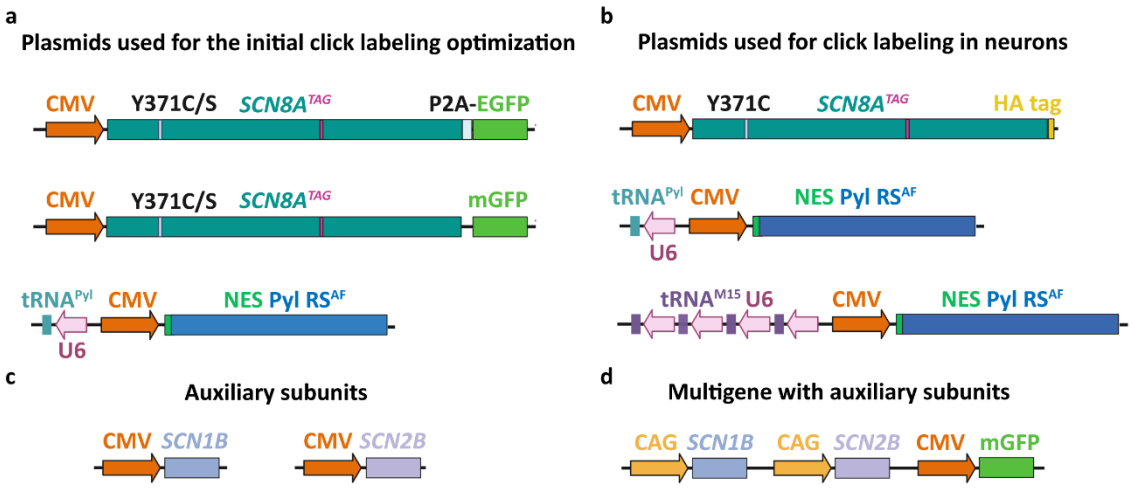

Scheme 6. The schematic representation of the plasmids used for the $Na_V1.6$ genetic code expansion and click labeling in neuronal cell lines and neurons. a: *Plasmids used for the initial optimization of the m$Na_V1.6$ genetic code expansion and click labeling in neuronal cell lines. The mSCN8A$^{WT/TAG}$ genes under the cytomegalovirus (CMV) promoter were fused to a self-cleaving P2A sequence and enhanced (E)GFP. Alternatively, mSCN8A$^{WT/TAG}$ was fused to monomeric (m)GFP. $Na_V1.6$ plasmids were co-transfected with a codon non-optimized NES PylRS^{AF}/U6-tRNA^{Pyl}.* ***b:*** *For the m$Na_V1.6$ genetic code expansion and click labeling in primary neurons, P2A-GFP was replaced with a small HA tag. The HA tag-containing plasmids were co-transfected with codon-optimized NES PylRS^{AF}/U6-tRNA^{Pyl} or NES PylRS^{AF}/4xU6-tRNA^{M15}.* ***c:*** *The membrane expression and functionality of m$Na_V1.6$ in neuronal cell lines were ensured by transfecting auxiliary β1 and β2 subunits along with plasmids shown in a and b.* ***d:*** *For patch clamp recordings of recombinant $Na_V1.6$-HA, neuronal cell lines were co-transfected with a multigene containing β1, β2, and mGFP instead of plasmids shown in c. The scheme was generated in BioRender.com.*

Next, I chose the potential TAG (click labeling) sites for the UAA incorporation (**Scheme 3**). However, due to the complex structure of $Na_V1.6$, I faced difficulties selecting those labeling positions. The crystal structure of the mammalian Na_V was unavailable when my project started. Also, the $Na_V1.6$ α subunit has a complex 3D organization and undergoes heavy posttranslational glycosylation. Therefore, predicting if the selected positions would be accessible for tetrazine dyes was difficult. Furthermore, numerous mutations of the *SCN8A* gene have been implicated in neurological conditions[13,14]. These positions/regions had to be avoided to exclude any possibility that UAA incorporation would affect the function or localization of the $Na_V1.6$. Likewise, I had to avoid all the domains indispensable for the function of $Na_V1.6$ or its interaction with partner proteins (e.g., S4 voltage-sensors, P loops)[50]. Since I was interested in membrane labeling of $Na_V1.6$ with cell-impermeable dyes, I chose positions in the extracellular loops of $Na_V1.6$. Based on limited information, I selected and introduced the following TAG mutation into *mSCN8A^{WT}*: R914TAG, K1224TAG, K1425TAG, K1546TAG, A1601TAG, K1606TAG, K1675TAG, and K1731TAG (**Scheme 3**). Since I later identified K1425TAG and K1546TAG as

the most promising mutants for click labeling in neurons, I did not test the other amber (TAG) mutants extensively. For the electrophysiological recordings of Na^+ currents originating from recombinant $Na_V1.6^{WT/TAG}$, I introduced either Y371S or Y371C mutation that provided resistance to sodium channel blocker tetrodotoxin (TTX) as previously described(**Scheme 3**)[60,109,234,253]. For the click labeling of $Na_V1.6$ in primary neurons, P2A-EGFP was replaced by an HA tag, which will be discussed later (**Scheme 6b**).

I also generated plasmids in which monomeric (m)GFP or EGFP were fused directly to the C terminus of $Na_V1.6^{WT/TAG}$ ($Na_V1.6$-$GFP^{WT/TAG}$; **Scheme 6a**). At that time, I was still optimizing molecular biology protocols for mutagenesis, cloning, and amplification of recombinant $Na_V1.6$ in XL-II gold bacteria. That is why $Na_V1.6$-GFP constructs were propagated in TOP10 *E. coli*. As these constructs were used in some pilot experiments, I will mention them in the following sections. However, the results obtained with these plasmids were not included in my published paper[75]. Also, these initial plasmids were later replaced by $Na_V1.6$-EGFP constructs propagated in XL-II gold bacteria.

b) Genetic code expansion of clickable $Na_V1.6$ in neuronal cell lines

To click label $Na_V1.6^{TAG}$, I first wanted to optimize the expression of the WT and amber mutants in the readily transfected intermediate host cell line. Since neuronal ND7/23 and N1E-115-1 cell lines share similarities with primary neurons (they express ion channels, including Na_V, and can grow processes)[254-256], I reasoned that they would provide a more native environment for the proper expression and functioning of the $Na_V1.6$ than the standard HEK293T cell line. ND7/23 cells have been extensively used for the electrophysiological recordings of recombinant voltage-gated sodium channels[13,83,84,109,242]. Therefore, I first attempted to express and click label $Na_V1.6$ in those cells. I identified optimal transfection conditions by testing different transfection reagents (JetPrime, Lipofectamine 2000, and 3000), different ratios of DNA and the transfection reagents, and different amounts of DNA. Regardless of the transfection protocol, click labeling conditions, or plasmids that were used, the general workflow included: co-transfections with previously described NES $PylRS^{AF}$/$tRNA^{Pyl150}$, $mNa_V1.6^{WT/TAG}$, and mouse (m)β subunits(**Scheme 6c**). Transfections were carried out in the presence or absence of the unnatural amino acid TCO*A-Lys. To reduce the number of plasmids that were delivered to the cells and to ensure that there was a sufficient amount of auxiliary β subunits[66], I later generated stable cell lines that expressed mβ1, or mβ1 and mβ2. To find optimal click labeling conditions, I tested different tetrazine (tz) dyes and different concentrations of the dyes. I also attempted labeling on ice vs. 37 °C and labeling at different time points after transfection (24 h or 48 h). Upon click

labeling, cells were fixed and imaged with widefield microscopy. In addition, to improve the surface expression of $Na_V1.6$, I incubated ND7/23 at 30 °C[242]. This section summarizes and shows the most relevant results that allowed me to establish GCE and click labeling of $Na_V1.6$ in neuronal cell lines.

Initially, I expressed and click labeled $Na_V1.6^{WT/TAG}$-P2A-EGFP along with mβ1, or mβ1 and mβ2 (**Scheme 6a** and **c**) in ND7/23 cells. I followed protocols that had been used for the click labeling of membrane proteins in HEK293T cells[170]. Instead of JetPrime, I used Lipofectamine 2000 transfection reagents since the cell survival was better with the latter. Also, Lipofectamine 2000 provided a higher transfection efficiency. In cells transfected with $Na_V1.6^{WT/TAG}$-P2A-EGFP, I observed the EGFP fluorescent signal, indicating that the expression of these constructs had been successful. However, click labeling of $Na_V1.6^{WT/TAG}$-P2A-EGFP with Cy5-tz was unsuccessful. Since cytosolic EGFP produced by P2A self-cleaving in the $Na_V1.6^{WT/TAG}$-P2A-EGFP could not be used to estimate the amount of $Na_V1.6$ WT or TAG amber mutants on the membrane, I expressed $Na_V1.6$-mGFP plasmid in ND7/23 cells (**Scheme 6a**). The widefield microscopy of $Na_V1.6$-mGFP-expressing cells indicated that $Na_V1.6$ WT and TAG amber mutants mostly remained inside the cytoplasm (data not shown).

To improve $Na_V1.6$ membrane localization, I generated stable cell lines that expressed either mβ1 (ND7/23^{β1}) or mβ1 and mβ2 (ND7/23^{β1β2}) by using the commercially available Super PiggyBac Transposase System. Although the membrane localization of $Na_V1.6$-mGFP in stable ND7/23^{β1} and ND7/23^{β1β2} cell lines improved, particularly when cells were incubated at 30 °C after the transfection, most channels remained in the cytosol (**Fig. 1a**).

Therefore, I tested an alternative host, a mouse neuroblastoma N1E-115-1 cell line. Those cells were a promising candidate for the GCE of the recombinant $Na_V1.6$ since they were previously used for the electrophysiological studies of voltage-gated sodium channels, including $Na_V1.6$[257,258]. Similarly to ND7/23, I generated N1E-115-1^{β1} and N1E-115-1^{β1β2} stable cell lines. The widefield microscopy showed higher $Na_V1.6^{WT}$-mGFP membrane localization in both stable N1E-11-5-1 cell lines compared to ND7/23 cells (**Fig. 1b**).

After identifying a suitable host for the GCE of voltage-gated sodium channels, I expressed and clicked labeled $Na_V1.6$-P2A-EGFP in N1E-115-1^{β1β2} cells. I first attempted click labeling with Cy5-tz following a published protocol[170]. However, click labeling with this dye resulted in high background and significant dye accumulations (data not shown). To find the optimal labeling conditions and reduce the background, I attempted labeling on ice[153] and introduced a washing

step in a warm culturing medium before labeling[148]. I also used an alternative far red dye, AF647-tz. These optimized click labeling conditions resulted in what seemed to be a successful click labeling of two $Na_V1.6$ amber mutants (K1425TAG and K1546TAG) in N1E-115-$1^{\beta1\beta2}$ cells (**Fig. 2**). The pale click labeling of both amber mutants was also observed in ND7/$23^{\beta1\beta2}$ cells (**Fig. 2**). The expression level and click labeling of $Na_V1.6^{K1546TAG}$ was higher than the $Na_V1.6^{K1425TAG}$ in both neuronal cell lines. However, later on, I realized that the membrane signal did not represent a real click labeling (this will be explained and discussed in **Section 4.1d**).

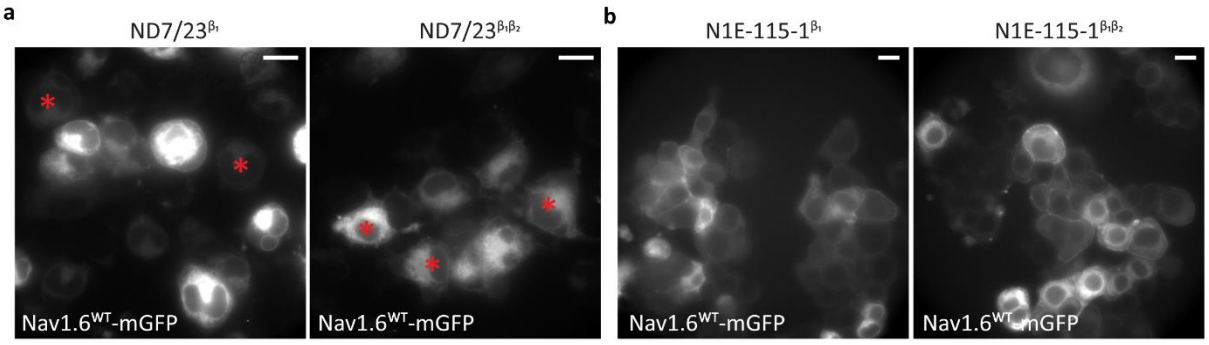

Figure 1. Comparison of the Nav1.6^{WT}-mGFP expression on the cell membrane of stable neuronal cell lines. *Neuronal ND7/23 or N1E-115-1 cells that stably expressed mβ1, or mβ1 and mβ2 auxiliary subunits (hereafter referred to as ND7/23$^{\beta1}$, ND7/23$^{\beta1\beta2}$, N1E-115-1$^{\beta1}$, N1E-115-1$^{\beta1\beta2}$) were transfected with $Na_V1.6^{WT}$-mGFP plasmid using Lipofectamine 2000 transfection reagent. Two days after the transfection, cells were fixed and imaged with widefield microscopy.* ***a:*** *The representative widefield images show that in most ND7/23$^{\beta1}$ and ND7$^{\beta1\beta2}$ cells, $Na_V1.6$ remained inside the cytosol (red asterisks) while the low membrane signal was observed.* ***b:*** *Contrary to ND7/23 cells, in N1E-115-1$^{\beta1}$ and N1E-115-1$^{\beta1\beta2}$, a higher $Na_V1.6$ signal was observed on the cell membrane. Scale bars: 20 µm.*

c) Electrophysiological characterization of clickable $Na_V1.6$ in neuronal cell lines

After identifying optimal click labeling conditions, it was necessary to examine if the introduction of TCO*A-Lys into $Na_V1.6^{TAG}$ altered any electrophysiological properties of the channel. Since the click labeling efficiency of the K1546TAG amber mutant was higher than the K1425TAG, the electrophysiological features of this mutant were assessed first. For the electrophysiological recordings, TTXr (Y371S) variants[60,253] of $Na_V1.6^{WT/TAG}$-P2A-EGFP plasmids were expressed in N1E-115-$1^{\beta1\beta2}$ cells. The Y371S mutation ensured that Na^+ currents originating only from the recombinant and not the endogenous $Na_V1.6$ would be recorded with the whole-cell patch clamp. The recordings were performed 48 h after transfection in the presence of TTX. Since Y371S variants exhibited very high Na^+ current amplitude that could not be analyzed, I replaced Y371S with an alternative TTXr mutation (Y371C)[109]. After confirming that plasmids with the Y371C mutation could be click labeled (**Fig. 3a**), the recombinant Na^+ currents were recorded. Importantly, the detection of the recombinant Na^+ currents provided additional proof that

$Na_V1.6^{WT/TAG}$-P2A-EGFP was expressed on the cell membrane. The whole-cell patch clamp recordings showed a slight difference in Na^+ current density between K1546TAG and WT channels that did not appear significant (**Fig. 3b, Appendix Table 2**). There was no difference in the activation of K1546TAG and WT channels. However, a slight depolarizing shift of the K1546TAG inactivation curve appeared significant (**Fig. 3b, Appendix Table 2**). Hence, the K1425TAG mutant was measured as well.

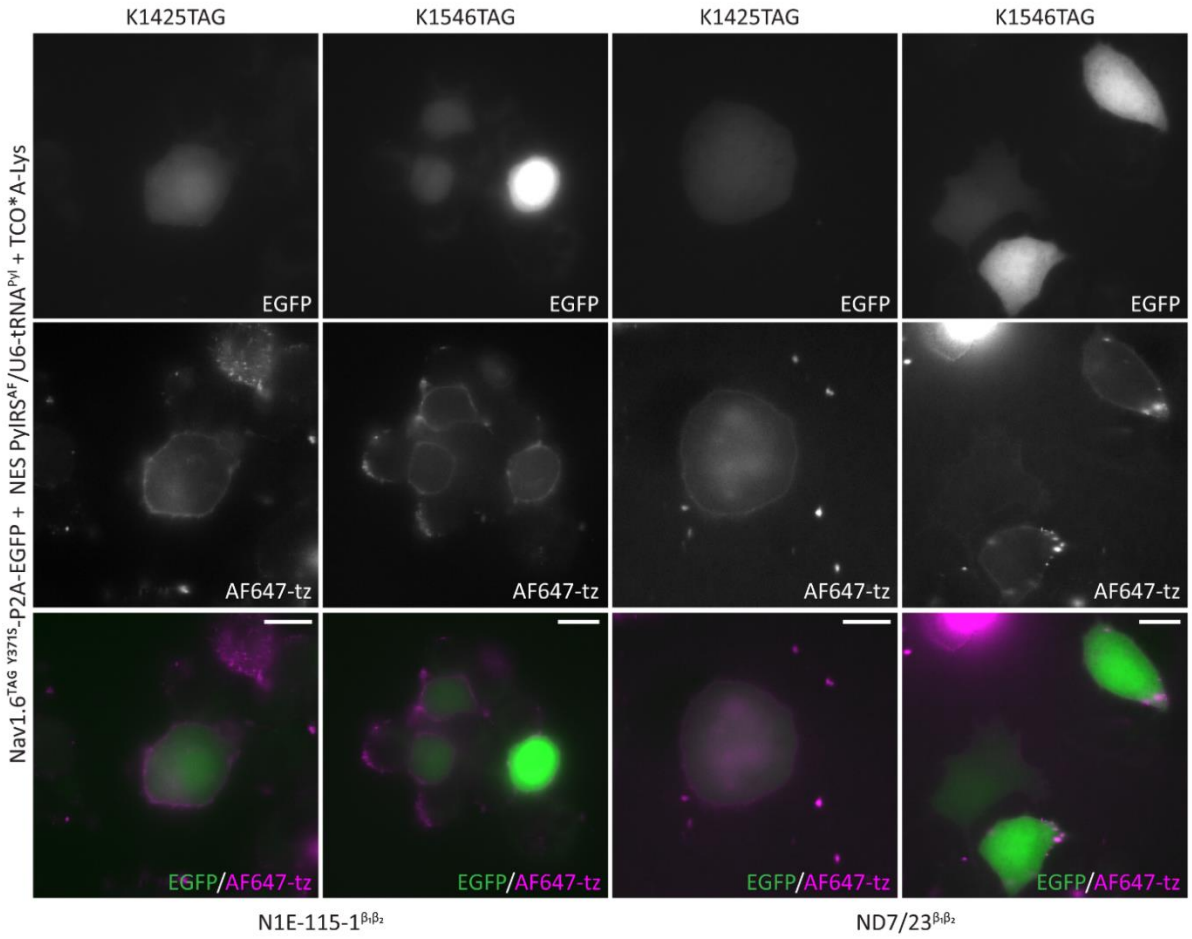

Figure 2. GCE and click labeling of Nav1.6^{Y371S}-P2A-EGFP in stable neuronal cell lines. *Neuronal ND7/23$^{\beta1\beta2}$ or N1E-115-1$^{\beta1\beta2}$ cells were co-transfected with codon non-optimized NES PylRS^{AF}/U6-tRNA^{Pyl} and with tetrodotoxin (TTX)-resistant Y371S versions of $Na_V1.6$-P2A-EGFP amber mutants (K1425TAG or K1546TAG) using Lipofectamine 2000 transfection reagent. Transfected cells were incubated with the unnatural amino acid TCO*A-Lys. Two days after the transfection, cells were washed for ~2 h, click labeled with AF647-tetrazine (tz), fixed, and imaged with widefield microscopy. The representative images show that both mutants were click-labeled in both cell lines. The expression level (EGFP) and click labeling signal (AF647-tz) of the K1546TAG amber mutant were higher than those of the K1425TAG. The EGFP and click signals were paler and present in fewer ND7/23$^{\beta1\beta2}$ cells than the N1E-115-1$^{\beta1\beta2}$. Scale bars: 20 µm.*

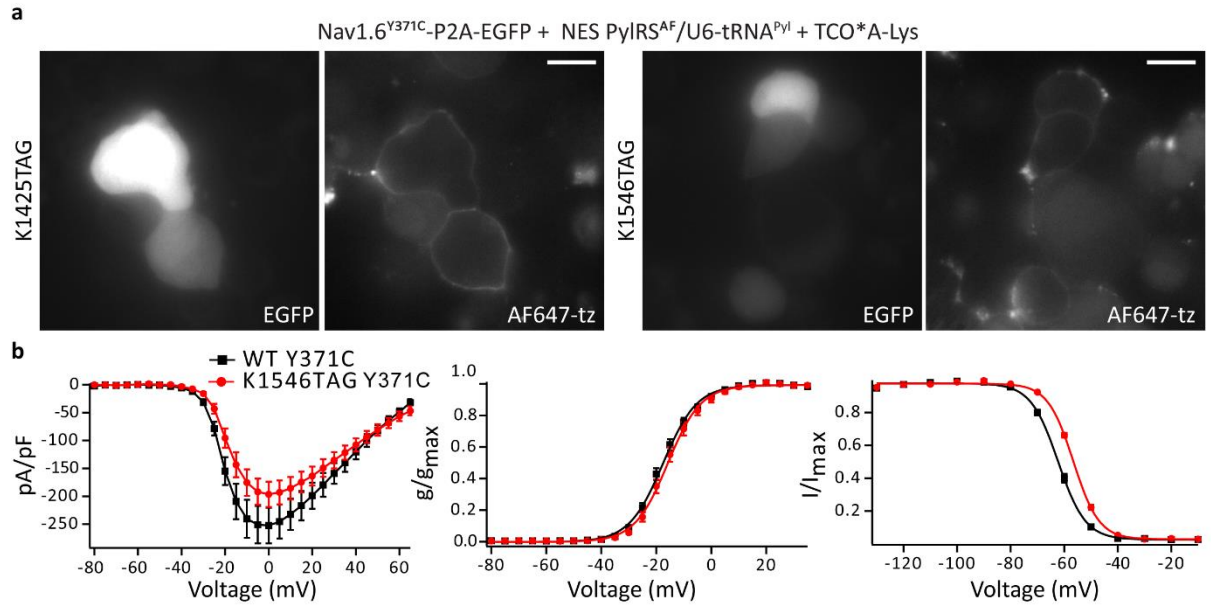

Figure 3. Click labeling and biophysical characterization of Nav1.6$^{K1546TAG,\ Y371C}$-P2A-EGFP in N1E-115-1$^{\beta1\beta2}$ cell line. *Neuronal N1E-115-1$^{\beta1\beta2}$ cells were co-transfected with codon non-optimized NES PylRS^{AF}/U6-tRNA^{Pyl} and with TTX-resistant Y371C versions of Na$_V$1.6-P2A-EGFP WT or amber mutants (K1425TAG or K1546TAG) using Lipofectamine 2000 transfection reagent. Transfected cells were incubated in the presence of the unnatural amino acid TCO*-Lys for two days. Afterwards, cells were click labeled with AF647-tz, fixed, and imaged via widefield microscopy (a). Alternatively, after two days, cells were re-seeded in 35 mm Petri dishes and recorded with a whole-cell patch clamp (b).* ***a:*** *The representative images show that both amber mutants that bore Y371C mutation were successfully click-labeled in N1E-115-1$^{\beta1\beta2}$ cells. Scale bars: 20 µm.* ***b:*** *Representative Na$^+$ current traces obtained from N1E-115-1$^{\beta1\beta2}$ cells that expressed Na$_V$1.6$^{WT,\ Y371C}$-P2A-EGFP (black), or Na$_V$1.6$^{K1546TAG,\ Y371C}$-P2A-EGFP (red). Peak Na$^+$ current densities normalized to cell capacitance were plotted versus voltage (left graph). Voltage-dependence of the activation (middle graph). Voltage-dependence of the fast inactivation (right graph). The K1546TAG amber mutation caused a significant depolarizing shift of voltage-dependent fast inactivation. Number of recorded cells $(n)_{WT}$ = 14 and $n_{K1546TAG}$ = 13. The lines represent the Boltzmann functions fit to the data points (middle and right graph). Means ± SEMs are shown in the graphs. Further details on the statistical analysis are provided in Appendix Table 2. and the Materials and methods.*

The low expression level of Na$_V$1.6^{K1425TAG} (**Fig. 3a**) resulted in lower Na$^+$ currents amplitude (data not shown). Therefore, I attempted to improve the transfection efficiency by testing different DNA concentrations for Lipofectamine 2000 and by probing Lipofectamine 3000 transfection reagent. Lipofectamine 3000 improved transfection efficiency (I observed more EGFP positive cells that appeared brighter**; Fig. 4a**), click labeling efficiency (**Fig. 4a)** and increased Na$^+$ current amplitude**.** However, the whole-cell patch clamp results showed a significantly lower current density of the K1425TAG amber mutant compared to the WT (**Fig. 4b, Appendix Table 2**). The other electrophysiological parameters were unchanged (**Fig. 4c–h, Appendix Table 2**). Since Na$_V$1.6^{K1425TAG} exhibited identical electrophysiological properties to WT except for

the current density, I decided to use this mutant. Therefore, other TAG amber mutants (**Section 4.1a**) were not measured.

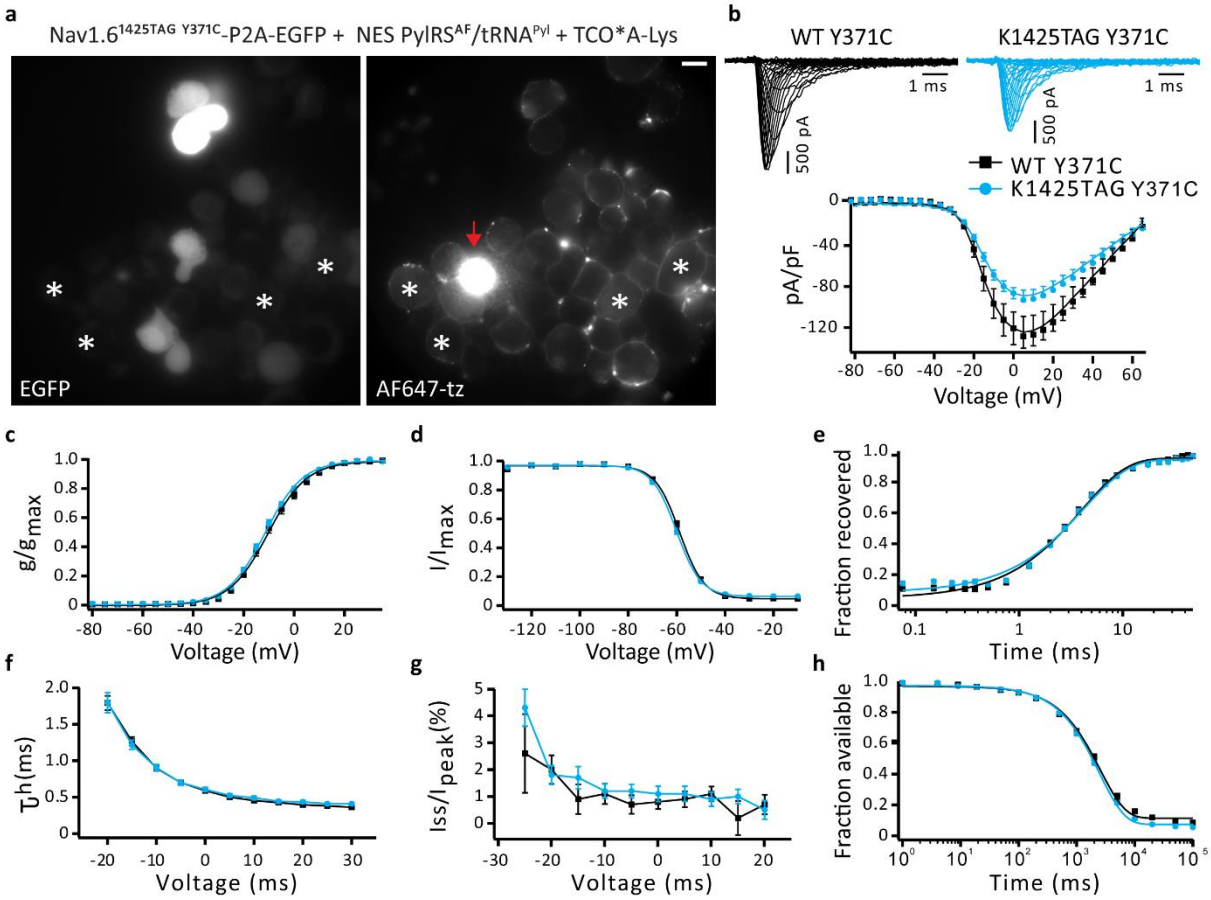

Figure 4. Characterization of the expression, click labeling, and functionality of the Na$_V$1.6$^{K1425TAG, Y371C}$-P2A-EGFP in N1E-115-1^{β1β2} cell line. *Neuronal N1E-115-1^{β1β2} cells were co-transfected with codon non-optimized NES PylRS^{AF}/U6-tRNA^{Pyl} and with TTX-resistant Y371C versions of Na$_V$1.6-P2A-EGFP WT or K1425TAG amber mutant using Lipofectamine 3000 transfection reagent. Transfected cells were incubated in the presence of the unnatural amino acid TCO*-Lys for two days. Afterwards, cells were click labeled with AF647-tz, fixed, and imaged with widefield microscopy (a). Alternatively, after two days, cells were re-seeded in 35 mm Petri dishes and recorded with whole-cell patch clamp (b–h).* ***a:*** *The representative widefield image shows that the transfection of N1E-115-1^{β1β2} cells with Lipofectamine 3000 improved expression and click labeling of the Na$_V$1.6$^{K1425TAG, Y371C}$. The red arrow indicates AF647-tz dye accumulation, while white asterisks indicate EGFP-negative cells that appeared labeled with click chemistry. Scale bars: 20 µm.* ***b:*** *Representative Na$^+$ current traces obtained from N1E-115-1^{β1β2} cells that expressed Na$_V$1.6$^{WT, Y371C}$-P2A-EGFP (black; upper left panel) or Na$_V$1.6$^{K1425TAG, Y371C}$-P2A-EGFP (blue; upper right panel). Peak Na$^+$ current densities normalized to the cell capacitance were plotted versus voltage (lower panel; n_{WT} = 18 and $n_{K1425TAG}$ = 20). K1425TAG amber mutation caused a significant current density reduction compared to the WT.* ***c:*** *Voltage-dependence of the activation (n_{WT} = 18 and $n_{K1425TAG}$= 20).* ***d:*** *Voltage-dependence of the fast inactivation (n_{WT} = 18 and $n_{K1425TAG}$ = 20). The lines represent the Boltzmann functions fit to the data points (c, d).* ***e:*** *Time course of recovery from fast inactivation at -100 mV (n_{WT} = 17 and $n_{K1425TAG}$ = 20).* ***f:*** *Voltage dependence of the major time constant of fast inactivation $τ_h$ (n_{WT}= 18 and $n_{K1425TAG}$ = 20).* ***g:*** *Voltage dependence of the persistent current (I_{ss}/I_{peak}).*

h: *Entry into slow inactivation. The lines represent fits of a first-order exponential function to the data points. Mean ± SEMs are shown. Further details on the statistical analysis are provided in Appendix Table 2 and the Materials and methods. The results shown in figure (b–h) were published in[75].*

d) Unsuccessful click labeling of $Na_V1.6$ in neuronal cell lines

While optimizing $Na_V1.6^{TAG}$-P2A-EGFP click labeling in neuronal cell lines, I occasionally observed an unexpected AF647-tz membrane signal in EGFP negative cells (**Fig. 4a**). Likewise, I noticed that click labeling signal did not always correlate with the EGFP intensity (**Fig. 4a**). To investigate this closer, I performed control experiments in which N1E-115-$1^{\beta1\beta2}$ cells were co-transfected with $Na_V1.6^{WT}$ and NES $PylRS^{AF}/tRNA^{Pyl}$ or with NES $PylRS^{AF}/tRNA^{Pyl}$ alone, in the presence or absence of TCO*A-Lys. As an additional control, I had untransfected cells propagated with or without TCO*A-Lys. Two days after the transfection, cells were fixed, click labeled with AF647-tz, and imaged with widefield microscopy. The results indicated that the combination of NES $PylRS^{AF}/tRNA^{Pyl}$ and TCO*A-Lys resulted in the membrane signal that resembled click labeling (**Fig. 5**). Such signal was not detected in the absence of TCO*A-Lys or the absence of NES $PylRS^{AF}$ (**Fig. 5**).

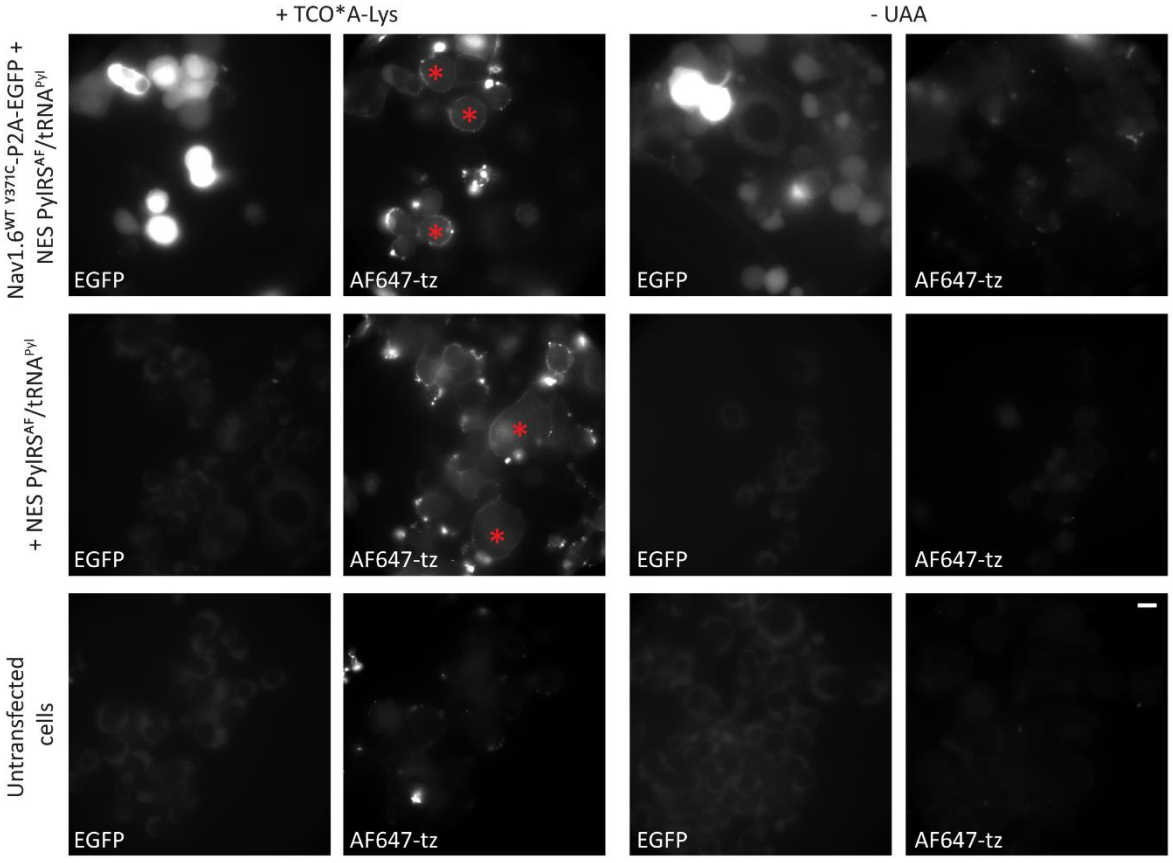

Figure 5. The false click labeling in neuronal cell lines transfected with orthogonal translational machinery. *Neuronal N1E-115-$1^{\beta1\beta2}$ cells were co-transfected with $Na_V1.6^{WT,\ Y371C}$-P2A-EGFP, and codon non-optimized*

*NES PylRS^{AF}/U6-tRNA^{Pyl} or NES PylRS^{AF}/U6-tRNA^{Pyl} alone, using Lipofectamine 3000 transfection reagent. Transfected cells were incubated with or without the unnatural amino acid TCO*A-Lys. As an additional control, untransfected cells were incubated with or without TCO*A-Lys. Two days after the transfection, cells were washed for ~2 h, click labeled with AF647-tz, fixed, and imaged with widefield microscopy. The representative images show that the abundant membrane signal resembling click labeling was present only when cells were transfected with NES PylRS^{AF}/U6-tRNA^{Pyl} in the presence of TCO*A-Lys. Red asterisks indicate cells with unspecific membrane signals resembling click labeling. Scale bars: 20 µm.*

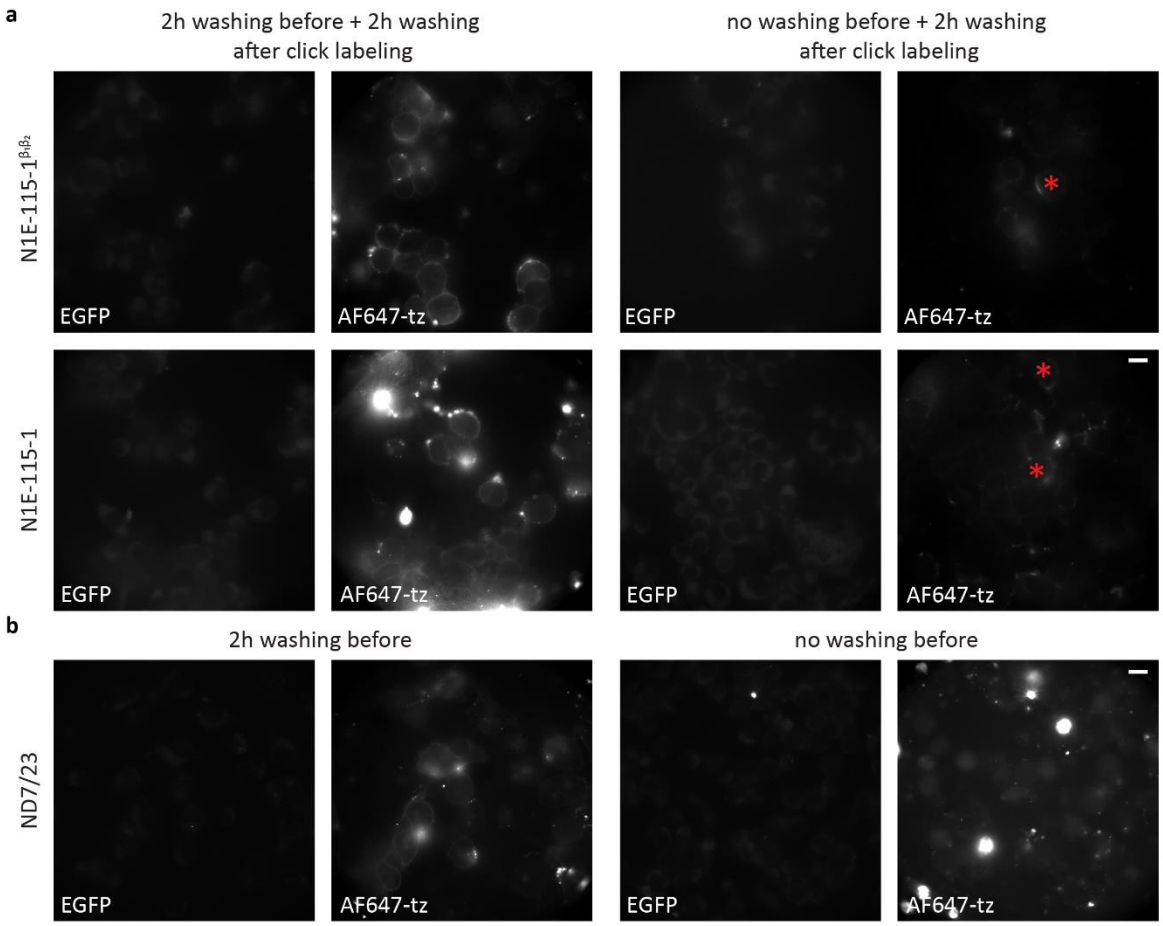

Figure 6. Cell washing before click labeling results in the appearance of the unspecific membrane signal in neuronal cell lines. *Neuronal N1E-115-1^{β1β2}, N1E-115-1, or ND7/23 cells were co-transfected with codon non-optimized NES PylRS^{AF}/U6-tRNA^{Pyl} using Lipofectamine 3000 transfection reagent. Transfected cells were incubated in the presence of the unnatural amino acid, TCO*A-Lys. Two days after the transfection, cells were either washed for ~2 h and click labeled with AF647-tz or click labeled without washing. N1E-115-1 WT and stable cells were washed for an additional 2 h after the click labeling and fixed s, while ND7/23 cells were fixed immediately. Upon fixation, cells were imaged with widefield microscopy.* ***a:*** *Representative images showing that in both N1E-115-1^{β1β2} and N1E-115-1 cells, membrane signals appear only when the 2 h washing step was performed before click labeling. Such a signal did not appear when the washing step was performed after click labeling.* ***b:*** *Representative images showing that a membrane signal in ND7/23 cells appeared when the 2 h washing step was performed before click labeling. Scale bars: 20 µm.*

To determine what was the exact cause of the click labeling-like signal, I performed a series of control experiments in which I tested the following: labeling on ice vs. labeling at 37 °C, labeling with different concentrations of Cy5-tz or AF647-tz, transfection with Lipofectamine 2000 and 3000 transfection reagents, transfection of different cell lines (stable vs. WT ND7/23 and N1E-115-1), and click labeling 24 h or 48 h after the transfection. I also tried cell re-seeding before labeling. The results of these experiments indicated that washing before or after labeling might be a problem. The subsequent experiments showed that washing before click labeling contributed significantly to the click labeling-like signal, most likely by stressing the cells (**Fig. 6**). The signal was observed in both neuronal cell lines (**Fig. 6a** and **b**). The observations from these experiments excluded the possibility that stable cell lines contributed to the false click labeling since such membrane signal was also observed in WT cells (**Fig. 6a** and **b**).

After successfully removing the background membrane signal, click labeling in N1E-115-1$^{\beta1\beta2}$ cells expressing Na$_V$1.6^{TAG} was still unsuccessful (**Fig. 7**). Therefore, I concluded that neuronal cell lines, although suitable for electrophysiological recordings, were not a good host for click labeling of the Na$_V$1.6.

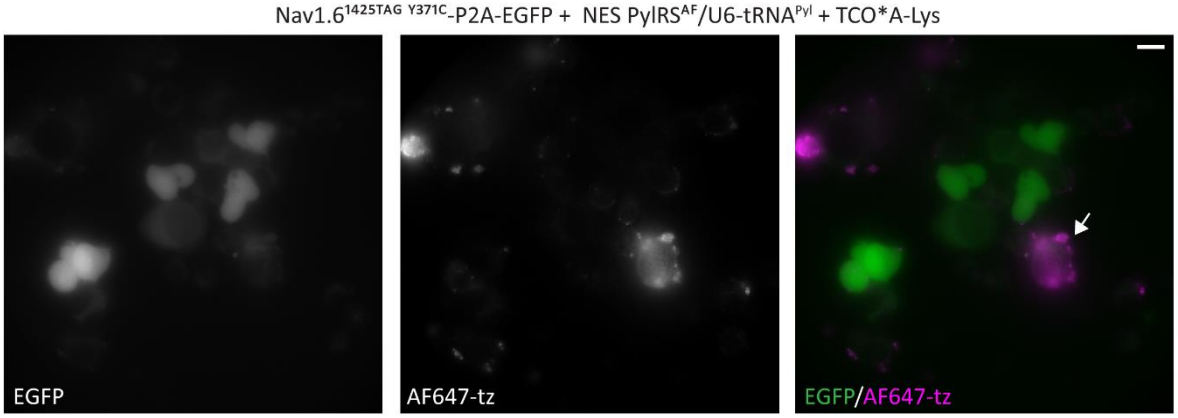

Figure 7. Unsuccessful click labeling of Na$_V$1.6^{TAG}-P2A-EGFP amber mutant in neuronal cell lines. *Neuronal N1E-115-1$^{\beta1\beta2}$ cells were co-transfected with codon non-optimized NES PylRS^{AF}/U6-tRNA^{Pyl} and Na$_V$1.6$^{K1425TAG,\ Y371C}$-P2A-EGFP using Lipofectamine 3000 transfection reagent. Transfected cells were incubated with the unnatural amino acid TCO*A-Lys. Two days after the transfection, cells were click labeled with AF647-tz, fixed, and imaged with widefield microscopy. Representative images show unsuccessful click labeling of the Na$_V$1.6^{K1425TAG} amber mutant in N1E-115-1$^{\beta1\beta2}$ cells. The white arrow indicates AF647-tz dye accumulations. Scale bars: 20 µm.*

e) Click labeling of Na$_V$1.6-mGFP in primary neurons

Although the Na$_V$1.6 click labeling in neuronal cell lines was unsuccessful (**Fig. 7**), the pilot experiments that involved click labeling of Nav1.6^{K1546TAG}-mGFP in primary mouse neurons indicated that this mutant could be labeled with AF647-tz (**Fig. 8**).

These results prompted me to establish $Na_V1.6$ click labeling directly in primary neurons. Since $Na_V1.6$ labeling was pale and frequent AF647-tz accumulations caused a high background (**Fig. 8**), further optimization of transfection and click labeling conditions were necessary. To this aim, I used a smaller AIS component with a less complex structure, the NF186 (**Fig. 9a, Scheme 4**). The following section describes the establishment and optimization of NF186 click labeling in cell lines and primary neurons.

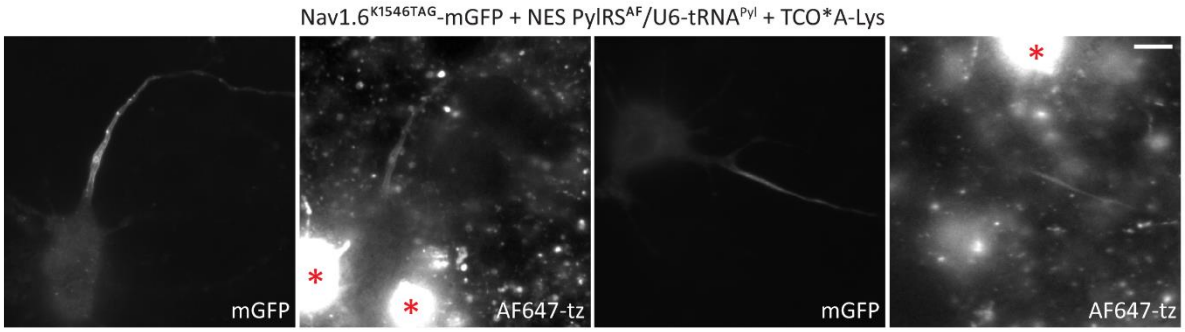

Figure 8. Click labeling of $Na_V1.6^{K1546TAG}$-mGFP plasmid in primary neurons. *Mouse cortical neurons were co-transfected on the day in vitro (DIV) 8 with codon non-optimized NES $PylRS^{AF}$/U6-$tRNA^{Pyl}$ and $Na_V1.6^{K1546TAG}$-mGFP using Lipofectamine 2000 transfection reagent. Transfected neurons were incubated with the unnatural amino acid TCO*A-Lys. Four days after the transfection, TCO*A-Lys was removed, and neurons were click labeled with AF647-tz, fixed, and imaged with widefield microscopy. Representative images of mouse neurons expressing $Na_V1.6^{K1546TAG}$-mGFP show specific localization and click labeling of sodium channels in the AIS. Red asterisks indicate AF647-tz accumulations in the extracellular space and surrounding dead neurons. Scale bars: 10 µm.*

4.2. Genetic code expansion and click labeling of NF186

The results described in section 4.2a–c were published in Stajković et al. "Direct fluorescent labeling of NF186 and $Na_V1.6$ in living primary neurons using bioorthogonal click chemistry." bioRxiv (2022)[75].

a) Genetic code expansion and click labeling of NF186 in neuronal cell lines

Before attempting NF186 click labeling in primary neurons, I assessed the expression level and click labeling efficiency of different NF186 amber mutants in intermediate host cell lines. To identify a suitable intermediate host for the GCE of NF186, I transfected HEK293T, N1E-115-1, or ND7/23 cells with a previously described plasmid that contained rat *Nfasc* under control of the

CMV promoter (**Scheme 7**)[101]. A small N-terminal HA tag in the NF186 plasmid (HA-NF186^{WT}) allowed me to immunolabel NF186^{WT} in different cell lines (**Fig. 9a**).

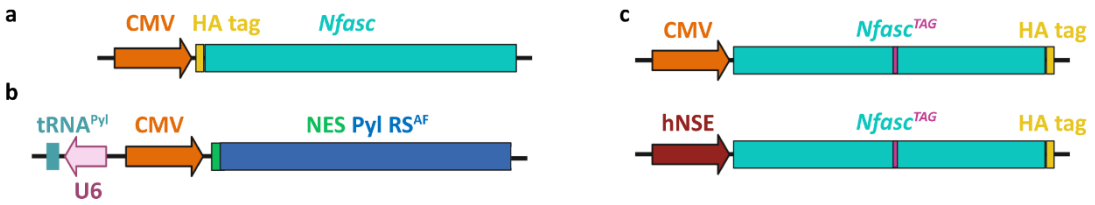

Scheme 7. The schematic representation of the plasmids used for the NF186 genetic code expansion and click labeling optimization in neuronal cell lines and neurons. a: *A plasmid containing rat Nfasc gene under strong CMV promoter with the N-terminal HA tag[101,115,117]. **b:** A plasmid encoding codon-optimized NES PylRS^{AF} and U6-tRNA^{Pyl} used for NF186 click labeling in neuronal cell lines and neurons. **c:** The plasmids containing Nfasc under CMV or weak human neuron-specific enolase (hNSE) promoters. These plasmids were modified by moving the HA tag from N to the C terminus to ensure immunodetection of full-length NF186 with an anti-HA antibody. The scheme was generated in BioRender.com.*

Although HEK293T cells have been previously used for NF186 microscopy studies[101], I wanted to test ND7/23 and N1E-115-1 cell lines as intermediate hosts for the GCE of NF186 because of their neuronal properties. Therefore, I compared NF186^{WT} expression levels in neuronal cell lines to the HEK293T cells (**Fig. 9b**).

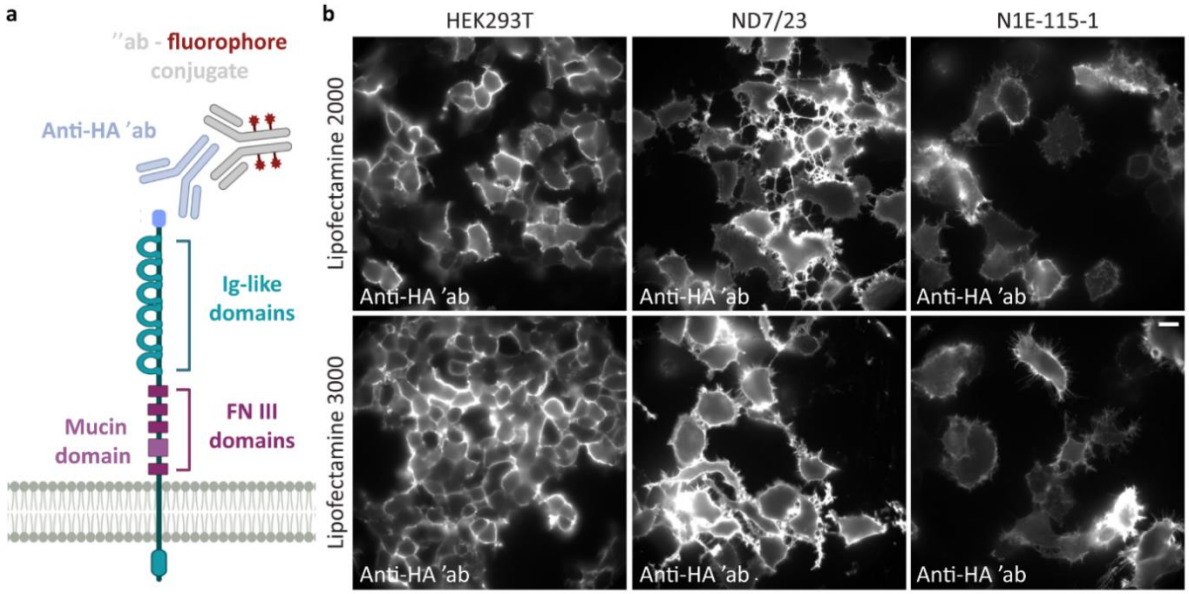

Figure 9. Optimization of the NF186^{WT} expression in neuronal cell lines. a: *A structure of the recombinant HA-NF186^{WT}. Cell adhesion molecule NF186 consists of a small intracellular tail (cyan), transmembrane domain (dark cyan), three extracellular fibronectin type III repeats (FN III; dark magenta), mucin domain (magenta), and six extracellular immunoglobulin (Ig)-like domains (cyan)[89]. An HA tag (purple) introduced at the N terminus of NF186 allows its immunodetection in living cells. **b:** Comparing the HA-NF186^{WT} expression in standard and neuronal cell lines. HEK293T, ND7/23, or N1E-115-1 cells were transfected with HA-NF186^{WT} plasmid using Lipofectamine 2000 or*

Lipofectamine 3000 transfection reagents. The following day, the cells were fixed, immunostained with an anti-HA antibody (ab), and imaged with widefield microscopy. Representative images show that NF186 expression was higher in HEK293T and ND7/23 cells than the N1E-115-1. Scale bars: 20 µm. The scheme was generated in BioRender.com.

The widefield microscopy showed abundant HA-NF186^{WT} expression in ND7/23 cells, similar to that observed in HEK293T cells. In contrast, the HA-NF186^{WT} expression in N1E-115-1 cells was lower compared to HEK293T and ND7/23 (**Fig. 9b**). Therefore, I used ND7/23 cells as a GCE host. To identify optimal transfection conditions, I tested two different transfection reagents, Lipofectamine 2000 and Lipofectamine 3000. Both transfection reagents provided robust expression of NF186 (**Fig. 9b**). Since Lipofectamine 2000 provided a sufficient NF186 expression, I used this reagent in further experiments.

For click labeling of NF186, I selected potential TAG click labeling sites using SWISS-MODEL based on the crystal structure of a titin fragment (PDB 3B43)[259,260]. To immunolabel only full-length recombinant NF186, I modified HA-NF186^{WT} plasmid by moving the HA tag from N to the C terminus (CMV-NF186-HA). Afterwards, I introduced the TAG amber codon into the rat *Nfasc* gene at the following positions: K519TAG, K534TAG, K570TAG, K604TAG, K680TAG, and K809TAG (**Fig. 10a**).

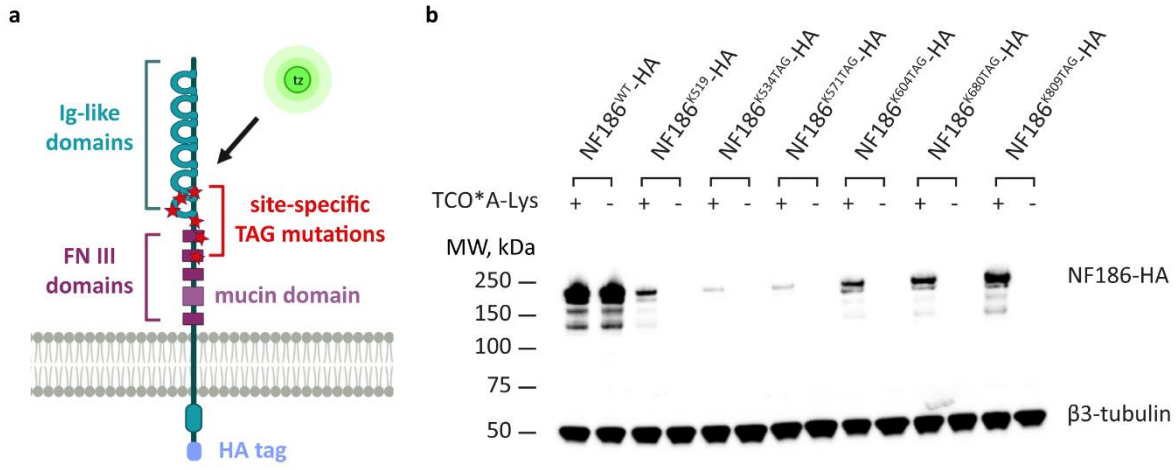

Figure 10. Western blot expression analysis of NF186^{WT}-HA and NF186^{TAG}-HA amber mutants in ND7/23 cell line. a: *A structure of the recombinant NF186-HA with positions of six potential TAG click labeling sites. In order to click label NF186, I introduced the corresponding TAG amber mutations in the extracellular domain of rat Nfasc: K519TAG, K534TAG, K571TAG, K604TAG, K680TAG, and K809TAG (red stars). An HA tag (purple) was moved from N to C terminus, allowing the detection of full-length NF186 and click labeling with ATTO488-tz (green).* ***b:*** *Western blot analyses of the NF186-HA expression. ND7/23 cells were co-transfected with codon-optimized NES PylRS^{AF}/U6-tRNA^{Pyl} and CMV-NF186^{WT}-HA or with one of the CMV-NF186^{TAG}-HA amber mutants (K519TAG, K534TAG, K571TAG, K604TAG, K680TAG, K809TAG). Transfected cells were incubated with or without the unnatural amino acid TCO*A-Lys. A day after transfection, cell lysates were collected, and the expression of NF186 was analyzed with a western blot. Recombinant NF186-HA was detected with anti-HA antibody. The endogenous β3-tubulin detected*

with the anti-β3-tubulin antibody was used as a loading control. The scheme shown in (a) was generated in BioRender.com and published in[75].

To assess if NF186 amber mutants could be expressed and labeled with click chemistry, I co-transfected ND7/23 cells with improved codon-optimized NES PylRS^{AF}/tRNA^{Pyl97} and CMV-NF186$^{WT/TAG}$-HA (**Scheme 7b** and **c**). The transfected cells were incubated with or without TCO*A-Lys. A day after transfection, I collected lysates for western blot analysis (**Fig. 10b**). Alternatively, I click labeled cells, fixed and immunostained them with anti-HA antibody (**Fig. 11** and **12**). Since click labeling of Nav1.6^{K1546TAG}-mGFP with AF647-tz in primary neurons resulted in a high background (**Fig. 8**), I used another cell-impermeable tetrazine dye (ATTO488-tz) instead.

Western blot analysis showed that all six CMV-NF186^{TAG}-HA amber mutants were expressed in the presence of TCO*A-Lys. NF186^{TAG}-HA expression was not detected in the absence of the UAA (**Fig. 10b**). Expression levels of amber mutants were lower compared to the NF186^{WT} (NF186^{K809TAG}>> NF186^{K680TAG}, NF186^{K519TAG}, NF186^{K604TAG}>>>NF186^{K534}, NF186^{K570}). The lower expression of amber mutants in comparison to WT was expected since the GCE is not 100% efficient in mammalian cells.

Confocal microscopy confirmed the results of the western blot analysis (**Fig. 11** and **12**). Furthermore, it revealed that all six amber mutants could be labeled with ATTO488-tz in living ND7/23 cells (**Fig. 12**). Click labeling was not detected in the absence of the UAA (**Fig. 12**), additionally confirming the click labeling specificity.

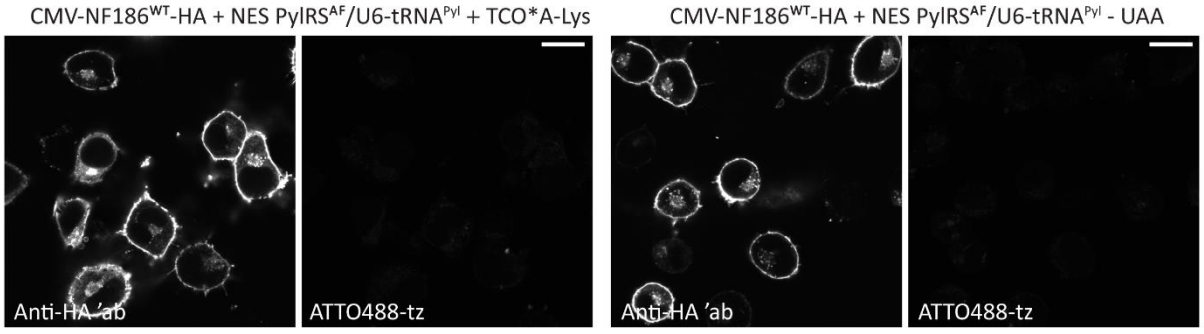

Figure 11. The membrane signal resembling click labeling is not detected in ND7/23 cells co-transfected with NF186^{WT}-HA and the orthogonal translational machinery elements. *Neuronal ND7/23 cells were co-transfected with codon-optimized NES PylRS^{Pyl}/U6-tRNA^{Pyl} and CMV-NF186^{WT}-HA using a Lipofectamine 2000 transfection reagent. Transfected cells were incubated with or without the unnatural amino acid TCO*A-Lys. The following day, cells were click labeled with ATTO488-tz, fixed, immunostained with anti-HA antibody, and imaged with confocal microscopy. The representative images show that WT protein was expressed independently of the TCO*A-Lys. Scale bars: 20 µm. The confocal images shown in the figure were published in[75].*

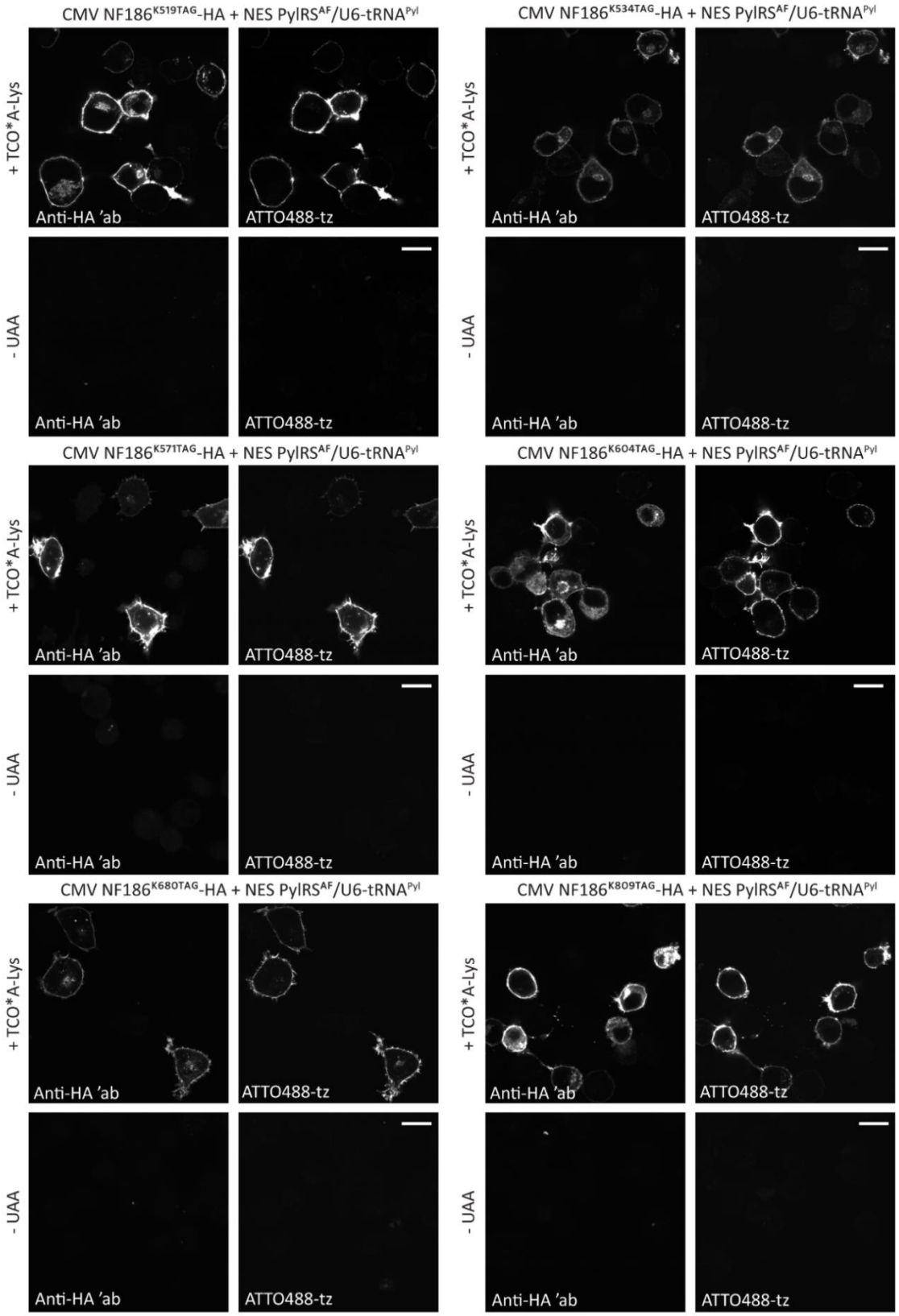

Figure 12. GCE and click labeling of CMV-NF186^{TAG}-HA amber mutants in ND7/23 cell line. *Neuronal ND7/23 cells were co-transfected with codon-optimized NES PylRS^{AF}/U6-tRNA^{Pyl} and one of the CMV-NF186^{TAG}-HA amber*

*mutants (K519TAG, K534TAG, K571TAG, K604TAG, K680TAG, and K809TAG). Transfected cells were incubated with or without the unnatural amino acid TCO*A-Lys. A day after transfection, cells were click labeled with ATTO488-tz, fixed, immunostained with anti-HA antibody, and imaged with confocal microscopy. Representative images show that all six amber mutants were successfully click-labeled in the presence of TCO*A-Lys. Click labeling signal was not detected in the absence of the TCO*A-Lys. Scale bars: 20 μm. The results shown in the figure were published in[75].*

b) Genetic code expansion and click labeling of NF186-HA in primary neurons

After establishing click labeling in neuronal cell lines, I attempted to click label NF186-HA amber mutants (**Fig. 10a**) in primary neurons. To this aim, I first assessed the localization of recombinant NF186-HA in neurons. This was an important step since the overexpression of the AIS components can affect targeting machinery, resulting in their mislocalization[26,96,117,261]. Since all amber mutants except NF186^{K809TAG} had considerably lower expression than the NF186^{WT} (**Fig. 10b**), I reasoned that this would be enough for their proper localization. Hence, I co-transfected rat cortical neurons at DIV 7 with codon-optimized NES PlyRS^{AF}/tRNA^{Pyl} and CMV-NF186$^{WT/TAG}$-HA in the presence of TCO*A-Lys (**Scheme 7b** and **c**). Four days after the transfection, I click labeled neurons with ATTO488-tz and immunostained them with an anti-HA antibody. I observed that all six mutants were successfully click-labeled (data not shown). However, confocal microscopy showed that NF186^{WT}-HA expressed from the CMV promoter was mislocalized in most of the neurons (**Fig. 13a**). The HA signal was mainly detected in soma and processes (**Fig. 13a**). Less frequently, the HA signal was detected exclusively in the AIS (**Fig. 13a**). Although NF186^{TAG}-HA localization was better than the one of WT, the HA signal was ectopically expressed along distal axons in many neurons (**Fig. 13b**).

To further improve the localization of NF186, I replaced the CMV promoter with a weak hNSE promoter (**Scheme 7c**; hNSE-NF186$^{WT/TAG}$-HA) that had been used to lower HA-NF186^{WT} expression[117]. As in all previous experiments, I tested new plasmids in ND7/23 cells before attempting click labeling in neurons. Widefield microscopy confirmed that hNSE promoter reduced the expression of NF186 WT (**Fig. 14a**) and amber mutants (**Fig. 14b**) compared to the CMV promoter. As expected, click labeling was unsuccessful due to the reduced expression of amber mutants (**Fig. 14b**).

After confirming that the hNSE promoter successfully reduced the expression of NF186$^{WT/TAG}$-HA, I expressed and attempted to click label new hNSE-NF186 amber mutants in primary neurons. To this end, I co-transfected DIV 7 rat cortical neurons with NES PylRS^{AF}/tRNA^{Pyl} and hNSE-NF186$^{WT/TAG}$-HA in the presence of TCO*A-Lys. Four days later, I click labeled neurons with ATTO488 tz, fixed, and co-immunostained them with anti-HA and

anti-ankG antibodies. The ankG immunostaining was used to detect the axon initial segments. Confocal microscopy revealed that replacement of the CMV promoter resulted in lower expression of NF186^{WT} and NF186^{TAG} and improved localization to the AIS of most neurons (**Fig. 15** and **16a–b**). Expectedly, due to the overexpression, some neurons still showed ectopic localization of NF186. Such ectopic signals were more frequent in neurons expressing NF186^{WT} or NF186^{K809TAG}. All six mutants were successfully click-labeled when expressed from the hNSE promoter (**Fig. 15** and **16b**). With the ATTO488-tz, there were few dye accumulations compared to Cy5-tz or AF647-tz, and the background was minimal (**Fig. 15** and **16b**).

c) The selection of the most optimal clickable NF186^{TAG}-HA amber mutant in primary neurons

After establishing click labeling of NF186^{TAG}-HA in primary neurons, I wanted to select the best click-labeled amber mutant whose overexpression did not affect the AIS structure. To this end, I transfected neurons with hNSE-NF186$^{WT/TAG}$-HA and immunostained them with anti-HA and anti-ankG antibodies. Afterwards, I imaged immunolabeled neurons with confocal microscopy and measured the AIS lengths in ankG channel using a custom-written MATLAB script[34,248]. Anti-HA immunostaining allowed the identification of neurons expressing NF186-HA, while anti-ankG immunostaining allowed the detection of the total AIS population (AIS of transfected and surrounding untransfected neurons). By comparing the AIS lengths of the neurons expressing NF186-HA and surrounding untransfected ones, I could judge if the NF186-HA overexpression affected the AIS structure (**Fig. 16c**).

I excluded NF186^{K534TAG}-HA and NF186K^{570TAG}-HA amber mutants from the analysis since few neurons expressed those two amber mutants. Furthermore, click labeling of NF186^{K534TAG}-HA and NF186K^{570TAG}-HA was frequently weak (**Fig. 15**). Although NF186^{K809TAG} showed bright click labeling, this mutant was not further analyzed due to its frequent ectopic expression along the distal axon (**Fig. 15**). Therefore, the AIS length was measured in three remaining amber mutants (NF186K^{K519TAG}-HA, NF186^{K680TAG}-HA, NF186^{K604TAG}-HA) and NF186^{WT}HA (**Fig. 16a** and **b**). The quantitative analysis of the AIS length revealed that neurons expressing recombinant NF186$^{WT/TAG}$-HA were slightly longer than surrounding untransfected cells (**Fig. 16c**). However, the differences in the AIS lengths between the NF186-expressing cells and surrounding untransfected cells were not statistically significant (**Fig. 16c, Appendix Table 3**). Hence, the expression of recombinant NF186^{TAG}-HA did not alter the AIS structure significantly.

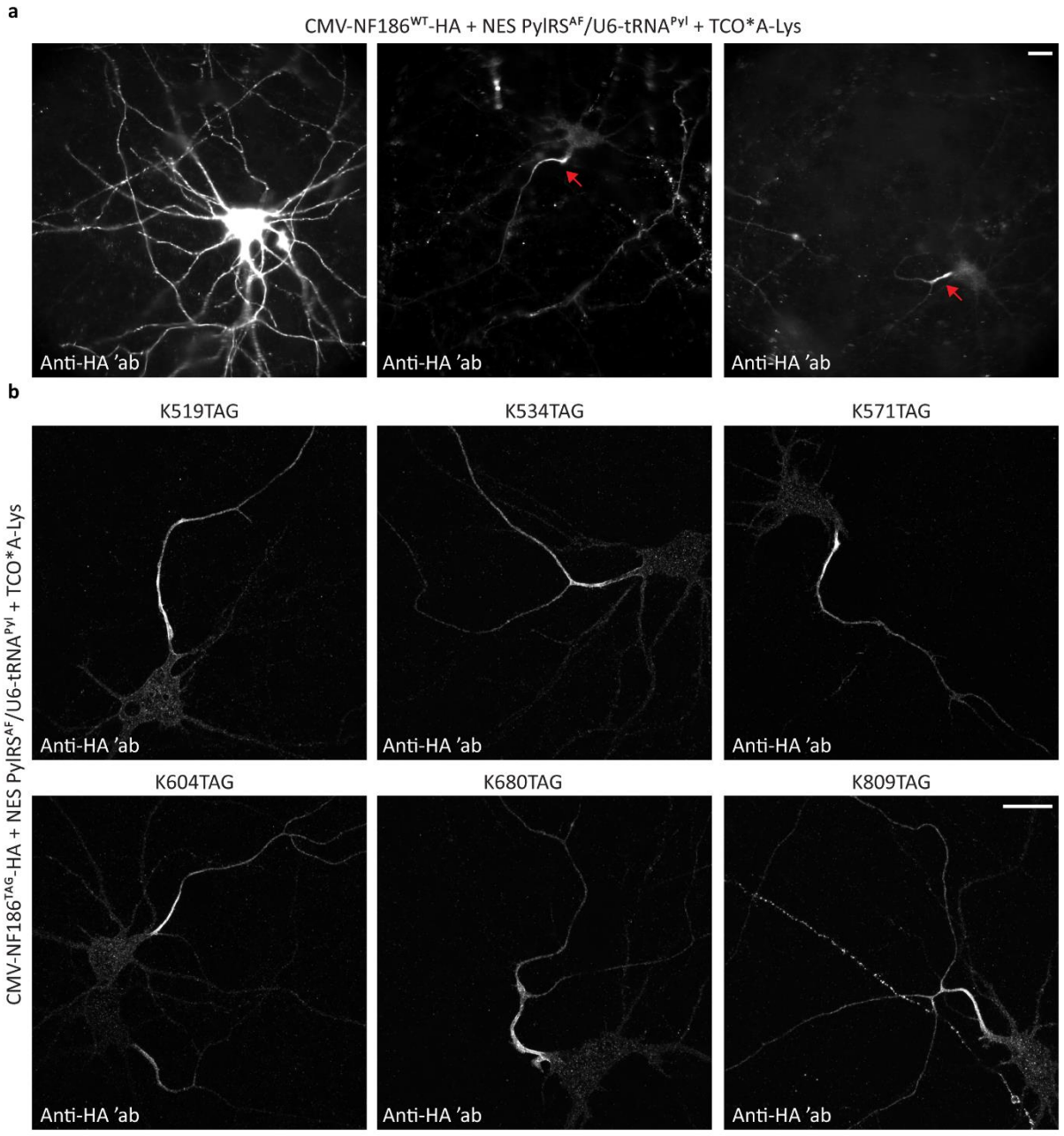

Figure 13. Recombinant NF186-HA under the CMV promoter frequently mislocalizes in primary neurons due to overexpression. *Rat cortical neurons were co-transfected on DIV 7 with codon-optimized NES PylRS^{AF}/U6-tRNA^{Pyl} and with CMV-NF186^{WT}-HA (a) or with one of the CMV-NF186^{TAG}-HA amber mutants (K519TAG, K534TAG, K571TAG, K604TAG, K680TAG, or K809TAG; b). Transfected neurons were incubated with or without the unnatural amino acid TCO*A-Lys. Four days after the transfection, neurons were click labeled with ATTO488-tz, fixed, and immunostained with anti-HA antibody. Afterwards, neurons were imaged with widefield (a) or confocal microscopy (b).* ***a:*** *The representative widefield images show frequent mislocalization of the CMV-NF186^{WT}-HA in primary neurons. Many neurons expressed NF186 in soma and processes (left panel). Some neurons ectopically expressed NF186 in the distal axon (middle panel), while others show proper NF186 localization in the AIS (right panel). Red arrows indicate NF186^{WT} localizing in the distal axon or AIS.* ***b:*** *The representative confocal images show that the reduced expression of*

NF186^{TAG}-HA amber mutants improved their localization. However, NF186 was still ectopically along the distal axon. The Z-stack images in b are shown as maximum intensity projections. Scale bars: 20 µm. The results shown in the figure were published in[75].

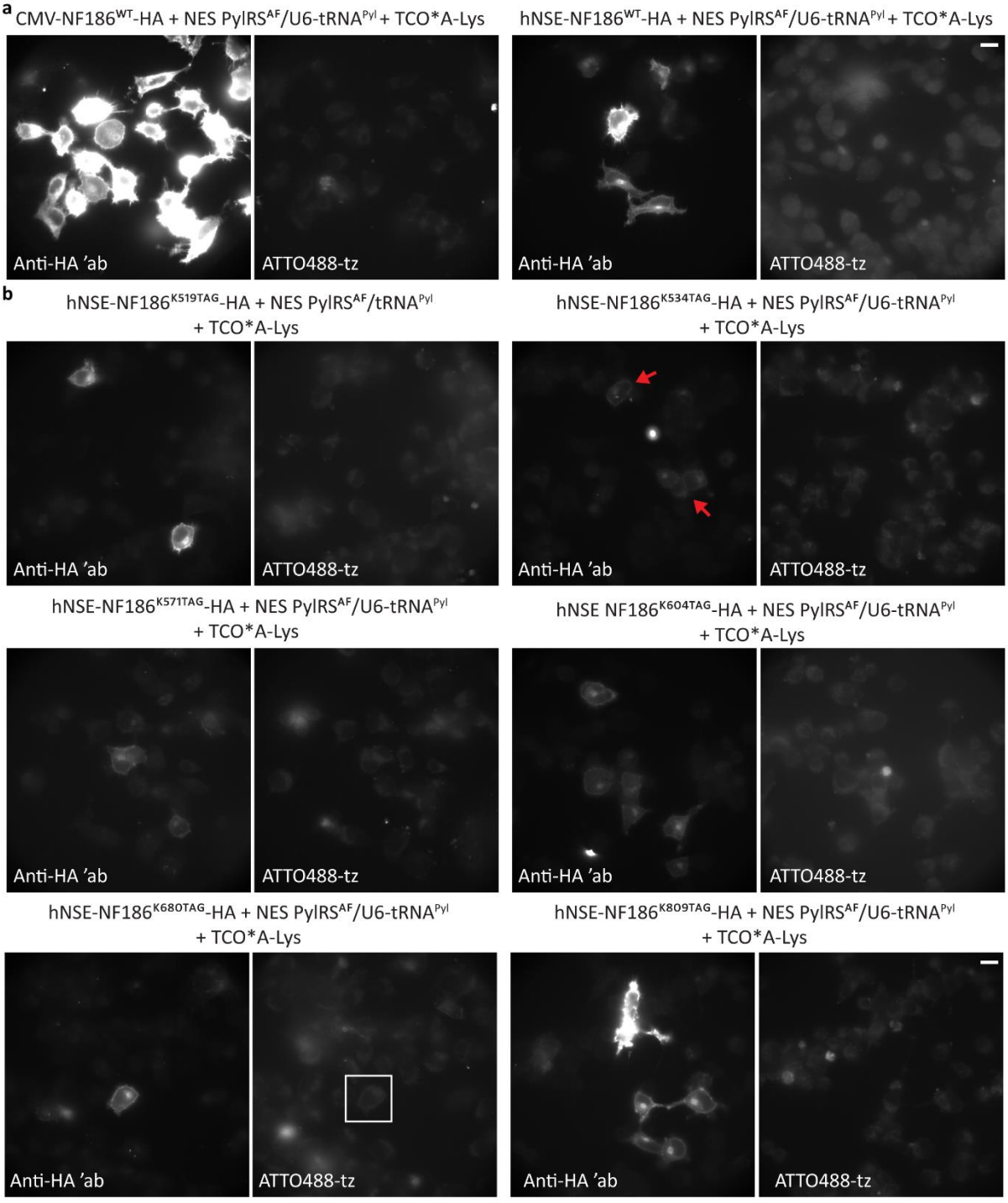

Figure 14. A weak hNSE promoter reduces the expression of NF186-HA, resulting in unsuccessful click labeling in ND7/23 cells. *Neuronal ND7/23 cells were co-transfected with codon-optimized NES PylRS^{AF}/U6-tRNA^{Pyl} and NF186^{WT}-HA under either CMV or hNSE promoter. Alternatively, cells were transfected with one of the*

*hNSE-NF186^{TAG}-HA amber mutants (K519TAG, K534TAG, K571TAG, K604TAG, K680TAG, and K809TAG). Transfected cells were incubated with or without the unnatural amino acid TCO*A-Lys. A day after the transfection, cells were click labeled with ATTO488-tz, fixed, immunostained with anti-HA antibody, and imaged with widefield microscopy.* ***a:*** *A weak hNSE promoter reduced the expression of NF186^{WT}-HA in ND7/23 cells compared to the CMV promoter.* ***b:*** *The hNSE promoter reduced NF186^{TAG}-HA expression, resulting in unsuccessful click labeling. The representative images show rare ND7/23 cells expressing NF186 NF186^{TAG}-HA amber mutants. The white box indicates potentially click-labeled cells, while red arrows indicate cells with weak HA signals. The scale bars: 20 µm.*

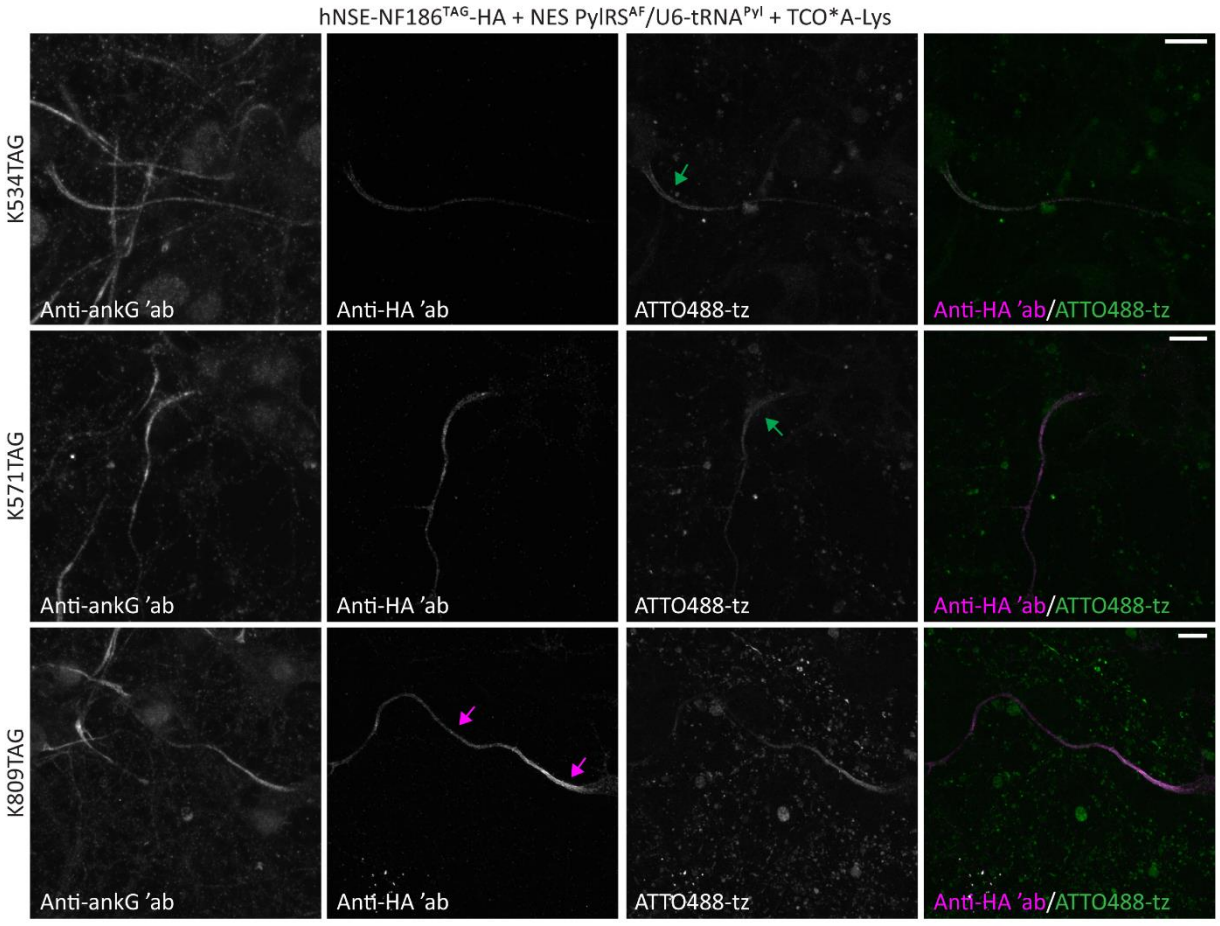

Figure 15. GCE and click labeling of the hNSE-NF186^{TAG}-HA in primary neurons—examples of the amber mutants that were poorly labeled or mislocalized *Rat cortical neurons were co-transfected in DIV 7 with codon-optimized NES PylRS^{AF}/U6-tRNA^{Pyl} and with one of the hNSE-NF186^{TAG}-HA amber mutants (K534TAG, K571TAG, or K809TAG). Transfected neurons were incubated in the presence of the unnatural amino acid TCO*A-Lys. Four days after the transfection, the neurons were click labeled with ATTO488-tz, fixed, and immunostained with anti-HA and anti-ankG antibodies. Afterwards, neurons were imaged with confocal microscopy. Representative images show that the click labeling signal was low (green arrows) in neurons expressing NF186^{K534TAG} (upper panels) and NF186^{K571TAG} (middle panels). Although click labeling of neurons expressing NF186^{K680TAG} was bright, this amber mutant showed frequent ectopic expression along the distal axon (magenta arrows). The Z-stack images are shown as maximum intensity projections in all panels. Scale bars: 10 µm. The results shown in the figure were published in[75].*

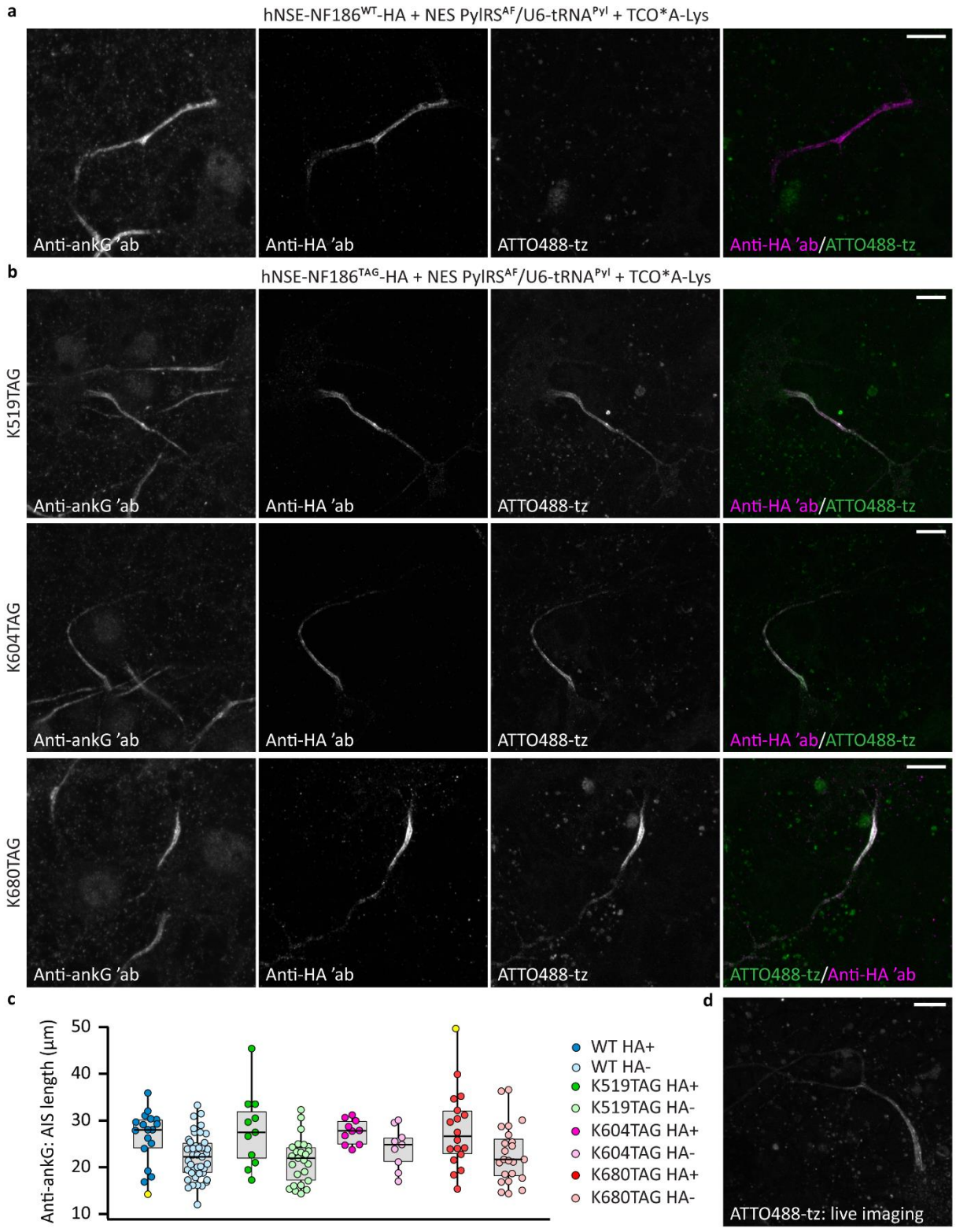

Figure 16. GCE and click labeling of hNSE-NF186^{TAG}-HA in primary neurons—examples of the successfully click-labeled amber mutants localizing in the AIS. *Rat cortical neurons were co-transfected in DIV 7 with codon-optimized NES PylRS^{AF}/U6-tRNA^{Pyl} and with one of the hNSE-NF186^{TAG}-HA amber mutants (K519TAG,*

*K604TAG, or K680TAG). Transfected neurons were incubated in the presence of the unnatural amino acid TCO*A-Lys. Four days after the transfection, the neurons were labeled with ATTO488-tz (a–d), fixed, and immunostained with anti-HA and anti-ankG antibodies (a–c). Afterwards, fixed (a–c) or living (d) neurons were imaged with confocal microscopy.* ***a:*** *Representative image of the neuron expressing NF186^{WT}-HA. The hNSE promoter improved the localization of WT NF186 by reducing its expression level.* ***b:*** *Representative confocal images of three remaining amber mutants expressed from hNSE promoter (K519TAG, K604TAG, or K680TAG) with proper localization and successful click labeling.* ***c:*** *The AIS lengths distribution measured in confocal images (in ankG channel) of neurons expressing WT, K519TAG, K604TAG, or K680TAG NF186-HA (HA+) and corresponding surrounding untransfected cells (HA-). The box plots show the median (the black lines inside the box), the 25th and 75th percentiles (the box boundaries), the single data points (the dots), and the outliers (the yellow dots). The lengths of the whiskers are defined by minimum and maximum data points. The non-parametric Kruskal-Wallis test with Dunn-Bonferroni posthoc did not show any significant differences between the HA+ and HA- AIS lengths for WT and the three clickable mutants (p_{WT} = 0.206, $p_{K519TAG}$ = 0.265 $p_{K604TAG}$ = 1.000, and $p_{K680TAG}$ = 0.605; number (n) of analyzed AIS: $n_{WT\ HA+}$ = 18, $n_{WT\ HA-}$ = 41, $n_{K519TAG\ HA+}$ = 11, $n_{K519TAG\ HA-}$ = 25, $n_{K604TAG\ HA+}$ = 10, $n_{K604TAG\ HA-}$ = 9, $n_{K680TAG\ HA+}$ = 18, and $n_{K680TAG\ HA-}$ = 23). The details of the statistical analysis are provided in Appendix Table 3 and Material and methods.* ***d****: The representative image shows a living neuron expressing NF186^{K680TAG}-HA labeled with ATTO488-tz. The Z-stack images are shown as maximum intensity projections. Scale bars: 10 µm (a, b, and d). The results shown in the figure were published in*[75]*.*

Since the overexpression of neither of the three NF186^{TAG}-HA amber mutants affected the AIS structure, I used additional criteria to select the best one. To this end, I estimated the UAA incorporation rate for NF186K^{K519TAG}-HA, NF186^{K680TAG}-HA, and NF186^{K604TAG}-HA using an iPASS (identification of permissive amber sites for suppression) tool [224]. This tool allowed me to calculate the iPASS score that positively correlates with the UAA incorporation efficiency. This means the iPASS score can predict at which positions the UAAs will be incorporated the most efficiently. The calculated iPASS score for NF186^{K680TAG}-HA was the highest (1.83), followed by the NF186^{K604TAG}-HA (1.63) and NF186^{K519TAG}-HA (1.61). Therefore, the iPASS tool predicted that the UAA should be the most efficiently incorporated into NF186^{K680TAG}. In line with the iPASS prediction of the highly-efficient GCE, the NF186^{K680TAG}-HA amber mutant also showed bright click labeling in most neurons. Due to these reasons, I identified the K680TAG mutant to be the best-performing out of the 3 TAG amber mutants that were measured. Hence, I used K680TAG amber mutant in further experiments. Afterwards, I demonstrated that, in addition to fixed-cell imaging, NF186^{K680TAG}-HA could be imaged in living neurons (**Fig. 16d**).

4.3. Genetic code expansion and click labeling of $Na_V1.6$ in primary neurons

The results described in section 4.3a–c were published in Stajković et al. "Direct fluorescent labeling of NF186 and Na_V1. 6 in living primary neurons using bioorthogonal click chemistry." bioRxiv (2022)[75]*. The electrophysiological recordings described in sections 4.3b and c were performed in collaboration with the laboratory of Prof. Dr. Lerche. My contribution includes*

the $Na_V1.6$ mutagenesis, transfection, and cell preparation for the electrophysiological recordings. Whole-cell patch clamp recordings of neuronal cell lines expressing recombinant $Na_V1.6$-HA and the data analysis (section 4.3.b) were performed by Dr. Yuanyuan Liu, a member of the laboratory of Prof. Dr. Lerche. This section briefly summarizes the results of the electrophysiological recordings of the $Na_V1.6^{K1546TAG}$-HA published in[75]*. Electrophysiological recordings of loss-of-function (LOF) variants in N1E-115-1 cells were performed by the laboratory members of Prof. Dr. Holger Lerche: Dr. Yuanyuan Liu, Hang Lyu, and Nan Zhang (section 4.3.c). These results were also published in*[75].

After optimizing the conditions for the transfection and click labeling of transmembrane AIS component NF186, I attempted to apply the same approach for the click labeling of $Na_V1.6$ in primary neurons. Similarly to NF186, I introduced an HA tag to the C terminus of $Na_V1.6^{WT/TAG}$ (**Scheme 3.** and **6b**). The C-terminal HA tag ensured that only the full-length $Na_V1.6$-HA was detected with an anti-HA antibody. Unlike EGFP, the anti-HA primary antibody in combination with AF555 or AF647-conjugated secondary antibodies allowed me to use clickable ATTO488-tz dye that formed fewer dye accumulations than the AF647-tz. Before attempting to click label $Na_V1.6$ in primary neurons, I validated the functionality of the new $Na_V1.6^{WT/TAG}$-HA constructs in neuronal cell lines.

a) Validation of new $Na_V1.6$-HA constructs in neuronal cell lines

To confirm that the full-length $Na_V1.6$-HA proteins were expressed on the membrane of neuronal cell lines, I co-transfected ND7/23 or N1E-115-1 with an improved codon-optimized NES $PylRS^{AF}/tRNA^{Pyl}$, $Na_V1.6^{WT/TAG}$-HA, and mβ1 and mβ2 auxiliary subunits (**Scheme 6b** and **c**). I used the WT cell lines because it seemed that the quality of β1β2 stable cells was lower after the transfection (cells had slightly changed morphology and their survival rate seemed lower). Transfected cells were click labeled with ATTO488-tz after two days, fixed, and immunostained with anti-HA antibody. Confocal microscopy showed that WT and both amber mutants (K1425TAG and K1546TAG) were expressed in ND7/23 and N1E-115-1 cells (**Fig. 17**). In ND7/23 cells, $Na_V1.6^{WT}$-HA remained mainly in the cytoplasm while a low $Na_V1.6^{WT}$-HA signal was detected on the cell membrane (**Fig. 17a** and **b**). Consistently with the results obtained with

$Na_V1.6$-GFP (**Fig. 1)**, $Na_V1.6^{WT}$-HA surface expression was higher in N1E-115-1 than in the ND7/23 (**Fig. 17a** and **b**).

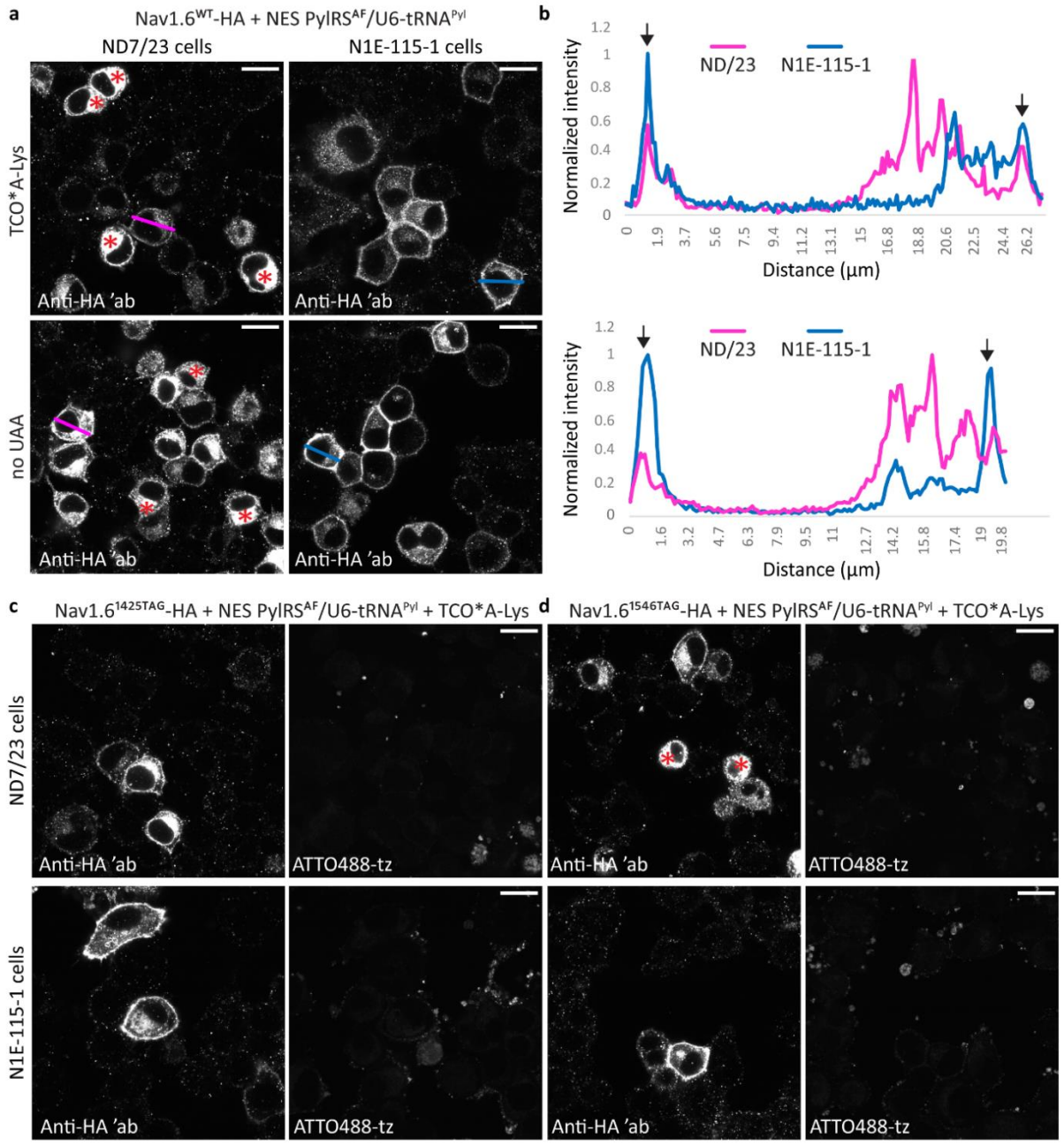

Figure 17. Validation of Nav1.6-HA plasmids in neuronal cell lines. *N1E-115-1 or ND7/23 cells were co-transfected with codon-optimized NES PylRS^{AF}/U6-tRNA^{Pyl}, mβ1 and mβ2 auxiliary subunits, and $Na_V1.6^{WT/TAG}$-HA using a Lipofectamine 3000 reagent. Transfected cells were incubated with or without the unnatural amino acid TCO*A-Lys. Two days after transfection, cells were click labeled with ATTO488-tz, fixed, immunostained with anti-HA antibody, and imaged with confocal microscopy.* ***a:*** *The $Na_V1.6^{WT}$-HA was expressed independently of the TCO*A-Lys in both neuronal cell lines. In ND7/23 cells, $Na_V1.6^{WT}$-HA frequently remained in the cytosol (red asterisks), while a low signal was observed on the cell surface. On the contrary, in N1E-115-1 cells, $Na_V1.6^{WT}$-HA was mainly detected on the cell surface.* ***b:*** *The graphs show the normalized line profile fluorescence intensity measurements for $Na_V1.6^{WT}$-HA signals*

*in the cytosol and cell surface. The measurements were performed in ND7/23 and N1E-115-1 cells (pink line and blue lines, respectively) shown in a. The blue and magenta lines indicate cells and regions of the cells used for the line profile measurements. The line profiles were determined for cells incubated with (upper graph) or without (lower graph) TCO*A-Lys after the transfection. The black arrows in the graphs indicate the membrane $Na_V1.6^{WT}$-HA signal.* ***c:*** *Click labeling of the ND7/23 and N1E-115-1 cells expressing $Na_V1.6^{K1425TAG}$-HA with ATTO488-tz dye was unsuccessful due to the insufficient expression of the channels on the cell surface.* ***d:*** *Click labeling of the ND7/23 and N1E-115-1 cells expressing $Na_V1.6^{K1546TAG}$-HA with ATTO488-tz dye was unsuccessful due to the insufficient expression of the channels on the cell surface. Scale bars: 20 µm (a, c, and d). The results shown in the figure (a—upper panels, b—upper graph, c, and d) were published in[75].*

Similar to what I observed in experiments involving $Na_V1.6$-P2A-GFP (**Fig. 3b** and **4b)**, the expression levels of $Na_V1.6$-HA amber mutants were lower than the WT (**Fig. 17c**). Click labeling of new $Na_V1.6^{TAG}$-HA constructs in neuronal cell lines was unsuccessful most likely due to the insufficient channel expression on the membrane (**Fig. 17c**). Therefore, I set out to click label $Na_V1.6^{TAG}$-HA in primary neurons. In parallel with click labeling and microscopy, the electrophysiological recordings of new $Na_V1.6^{Y371C}$-HA plasmids expressed in neuronal cell lines were repeated. However, in the meantime, I found out that the click labeling of K1546TAG in neurons is brighter than the labeling of K1425TAG. Therefore, only the K1546TAG amber mutant was re-measured with the whole-cell patch clamp (this will be discussed in detail in the following section).

b) The selection of the most optimal new clickable $Na_V1.6^{TAG}$-HA amber mutants

After validating new $Na_V1.6$-HA plasmids in neuronal cell lines, I attempted click labeling of sodium channels in primary neurons (**Fig. 18**). I co-transfected rat cortical neurons at DIV 8 with an improved codon-optimized NES $PylRS^{AF}/tRNA^{Pyl}$ and $Na_V1.6^{WT/TAG}$-HA in the presence or absence of TCO*A-Lys (**Scheme 6b**). Four days after the transfection, neurons were click labeled with ATTO488-tz (**Fig. 18a**), fixed, and immunostained with an anti-HA antibody (**Fig. 18b** and **c**). Alternatively, living neurons were imaged immediately upon click labeling (**Fig. 18c,** right panels). Confocal microscopy showed that WT and both clickable TAG $Na_V1.6$-HA were expressed in the AIS. Both amber mutants were click labeled with ATTO488-tz, albeit the expression level and the labeling efficiency of K1425TAG were lower than the K1546TAG. Live imaging of click-labeled neurons was also successful. However, since the quality of $Na_V1.6^{K1425TAG}$-HA click labeling was low, I had difficulties identifying living neurons that expressed this mutant. Expectedly, only WT $Na_V1.6$-HA was expressed in the absence of TCO*A-Lys, while amber mutants were not (**Fig. 19**). The click labeling was not detected in WT or amber mutant-transfected neurons in the absence of the UAAs (**Fig. 19**).

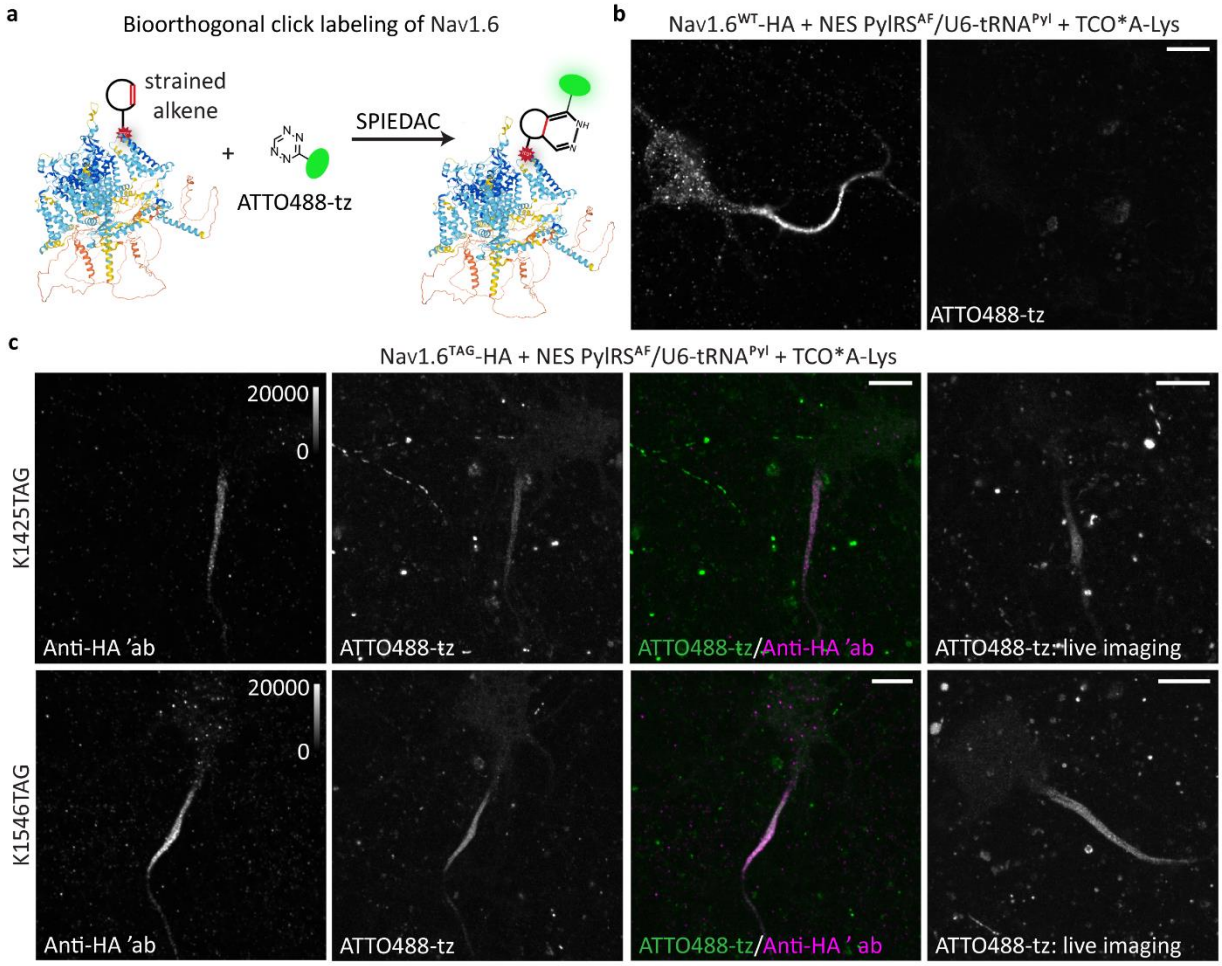

Figure 18. GCE and click labeling of $Na_V1.6^{TAG}$-HA in primary neurons. a: *A scheme depicting labeling of $mNa_V1.6^{K1546TAG}$ amber mutant with ATTO488-tz via bioorthogonal SPIEDAC click reaction. The structure of $mNa_V1.6$ was generated in AlphaFold Protein Structure Database[262,263] and modified in BioRender.com.* ***b–c:*** *Rat cortical neurons were co-transfected on DIV 8 with codon-optimized NES $PylRS^{AF}$/U6-$tRNA^{Pyl}$ and $Na_V1.6^{WT/TAG}$-HA using a Lipofectamine 2000 transfection reagent. The transfected neurons were incubated with the unnatural amino acid TCO*A-Lys. Four days after the transfection, cells were click labeled with ATTO488-tz, fixed, immunostained with anti-HA antibody, and imaged with confocal microscopy. Alternatively, living neurons were imaged immediately upon click labeling with confocal microscopy (right panels in c).* ***b****: Rat cortical neurons co-expressing $Na_V1.6^{WT}$-HA and the orthogonal translational machinery. The confocal images are shown as single planes.* ***c:*** *Both $Na_V1.6^{TAG}$-HA amber mutants (K1425TAG and K1546TAG) were successfully expressed and click labeled with ATTO488-tz in fixed and living neurons. The K1546TAG amber mutant was expressed at a higher level and exhibited brighter click labeling than the K1425TAG. The Z-stack images are shown as maximum intensity projections. The brightness and contrast of the panels showing the HA channel were linearly adjusted to show the 0–20,000 display range, as indicated by the look-up table (LUT) intensity scale bars. LUT intensity scale bars show the minimum and maximum grey values. The brightness and contrast of the panels showing the click channels were also linearly adjusted to show the 100–3100 display ranges (LUT scale bars were shown). Scale bars: 10 µm. The panels in b and c (except for the panel showing a living neuron expressing K1425TAG) were published in[75].*

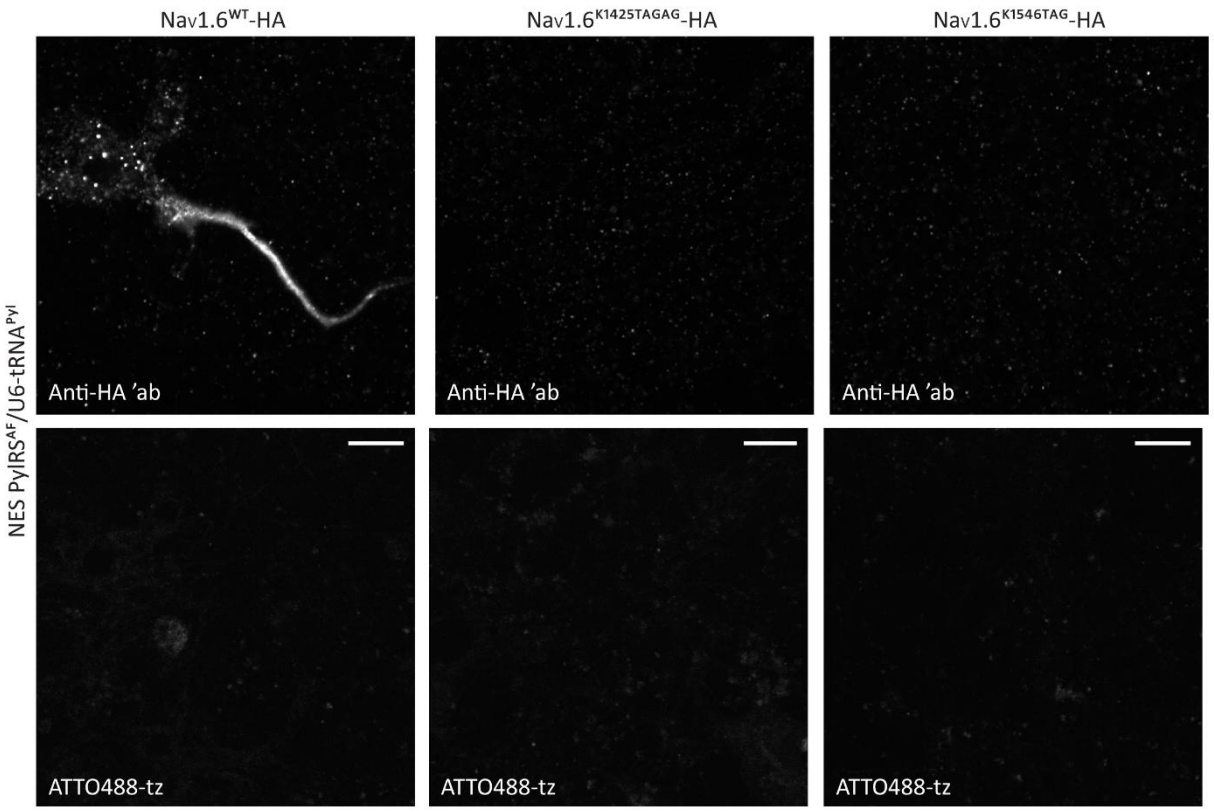

Figure 19. The Nav1.6^{TAG}-HA amber mutants are not expressed and click labeled without the unnatural amino acid TCO*A-Lys in primary neurons. *Rat cortical neurons were co-transfected on DIV 8 with codon-optimized NES PylRS^{AF}/U6-tRNA^{Pyl} and Nav1.6$^{WT/TAG}$-HA using a Lipofectamine 2000 transfection reagent. The transfected neurons were incubated without the unnatural amino acid TCO*A-Lys. Four days after the transfection, cells were click labeled with ATTO488-tz, fixed, immunostained with anti-HA antibody, and imaged with confocal microscopy. As expected, only Nav1.6^{WT}-HA was expressed in the absence of TCO*A-Lys, while click labeling was absent in all the conditions. Scale bars: 10 µm. The single plane confocal images shown in the figure were published in[75].*

Since the initial electrophysiological recordings showed that the biophysical properties (e.g., fast inactivation) of the K1425TAG were more similar to WT than the ones of K1546TAG, I attempted to increase its GCE efficiency. To this aim, I probed a plasmid that contained four copies of improved orthogonal tRNA^{M15} (**Scheme 6b, Fig. 20**)[151] and alternative transfection reagents (**Fig. 21**). I also tested two additional amber mutants, Nav1.6^{K1675TAG} and Nav1.6^{K1224TAG} (**Fig. 22).** To test the improved orthogonal tRNA^{M15}, I co-transfected, click labeled (fixed and immunostained for fixed-cell imaging), and imaged rat cortical neurons as described above. The difference was that I used a plasmid containing codon-optimized NES PylRS^{AF} and 4xtRNA^{M15}

(NES PylRS^{AF}/4xtRNA^{M15}; **Fig. 20**)[97,241]. Confocal microscopy of fixed and living neurons showed no apparent improvement in click labeling efficiency compared to tRNA^{Pyl} (**Fig. 18c**).

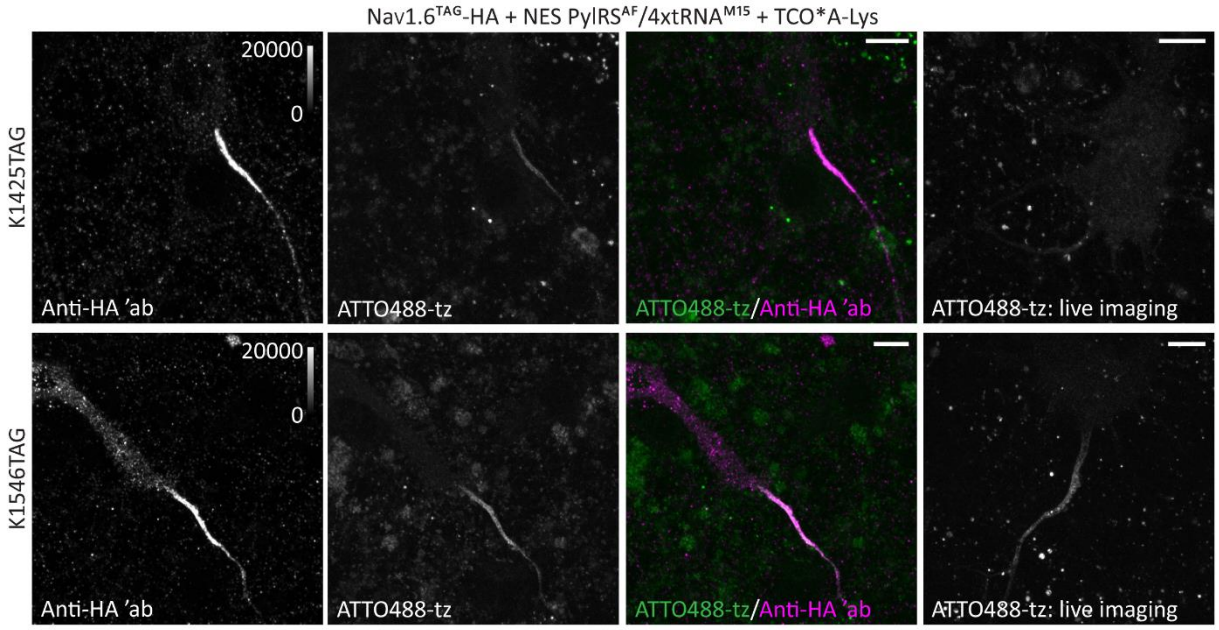

Figure 20. The orthogonal tRNA^{M15} does not improve expression and click labeling of the Na$_V$1.6^{TAG}-HA amber mutants in primary neurons. *Rat cortical neurons were co-transfected on DIV 8 with codon-optimized NES PylRS^{AF}/4xU6-tRNA^{M15} and one of the Na$_V$1.6^{TAG}-HA amber mutants (K1425TAG or K1546TAG) using Lipofectamine 2000 transfection reagent. The transfected neurons were incubated with the unnatural amino acid TCO*A-Lys. Four days after the transfection, cells were click labeled with ATTO488-tz, fixed, immunostained with an anti-HA antibody, and imaged with confocal microscopy. Alternatively, living neurons were imaged immediately upon click labeling with confocal microscopy (right panels). The representative images show that both Na$_V$1.6^{TAG}-HA amber mutants (K1425TAG and K1546TAG) were successfully expressed and click labeled with ATTO488-tz. However, 4xU6-tRNA^{M15} did not seem to improve the expression and click labeling efficiency of Na$_V$1.6^{TAG}-HA compared to U6-tRNA^{Pyl}. The Z-stack images are shown as maximum intensity projections. For comparison of 4xU6-tRNA^{M15} and U6-tRNA^{Pyl}, the brightness and the contrast of the panels showing the HA channel were linearly adjusted to show the same display range (0–20,000) as shown in Figure 18 [as indicated by the look-up table (LUT) intensity scale bars]. The LUT intensity scale bars show the minimum and maximum grey values. The brightness and contrast of the panels showing the click channels were also linearly adjusted to show the 100–3100 display ranges (as in Figure 18). The scale bars: 10 µm.*

Next, I tested Lipofectamine 3000 transfection reagent, which had been reported to improve transfection efficiency compared to Lipofectamine 2000[264]. I also observed slightly higher expression when Lipofectamine 3000 was used for transfection in neuronal cell lines. Therefore, I transfected rat cortical neurons with codon-optimized NES PylRS^{AF}/tRNA^{Pyl} and Nav1.6^{TAG}-HA, click labeled, and immunostained in the same way as for Lipofectamine 2000. I tested different protocols and different ratios of DNA to Lipofectamine 3000 reagent. Confocal microscopy

showed that the manufacturer's Lipofectamine 3000 transfection protocol worked the best (details are provided in Materials and methods), resulting in the improved expression and bright click labeling of the amber mutants (**Fig. 21**). However, when Lipofectamine 3000 was used, I observed fewer neurons expressing $Na_V1.6^{TAG}$-HA compared to Lipofectamine 2000 transfection (~5 vs. ~16 neurons per eight-well Lab-Tek II chambered cover glasses, respectively). Despite the improved expression level of the amber mutant in individual neurons, providing enough AIS for quantitative analysis and live cell imaging studies was challenging due to the low number of transfected neurons.

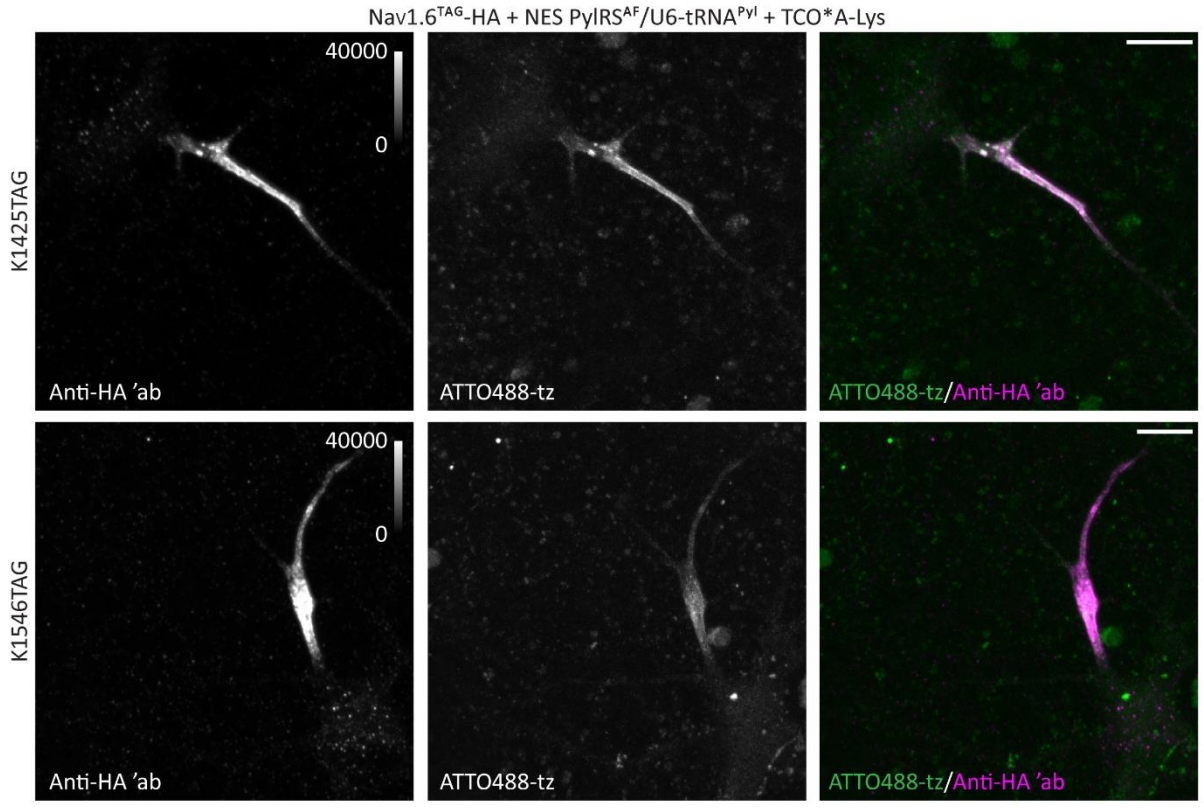

Figure 21. Optimizing the expression and click labeling of $Na_V1.6^{TAG}$-HA amber mutants in primary neurons with Lipofectamine 3000 transfection reagent. *Rat cortical neurons were co-transfected on DIV 8 with codon-optimized NES $PylRS^{AF}$/U6-$tRNA^{Pyl}$ and one of the $Na_V1.6^{TAG}$-HA amber mutants (K1425TAG or K1546TAG) using an alternative Lipofectamine 3000 transfection reagent. The transfected neurons were incubated with the unnatural amino acid TCO*A-Lys. Four days after the transfection, cells were click labeled with ATTO488-tz, fixed, immunostained with anti-HA antibody, and imaged with confocal microscopy. The representative images show that Lipofectamine 3000 improved the expression and click labeling of $Na_V1.6^{TAG}$-HA amber mutants (K1425TAG and K1546TAG). The Z-stack images are shown as maximum intensity projections. The brightness and the contrast of the panels showing the HA channel were linearly adjusted to show the (0–40,000) display range, as indicated by the look-up table (LUT) intensity scale bars. The LUT intensity scale bars show the minimum and maximum grey values. The brightness and contrast of the panels showing the click channels were also linearly adjusted to show the 100–3100*

display ranges (as in Figure 18; LUTs are not shown). Scale bars: 10 µm. The panels showing $Na_V1.6^{K1425TAG}$-HA were published in[75].

Finally, I attempted click labeling of two $Na_V1.6$-HA amber mutants (K1224TAG and K1675TAG), which showed more robust expression in cell lines than the other spare amber mutants (R914TAG, K1675TAG, and K1731TAG; **Scheme 3**). I transfected DIV 8 rat cortical neurons with Lipofectamine 2000, click labeled, and immunostained them as described for K1546TAG and K1425TAG. Confocal microscopy showed that few neurons expressed $Na_V1.6^{K1224TAG}$-HA, while I found no neurons that expressed $Nav1.6^{K1675TAG}$-HA.

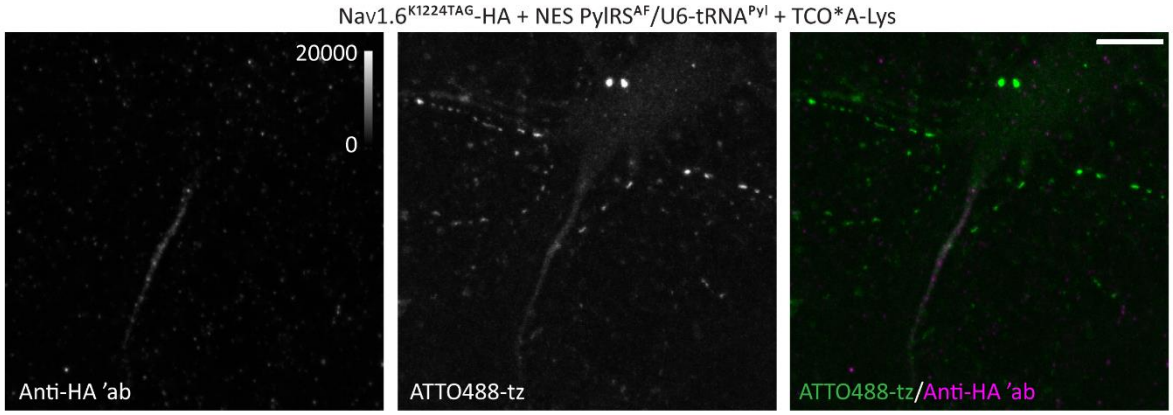

Figure 22. GCE and click labeling of the additional $Na_V1.6^{K1224TAG}$-HA amber mutant in primary neurons. *Rat cortical neurons were co-transfected on DIV 8 with codon-optimized NES $PylRS^{AF}$/U6-$tRNA^{Pyl}$ and $Na_V1.6^{K1224TAG}$-HA amber mutant using Lipofectamine 2000 transfection reagent. The transfected neurons were incubated with the unnatural amino acid TCO*A-Lys. Four days after the transfection, cells were click labeled with ATTO488-tz, fixed, immunostained with anti-HA antibody, and imaged with confocal microscopy. The representative images show that click labeling of $Na_V1.6^{K1224TAG}$-HA amber mutant was successful. The Z-stack images are shown as maximum intensity projections. The brightness and the contrast of the panel showing the HA channel were linearly adjusted to show the same display range (0–20,000) as shown in Figure 18 [as indicated by the look-up table (LUT) intensity scale bars]. The LUT intensity scale bars show the minimum and maximum grey values. The brightness and contrast of the panels showing the click channels were also linearly adjusted to show the 100–3100 display ranges (as in Figure 18; LUT is not shown). Scale bars: 10 µm.*

Since click labeling of $Nav1.6^{K1224TAG}$-HA was pale, I did not test this mutant further (**Fig. 22**). Instead, I sought alternative ways to improve expression levels of amber mutants and their labeling efficiency (particularly K1425TAG). To this aim, I used viral-based vectors to deliver orthogonal translational machinery to primary neurons. Details on the viral vectors are described in **Sections 4.4a** and **b**.

After demonstrating that click labeling of $Na_V1.6$-HA in primary neurons was possible, I wanted to assess whether the TCO*A-Lys incorporation and the overexpression of recombinant $Na_V1.6$ affected the AIS structure (**Fig. 23a**). For the AIS quantitative analysis, neurons were transfected, click labeled, and immunostained with anti-HA and anti-ankG antibodies (details are provided in Materials and Methods; **Fig. 23b**). Similarly to NF186, I compared the AIS length of the neurons expressing $Na_V1.6^{TAG}$-HA to the AIS length of the surrounding untransfected neurons by using a custom-written MATLAB script[34,248]. The anti-HA antibody was used to identify neurons that expressed $Na_V1.6^{TAG}$-HA [HA positive (+)], while the anti-ankG was used to identify total AIS [HA+ and HA negative (-)]. Contrary to the NF186, I measured only the AIS length of the neurons expressing amber mutants, as I observed no mislocalization of $Nav1.6^{WT}$-HA. Quantitative measurements of the AIS showed that its length was not significantly affected by the overexpression of recombinant $Na_V1.6^{TAG}$-HA (**Fig. 23b, Appendix Table 4**).

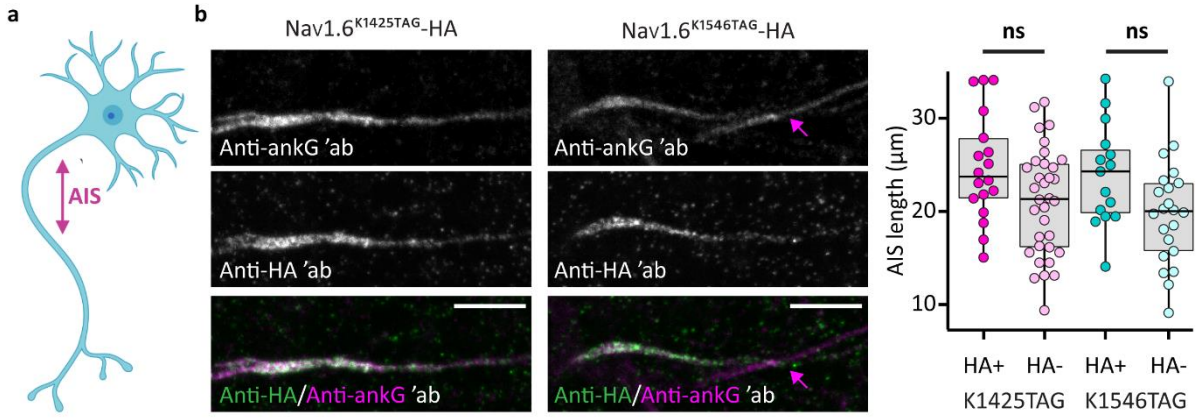

Figure 23. The TCO*A-Lys incorporation and the overexpression of $Na_V1.6^{TAG}$-HA in primary neurons do not alter the AIS structure. a: *A schematic representation of the cultured primary neuron with annotated AIS.* ***b:*** *Rat cortical neurons were co-transfected on DIV 8 with codon-optimized NES $PylRS^{AF}$/U6-$tRNA^{Pyl}$ and one of the $Na_V1.6^{TAG}$-HA amber mutant (K1425TAG and K1546TAG) using Lipofectamine 2000 transfection reagent. The transfected neurons were incubated with the unnatural amino acid TCO*A-Lys. Four days after the transfection, cells were click labeled with ATTO488-tz, fixed, immunostained with anti-HA and anti-ankG antibodies, and imaged with confocal microscopy. The representative images show co-localization of the recombinant $Na_V1.6^{TAG}$-HA (anti-HA immunostaining) with AIS marker ankG (anti-ankG immunostaining). As expected, the localization of recombinant $Na_V1.6$ was more robust in the distal AIS. The Z-stack images are shown as maximum intensity projections. Scale bars: 10 µm. The graph shows the distribution of the AIS lengths measured in the confocal images of the anti-ankG immunostained neurons expressing either $Na_V1.6^{K1425TAG}$-HA or $Na_V1.6^{K1546TAG}$-HA (HA+) and corresponding surrounding untransfected cells (HA-). The box plots indicate the median (the black lines inside the box), the 25^{th} and 75^{th} percentiles (the box boundaries), and the single data points (the dots). The minimum and maximum data points define the whiskers' lengths. One-way ANOVA with Tukey posthoc did not show significant differences between the HA+ and HA- AIS lengths ($p_{K1425TAG} = 0.124$, $p_{K1546TAG} = 0.136$; number (n) of analyzed cells: $n_{K1425TAG\ HA+} = 18$, $n_{K1425TAG\ HA-} = 34$, $n_{K1546TAG\ HA+} = 15$, and $n_{K1546TAG\ HA-} = 22$). The details of the statistical analysis are shown in*

Appendix Table 4. and the Materials and methods. The scheme (a) was generated in Biorender.com.The results shown in figure (b) were published in[75].

I then attempted to assess if the overexpression of recombinant $Na_V1.6^{TAG}$-HA changed the number of sodium channels in transfected neurons compared to untransfected ones by measuring $Na_V1.6$ fluorescence intensity. To this aim, I transfected neurons with $Na_V1.6^{TAG}$-HA and immunostained them with anti-HA and anti-$Na_V1.6$ antibodies. The anti-HA antibody was used to identify neurons that expressed $Na_V1.6^{TAG}$-HA (HA+), while anti-$Na_V1.6$ was used to identify the total population of 1.6 sodium channel isoform. However, due to the very low anti-$Na_V1.6$ signal, I could not acquire a sufficient number of bright neurons that could be used for quantitative measurements of the AIS fluorescence intensity.

Finally, I wanted to validate the functionality of the new $Na_V1.6^{TAG}$-HA constructs (**Fig. 24**). Since $Nav1.6^{K1546TAG}$-HA click labeling in neurons was brighter than the $Nav1.6^{K1425TAG}$-HA, the biophysical parameters of this mutant were assessed. To this aim, I co-transfected $N1E\text{-}115\text{-}1^{WT}$ cells with codon-optimized NES $PylRS^{AF}/tRNA^{Pyl}$, TTXr versions of $Na_V1.6^{WT/K1546TAG,\ Y371C}$-HA, and with a plasmid that bore mβ1, mβ2 and mGFP genes (**Scheme 6b** and **c**). The mGFP was used to identify cells expressing mβ1 and mβ2. TTX ensured that only Na^+ currents originating from recombinant $Na_V1.6$ would be recorded. The electrophysiological recordings detected a small significant shift (~2.8 mV) in the inactivation curve of the K1546TAG amber mutant compared to the WT (**Fig. 24c, Appendix Table 5**). Since this difference was smaller than the one observed for P2A-EGFP constructs (~5.6 mV) and click labeling of K1546TAG was bright, it was possible to use this amber mutant in further experiments.

I then attempted to further improve $Na_V1.6^{K1546TAG}$ click labeling in neurons by testing alternative, more stable UAAs, such as endo-BCN-Lys^{265} and TCO4en/eq-Lys^{198} (**Fig. 25**). Confocal microscopy revealed that both UAAs were successfully incorporated into $Nav1.6^{K1546TAG}$. Likewise, both UAAs were successfully click-labeled with ATTO488-tz (**Fig. 25**). However, neither of those two seemed to be better than the TCO*A-Lys. The endo-BCN-Lys produced frequent somatic background (**Fig. 25a**). When TCO4en/eq-Lys was used, only a few neurons expressing $Na_V1.6^{TAG}$ were detected (**Fig. 25b**) probably due to the incompatibility of the NES $PylRS^{AF}/tRNA^{Pyl}$ with this UAA.

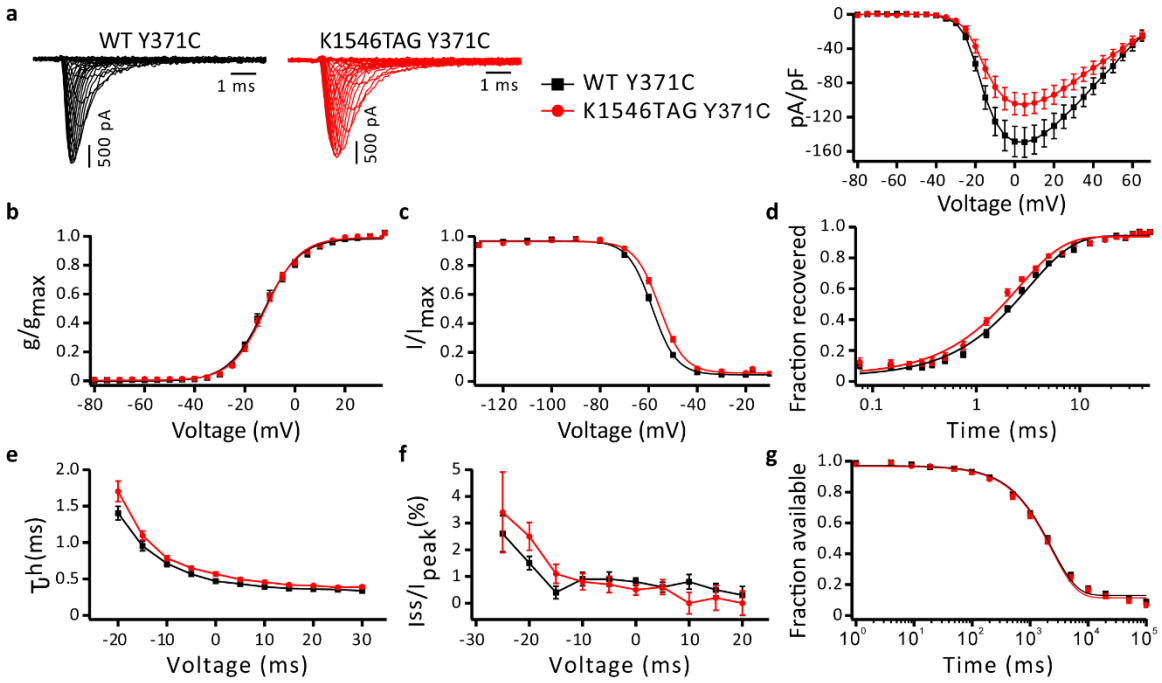

Figure 24. Biophysical characterization of $Na_V1.6^{K1546TAG}$-HA in N1E-115-1 cell line. *Neuronal N1E-115-1 cell line was co-transfected with codon-optimized NES $PylRS^{AF}$/U6-$tRNA^{Pyl}$, multigene containing mβ1, mβ2, and mGFP, and TTX-resistant Y371C versions of $Na_V1.6$-HA WT or K1546TAG amber mutant using Lipofectamine 3000 transfection reagent. Transfected cells were incubated in the presence of the unnatural amino acid TCO*-Lys for two days. Afterwards, cells were re-seeded and recorded via whole-cell patch clamp.* ***a:*** *Representative Na^+ current traces obtained from N1E-115-1 cells that expressed either $Na_V1.6^{WT,\ Y371C}$-HA (black) or $Na_V1.6^{K1546TAG,\ Y371C}$-HA (red). Peak Na^+ current densities normalized by the cell capacitance were plotted versus voltage (n_{WT} = 20 and $n_{K1546TAG}$ = 18).* ***b:*** *Voltage-dependence of the activation (n_{WT} = 20 and $n_{K1546TAG}$ = 18).* ***c:*** *Voltage-dependence of the fast inactivation (n_{WT} = 20 and $n_{K1546TAG}$ = 17). The K1546TAG amber mutation caused a significant depolarizing shift of voltage-dependent fast inactivation. The lines represent the Boltzmann functions fit to the data points (b, c).* ***d:*** *Time course of recovery from fast inactivation at -100 mV (n_{WT} = 20 and $n_{K1546TAG}$ = 18). The K1546TAG amber mutation significantly accelerated the recovery from fast inactivation.* ***e:*** *Voltage dependence of the major time constant of fast inactivation τh. K1546TAG amber mutation significantly delayed the transition from activation to fast inactivation.* ***f:*** *Voltage dependence of the persistent current (I_{ss}/I_{peak}).* ***g:*** *Entry into slow inactivation. The lines represent fits of a first-order exponential function to the data points. Mean ± SEMs are shown. Further details on the statistical analysis are provided in Appendix* ***Table 5*** *and Materials and methods. The results shown in the figure were published in[75].*

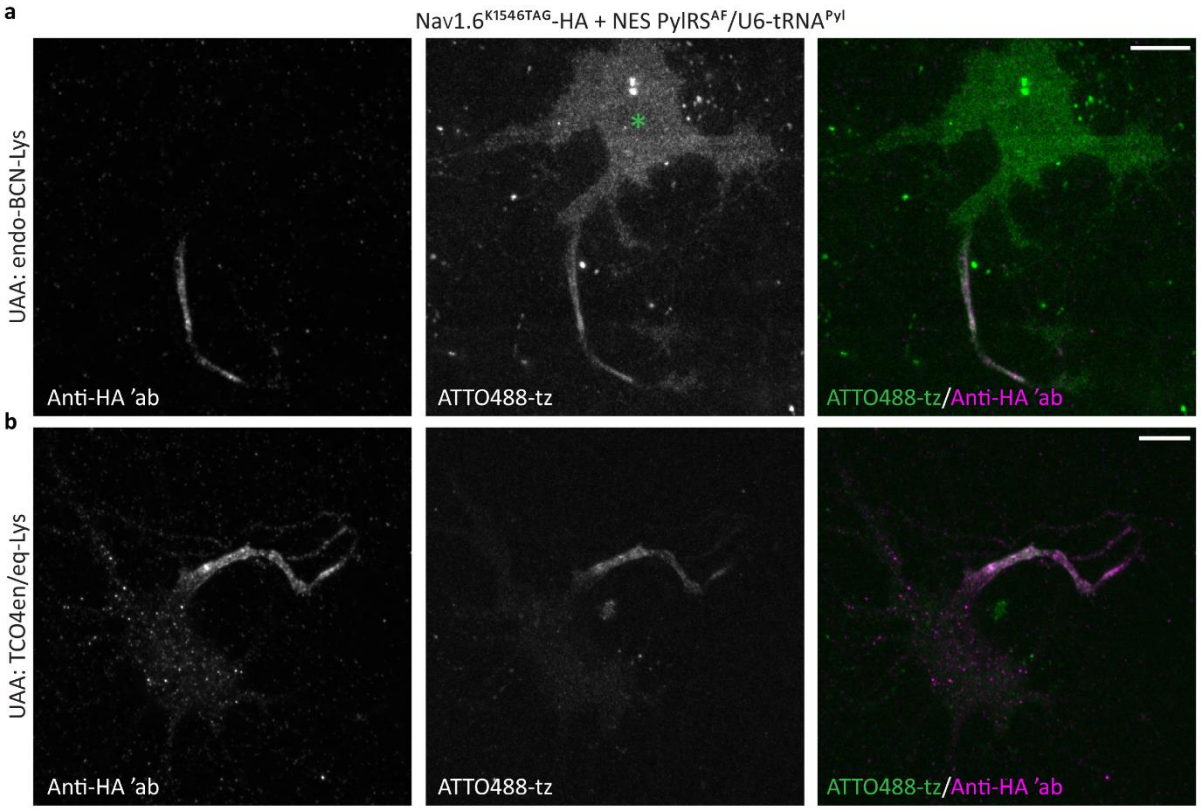

Figure 25. The alternative unnatural amino acids provide a successful GCE and click labeling of the $Na_V1.6^{K1546TAG}$-HA in primary neurons. *Rat cortical neurons were co-transfected on DIV 8 with codon-optimized NES $PylRS^{AF}$/U6-$tRNA^{Pyl}$ and $Na_V1.6^{K1546TAG}$-HA amber mutant using Lipofectamine 2000 transfection reagent. The transfected neurons were incubated with unnatural amino acid endo-BCN-Lys (a) or TCO4en/eq-Lys (b). Four days after the transfection, cells were click labeled with ATTO488-tz, fixed, immunostained with anti-HA antibody, and imaged with confocal microscopy.* ***a:*** *The representative images show that click labeling of incorporated endo-BCN-Lys was successful, albeit there was a frequent background in the soma (indicated by a green asterisk).* ***b:*** *The representative images show that click labeling of incorporated TCO4en/eq-Lys was successful. However, there were only a few HA+ and click-labeled neurons. The Z-stack images are shown as maximum intensity projections. Scale bars: 10 µm.*

c) Application of click labeling for localization studies of pathogenic $Na_V1.6$ variants

After I successfully established $Na_V1.6^{TAG}$-HA click labeling in neurons and confirmed the functionality of the K1546TAG amber mutant by whole-cell patch clamp, I wanted to demonstrate the applicability of this approach for localization studies of pathogenic $Na_V1.6$ variants. Recently, new generalized epilepsy-causing mutations of the human (*h)SCN8A* gene (I1654N and T1787P) have been reported[13]. Both mutations showed a loss-of-function effect (LOF), i.e., they caused loss of Na^+ currents in neuronal cell lines and altered firing in mouse hippocampal neurons. However, due to a lack of suitable labeling approaches, it remains elusive if the LOF effect was caused by reduced expression of mutated channels on the neuronal surface or impaired function of the $Na_V1.6$. To answer this question, I used click labeling to study the localization of LOF $Na_V1.6$ variants.

To use the click labeling to study the localization of LOF variants, I introduced LOF mutations that corresponded to the ones described for the *hSCN8A* (I1652N and T1785P) into clickable *mSCN8A*$^{K1546TAG,\ Y371C,}$ and *mSCN8A*$^{K1425TAG,\ Y371C}$ genes. Before starting the microscopy studies, I wanted to confirm that these mutations had an equivalent LOF effect on the mouse $Na_V1.6$ to the one they have on the human $Na_V1.6$. Hence, I co-transfected N1E-115-1^{WT} cells with codon-optimized NES PylRS^{AF}/tRNA^{Pyl}, control (TAG-only) or LOF (TAG and pathogenic mutation) $Na_v1.6^{Y371C}$-HA plasmids, and multigene construct containing mGFP, β1, and β2 genes. The whole-cell patch clamp recordings of $Na_V1.6$ currents in N1E-115-1^{WT} cells confirmed that both LOF variants caused a significant reduction of Na^+ currents compared to the control (**Fig. 26a** and **b, Appendix Table 6**). Therefore, I could use these plasmids for localization studies.

To study the localization of LOF $Na_V1.6$-HA variants, I then co-transfected mouse hippocampal neurons at DIV 7–8 with NES PylRS^{AF}/tRNA^{Pyl} and control (TAG-only), or LOF $Na_v1.6^{K1546TAG,\ Y371C}$-HA plasmids. Four days later, I click labeled neurons with ATTO488-tz and immunostained them with an anti-HA antibody. Click labeling allowed the detection of the $Na_V1.6$-HA membrane population, while anti-HA immunostaining was used to detect the total $Na_V1.6$-HA population (cytosolic and membrane $Na_V1.6$-HA). Surprisingly, confocal microscopy revealed that both LOF variants were expressed on the neuronal surface despite almost complete loss of Na^+ currents in N1E-115-1^{WT} cells (**Fig. 26c**). I further confirmed microscopy results by measuring the AIS fluorescence intensity of the ATTO488-tz and HA signal in neurons expressing control of LOF variants. The quantitative analysis showed no significant difference in the AIS fluorescence between control and LOF variants (**Fig. 26d**).

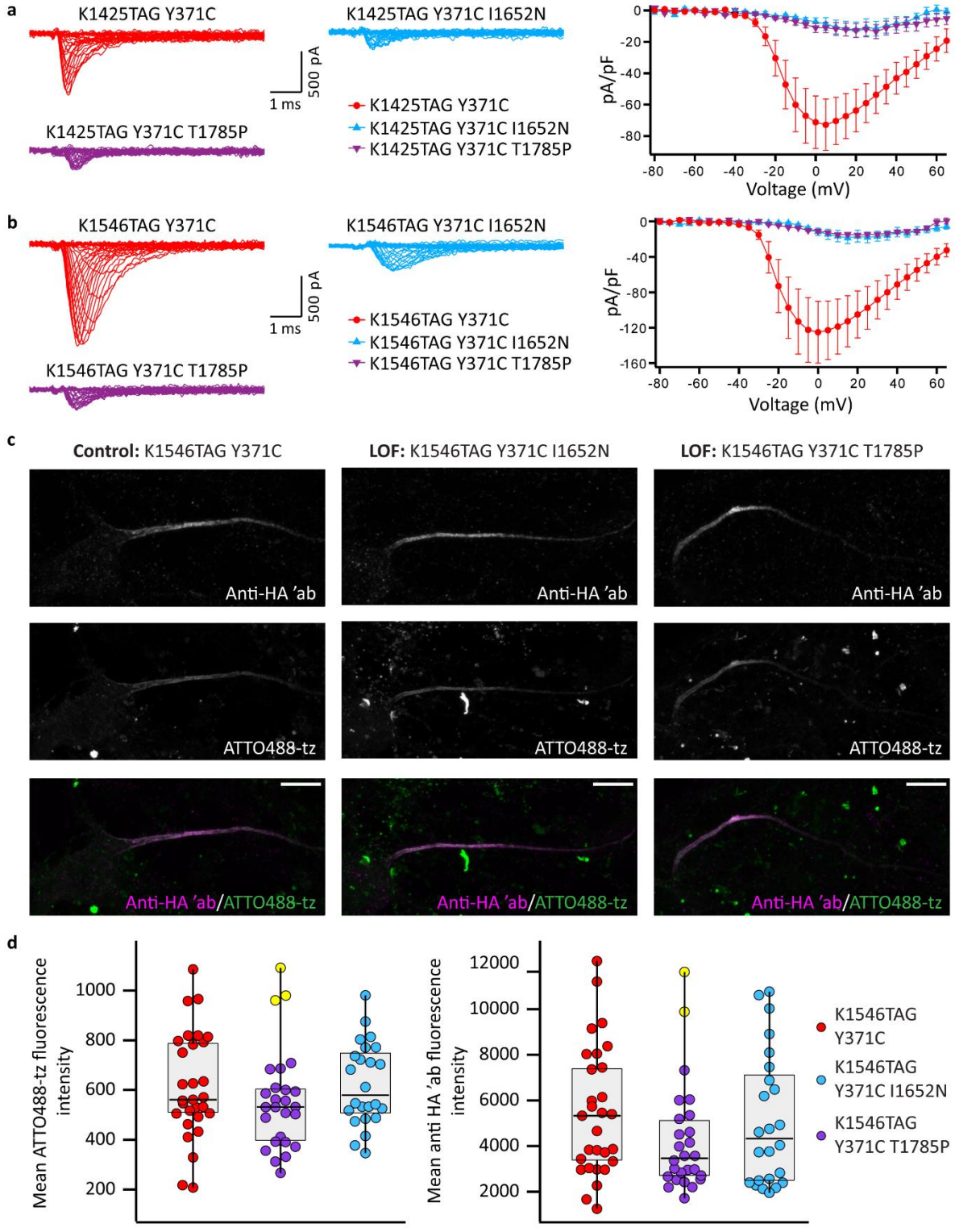

Figure 26. The localization study of click-labeled $Na_V1.6^{TAG}$-HA pathogenic variants in primary neurons. a–b: *N1E-115-1 cells were co-transfected with codon-optimized NES $PylRS^{AF}$/U6-$tRNA^{Pyl}$, a plasmid containing mβ1, mβ2, and mGFP, and TTX-resistant clickable $Na_V1.6^{TAG,\ Y371C}$-HA (with or without loss-of-function mutations) using Lipofectamine 3000 transfection reagent. Transfected cells were incubated in the presence of the unnatural amino acid*

TCO-Lys for two days. Afterwards, cells were re-seeded and recorded with a whole-cell patch clamp.* ***a:*** *Representative Na^+ current traces obtained from N1E-115-1 cells expressing either control—$Na_V1.6^{K1425TAGY371C}$-HA (red) or one of the loss-of-function (LOF) variants—$Na_V1.6^{K1425TAG,\ Y371C,\ I1652N}$-HA (blue) or $Na_V1.6^{K1425TAG,\ Y371C,\ T1785P}$-HA (purple). Both LOF pathogenic mutations significantly reduced the peak Na^+ current density of clickable $Na_V1.6$ compared to the control ($Na_V1.6^{K1425TAG,\ Y371C}$-HA: -72.9 ± 16.4 pA/pF, n = 11; $Na_V1.6^{K1425TAG,Y371C,I1652N}$-HA: -12.3 ± 5.0 pA/pF, n = 8, p = 0.0015; $Na_V1.6^{K1425TAG,Y371C,T1785P}$-HA: -12.7 ± 4.4 pA/pF, n = 12, p = 0.0006; ANOVA on ranks with Dunn's posthoc test).* ***b:*** *Representative Na^+ current traces obtained from N1E-115-1 cells that expressed either control—$Na_V1.6^{K1546TAG\ Y371C}$-HA (red) or one of the LOF variants—$Na_V1.6^{K1546TAG\ Y371C\ I1652N}$-HA (blue) or $Na_V1.6^{K1546TAG\ Y371C\ T1785P}$-HA (purple). Both LOF pathogenic mutations significantly reduced the peak Na^+ current density of clickable $Na_V1.6$ compared to the control ($Na_V1.6^{K1546TAG,\ Y371C}$-HA: -125.1 ± 34.8 pA/pF, n = 13; $Na_V1.6^{K1546TAG,\ Y371,I1652N}$-HA: -18.7 ± 6.3 pA/pF, n = 8, p = 0.0018; $Na_V1.6^{K1546TAG,Y371C,T1785P}$-HA: -15.4 ± 2.0 pA/pF, n = 8, p = 0.0014; ANOVA on ranks with Dunn's posthoc test). Mean ± SEMs are shown (a, b).* ***c:*** *The representative images show DIV 12 mouse hippocampal neurons expressing either control—$Na_V1.6^{K1546TAG\ Y371C}$-HA or one of the LOF pathogenic variants—$Na_V1.6^{K1546TAG\ Y371C\ I1652N}$-HA or $Na_V1.6^{K1546TAG\ Y371C\ T1785P}$-HA. For days after transfection, neurons were click labeled with ATTO488-tz, fixed, immunostained with anti-HA antibody, and imaged with confocal microscopy. Both LOF pathogenic variants were present at the AIS of mouse hippocampal neurons.* ***d:*** *Distribution of the ATTO488-tz (left graph) or anti-HA (right graph) fluorescence intensity measured in confocal images of click-labeled and anti-HA immunostained mouse hippocampal neurons expressing either control—$Na_V1.6^{K1546TAG\ Y371C}$-HA (red) or one of the LOF pathogenic variants—$Na_V1.6^{K1546TAG\ Y371C\ I1652N}$-HA (blue) or $Na_V1.6^{K1546TAG\ Y371C\ T1785P}$-HA (purple). The box plots indicate the median (the black lines inside the box), the 25^{th} and 75^{th} percentiles (the box boundaries), the single data points (the dots), and the outliers (the yellow dots). The minimum and maximum data points define the lengths of the whiskers. The non-parametric Kruskal-Wallis test did not show any significant differences between the control and the LOFs measured in click or HA channel ($p_{ATTO488\text{-}tz}$ = 0.324; $p_{anti\text{-}HA}$ = 0.190; $n_{K1546TAG,\ Y371C}$ = 29, $n_{K1546TAG,\ Y371C,I1652N}$ = 24 and $n_{K1546TAG\ Y371C\ T1785P}$ = 26). The Z-stack images are shown as maximum intensity projection (c). The scale bars: 10 µm (c). Details on the statistical analysis (d) are provided in Appendix Table 6 and Materials and Methods. The results shown in the figure were published in*[75]*.*

4.4. Strategies to improve genetic code expansion and click labeling efficiency in neurons

The results described in section 4.4b (except for the quantitative analysis of GFP^{Y39TAG}/mCherry ratio in primary neurons) were published in Stajković et al. "Direct fluorescent labeling of NF186 and $Na_V1.6$ in living primary neurons using bioorthogonal click chemistry." bioRxiv (2022)[75]*. The AAVs described in this section were generated by Ning Meng, a Ph.D. candidate in the laboratory of Prof. Dr. Dirk Grimm. I performed all the experiments that included AAVs. I also analyzed all the data except for the quantitative analysis of the GFP^{Y39TAG}/mCherry ratio in primary neurons. This analysis was carried out by Aleksandra Arsić, a member of Dr. Ivana Nikić-Spiegel's laboratory.*

After successfully establishing the click labeling of the AIS components, I aimed to further increase the efficiency of GCE and click labeling in neurons. To this aim, I probed different viral-vectors to efficiently deliver orthogonal translational machinery elements and amber mutants to neurons. I tested a commercially available, baculovirus-based system for gene delivery, MultiBacMam[233], and AAV-based viral vectors. In addition, I tried to optimize the expression levels of orthogonal tRNA and NES PylRS^{AF}.

a) MultiBacMam system

To test MultiBacMam suitability for the delivery of the GCE components to the neurons, I first established the insect cell culture. I chose *Spodoptera frugiperda* (Sf)21 cells as a model system since they are commonly used for the production of recombinant MultiBacMam baculoviruses[233,243]. I tested different conditions for insect cell propagation (e.g., adherent vs. suspension culture and plastic flasks vs. glass flasks). Growing Sf21 cells in suspension in glass flasks provided the most optimal conditions for insect cell proliferation. Plastic flasks were unsuitable since Sf21 cells adhered firmly to the bottom of the dish and could not be efficiently detached.

Before starting baculovirus production, I inserted GOIs into the engineered baculovirus genome—bacmid (DH10EMBacVSV; **Schemes 8** and **9a**). To this end, I cloned genes encoding the GCE elements and amber mutant into transfer vectors (donors and acceptor) provided with a commercial MultiBacMam^{TM} kit (**Scheme 8**). For the optimization of the baculovirus production, I cloned a dual fluorescent reporter consisting of nuclear localization sequence (NLS)-near-infrared fluorescent protein (iRFP) fused to GFP^{Y39TAG} (NLS-iRFP-GFPY39^{TAG}) into a donor vector. The codon-optimized NES PylRS^{AF}/U6-tRNA^{Pyl} was cloned into the acceptor vector. Donor and acceptor vectors contained locus of X over P1 (loxP/Lox) sites that allowed me to combine GOIs into a multigene via Cre-Lox recombination (**Scheme 8**). The subsequent steps involved: the selection of a multigene with the desired combination of genes, the multigene insertion into the DH10MBacVSV genome via T7 transposition, bacmid selection by blue-white screening, amplification, and isolation of the bacmid that carried GOIs (**Scheme 8;** the details are provided in Materials and Methods).

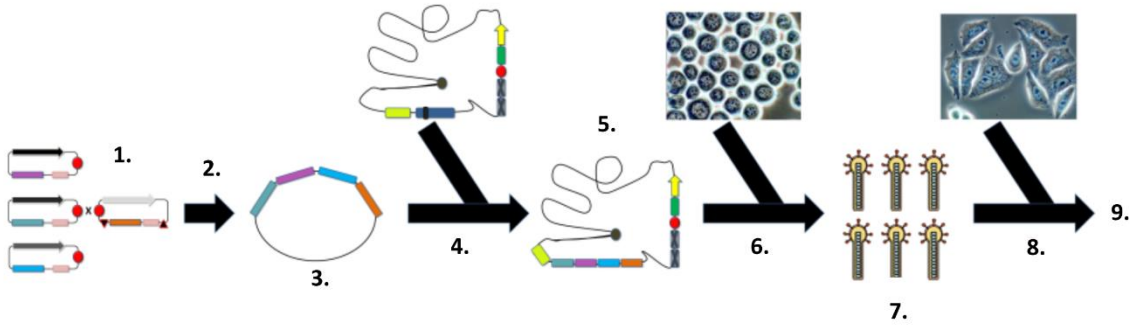

Scheme 8. A general workflow of the MultiBacMam^{TM} system. *In the first step (**1.**), genes encoding amber mutant and orthogonal translational machinery elements (or genes encoding any other proteins of interest) are cloned into transfer vectors (donor and acceptors). The transfer vectors contain LoxP sites that allow the generation of large multigene via Cre-Lox recombination (**2.**). The multigene containing the right combination of the genes is selected using different combinations of antibiotics and special bacterial strains (pir^{+} E. coli). The multigene is inserted into the baculovirus genome via Tn7 transposition (**4.**). The successful transposition events are detected via blue-white selection, and bacmids are amplified (**5.**). In order to generate baculoviruses, insect cells are transfected with the bacmid (**6.**). Baculoviruses are further amplified, collected, and purified (**7.**). In the final step, mammalian cells are transduced (**8.**) and analyzed (**9.**). The scheme was obtained and adapted from the MultiBacMam^{TM} manual (Geneva Biotech).*

To produce baculoviruses (**Scheme 9**), I transfected Sf21 cells with the bacmid that carried genes encoding the GCE elements (NES PylRS^{AF} and U6-tRNA^{Pyl}) and amber mutant (NLS-iRFP-GFP^{Y39TAG}). I determined optimal conditions for baculovirus production by seeding different numbers of Sf21 cells and probing different transfection reagents (Cellfectin II vs. FuGene). The mCherry gene expressed under the control of an insect cell-specific promoter that was present in the bacmid (**Scheme 9a**) allowed the detection of successfully transfected [mCherry positive (+) cells] under an epifluorescent microscope (**Scheme 9b**). Approximately 48–60 h after the transfection (before the cells reached confluence), I collected initial viral stock (V0 generation).

Afterwards, baculovirus was amplified by transducing Sf21 in suspension with V0 (V1 generation; **Scheme 9b**). The large amounts of baculoviral stocks were produced by transducing Sf21 with V1 (V2 generation; **Scheme 9b**). In order to prevent the accumulation of defective viruses, Sf21 cells had to be counted and split every day. I also followed the fluorescence and morphology of the transduced cells under the microscope daily. The presence of many large and swollen mCherry+ cells indicated that proliferation was about to arrest. Furthermore, mCherry gave the medium pink color, allowing me to monitor the amplification of the virus with the naked eye (**Scheme 9b**). The baculovirus amplification was followed by

proliferation arrest. After the proliferation had been arrested, to avoid the production of defective viruses, V1 and V2 viral stocks had to be collected after 48–60 h. Afterwards, V1 and V2 viral stocks were filtered to remove cell debris.

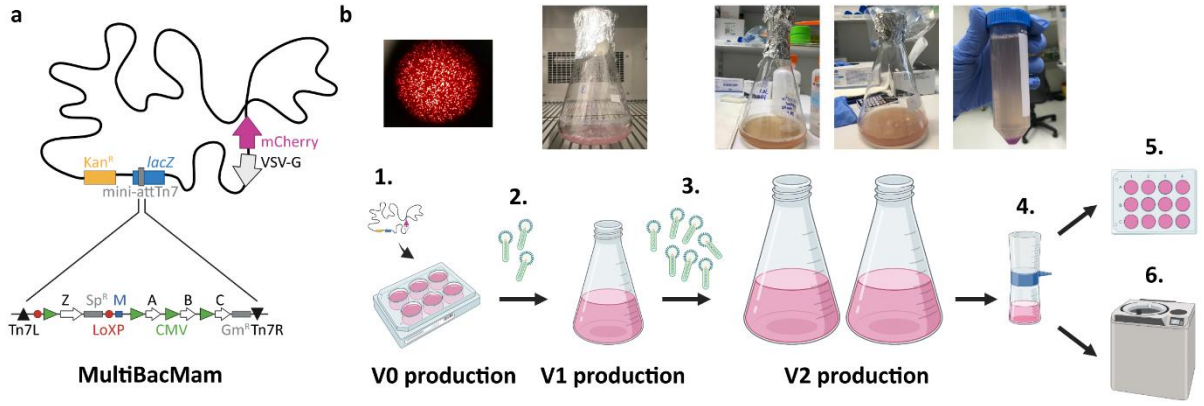

Scheme 9. The baculoviruses production via the MultiBacMam™ system. a: *A schematic representation of a MultiBacMam genome (bacmid). The bacmid (DH10EmBacVSV™) is engineered to contain the elements required to successfully produce recombinant baculoviruses. The mCherry gene under insect cell-specific promoter facilitates the detection of transduced Sf21 cells by giving the suspension culture pink color. The vesicular stomatitis virus (VSV) glycoprotein increases the transduction efficiency of mammalian cells. Tn7L, Tn7R, and mini attTn7 elements allow Tn7 transposition and multigene insertion into bacmid, while lacZ gene allows blue-white selection. The F replicon limits the number of bacmid to one per cell.* ***b:*** *The baculovirus production and amplification. After the transfection of the Sf21 cells with bacmid in six-well plates, the successfully transduced cells are identified by estimating the mCherry fluorescent signal, and V0 is collected (**1.**). V1 generation is produced by the transduction of Sf21 cells in suspension with V0 (**2.**). After the cells stop dividing and the culture acquires pink color, V1 is collected and used to produce large amounts of the baculovirus (V2 generation) (**3.**). After the V1-transduced cells stop dividing and the culture acquires pink color, V2 is collected (**4.**). Afterwards, the virus titer can be determined (**5.**), or the virus can be concentrated by ultracentrifugation (**5.**). The scheme was generated in BioRender.com. The scheme of the bacmid (a) was generated based on the scheme available in the MultiBacMam™ manual (Geneva Biotech).*

I observed that the time until the proliferation arrest of transduced Sf21 (V1 generation) took 5–9 days and depended on the bacmid transfection efficiency (estimated by mCherry fluorescence). The presence of a higher number of mCherry+ cells would result in faster production of V1. The proliferation of V1-infected cells (V2 generation) usually took shorter (3–5 days) since V1 contains more infective particles than V0. In some instances, cells did not stop dividing. The reason was usually the poor quality of Sf21 cells or the low quality of the V0 or V1 viral stocks. Before carrying out experiments in mammalian cells, I assessed the functionality of baculoviruses by transducing Sf21 cells with different amounts of the V2 virus and estimating the number of mCherry+ cells and the overall appearance of the transduced cells.

After generating the V2 viral stocks, I attempted to optimize transduction in standard HEK293T and neuronal ND7/23 cell lines. To this end, I seeded cells in eight-well Lab-Tek II chambered cover glasses. The following day, I transduced them by replacing the culturing medium with the V2 virus that carried NES PylRS^{AF}, U6-tRNA^{Pyl,} and NLS-iRFP-GFP^{Y39TAG} genes in its genome. Since fetal bovine serum (FBS) could affect the binding of the virus, cells were extensively washed in Opti-MEM Reduced serum media and phosphate-buffered saline (PBS) before the transduction. To find optimal transduction conditions, I probed different amounts of V2 viral stock (300 µl, 600 µl, and 1000 µl) for the transduction and incubation with V2 at different temperatures (RT vs. 37 °C). I also tested different times for the expression of amber mutant (24 h, 48 h, and 72 h post-transduction). Approximately 4 h after the transduction, I exchanged medium and added non-reactive unnatural amino acid, BOC-Lys. To improve transduction efficiency and protein expression, I supplied cells with 3 mM sodium butyrate, following the recommendation of the MultiBacMam^{TM} kit manufacturer.

The widefield microscopy showed that cells were successfully transduced with the baculovirus (estimated by the fluorescence of the iRFP that was expressed independently of the UAAs and orthogonal translational machinery; **Fig. 27a**). However, the BOC-Lys incorporation was unsuccessful since the GFP^{Y39TAG} signal was absent in all the conditions (data not shown). By checking the iRFP fluorescence, I observed that the transduction efficiency was higher in HEK293T cells (**Fig. 27a**) than in the ND7/23 cells (**Fig. 27b**). The transduction efficiency was the highest in the cells transduced at 37 °C and fixed at 48 h or 72 h upon transduction (**Fig. 27a**). The higher amounts of virus resulted in a higher iRFP signal (600 µl and 1000 µl; **Fig. 27a**). Hence, I conducted further experiments in HEK293T cells at 37 °C. I used 600 µl or 1000 µl of the V2. The fluorescence signal was analyzed 48 h upon transduction.

Since I did not observe any GFP^{Y37TAG} signal, I wanted to determine if one of the GCE components was deficient. To this end, before transduction, I transfected HEK293T cells with either U6-tRNA^{Pyl} or NES PylRS^{AF} and compared those to the transduced-only cells. The widefield microscopy revealed that tRNA^{Pyl} was deficient since the robust GFP^{Y39TAG} signal was detected only in the cells transfected with additional tRNA^{Pyl} (**Fig. 28a**). Since I also determined that the titer of the V2 stock was low (~4) I attempted to concentrate V2 by using Amicon centrifugal filter

units[244]. However, widefield microscopy indicated that the Amicon-concentrated V2 did not improve transduction efficiency (**Fig. 28b**).

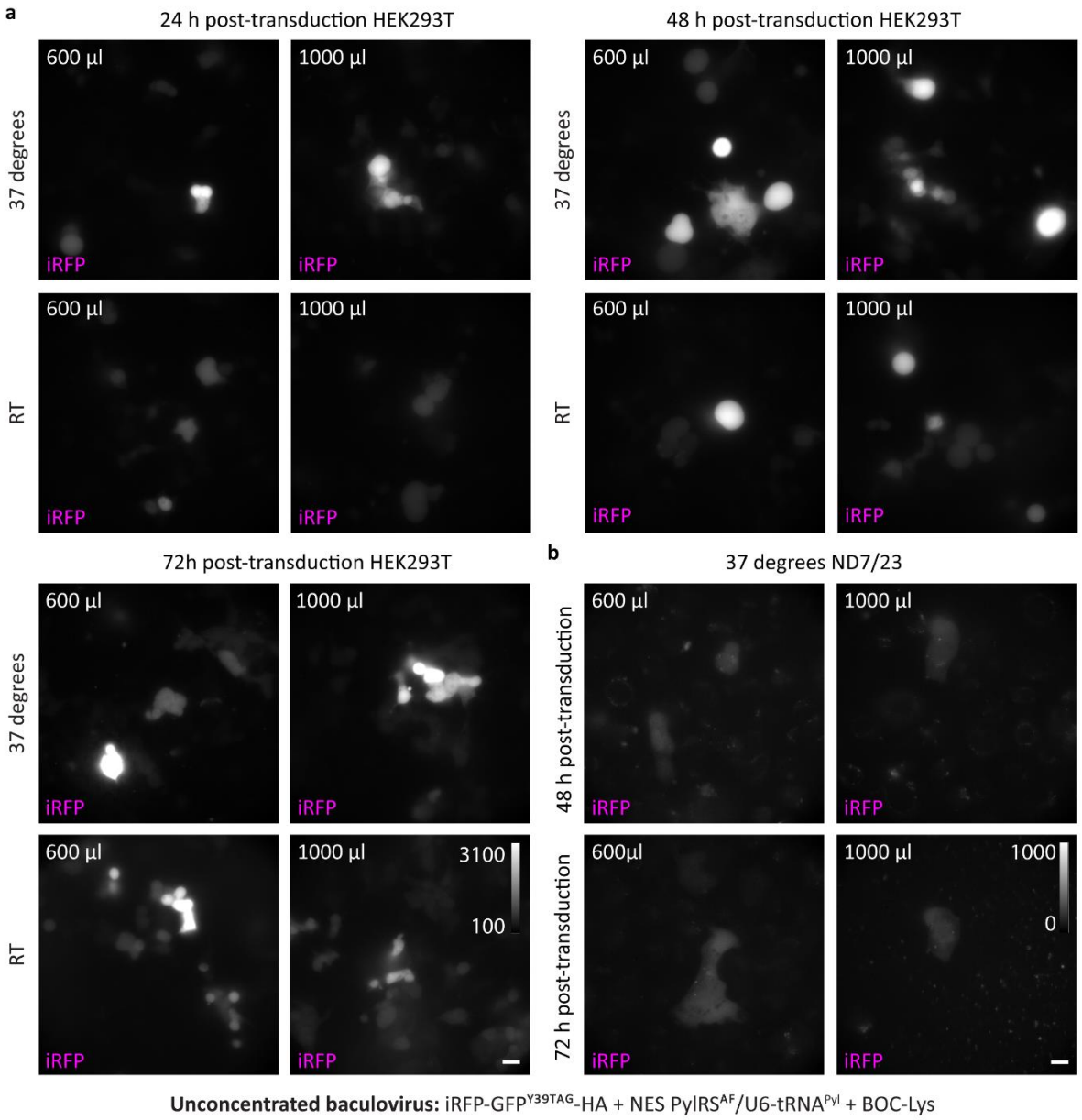

Unconcentrated baculovirus: iRFP-GFP^{Y39TAG}-HA + NES PylRS^{AF}/U6-tRNA^{Pyl} + BOC-Lys

Figure 27. Optimization of the transduction condition with baculoviruses in mammalian cell lines. *Standard HEK293T and neuronal ND7/23 cell lines were transduced with different amounts of the unconcentrated baculovirus carrying codon-optimized NES PylRS^{AF}/U6-tRNA^{Pyl} and iRFP-GFP^{Y39TAG}. The transduction was carried out at room temperature (RT) or 37 °C. The unnatural amino acid BOC-Lys and 3 mM sodium butyrate were added upon transduction. After 24 h, 48 h, or 72 h, cells were fixed and imaged with widefield microscopy.* ***a:*** *Comparison of different transduction conditions with unconcentrated baculoviruses in HEK293T cells. The representative images show that the highest iRFP signal was observed in cells transduced at 37 °C that were fixed 48 h or 72 h after the transduction.* ***b:*** *Comparison of the different transduction conditions with baculoviruses in ND7/23 neuronal cell line. Representative images show a low iRFP signal in a few ND7/23 cells. The brightness and the contrast were linearly adjusted to show*

the same display range (a: 100–3100; b: 0–1000), as indicated by the look-up table (LUT) intensity scale bars. The LUT intensity scale bars show the minimum and maximum grey values. Scale bars: 20 µm.

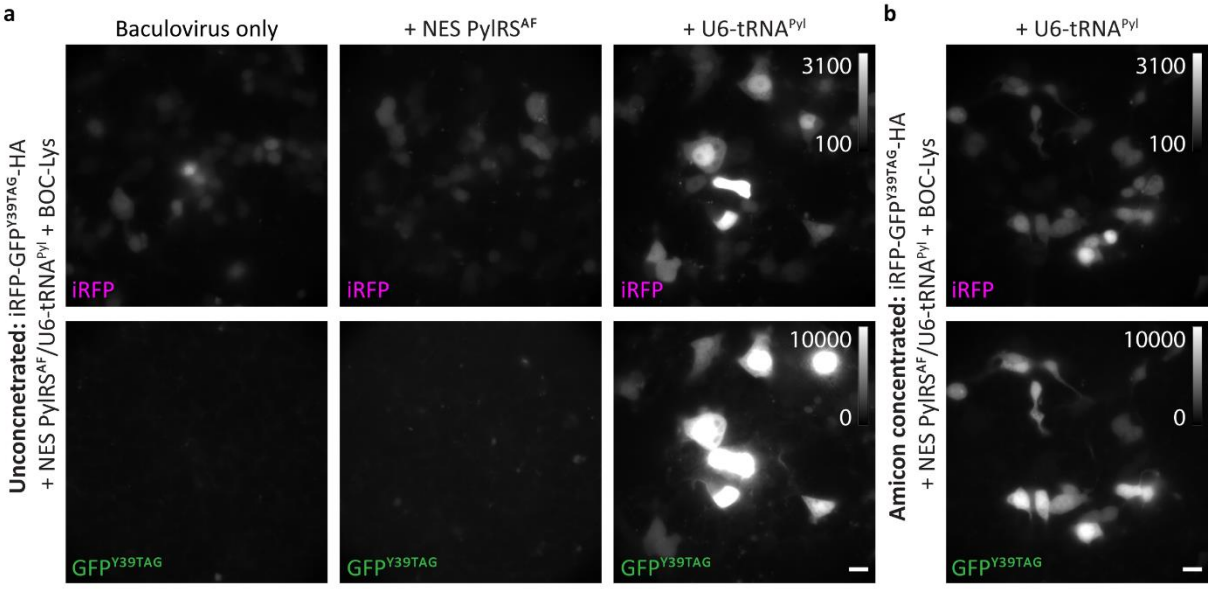

Figure 28. Orthogonal tRNA^{Pyl} is a limiting component for the successful GCE in mammalian cells transduced with baculoviruses. *HEK293T cells were transfected with codon-optimized NES PylRS^{AF} or U6-tRNA^{Pyl}. Afterwards, transfected or untransfected (control) cells were transduced with the unconcentrated (a) or amicon-concentrated (b) baculovirus carrying codon-optimized NES PylRS^{AF}/U6-tRNA^{Pyl} and iRFP-GFP^{Y39TAG}. The transduction was carried out at 37 °C. The unnatural amino acid BOC-Lys and 3 mM sodium butyrate were added upon transduction. After 48h, the cells were fixed and imaged with widefield microscopy.* ***a:*** *The representative images show that the GFP^{Y39TAG} signal was detected only when additional orthogonal tRNA^{Pyl} was delivered via transfection.* ***b:*** *The representative images show that the amicon-concentrated baculovirus did not improve the transduction efficiency. The brightness and contrast of the images in a and b were linearly adjusted to show the same display range (iRFP: 100–3100, GFP^{Y39TAG}: 0–10,000), as indicated by the look-up table (LUT) intensity scale bars. The LUT intensity scale bars show the minimum and maximum grey values. Scale bars: 20 µm.*

I next attempted to increase virus titer by concentrating V2 stocks with ultracentrifugation at high speed (**Scheme 9b**) as described previously[227,233]. Afterwards, I transduced HEK293T with different amounts of the concentrated virus (10 µl, 30 µl, 60 µl, and 120 µl). The widefield microscopy showed that ultracentrifugation improved transduction efficiency as a more robust iRFP signal was observed in cells transduced with concentrated V2 (**Fig. 29a**) compared to the unconcentrated one (**Fig. 27a**). Occasionally, GFP^{Y39TAG} positive (+) cells were observed in cell transduced with concentrated V2 (**Fig. 29a**). When cells transduced with concentrated V2 were supplied with additional tRNA^{Pyl}, robust iRFP and GFP^{Y39TAG} signals were observed (**Fig. 29b**).

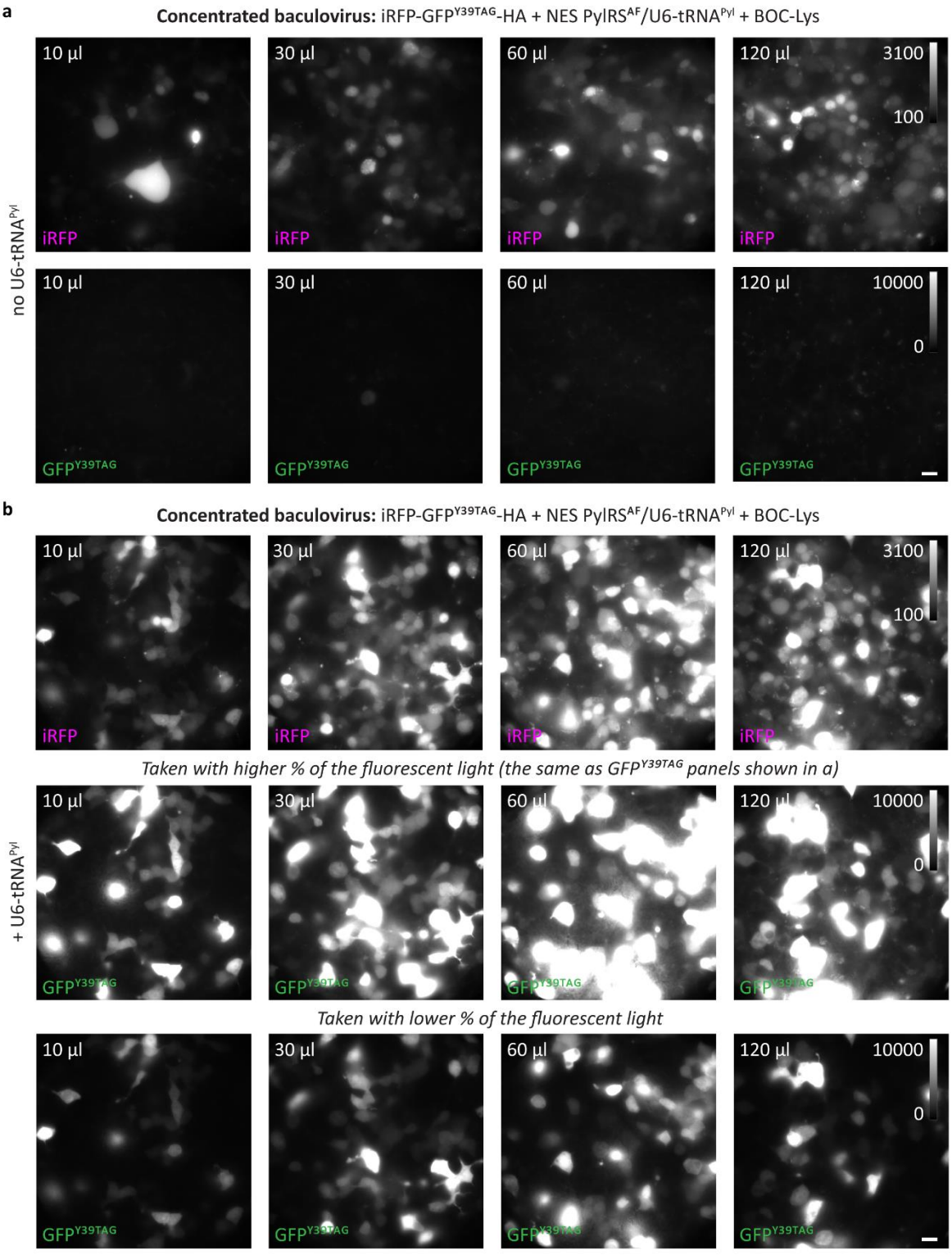

Figure 29. Concentrating baculoviruses with ultracentrifugation improves transduction efficiency but not GCE efficiency. *The HEK293T cells were transfected with U6-tRNA^{Pyl}. Afterwards, transfected or untransfected (control) cells were transduced with different amounts of the baculoviruses carrying codon-optimized NES PylRS^{AF}/U6-tRNA^{Pyl} and iRFP-GFP^{Y39TAG}. Baculoviruses were concentrated with ultracentrifugation at high-speed to improve the*

transduction efficiency. The transduction was carried out at 37 °C. The unnatural amino acid BOC-Lys and 3 mM sodium butyrate were added upon transduction. After 48h, the cells were fixed and imaged with widefield microscopy. ***a:*** *The representative images show that ultracentrifugation at high-speed improved transduction efficiency. However, when additional tRNA^{Pyl} was not delivered, a low GFP^{Y39TAG} signal was detected in a few cells.* ***b:*** *The representative images show that when additional tRNA^{Pyl} was delivered via transfection, robust iRFP and GFP^{Y39TAG} signals were detected. For comparison of the iRFP and GFP^{Y39TAG} signals between cells transfected with U6-tRNA^{Pyl} (b) and untransfected ones (a), the brightness and the contrast were linearly adjusted to show the same display range (0–10,000), as indicated by look-up table (LUT) intensity scale bars (a, b). LUT intensity scale bars show the minimum and maximum grey values. Scale bars: 20 µm.*

To check whether baculoviruses could be used for GCE of the AIS components, I generated a bacmid that carried CMV-NF186^{K680TAG}-HA, NES PylRS^{AF}, and U6-tRNA^{Pyl}. After I had produced and concentrated V2 viral stocks, I transduced HEK293T cells (with or without transfection with the additional tRNA^{Pyl}). The widefield microscopy showed that NF186 amber mutant was poorly expressed in HEK293T cells even when the additional tRNA^{Pyl} was supplied (**Fig. 30**).

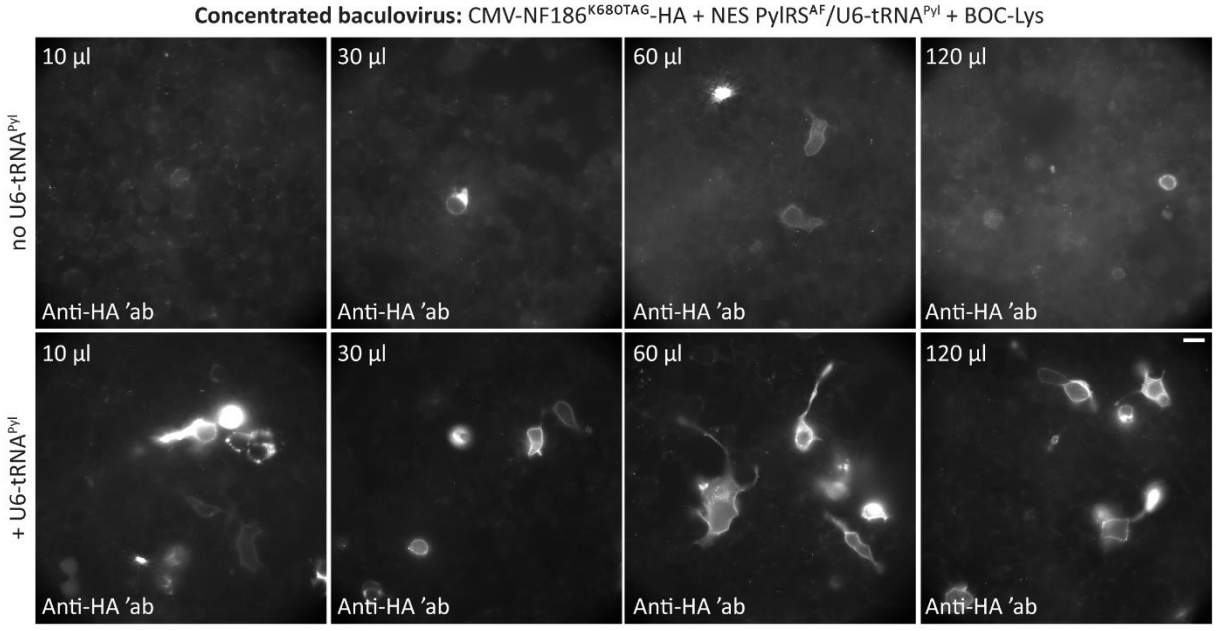

Figure 30. GCE efficiency of NF186^{TAG}-HA amber mutant in mammalian cells transduced with concentrated baculoviruses is low even when additional tRNA^{Pyl} was added. *The HEK293T cells were transfected with U6-tRNA^{Pyl}. Afterwards, transfected or untransfected (control) cells were transduced with different amounts of the baculoviruses carrying codon-optimized NES PylRS^{AF}/U6-tRNA^{Pyl} and CMV-NF186^{K680TAG}-HA. In order to improve the transduction efficiency, baculoviruses were concentrated via ultracentrifugation at high-speed. The transduction was carried out at 37 °C. The unnatural amino acid BOC-Lys and 3 mM sodium butyrate were added upon transduction. After 48h, the cells were fixed and imaged with widefield microscopy. The representative images show that when additional tRNA^{Pyl} was not delivered via transfection, a low HA signal was detected in a few cells (upper panels). When additional tRNA^{Pyl} was delivered via transfection, the expression level of NF186^{K680TAG}-HA was improved. However, the number of transduced cells remained low. Scale bars: 20 µm.*

In summary, the amount of the orthogonal $tRNA^{Pyl}$ proved to be a limiting factor for the expression of amber mutant in mammalian cells transduced with baculoviruses. The expression level of AIS component NF186 was low in HEK293T cells even when cells were supplied with additional $tRNA^{Pyl}$. In contrast to HEK293T cells, the ND7/23 cells were poorly transduced with baculoviruses. Therefore, I probed AAVs as alternative viral-based vectors for delivery of the orthogonal translational machinery to primary neurons.

b) Adeno-associated virus-based vectors

Despite their limiting cargo capacity[231], AAVs are a suitable alternative to baculoviruses since they have been utilized for proof-of-principle GCE of a small GFP^{TAG} in a mouse brain[173].

As a first step, I optimized transduction conditions by using a dual-fluorescent reporter (NLS-mCherry-GFP^{Y39TAG}) packed in engineered AAV7 or AAV9. The engineered AAVs displayed the small A2 peptide (NYSRGVD) on their surfaces (hereafter referred to as "AAV7A2" or "AAV9A2"), which previously improved the transduction efficiency of various cells[266]. To find which serotype was more suitable, I transduced primary neurons with NLS-mCherry-GFP^{Y39TAG} packed in either AAV7A2 or AAV9A2. At the same time, I tested different promotors for the reporter expression [CMV or minimal (m)CMV]. Upon transduction, neuronal viability and the mCherry fluorescence were monitored daily on the epifluorescent microscope. The mCherry was successfully expressed in all conditions. Microscopy results indicated that neurons transduced with CMV-NLS-mCherry-GFP^{Y39TAG} packed in AAV9A2 looked the healthiest and appeared to have the highest number of bright mCherry+ cells. In addition to the promoters and serotypes, I tested different DIVs for transduction (DIV 5 vs. DIV 8). I observed a robust mCherry fluorescence in neurons transduced at DIV 8. Therefore, in further experiments, I infected neurons at DIV 8 with the AAV9A2. After identifying a suitable serotype and DIV for the transduction, I probed if the AAV9A2 could be used for the GCE of the fluorescent reporter. To this end, I transduced rat cortical neurons at DIV 8 with the AAV9A2 bearing CMV-NLS-mCherry-GFP^{Y39TAG} (**Fig. 31a**; AAV#6) along with the AAV9A2 carrying different combinations of GCE elements (**Fig. 31a**; AAV#1–5). The NES $PylRS^{AF}$ was combined with one, two, or four copies of U6-$tRNA^{Pyl}$, with or without eRF^{E55D} (details are provided in **Fig. 31a**). I also tested CMV and mCMV promoters for

the expression of GCE elements (**Fig. 31a**). Three days after transduction, I fixed cells, imaged them, and estimated mCherry and GFP^{Y39TAG} fluorescence intensity.

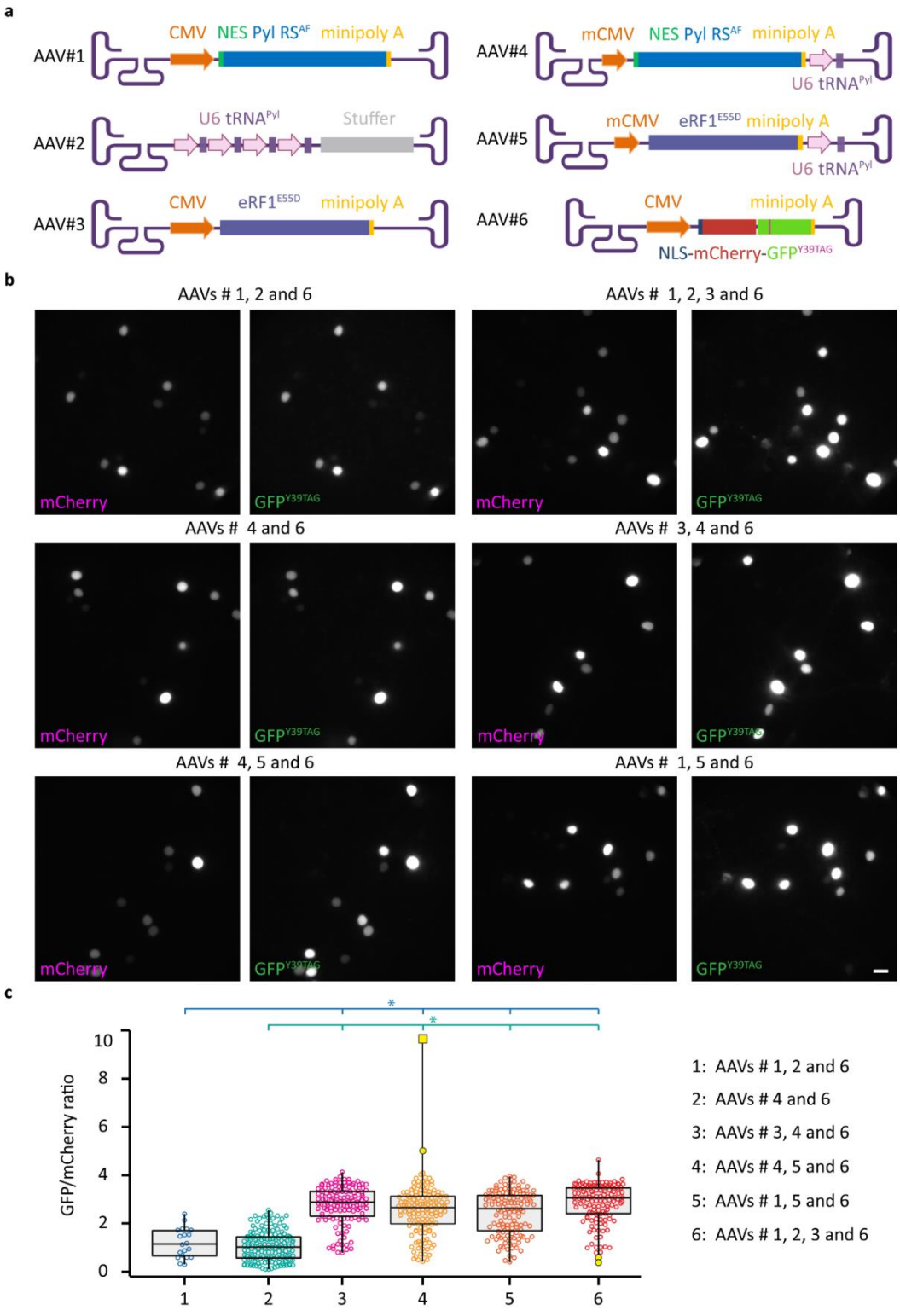

Figure 31. Adeno-associated viruses (AAVs) provide an efficient GCE of a dual-fluorescent reporter in primary neurons. a: *The schematic representations of the GCE elements packed in the AAVs. The scheme was initially*

*generated in BioRender.com and modified from[75]. **b–c:** Rat cortical neurons were co-transduced on DIV 8 with an AAV9A2 carrying the gene for a dual-fluorescent reporter (AAV#6: CMV-NLS-mCherry-GFP^{Y39TAG}) and different combinations of AAV9A2s carrying genes for GCE elements (AAV#1—CMV-NES PylR^{AF}; AAV#2—4xU6-tRNA^{Pyl}; AAV#3—CMV-eRF1^{E55D}; AAV#4—minimal (m)CMV-NES PylR^{AF} and U6-tRNA^{Pyl}; AAV#5—mCMV-eRF1^{E55D} and U6-tRNA^{Pyl}) depicted in a. The neurons were incubated with the unnatural amino acid TCO*A-Lys. Three days after the transduction, neurons were fixed and imaged with widefield microscopy. **b:** The representative images show neurons expressing a dual-fluorescent reporter (AAV#6) and different GCE elements (AAV#1 and 2, AAV#1, 2 and 3, AAV#4, AAV#3 and 4, AAV#1 and 5, and AAV#4 and 5). Scale bars: 20 µm. **c:** The quantitative analysis of the GFP^{Y39TAG}/mCherry ratio in neurons co-transduced with different AAVs combinations (shown in a and b). The box plots show the median (the black lines inside the box), the 25th and 75th percentiles (the box boundaries), the single data points (the dots), and the outliers (the yellow dots/squares). The minimum and maximum data points define the lengths of the whiskers. The nonparametric Kruskal-Wallis test with Dunn-Bonferroni posthoc showed no significant differences between AAV#1 and 2 and AAV#4 ($p_{1\ vs.2} = 1$). However, statistical analysis showed that AAV#1 and 2 and AAV#4 were significantly different from AAV#1, 2, and 3, AAV#1 and 5, AAV#4 and 5, and AAV#3 and 4 ($p_{1\ vs.3} = 0$, $p_{1\ vs.4} = 0$, $p_{1\ vs.5} = 0$, $p_{1\ vs.6} = 0$, $p_{2\ vs.3} = 0$, $p_{2\ vs.4} = 0$, $p_{2\ vs.5} = 0$, $p_{2\ vs.6} = 0$). The number of analyzed nuclei $(n)_1 = 169$, $n_2 = 151$, $n_3 = 129$, $n_4 = 133$, $n_5 = 129$, $n_6 = 127$). The blue (AAV#1 and 2) and green (AAV#4) asterisks in the graph indicate significant differences between the groups. The details of the statistical analysis are provided in Appendix Table 7 and the Material and Methods section. The quantitative analysis was performed by a colleague from the laboratory (Aleksandra Arsić).*

The widefield microscopy showed that a combination of AAV#1 and AAV#2 (CMV-NES-PylRS^{AF} and 4xU6-tRNA^{Pyl}) or AAV#4 (mCMV-NES-PylRS^{AF} and U6-tRNA^{Pyl}) resulted in the lowest GCE efficiency (**Fig. 31b**). When neurons were transduced with eRF1^{E55D}, the GCE efficiency improved, resulting in a higher GFP^{Y39TAG} signal (**Fig. 31b**). Quantitative measurements of the GFP^{Y39TAG}/mCherry ratio in transduced neurons confirmed widefield microscopy results (**Fig. 31c**, **Appendix Table 7**). There was no significant difference between the combination of AAV#1 and #2 and AAV#4. In contrast, both had a significantly lower GFP^{Y39TA}/mCherry ratio than the combinations that contained eRF1^{E55D} (**Fig. 31c**, **Appendix Table 7**).

Next, I attempted to express and click label AIS constituents in primary neurons by using AAV-based viral vectors. Due to the limiting cargo capacity of the AAVs, I had to combine the transfection of the large amber mutants (NF186^{TAG}-HA or Na$_V$1.6^{TAG}-HA) and the transduction with AAV9A2 that carried GCE elements (AAV#1–5). I first tried to click label NF186^{TAG}-HA since it was a smaller AIS constituent. At DIV 8, I transfected rat cortical neurons with hNSE-NF18^{K680TAG}-HA (plasmid#1; **Fig. 32a** and **b**) and transduced them with AAV9A2 that carried different combinations of GCE elements (AAV#1–5; **Fig. 32a** and **b**).

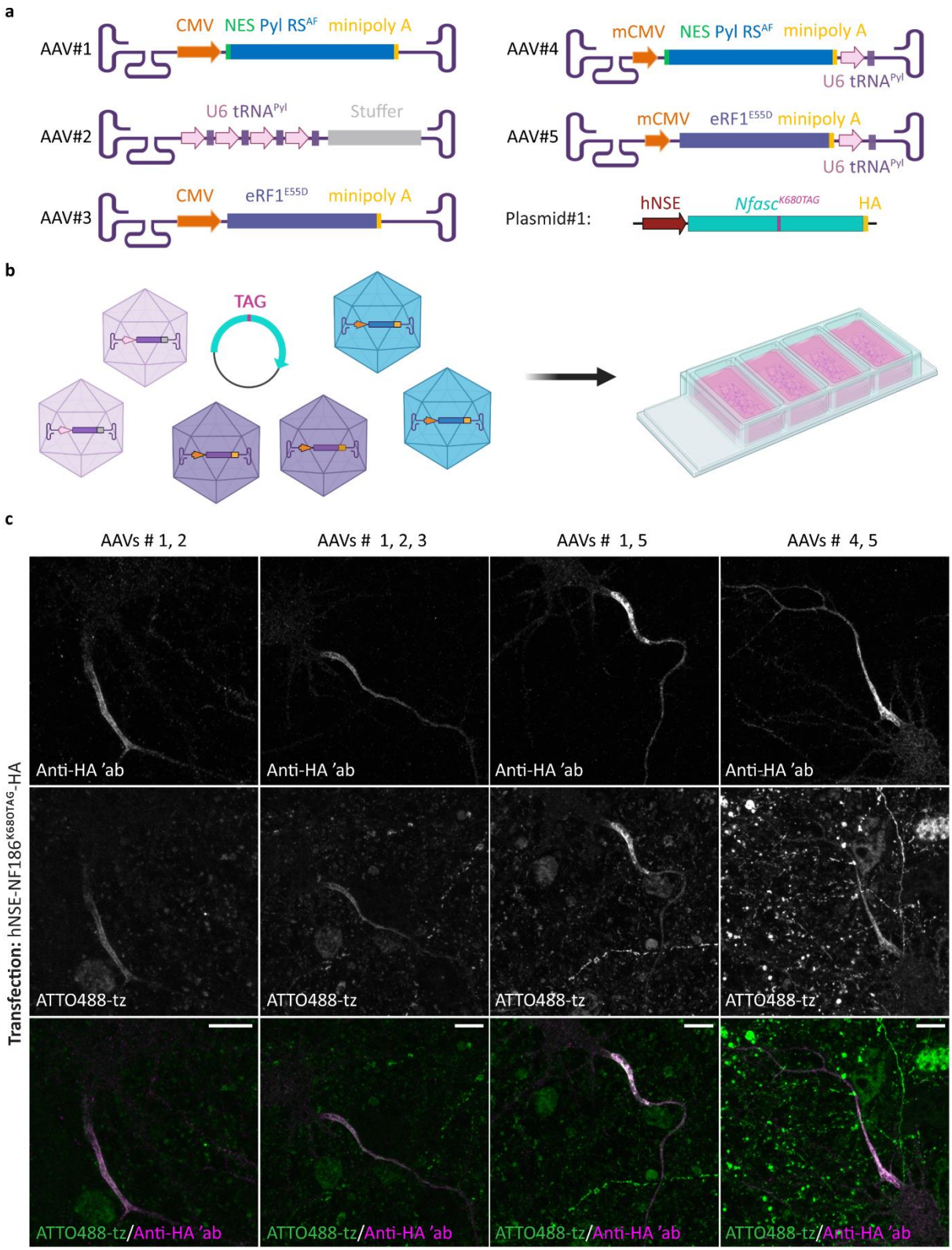

Figure 32. AAVs provide a successful GCE and click labeling of the AIS component NF186^{K680TAG}-HA in primary neurons. a: *The schematic representations of the AAV9A2 and the plasmid used for GCE and click labeling of NF186 in primary neurons.* ***b:*** *The schematic representation of the experimental design. The schemes were initially generated*

*in BioRender.com and modified from[75]. **c:** The Rat cortical neurons were transfected on DIV 8 with hNSE-NF186^{K680TAG}-HA amber mutant (plasmid#1) and transduced with different combinations of AAVs carrying genes for the GCE elements (AAV#1 and 2; AAV#1, 2, and 3; AAV#1 and 5; AAV#4 and 5). The neurons were incubated with the unnatural amino acid TCO*A-Lys. After three days, neurons were click labeled with ATTO488-tz, fixed, immunostained with an anti-HA antibody, and imaged with confocal microscopy. The Z-stack images are shown as maximum intensity projection. The representative confocal images show that AAV9A2 provides efficient GCE and click labeling of NF186 amber mutant. However, NF186 shows ectopic expression along the distal axons due to overexpression. Scale bars: 10 µm.*

Since a combination of AAV#1 and 2 performed similarly to AAV#4, I did not transduce neurons with the latter. For the same reason, I did not transduce neurons with AAV#4 and 3 (eRF1^{E55D}). Three days later, I click labeled neurons with ATTO488-tz, fixed, and immunostained them with anti-HA antibody. The confocal microscopy showed that click labeling of NF186 was successful (**Fig. 32c**). However, NF186 was frequently ectopically expressed along the distal axon in all conditions. The ectopic expression was not surprising for two reasons. First, a transfection with one plasmid (NF186^{TAG}-HA) is more efficient than transfections with multiple plasmids (NF186^{TAG}-HA and NES PylRS^{AF}/tRNA^{Pyl}). Second, the delivery of the GCE elements with the AAVs is more efficient and hence leads to a higher GCE efficiency. Furthermore, in some conditions, I observed a background in the ATTO488-tz channel coming most likely from cell debris that accumulated tetrazine dye and the UAAs. Since it showed the lowest GCE efficiency, a combination of AAV#1 and AAV#2 resulted in the lowest number of neurons ectopically expressing NF18^{K680TAG}-HA and showed the lowest background in the ATTO488-tz channel.

Since the AAVs seemed to improve the expression of NF186, I proceeded with experiments involving $Na_V1.6$. Using the same protocol described above, I transfected neurons with $Na_V1.6^{TAG}$-HA and transduced them with AAVs that bore different GCE elements. Three days later, I click labeled neurons with ATTO488-tz, fixed and immunostained them with an anti-HA antibody. Afterwards, I imaged neurons with confocal microscopy or counted HA+ neurons with widefield microscopy. The confocal microscopy showed that a combination of AAV#1 and AAV#2 improved the $Na_V1.6^{TAG}$-HA expression level and click labeling in comparison to the transfection with $Na_V1.6^{TAG}$-HA and GCE elements (**Fig. 33** and **Fig. 18**). Furthermore, the widefield microscopy showed that the number of transduced neurons expressing $Na_V1.6^{TAG}$ was ~2.7 times higher than the transfected neurons (40 neurons vs. 15 neurons per well in eight-well Lab-Tek II chambered cover glasses, respectively). I also observed that the co-transduction with the eRF1^{E55D} further improved the expression and click labeling efficiency of $Na_V1.6$ (data not shown). However, the background of ATTO488-tz labeling was high, while the surrounding dead cell

debris frequently hindered the click labeling signal (data not shown). Therefore, I used a combination of AAV#1 and 2 in further experiments.

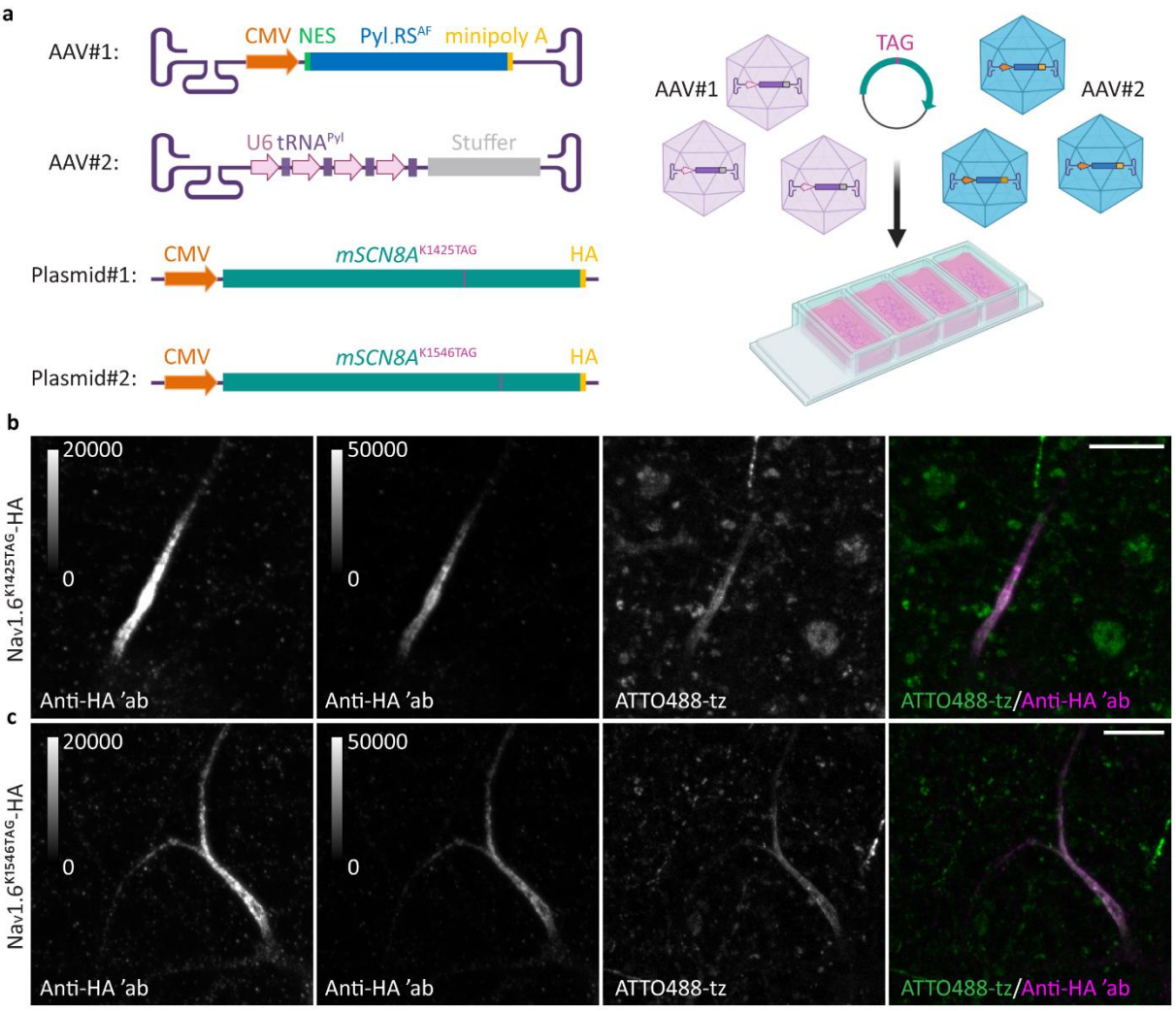

Figure 33. AAVs provide a highly efficient GCE and click labeling of the AIS component Nav1.6 in primary neurons. a: *The schematic representations of the AAV9A2 and the plasmids used for GCE and click labeling of Nav1.6 in primary neurons and the experimental design. The scheme was initially generated in BioRender.com and modified from[75]. **b:** The Rat cortical neurons were transfected on DIV 8 with Nav1.6^{TAG}-HA amber mutants (plasmid#1 and 2) and transduced with AAV9A2 (as shown in a). The neurons were incubated with the unnatural amino acid TCO*A-Lys. After three days, neurons were click labeled with ATTO488-tz, fixed, immunostained with an anti-HA antibody, and imaged with confocal microscopy. The Z-stack images are shown as maximum intensity projection. The representative confocal images show that AAV9A2 provides efficient GCE and click labeling of Nav1.6^{TAG}-HA amber mutants. For comparison with transfected neurons, the brightness and contrast of the panels showing the HA channel were linearly adjusted to show the same display range (0–20,000), as shown in Figure 18. In addition, they were adjusted to show a broader display range (0–50,000), as indicated by the look-up table (LUT) intensity scale bars. The LUT intensity scale bars show the minimum and maximum grey values. The brightness and contrast of the panels showing the click channels were also linearly adjusted to show the 100–3100 display ranges (LUTs are not shown), as in Figure 18. Scale bars: 10 µm. The confocal images shown in the figure were published in[75].*

c) Engineering orthogonal translational machinery elements to improve genetic code expansion in mammalian cells and neurons

Apart from probing the viral-based vectors, I attempted to enhance the expression level of the orthogonal translational machinery to improve the GCE efficiency in mammalian cells and primary neurons.

To optimize the expression levels of the orthogonal translational machinery elements, I engineered orthogonal aaRS and $tRNA^{Pyl}$ genes (**Scheme 10**). The modifications included the codon optimization in the gene encoding $PylRS^{AF}$ and the addition of the NES signal[97,150]. As the previous sections (**4.2** and **4.3**) mentioned, I combined the improved codon-optimized NES $PylRS^{AF}$ with $tRNA^{Pyl}$ expressed from a commonly used, strong U6 promoter[97]. In addition, I engineered and probed alternative type 3 polymerase III promoters—7SK, MRP/7-2, and Y3. Furthermore, I attempted to improve $tRNA^{Pyl}$ stability by removing the variable polyT tail (**Scheme 10a**). To this end, I inserted a self-cleaving hepatitis delta virus (HDV) ribozyme between the $tRNA^{Pyl}$ 3' end and polyT sequence[216,217]. The HDV ribozyme ensured that polyT was cleaved after the transcription. I combined codon-optimized NES $PylRS^{AF}$ with cassettes that consisted of one of the type 3 polymerase III promoters and $tRNA^{Pyl}$ followed by polyT tail, with or without HDV ribozyme in between these two (**Scheme 10a**). Furthermore, as mentioned in section 4.3, I generated a plasmid that contained four copies of improved $tRNA^{M15}$ expressed from U6 promoter ($4xU6\text{-}tRNA^{M15}$)[151] and codon-optimized NES $PylRS^{AF}$ (**Scheme 10b;** NES $PylRS^{AF}$/$U6\text{-}tRNA^{M15}$)[97].

This section briefly describes preliminary microscopy results obtained in neuronal cell lines and primary neurons transfected with engineered plasmids and a dual fluorescent reporter (NLS-iRFP-GFP^{Y39TAG}; **Scheme 10c**). To confirm that the engineered promoters were functional, I first probed new plasmids in a commonly used GCE host, the HEK293T cell line. I co-transfected those cells with NLS-iRFP-GFP^{Y39TAG} (**Scheme 10c**) and with each of the engineered plasmids (**Scheme 10a** and **b)** in the presence or absence of unnatural amino acid BOC-Lys. In addition, I co-transfected cells with NLS-iRFP-GFP^{Y39TAG} and previously published codon non-optimized NES $PylRS^{AF}$/$U6\text{-}tRNA^{Pyl}$ plasmid (**Scheme 10d**)[150]. Codon non-optimized NES $PylRS^{AF}$/$U6\text{-}tRNA^{Pyl}$ allowed me to assess if the new constructs improved GCE efficiency. The following day I fixed cells and imaged them with widefield microscopy. All the other experiments described in this section were performed in the same way unless stated otherwise. The microscopy results showed that all engineered type 3 polymerase III promoters provided the

successful GCE of the GFP^{Y39TAG}, albeit with different efficiencies (**Fig. 34**). As expected, in the absence of BOC-Lys only iRFP was detected (data not shown).

After confirming the functionality of new plasmids, I wanted to check if alternative promoters are functional in neuronal cell lines that I had used as intermediate hosts for the GCE of neuronal proteins (ND7/23 and N1E-115-1). In both neuronal cell lines, the GCE was successful (**Fig. 35** and **Fig. 36**). Widefield microscopy showed that the transfection efficiency (iRFP fluorescent signal) and the amber codon suppression efficiency (GFP^{Y39TAG} fluorescent signal) were lower in N1E-115-1 than in the HEK293T and ND7/23 cell lines. In ND7/23 cells, the expression levels of iRFP and GFP^{Y39TAG} appeared even higher than in the HEK293T cells. Regarding the efficiency of the new plasmids, preliminary results indicated that alternative promoters (7SK and MRP/7-2, and Y3) were less efficient than the U6. Furthermore, HDV ribozyme did not seem to improve the GCE efficiency. The plasmid containing codon-optimized NES $PylRS^{AF}$ and U6-$tRNA^{Pyl}$ was more efficient than the codon non-optimized counterpart. However, further quantitative analysis is needed to confirm the microscopy results. Also, the efficiency of the plasmid containing 4xU6-$tRNA^{M15}$ was unclear without quantitative analysis.

To confirm the results obtained in intermediate hosts, I co-transfected DIV 8 mouse cortical neurons with engineered plasmids encoding orthogonal translational machinery and a dual fluorescent reporter consisting of iRFP (without NLS) fused to GFP^{Y39TAG}. After three days, I fixed neurons and assessed iRFP and GFP^{Y39TAG} fluorescence with widefield microscopy. The preliminary results indicated that codon-optimized NES $PylRS^{AF}$ was more efficient than the codon non-optimized version **(Fig. 37**) and that the U6 promoter was the most efficient for the $tRNA^{Pyl}$ expression **(Fig. 38**).

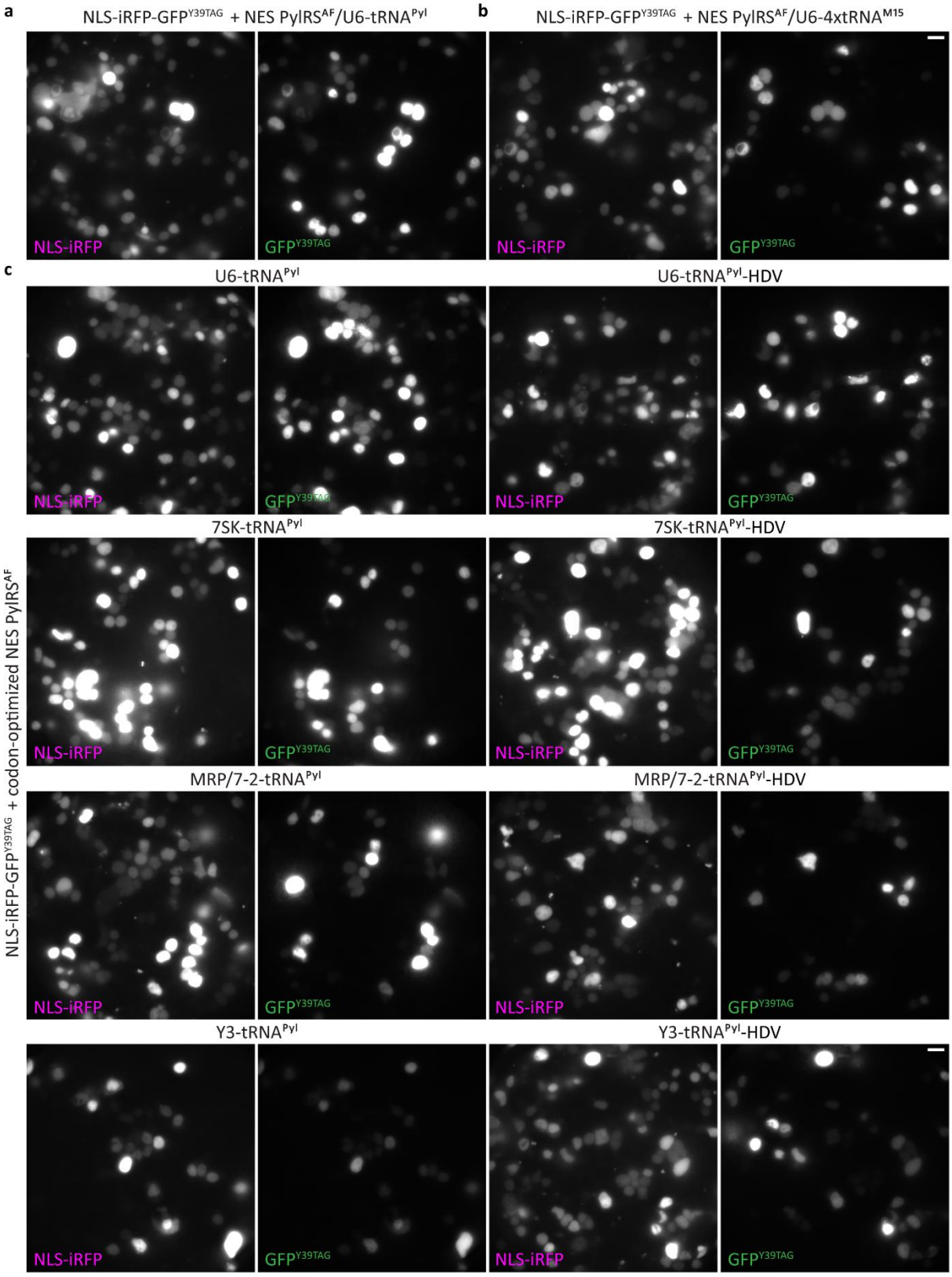

Figure 34. The functionality conformation of the engineered plasmids encoding the GCE elements in the standard cell line. *HEK293T cells were co-transfected with a dual-fluorescent reporter (NLS-iRFP-GFP^{Y39TAG}) and*

different plasmids that bore GCE elements. Cells were incubated with BOC-Lys overnight, fixed, and imaged with widefield microscopy. ***a:*** *The representative images of the HEK293T cells co-transfected with NLS-iRFP-GFP^{Y39TAG} and codon non-optimized NES PylRS^{AF}/U6-tRNA^{Pyl}.* ***b:*** *The representative images of the HEK293T cells co-transfected with NLS-iRFP-GFP^{Y39TAG}, codon-optimized NES PylRS^{AF} and four copies of improved U6-tRNA^{M15}.* ***c:*** *The representative images of the HEK293T cells co-transfected with NLS-iRFP-GFP^{Y39TAG}, codon-optimized NES PylRS^{AF} and tRNA^{Pyl} expressed from different type 3 polymerase III promoters (U6, 7SK, MRP/7-2, or Y3), with or without HDV sequence at the 3' end of the tRNA^{Pyl}. The widefield microscopy showed that all polymerase III promoters are functional. Scale bars: 20 μm.*

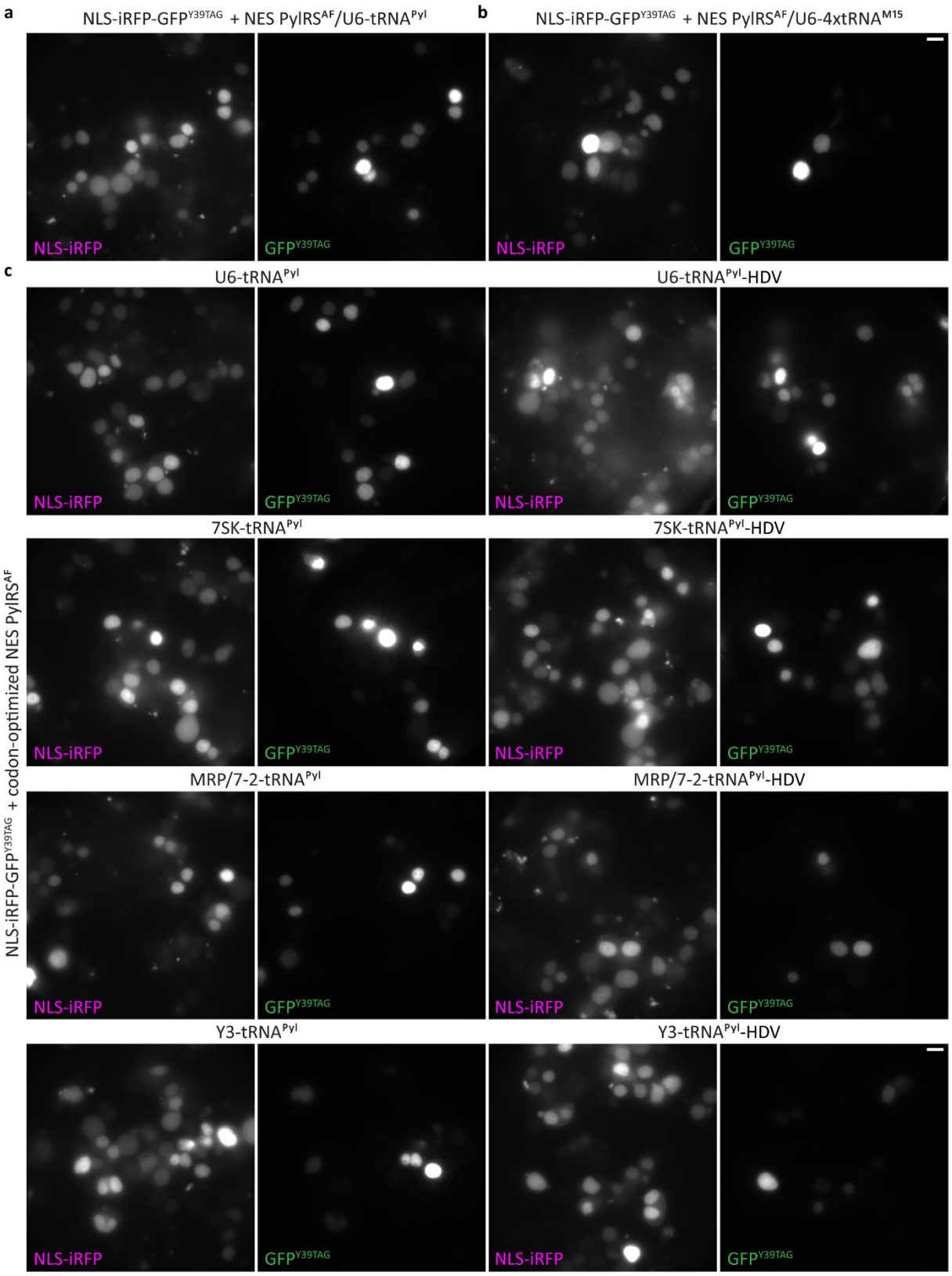

Figure 35. Comparison of the engineered type 3 polymerase III promoters in neuronal N1E-115-1 cell line. *Mouse neuroblastoma N1E-115-1 cells were co-transfected with a dual-fluorescent reporter (NLS-iRFP-GFP^{Y39TAG})*

and different plasmids that bore GCE elements. Cells were incubated with BOC-Lys overnight, fixed, and imaged with widefield microscopy. ***a:*** *The representative images of the N1E-115-1 cells co-transfected with NLS-iRFP-GFP^{Y39TAG} and codon non-optimized NES PylRS^{AF}/U6-tRNA^{Pyl}.* ***b:*** *The representative images of the N1E-115-1 cells co-transfected with NLS-iRFP-GFP^{Y39TAG}, codon-optimized NES PylRS^{AF} and four copies of improved U6-tRNA^{M15}.* ***c:*** *The representative images of the N1E-115-1 cells co-transfected with NLS-iRFP-GFP^{Y39TAG}, codon-optimized NES PylRS^{AF} and tRNA^{Pyl} expressed from different type 3 polymerase III promoters (U6, 7SK, MRP/7-2, or Y3), with or without HDV sequence at the 3' end of the tRNA^{Pyl}. The widefield microscopy showed that the strongest GFP^{Y39TAG} signal was observed when the U6 promoter was combined with codon-optimized NES PylRS^{AF}. Scale bars: 20 µm.*

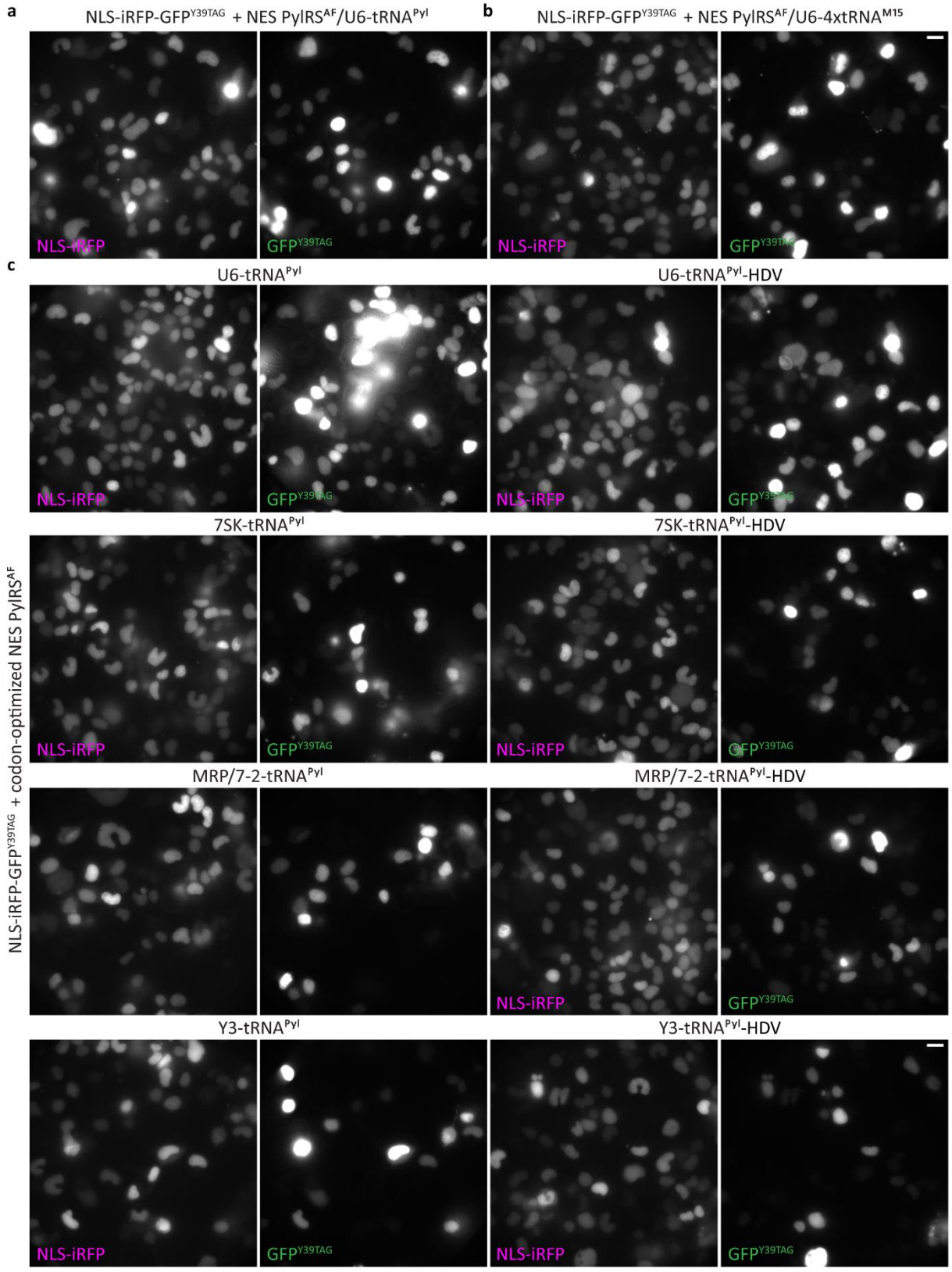

Figure 36. Comparison of engineered type 3 polymerase III promoters in neuronal ND7/23 cell line. *Rodent ND7/23 neuroblastoma cells were co-transfected with a dual-fluorescent reporter (NLS-iRFP-GFP^{Y39TAG}) and different*

plasmids that bore GCE elements. Cells were incubated with BOC-Lys overnight, fixed, and imaged with widefield microscopy. ***a:*** *The representative images of the ND7/23 cells co-transfected with NLS-iRFP-GFP^{Y39TAG} and codon non-optimized NES PylRS^{AF}/U6-tRNA^{Pyl}.* ***b:*** *The representative images of the ND7/23 cells co-transfected with NLS-iRFP-GFP^{Y39TAG}, codon-optimized NES PylRS^{AF} and four copies of improved U6-tRNA^{M15}.* ***c:*** *The representative images of the N1E-115-1 cells co-transfected with NLS-iRFP-GFP^{Y39TAG}, codon-optimized NES PylRS^{AF} and tRNA^{Pyl} expressed from different type 3 polymerase III promoters (U6, 7SK, MRP/7-2, or Y3), with or without HDV sequence at the 3' end of the tRNA^{Pyl}. The widefield microscopy showed robust iRFP and GFP^{Y39TAG} signals in many cells. The strongest GFP^{Y39TAG} signal was observed when the U6 promoter was combined codon-optimized NES PylRS^{AF}. Scale bars: 20 µm.*

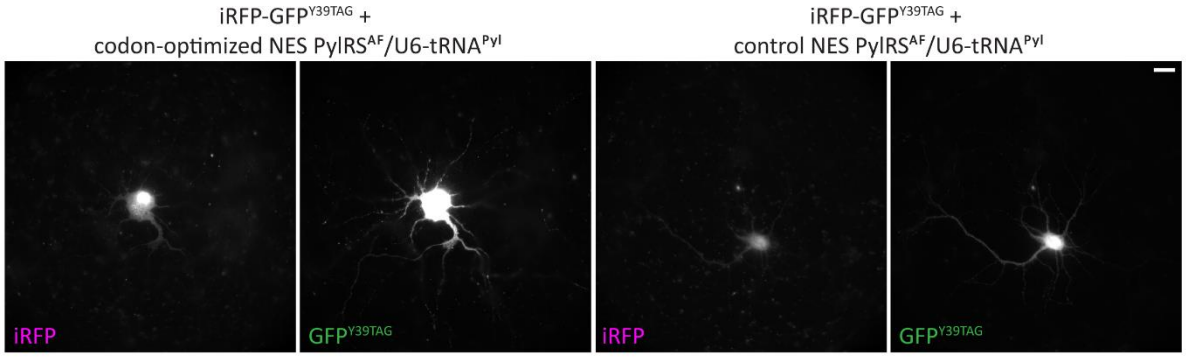

Figure 37. The codon-optimized NES PylRS^{AF} improves GCE efficiency in primary neurons. *Mouse cortical neurons were co-transfected with a dual-fluorescent reporter (NLS-iRFP-GFP^{Y39TAG}) and either codon-optimized NES PylRS^{AF}/U6-tRNA^{Pyl97} or a codon non-optimized version[150]. The neurons were incubated with BOC-Lys. After four days, they were fixed and imaged with widefield microscopy. The representative images show that the codon-optimized NES PylRS^{AF} provides higher GFP^{Y39TAG} expression in comparison to codon non-optimized version. Scale bars: 20 µm.*

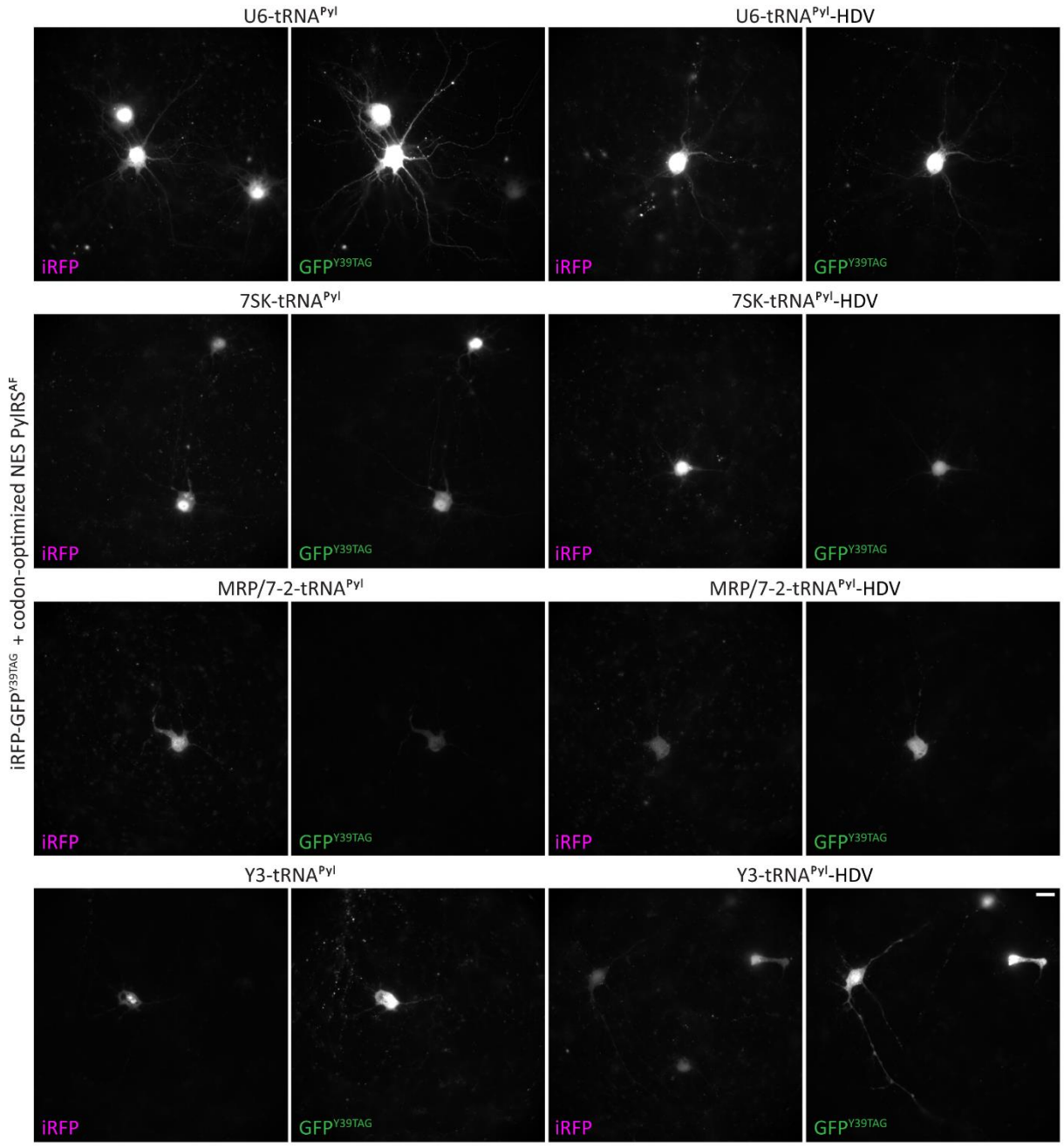

Figure 38. Comparison of engineered type 3 polymerase III promoters in primary neurons. *Mouse cortical neurons were co-transfected with a dual-fluorescent reporter (iRFP-GFP^{Y39TAG}), codon-optimized NES PylRS^{AF} and tRNA^{Pyl} expressed from different type 3 polymerase III promoters (U6, 7SK, MRP/7-2, or Y3), with or without HDV sequence at the 3' end of the tRNA^{Pyl}. The neurons were incubated with BOC-Lys. After four days, they were fixed and imaged with widefield microscopy. The representative images show that the codon-optimized NES PylRS^{AF}/U6-tRNA^{Pyl} provides the highest GFP^{Y39TAG} expression. Scale bars: 20 µm.*

4.5. dSTORM imaging of the AIS and the node of Ranvier components in neurons

The results described in section 4.5b were published in Arsić, A., Stajković, N., Spiegel, R., & Nikić-Spiegel, I. (2020). Effect of Vectashield-induced fluorescence quenching on conventional and super-resolution microscopy. Scientific reports, 10(1), 1-13[246]. Aleksandra Arsić and I are shared first authors in the publication. The data shown in section 4.5b (widefield and dSTORM imaging of immunolabeled AIS in different imaging mediums) were produced by me.

The final aim of my Ph.D. project was to combine click labeling with dSTORM microscopy to visualize AIS and node of Ranvier components at a single-molecule level. To this end, I first optimized dSTORM imaging of the AIS components in neurons immunolabeled with conventional primary and secondary antibodies, as previously described[16,28]. The optimization of SRM imaging also included probing different dSTORM imaging buffers. Afterwards, I optimized dSTORM imaging of click-labeled AIS components with the help of the AAV-based viral vectors and by testing click labeling with different tetrazine dyes.

a) dSTORM imaging of the immunolabeled primary neurons

I used conventional antibodies to optimize dSTORM imaging of the AIS in primary neurons and followed previously published protocols[16,28]. I maintained cortical neurons for at least 11 DIV before fixation and immunostaining. This ensured that $Na_V1.6$ and associated proteins were incorporated into the periodic skeleton[29]. I combined anti-AIS primary antibodies with the improved variant of the photoswitchable AF647-conjugated secondary antibody, the AF647 Plus [AF(+)647]. As previously reported[28], fixing neurons with 4% PFA in cytoskeletal preserving buffer (PEM) maintained the periodic arrangement of the AIS components (**Fig. 39**). Such fixation procedure allowed me to successfully perform dSTORM of neurons immunostained with anti-panNF or anti-panNa_V antibodies in GLOX βME imaging buffer (**Fig. 39a** and **b**). I also attempted dSTORM of neurons immunostained with anti-$Na_V1.6$ antibody. However, due to the poor quality of the immunostaining, dSTORM was less successful (**Fig. 39c**).

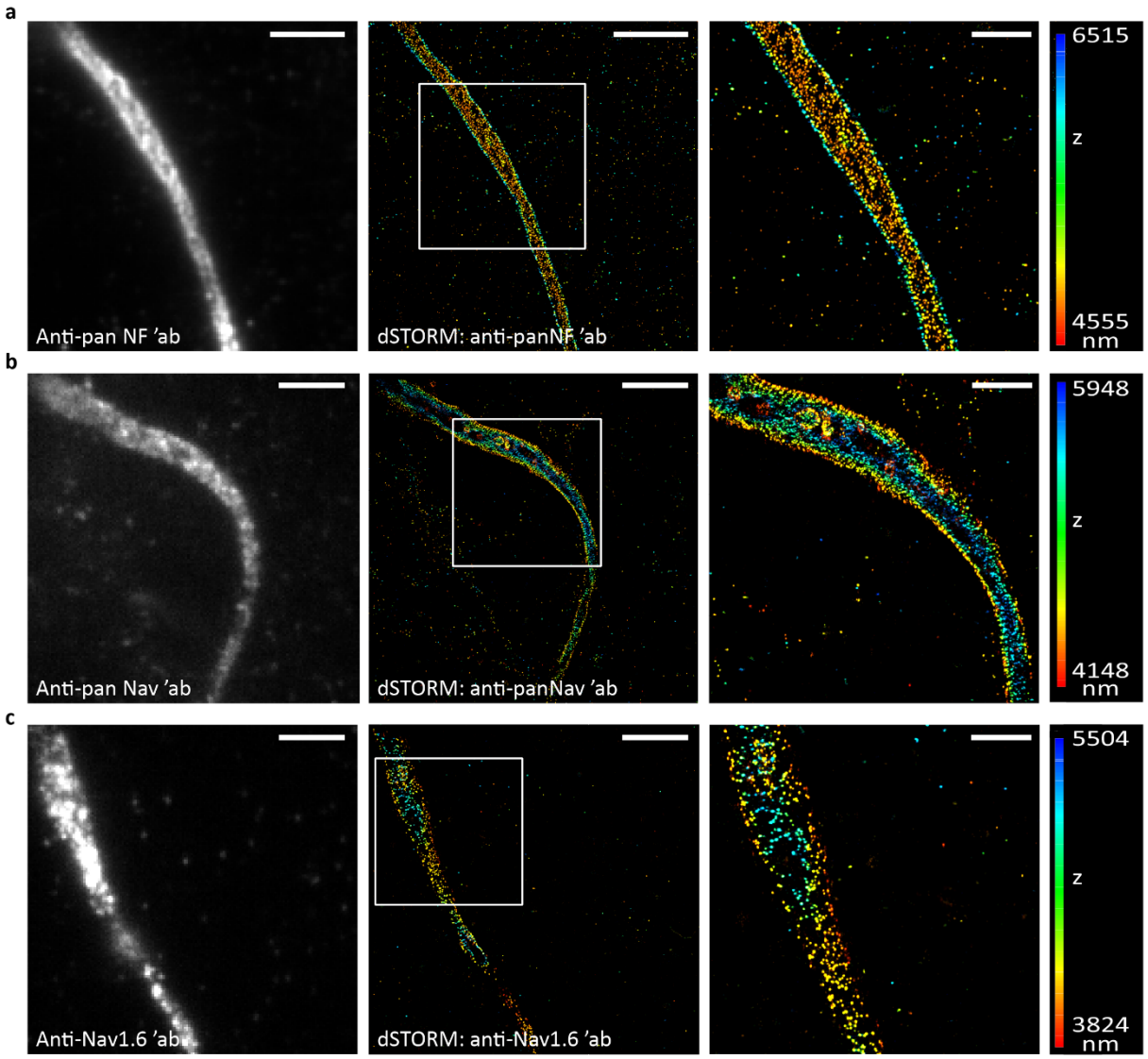

Figure 39. Optimization of dSTORM imaging of immunostained AIS components in primary neurons. *Mouse cortical neurons were fixed, immunostained with anti-pan neurofascin (NF; a), anti-panNa$_V$ (b), and anti-Na$_V$1.6 (c) antibodies, and imaged with dSTORM microscopy.* ***a:*** *The representative 3D dSTORM image of panNF in DIV 15 mouse cortical neurons shows its periodic distribution at the AIS.* ***b:*** *The representative 3D dSTORM image of panNa$_V$ in DIV 10 mouse cortical neurons shows its periodic distribution at the AIS.* ***c:*** *The representative 3D dSTORM image of Na$_V$1.6 in DIV 14 mouse cortical neurons does not show apparent periodic distribution at the AIS. The left panels show total internal reflection fluorescence (TIRF)/*highly inclined and laminated optical sheet *(HILO) images acquired with a 647 nm laser before dSTORM imaging. Middle panels show 3D dSTORM images. The right panels show an enlarged boxed region from 3D dSTORM images in the middle. The Z positions in the 3D dSTORM images are color-coded according to the height maps on the right. The height maps contain minimal and maximal Z-position values. Scale bars (HILO/TIRF and dSTORM images): 5 µm. Scale bars (dSTORM insets): 2 µm.*

b) Vectashield as an alternative buffer for dSTORM imaging of the AIS components

Prior to dSTORM imaging in GLOX βME, labeled samples are usually stored in PBS. However, storing the labeled samples in PBS can lead to fluorescence loss if the samples are not imaged within several days upon immunostaining or click labeling. Therefore, before attempting to establish dSTORM imaging of click-labeled neurons, I probed alternative imaging buffers that could help with fluorescence preservation. I chose Vectashield (VS), a commonly used mounting medium since it has been combined with AF647 for dSTORM imaging of cytoskeletal elements in cell lines[136].

To test Vectashield suitability for dSTORM imaging of the AIS, I fixed and immunostained mouse primary neurons with anti-panNa_V primary and AF647 or AF(+)647-conjugated secondary antibodies. The AF(+)647 is an improved variant of the AF647, whose suitability for dSTORM in Vectashield has not been probed previously. Surprisingly, the widefield imaging showed that the fluorescence of both AF647 and AF(+)647 was quenched when neurons were placed in Vectashield (**Fig. 40**).

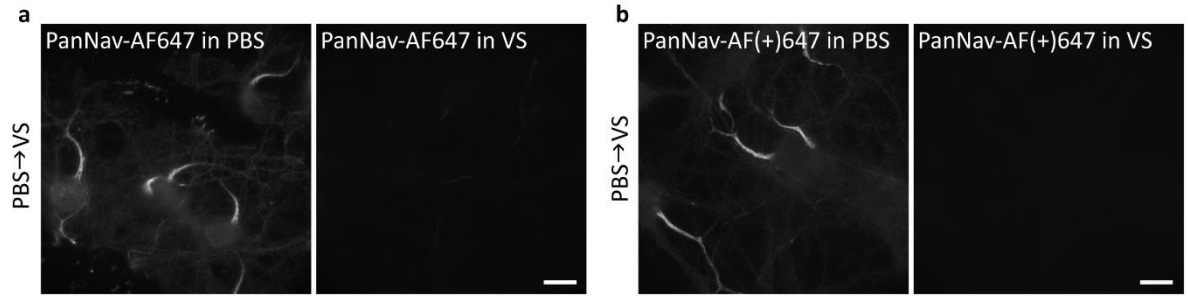

Figure 40. The effect of Vectashield (VS) imaging medium on the AF647 and AF(+)647 fluorescence intensity*. Mouse cortical neurons were fixed and immunostained with anti-panNa_V primary and Alexa Fluor (AF)647 or AF647 Plus [AF(+)647)] secondary antibodies. Afterwards, neurons were imaged with widefield microscopy. The same field of view was first imaged in PBS and afterwards in VS.* ***a:*** *Representative images show that VS quenches AF647 fluorescence.* ***b:*** *Representative images show that VS quenches AF(+)647 fluorescence. The brightness and contrast were linearly adjusted to show the same display range in PBS and VS. Scale bars: 20 µm. The figure and the figure legends were modified from[246].*

Despite the fluorescence loss, the photoswitching properties of the AF(+)647 were not affected by Vectashield, which allowed me to successfully performed dSTORM imaging (**Fig. 41a**). Furthermore, the periodic distribution of the Na_V was successfully resolved in Vectashield (**Fig. 41a**), similarly to GLOX βME (**Fig. 41b**). Likewise, dSTORM of the AF647 immunostained neurons was possible (data now shown).

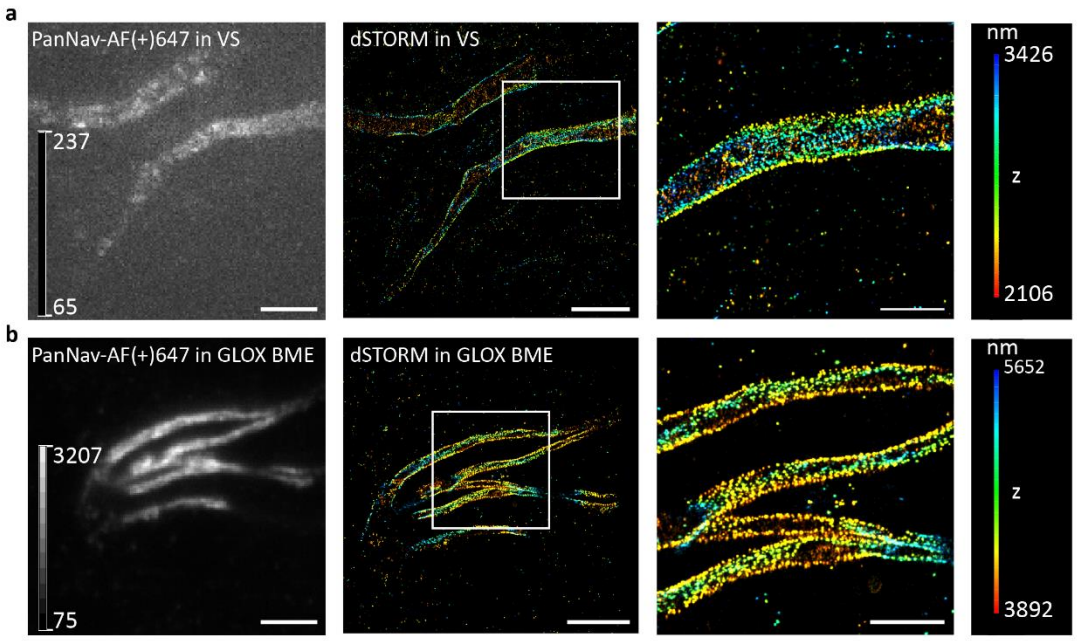

Figure 41. dSTORM imaging of the Na_V in different imaging mediums. *Mouse cortical neurons were fixed and immunostained with anti-panNa_V primary and AF(+)647) secondary antibodies. Afterwards, neurons were imaged with 3D dSTORM in Vectashield (VS) or GLOX βME imaging mediums.* ***a:*** *The representative 3D dSTORM image shows that the Na_V periodic distribution at the AIS can be resolved despite the VS quenching effect.* ***b:*** *The representative 3D dSTORM image shows that, as expected, in GLOX βME, the Na_V periodic distribution is resolved. The left panels show TIRF/HILO images acquired with a 647 nm laser before dSTORM imaging. Because of the VS quenching effect, an autoscale look-up table (LUT) intensity bar was used to ensure that AIS would be visible. The LUT intensity scale bars show minimum and maximum grey values. Middle panels show corresponding 3D dSTORM images. The right panels show an enlarged boxed region from 3D dSTORM images in the middle panels. The Z positions in the 3D dSTORM images are color-coded according to the height maps on the right. The height maps contain minimal and maximal Z-position values. Scale bars (HILO/TIRF and dSTORM images): 5 µm. Scale bars (dSTORM insets): 2 µm. The figure and the figure legends were modified from*[246].

However, dSTORM imaging in Vectashield was challenging due to the fluorescence quenching that hindered the identification of immunolabeled axon initial segments. Therefore, I had to select immunolabeled axon initial segments in PBS, save their positions, replace PBS with Vectashield, and image the selected neurons with dSTORM. To overcome this issue, I tested the suitability of 25% Vectashield for dSTORM of the AIS (**Fig. 42**). I chose this imaging medium since it has been previously used for dSTORM imaging in cell lines[136]. With both AF647 and AF(+)647, dSTORM imaging was successful (**Fig. 42**). The 25% VS effect on AF(+)647 fluorescence was similar to that observed for 100% Vectashield. Interestingly, the AF647 fluorescence was quenched to a lesser extent in 25% Vectashield (**Fig. 42a**). Therefore, I was able to search for immunolabeled AIS in 25% Vectashield when the AF647 was used.

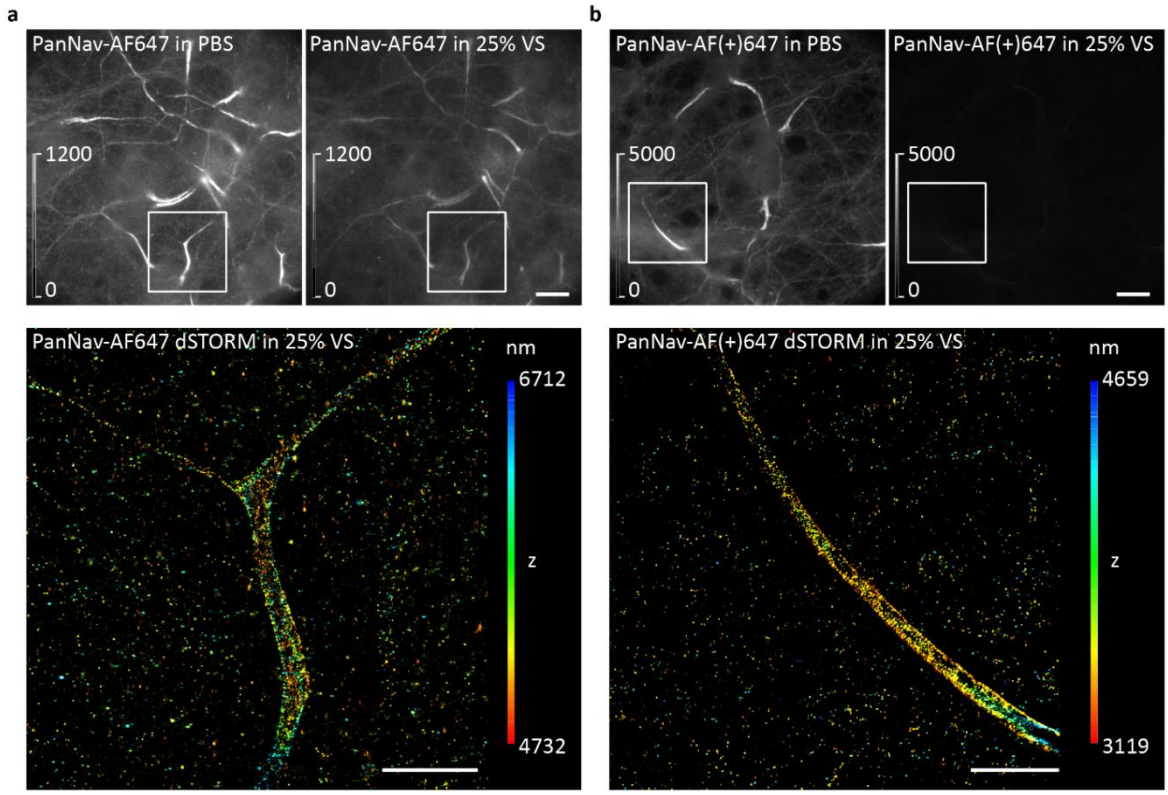

Figure 42. The 25% Vectashield (VS) effect on the AF647 and AF(+)647 fluorescence. *Mouse cortical neurons were fixed and immunostained with anti-panNa$_V$ primary and AF647 or AF(+)647) secondary antibodies. Afterwards, neurons were imaged with widefield and dSTORM microscopy. The same fields of view were first acquired in PBS and afterwards in 25% VS with widefield microscopy (upper panels in a and b). The neurons placed in 25% VS were also imaged with 3D dSTORM (lower panels in a and b).* ***a:*** *The widefield and 3D dSTORM images show the 25% VS effect on the AF647.* ***b****: The widefield and 3D dSTORM images show the 25% VS effect on the AF(+)647 fluorescence. In widefield microscopy images (a, b), the brightness and contrast were linearly adjusted to show the same display range in both PBS and 25% VS [as indicated by look-up table (LUT) intensity scale bars]. The LUT intensity scale bars show minimum and maximum grey values. The lower panels show corresponding 3D dSTORM images of the boxed regions from widefield images. The Z positions in the 3D dSTORM images are color-coded according to the height maps on the right. The height maps contain minimal and maximal Z-position values. Scale bars: 20 µm (widefield images) and 5 µm (dSTORM images). The figure and the figure legends were modified from*[246]*.*

Apart from dSTORM, the Vectashield quenching effect is important for conventional widefield and confocal microscopy. That is why I investigated this phenomenon further. The details on quantitative analysis of the AF647 and AF(+)647 fluorescence quenching in Vectashield have been published[246]. The details on the quantification of Vectashield and 25% Vectashield suitability for dSTORM imaging were described in the same publication. Since these results are published and out of the scope of my Ph.D. thesis, I did not describe them here again.

c) dSTORM imaging of click-labeled AIS and node of Ranvier components in neurons

After successfully establishing click labeling of AIS components in neurons, I attempted to combine it with dSTORM imaging. Since imaging in VS proved to be more challenging than in GLOX βME, I performed experiments that involved optimization of dSTORM imaging of click-labeled AIS components in the latter. I first attempted to establish the dSTORM of click-labeled NF186^{TAG}-HA. I started with NF186 since it was smaller and expressed at a higher level in comparison to $Na_V1.6$. As mentioned earlier in the text, AF647-tz produced high background and formed dye aggregates (**Fig. 8**). Hence, I tested AF647-Pyrimidyl-tetrazine (AF647-Pyr-tz) that had been used for click labeling of small synaptic proteins[98]. This dye produced fewer dye aggregates and, subsequently, less background than the AF647-tz. With lower background, I could use a high concentration of AF647-Pyr-tz, ensuring bright click labeling. Using a high dye concentration was necessary since AF647-Pyr-tz is less reactive than AF647-tz. As a result, dSTORM imaging of click-labeled NF186^{TAG}-HA in neurons was successful (**Fig. 43**).

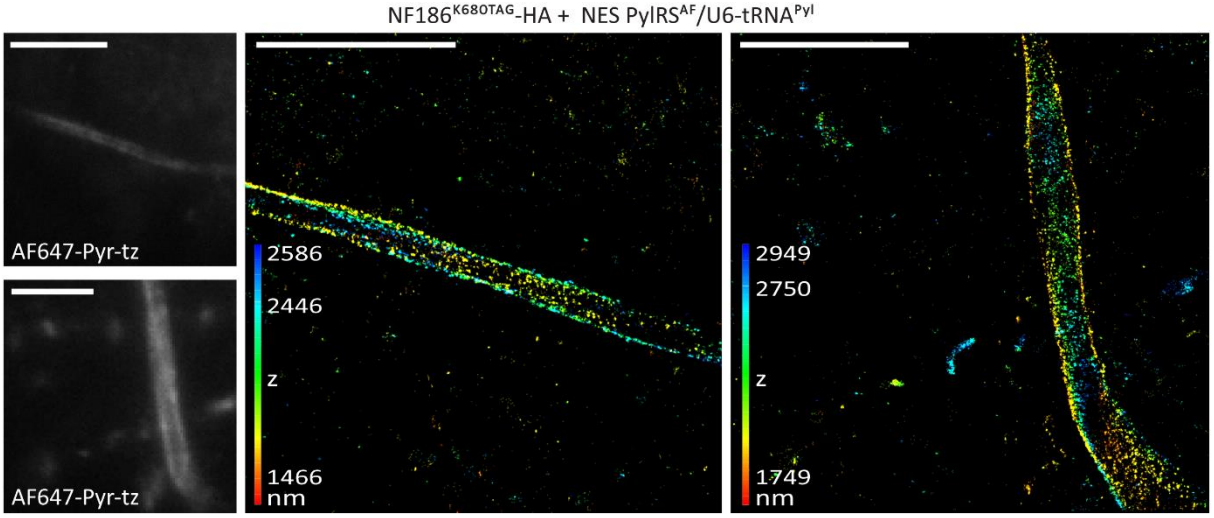

Figure 43. dSTORM microscopy of click-labeled NF186^{K680TAG}-HA in primary neurons. *The representative 3D dSTORM images of DIV 12 or DIV 14 rat cortical neurons expressing NF186^{K680TAG}-HA click-labeled with AF647-Pyr-tz. The neurons were transfected on DIV 8 or 10 with hNSE- NF186^{K680TAG}-HA and codon-optimized NES PylRS^{AF}/U6-tRNA^{Pyl}, in the presence of unnatural amino acid TCO*A-Lys. Four days after transfection, neurons were click labeled, fixed, and immunostained with anti-HA antibody. Afterwards, the neurons were imaged with 3D dSTORM microscopy in GLOX βME. The left panels show TIRF/HILO images acquired with a 647 nm laser in the click channel before dSTORM imaging. The middle and right panels show corresponding 3D dSTORM images. The Z positions in the 3D dSTORM images are color-coded according to the height maps. The height maps contain minimal and maximal Z-position values and the position of the focal planes. Scale bars (HILO/TIRF and dSTORM images): 5 µm.*

After establishing dSTORM imaging of click-labeled NF186, I attempted to do the same for $Na_V1.6$. Since the reports on the nanoscale organization of the $Na_V1.6$ isoform were lacking, I first assessed how the recombinant $Na_V1.6^{TAG}$-HA was incorporated into the membrane periodic skeleton (**Fig. 44**). To this end, I transfected DIV 8 rat cortical neurons with codon-optimized NES $PylRS^{AF}$/$tRNA^{Pyl}$ and $Na_V1.6^{K1546TAG}$-HA (**Fig. 44a**). Alternatively, I transfected DIV 8 neurons with $Na_V1.6^{K1546TAG}$-HA and transduced them with AAV#1 and 2 (**Fig. 44b**). After 4–6 days, I immunostained neurons with anti-HA primary and AF(+)647 secondary antibodies. Afterwards, I performed dSTORM of the HA+ neurons. The results showed that $Na_V1.6$ were successfully incorporated into the AIS skeleton since I observed periodic distribution in some parts of the AIS (**Fig. 44**). This arrangement also indicated that TCO*A-Lys incorporation and the overexpression of the $Na_V1.6$ did not affect the AIS nanostructure. At the moment, I am conducting additional experiments to quantify $Na_V1.6$-HA periodicity (data are not included in the thesis).

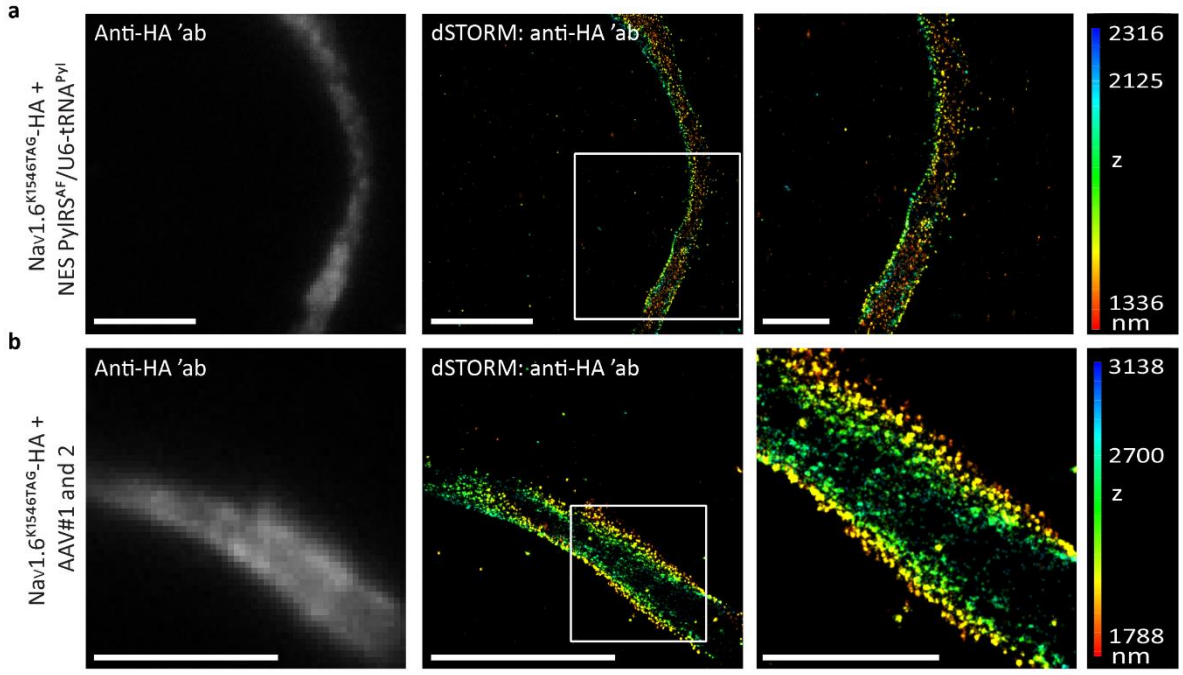

F*igure 44. dSTORM microscopy of immunostained neurons expressing $Na_V1.6^{K1546TAG}$-HA.* *Rat cortical neurons were transfected on DIV 8 with $Na_V1.6^{K1546TAG}$-HA amber mutant and codon-optimized NES $PylRS^{AF}$/U6-$tRNA^{Pyl}$ (a). Alternatively, neurons were transfected with $Na_V1.6^{K1546TAG}$-HA and transduced with AAV#1 and 2 (CMV-NES $PylRS^{AF}$ and 4x U6-$tRNA^{Pyl}$, respectively; b). Neurons were incubated with the unnatural amino acid TCO*A-Lys. After 4–6 days, neurons were fixed and immunostained with anti-HA primary and AF(+)647 secondary antibodies and imaged with 3D dSTORM in GLOX βME.* ***a–b:*** *The representative 3D dSTORM images of the anti-HA immunostained DIV 12 neurons expressing $Na_V1.6^{K1546TAG}$-HA. The left panels show TIRF/HILO images acquired with a 647 nm laser in the HA channel before dSTORM imaging. The middle panels show corresponding 3D dSTORM images. The right panels show an enlarged boxed region from 3D dSTORM images in the middle panels. The Z positions in the 3D dSTORM images are color-coded according to the height maps. The height maps contain minimal and maximal Z-position values*

and the position of the focal planes. Scale bars (HILO/TIRF and dSTORM images): 5 µm. The scale bar (3D dSTORM inset): 2 µm.

In the next step, I attempted dSTORM imaging of $Na_V1.6^{K1546TAG}$-HA that was click labeled with a high concentration of the AF647-Pyr-tz. The AAV-based delivery of the orthogonal translational machinery elements combined with transfection with the $Na_V1.6$-HA plasmid resulted in a larger number of neurons expressing recombinant $Na_V1.6$ at a higher level than the transfection (**Section 4.4b**). Therefore, I imaged only neurons transfected with $Na_V1.6$ and transduced with orthogonal translational machinery. In addition to AAV#1 and 2, I also tested AAV#4 since both (AAV#1 and 2 and AAV#4) provided lower background than other AAV combinations (**Section 4.4b**). Preliminary results suggested that dSTORM imaging of click-labeled $Na_V1.6$ is possible. However, in some instances, it was hard to distinguish labeling from the surrounding background due to low signal-to-noise-ratio (**Fig. 45**). Currently, I am working on further optimization of dSTORM imaging of click-labeled $Na_V1.6$.

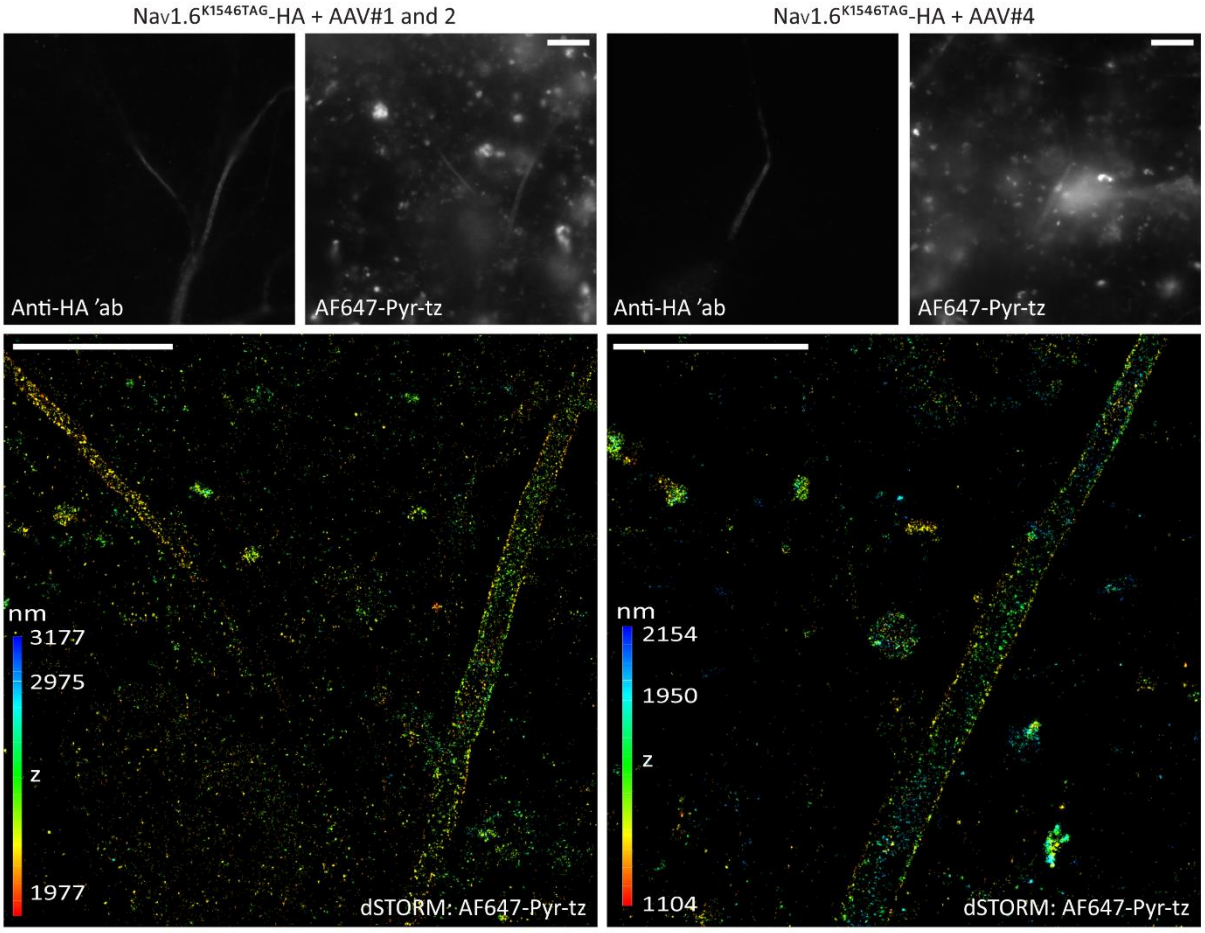

Figure 45. dSTORM microscopy of click-labeled $Na_V1.6^{K1546TAG}$-HA in primary neurons. *Rat cortical neurons were transfected on DIV 10 with $Na_V1.6^{K1546TAG}$-HA amber mutant and transduced with AAV#1 and 2 (CMV-NES $PylRS^{AF}$*

*and 4xU6-tRNA^{Pyl}, respectively) or AAV#4 (mCMV-NES PylRS^{AF}/U6-tRNA^{Pyl}) in the presence of unnatural amino acid TCO*A-Lys. Four days after the transduction (DIV 14), neurons were click labeled with AF647-Pyr-tz, fixed, and immunostained with anti-HA primary and AF555 secondary antibodies. The click-labeled neurons were imaged with 3D dSTORM in GLOX βME. The representative widefield images (upper panels) show neurons expressing Na$_V$1.6^{K1546TAG}-HA in HA and the corresponding click channel. The lower panels show 3D dSTORM of click-labeled AIS from the upper panel. For both AAVs combinations, 3D dSTORM of Na$_V$1.6^{K1546TAG}-HA was possible despite the high background. The Z positions in the 3D dSTORM images are color-coded according to the height maps. The height maps contain minimal and maximal Z-position values and the position of the focal planes. Scale bars of the widefield images: 10 µm. Scale bars of the dSTORM images: 5 µm.*

5. Discussion and further perspectives

Click labeling of the AIS components in neuronal cell lines and neurons

Labeling the AIS in living neurons is challenging due to the large sizes of its components (~140–480 kDa). Another reason is the complex and precisely regulated molecular organization of the AIS constituents that can be affected by the introduction of labeling tags. Until recently, AIS live labeling approaches have been limited to a) the bulky antibodies conjugated to fluorescent dyes, b) the N- or C-terminal FPs fusions with recombinant AIS proteins, and c) the labeling tags such as HaloTag or biotin acceptor domain (BAD)[65,83,84,96,101,119,120,123]. However, none of these approaches is ideal. On the one hand, the antibodies compatible with live-cell labeling are available only for some transmembrane AIS components (e.g., NF186). Also, the antibodies are large (~150 kDa) and cannot follow the fast dynamic changes of the AIS[96]. On the other hand, relatively large FPs and labeling tags (~30 kDa) can alter molecular interactions, trafficking, or localization of the AIS constituents[95]. Also, the overexpression of the recombinant AIS components can lead to their ectopic localization[26,95,96,117,261].

In addition, the existing labeling tags are not ideal for the SRM studies in general, including the studies of the AIS, as they place fluorophores further away from the target, increasing the linkage error[267]. New labeling approaches that bring fluorophores closer to the target proteins are in demand to reduce linkage error. Developing novel minimal labels became even more important with the development of new SRM methods such as MINFLUX, which has a resolution of ~1–5 nm[134]. With such high resolution, minimal tags are required since FPs and bulky antibodies will almost certainly limit localization accuracy and introduce artefacts[204].

An especially difficult-to-label AIS component is the voltage-gated sodium channel 1.6 isoform. Besides common problems associated with the AIS live labeling, plasmids encoding recombinant $Na_V1.6$ tend to rearrange during propagation in bacteria. The reasons are repetitive sequences and cryptic prokaryotic promoters in the *SCN8A* gene[236,251]. Also, since many highly conserved domains are indispensable for the proper functioning of the $Na_V1.6$, introducing even small tags can severely impact its function[13,14,50]. For these reasons, the number of studies involving $Na_V1.6$ live labeling and subsequent live-cell or fixed-cell imaging is limited. To my knowledge, there have been no reports on live-cell labeling of recombinant $Na_V1.6$ with fluorescent tags in cell lines. At present, there are, in total, seven reports in which FPs or extra- and intracellular labeling tags were used for the $Na_V1.6$ labeling in living primary neurons[65,80,83,84,87,123].

I overcame the issues associated with the existing AIS labeling methods, including $Na_V1.6$, by establishing a new approach that combines two modern technologies, GCE and bioorthogonal click chemistry (click labeling)[75]. The main advantages of click labeling are the small size of the UAA with attached organic dye (~0.2–2 kDa) and the possibility of introducing UAAs anywhere into the target protein[160,188]. These advantages minimize the potentially harmful effect of the labeling tag on the AIS constituents. An additional benefit of click labeling is the availability of commercial cell-permeable and cell-impermeable clickable dyes with different photophysical properties covering the visible spectrum. The variety of tetrazine dyes (e.g., bright and stable ATTO488-tz or SiR-tz, photoswitchable Cy5-tz, AF647-tz or AF647-Pyr-tz) allows combining click chemistry with various advanced microscopy techniques. The examples are recent reports in which different tetrazine dyes were used for live-cell labeling and imaging (ATTO488-tz, SiR-tz)[75,97] or super-resolution STED (SiR-tz) and dSTORM (AF647-Pyr-tz) imaging in neurons[97,98]. In these studies, cell-impermeable dyes were used to label membrane proteins and ion channels[75,98], while cell-permeable dyes were used for labeling of the intracellular cytoskeleton[97]. Recently, photoswitchable AF647-tz was combined with a powerful MINFLUX nanoscopy, allowing imaging of filopodia in cell lines with a resolution of ~2 nm[204]. Besides the abovementioned applications, clickable dyes attached directly to the target protein (1:1 ratio) could be particularly useful for quantitative SRM studies of neuronal proteins.

While I was establishing click labeling of the AIS, two papers reported labeling of small transmembrane regulatory proteins (TARPs) and neuronal cytoskeletal elements (NFL) in primary neurons using the same approach[97,98]. I contributed to the research article reporting click labeling of NFL as one of the co-authors. However, the AIS components, especially $Na_V1.6$, are much larger and have a more complex structure than the NFL and TARPs (260 kDa vs. ~35–68 kDa, respectively). As a result, the transfection and GCE efficiencies of the $Na_V1.6$ were low, leading to poor click labeling. Also, less complex structures of NFL and TARPs made it easier to select potential click labeling sites for those two. However, by optimizing transfection and labeling conditions, I expanded the application of click chemistry to large, spatially confined proteins with complex structures[75]. Furthermore, I efficiently delivered orthogonal translational machinery to neurons by taking advantage of the AAV-based viral vectors. The efficient delivery of orthogonal translational machinery increased GCE efficiency, resulting in a bright click labeling of the AIS in many neurons (~3x more neurons compared to the conventional transfection). With the new AAVs carrying orthogonal translational machinery elements, it will be much easier to establish efficient click labeling of other proteins and ion channels in neurons.

Previously, click labeling was applied for proof-of-principle studies of WT ion channels, such as NMDA, GABA-A, and Shaker B K_V, in conventional and neuronal cell lines[153,209,210]. However, click labeling of large ion channels has not been achieved in primary neurons. I demonstrated that this approach could be used to label WT and pathogenic $Na_V1.6$ in neurons, opening new opportunities to study ion channels and large neuronal proteins in their native environment with various microscopy techniques. In addition to clickable UAAs that allow visualization of molecules in living cells with microscopy, diverse UAAs have previously been exploited to study the functional properties of ion channels and receptors. The incorporation of bulky UAAs was used to study the role of specific amino acids in the inactivation of $K_V1.4$[163]. A similar approach could be applied to $Na_V1.6$. Furthermore, non-clickable photoresponsive UAAs could be used for site-specific optogenetic *in vitro* or *in vivo* studies of $Na_V1.6$ interactions, activity, and gating properties[175,179,206-208,268].

When I started establishing click labeling of the AIS components, this approach had been successfully applied for extracellular labeling and microscopy of receptors in mammalian cell lines[145,148]. There were also limited reports on the GCE-based incorporation of non-clickable UAAs in primary neurons[163,175,179] and proof-of-concept incorporation of clickable UAA into GFP in mouse brains[173]. Since the transfection efficiency of primary neurons is low, I initially attempted to establish GCE and click labeling of the $Na_V1.6$ in cell lines that are efficiently transfected and can be propagated fast. Choosing an optimal host cell line was important since HEK293T cells do not provide the most native environment for the $Na_V1.6$ expression. On the contrary, neuronal N1E-15-1 and ND7/23 share similarities with primary neurons and acquire neuronal-like phenotype upon differentiation, providing a more native environment for the proper folding and functioning of sodium channels[254-256].

Microscopy and patch clamp recordings showed that neuronal N1E-115-1 cells provided higher membrane expression of $Na_V1.6$ WT and TAG amber mutants than the ND7/23 cells. The Na^+ currents of my recombinant WT constructs recorded in ND7/23 (~0.5–1 nA) were lower than previously reported values for the recombinant $Na_V1.6$ plasmids (1–4 nA)[109], suggesting lower $Na_V1.6^{WT}$ expression in my experiments. The low Na^+ currents and $Na_V1.6$ membrane expression in ND7/23 cells were surprising since the electrophysiological recordings of recombinant $Na_V1.6$ are typically performed in those cells[13,83,84,109]. The low $Na_V1.6^{WT}$ expression could be due to the transfection of ND7/23 cells with multiple large constructs encoding GCE components (NES $PylRS^{AF}$/$tRNA^{Pyl}$) and $Na_V1.6$. Since the efficiency of multiple transfections is generally lower than one of the single transfection, this could have resulted in lower Na^+ currents measured in cells expressing recombinant $Na_V1.6^{WT}$. The Na^+ currents recorded in both ND7/23 and

N1E-115-1 cells expressing recombinant $Na_V1.6^{TAG}$ were lower than ones recorded in cells expressing $Na_V1.6^{WT}$, suggesting lower expression of $Na_V1.6^{TAG}$ amber mutants. The lower expression of $Na_V1.6^{TAG}$ constructs compared to $Na_V1.6^{WT}$ was expected since the GCE is not 100% efficient.

The results presented in this thesis implied that the N1E-115-1 provided a better environment than the ND7/23 cells for membrane expression of the sodium channels. As I showed, these cells allowed reliable electrophysiological recordings of the recombinant $Na_V1.6$ WT and TAG amber mutants. Therefore, in instances where primary neurons cannot be used (e.g., when activation or fast inactivation of recombinant $Na_V1.6$ needs to be determined), neuronal N1E-115-1 cell line can be a good alternative.

The N1E-115-1 cells proved to be a suitable host for the $Na_V1.6$ genetic code expansion and patch clamp recordings. However, I encountered multiple problems while attempting to click label $Na_V1.6^{TAG}$ in N1E-115-1 cells. The substantial dye aggregates resulted in a high background upon click labeling with commonly used Cy5-tz or AF647-tz. Although some aggregates were removed by extensive washing in culturing medium, I did not manage to remove them completely. Similar aggregates were observed in primary neurons, while they were less pronounced in the ND7/23 cells. Hence, the background was at least partially related to the cell type. The cells that formed clusters, or the ones seeded at a higher density, such as N1E-115-1 and primary neurons, possibly had more dye remaining between them. Likewise, the type[269,270] and the size[80] of the tetrazine dye may have contributed to the background, as the smaller ATTO488-tz did not form dye aggregates (I discuss this in more detail below).

Another critical problem with neuronal cell lines, particularly N1E-115-1, was false click labeling that I observed in the initial experiments. Since the false click labeling was mainly detected in cells expressing NES $PylRS^{AF}$/U6-$tRNA^{Pyl}$ in the presence of the UAAs, it was reasonable to assume that the unspecific amber codon suppression could have contributed to its appearance. However, experiments in which I compared different labeling conditions in the cells expressing NES $PylRS^{AF}$/U6-$tRNA^{Pyl}$, with and without UAA, revealed that the false labeling signal was present only when ~2 h washing step in a culturing medium before click labeling was performed. Furthermore, the click labeling-like signal was not observed in neurons. Therefore, the false click labeling was likely not a direct result of the unspecific amber codon suppression. However, I cannot entirely exclude that NES $PylRS^{AF}$/U6-$tRNA^{Pyl}$ with TCO*-A-Lys suppressed some endogenous codons in the absence of its substrate (amber mutant of the protein of interest), producing C-terminally extended proteins. Such proteins can be deleterious or act as stressors[271].

However, other reports suggest cells have mechanisms to remove C-terminally elongated and potentially harmful proteins[272]. I cannot explain why the washing in culturing medium before click labeling introduced a background while the washing after did not. A possible explanation would be that the cells that underwent transfection with orthogonal translation machinery in the presence of UAAs were more stressed. In such cells, medium change and washing before labeling could have been an additional stressor that made the tetrazine dyes somehow stick to the cell membrane. Importantly, washing before click labeling did not seem to affect neurons. Therefore, false click labeling was most likely the result of a combination of different stressors that occurred only in certain cell types. Based on these observations, when establishing click labeling of a new protein, it is essential to consider the host cell line carefully. Likewise, care should be taken that the cells are minimally stressed. Cell seeding number, transfection reagents, transfections with multiple plasmids, and medium change are just some critical factors that could affect cell viability and act as stressors. In addition, including the appropriate transfection and labeling controls is required to avoid false or unreliable results.

Even after I had reduced the background, click labeling of the $Na_V1.6$ was unsuccessful in neuronal cell lines. The most likely explanation was the insufficient $Na_V1.6^{TAG}$ expression on the cell surface. This observation was supported by the results from ND7/23 cells that expressed NF186-HA. After the $NF186^{TAG}$ expression had been reduced by exchanging the CMV with a weak hNSE promoter, previously successful click labeling became unsuccessful. Since neuronal cell lines were not optimal for $Na_V1.6$ click labeling, I aimed to establish it directly in primary neurons. However, establishing click labeling of large, spatially confined ion channels with a complex structure in primary neurons was technically challenging. Therefore, using a smaller target with a less complex structure facilitated the optimization of expression, transfection, and click labeling in neurons. $Na_V1.6$-associated protein NF186 was a perfect candidate due to its smaller size (~186 kDa), lack of repetitive domains, and less complex structural organization compared to $Na_V1.6$[89].

I used NF186 to establish the click labeling of the AIS in living neurons since it is a smaller target with a less complex structure than the $Na_V1.6$. However, NF186 itself represents an interesting target to study due to its essential roles in the AIS and node of Ranvier maintenance and establishment[9-11]. So far, FPs have been used to study NF186 targeting to the AIS during development in living neurons[118]. There are also studies in which antibodies were used to study NF186 regulation at the AIS[115] or to demonstrate NF186 roles in organizing extracellular matrix at the AIS[102]. Small UAA-based tags could be applied to study these processes in more detail

with SRM and live-cell microscopy without the risk of tag-induced perturbations. Furthermore, click labeling could be used to follow the NF186 plasticity in the AIS upon depolarization or injury, which has been impossible with fluorescent antibodies or GFP-based tags[95,96].

Click labeling optimization typically involves a selection of the amber mutant with the strongest expression level since such a mutant has the highest chance of being labeled. However, this rule cannot be applied to recombinant AIS components as their overexpression can affect the AIS structure[26,96,117,261]. For example, although NF186^{TAG} amber mutants under the control of a strong CMV promoter were successfully click labeled, I could not use them because they were ectopically expressed. Even after I lowered the expression level of NF186 by replacing CMV with a weak hNSE promoter[117], some amber mutants, such as K809TAG, remained mislocalized. Therefore, probing multiple amber mutants was required to find one with proper localization and bright click labeling.

An additional issue with the GCE inherent to (multiple) transfections was the difference in protein expression levels between individual cells. The non-uniform expression was especially problematic for the recombinant AIS components, NF186-HA and $Na_V1.6$-HA, since it resulted in their mislocalization in some neurons. In the other neurons, these AIS components localized properly. The unequal expression levels of recombinant NF186-HA and $Na_V1.6$-HA between neurons could explain why the AIS length of neurons expressing these two AIS components were slightly longer than that of the untransfected cells, although the difference did not appear significant. In addition, the combined expression of endogenous and recombinant NF186 or $Na_V1.6$ might have contributed to the slightly longer AIS length of the transfected neurons. The difference in the AIS length between transfected and untransfected neurons could be reduced by knocking down or silencing endogenous proteins with small interfering (si)RNA or short hairpin (sh)RNA[102,273]. It should also be kept in mind that the expression level and subsequent localization of the protein of interest will depend on its size. For example, smaller NF186 (186 kDa) was ectopically localized more frequently compared to the larger $Na_V1.6$ (~260 kDa) that localized properly at the AIS in almost all the instances. The slight $Na_V1.6$ mislocalization was observed in a few neurons only when its expression was increased using highly efficient AAVs, including those carrying eRF1^{E55D} (this will be discussed later in the text).

Another factor that affects UAA incorporation efficiency is the context around the TAG site[224]. Depending on the TAG position, the amber mutant could become more susceptible to readthrough (expression of amber mutant in the absence of UAA) or exhibit a lower expression level. For all of the tested amber mutants, I observed no readthrough in the absence of the UAA.

However, I did observe the difference in the expression levels between different NF186 or $Na_V1.6$ amber mutants. The expression level mostly correlated with the iPASS scores that predict the suppression efficiency of the amber mutants[224] [NF186; 1.86 (K680TAG) vs. 0.62 (K524TAG); $Na_V1.6$: 0.9 (K1425TAG) vs. 2.05 (K1546TAG)]. The position of amber mutation will affect not only not GCE but also click labeling efficiency. Even if certain TAG labeling sites provide the optimal expression level and do not affect the function or localization of a target protein, they also need to be accessible for tetrazine dye. An example is $Na_V1.6^{K1425TAG}$ which was poorly click labeled compared to $Na_V1.6^{K1546TAG}$. Although the expression level of the $Na_V1.6^{K1425TAG}$ was slightly lower than the $Na_V1.6^{K1546TAG}$, as shown by microscopy and patch clamp, the main reason for the poor click labeling of this mutant was most likely the UAA inaccessibility for tetrazine dye. This observation was supported by the microscopy results showing that the highly-efficient AAVs used for delivery of the GCE elements increased the expression levels of $Na_V1.6^{K1425TAG}$ while the click labeling improved only slightly. To further confirm these findings, I looked at the positions of incorporated UAAs using the recently developed AlphaFold Protein Structure Database (AlphaFold DB, https://alphafold.ebi.ac.uk) that predicts 3D protein structure models[263]. According to the predicted 3D $Na_V1.6$ structure, UAA incorporated at position K1546TAG is exposed on the protein surface, while one incorporated at K1425TAG is buried between different domains of the channel. Therefore, tetrazine dye seemed to have better access to the UAA incorporated at the K1546TAG position, explaining the higher efficiency of click labeling of the $Na_V1.6^{K1546TAG}$ amber mutant compared to the $Na_V1.6^{K1425TAG}$.

Since $Na_V1.6^{K1546TAG}$ showed bright click labeling with minimal changes in its biophysical properties manifested in ~2.8 mV shift of the inactivation curve compared to the $Na_V1.6^{WT}$, I used this amber mutant in further experiments. The previous reports in which a larger (17 amino acids) BAD domain had been introduced at position K1546 for labeling and live imaging studies of the $Na_V1.6$ support the suitability of this position for click labeling[80,84,87]. The $Na_V1.6$ function was minimally affected by BAD introduction, i.e., only current density was reduced[84]. I did not observe a significant difference in the current density of K1546TAG vs. WT, while the current density of low-expressed K1425TAG was significantly reduced compared to WT. Contrary to Akin et al., although small (2.8 mV), a shift in the inactivation curve of K1546TAG was significant[84]. These results were unexpected since I introduced only one amino acid change at the same position instead of 17 amino acids. The discrepancy in the results could have arisen from the lower number of recorded cells in the previous study (9 $Na_V1.6^{BAD}$-GFP vs. 6 $Na_V1.6^{WT}$-GFP) compared to the number of cells recorded in my work (18 $Na_V1.6^{TAG}$-HA vs. 20 $Na_V1.6^{WT}$-HA)[75,84]. Alternatively, the host cell line in which $Na_V1.6$ was recorded (ND7/23 vs. N1E-1115-1) or TTXr mutation (Y371S

vs. Y371C) could have led to the difference between the results reported in Akin et al. and my results.

In addition to the $Na_V1.6$ expression in the AIS, using confocal and PALM microscopy, Akin et al. detected ~230 nm $Na_V1.6$ nanoclusters in the somatic compartment[80]. Click labeling of the K546TAG amber mutant allowed the detection of the $Na_V1.6$ in the AIS. However, I did not observe previously reported membrane somatic nanoclusters[80] in living or fixed neurons. Possibly, such small clusters cannot be detected with click chemistry since, with this approach, there is no fluorescent signal amplification (one dye molecule labels one $Na_V1.6$). With the immunostaining of the HA tag, I also detected somatic $Na_V1.6$, which represented the total $Na_V1.6$ pool. However, as the immunostaining is done upon fixation and permeabilization, these immunostained somatic channels represented the total $Na_V1.6$ pool, and I could not distinguish between intracellular and extracellular somatic $Na_V1.6$.

After establishing click labeling of the AIS, I demonstrated the applicability of this approach for the AIS studies by investigating the localization of previously described pathogenic epilepsy-causing $Na_V1.6$ mutations with the LOF effect in cell lines and primary neurons[13]. The pathogenic mutants were expressed at the same level as the control in the AIS, as shown by click labeling, while the Na^+ currents recorded in neuronal cells were almost completely abolished, similarly to the previous work[13]. These results suggested that LOF mutations affected the function of the $Na_V1.6$ rather than its trafficking to the neuronal membrane. This conclusion was further supported by the fact that both mutations were located in the transmembrane domain IV and not in domains essential for trafficking and maintenance of the $Na_V1.6$ on the membrane (e.g., N-terminus and ABD)[83,84,87]. It would be interesting to use click chemistry to further explore the effect of these two pathogenic mutations. UAA-minimal tags can be utilized to follow the internalization or the stability and mobility of I1652N and T1785P $Na_V1.6$ variants in living neurons. Apart from these two, it would be interesting to click label other $Na_V1.6$ with LOF effect[13] and to determine if they are exported to AIS. Likewise, click labeling can be used to study the trafficking and localization of pathogenic variants with the gain of function effect[13]. If the pathogenic $Na_V1.6$ variants have a reduced or absent expression on the neuronal surface, they could be pulse-chased labeled with cell-permeable and cell-impermeable tetrazine dyes. The pulse-chase labeling with two tetrazine dyes has been previously used to study different populations of the same membrane receptor[148] and cytoskeletal elements[97]. Applying this approach to $Na_V1.6$ will allow studying if the pathogenic variants get internalized or retained in the cytosol. Trafficking and localization studies of the pathogenic $Na_V1.6$ represent one of many potential applications of click

labeling. Other potential applications include studies of different $Na_V1.6$ populations or expression of newly synthesized $Na_V1.6$ during the development and pathological conditions such as neuronal injury.

During my Ph.D. I established click labeling of the AIS in primary non-myelinated neurons. To study the nodes of Ranvier, it would be necessary to establish click labeling in myelinating co-cultures or slice cultures. This would allow studying the nodes of Ranvier components, NF186 and $Na_V1.6$, with live-cell and SRM microscopy in health and disease. To this end, expressing recombinant nodal components at the later DIV in primary neurons would be required. Later expression of NF186 and $Na_V1.6$ could be accomplished with inducible promoters[98]. For the expression in slice cultures, the AAVs described in my thesis could be used to efficiently deliver the GCE components. Also, these AAVs may allow NF186 or Nav1.6 labeling in human brain slice cultures[274].

To some extent, the short- and long-term AIS plasticity has been studied in living and fixed neurons[34,35,96,123]. However, it remains elusive whether the AIS in co-cultured neurons undergoes plasticity the same way as in non-myelinated cultured neurons. Likewise, the nodes of Ranvier plasticity have not been studied extensively with microscopy in living neurons. Therefore, it remains unclear if and how the nodes of Ranvier undergo plasticity. Click chemistry could be used to follow the nodes of Ranvier in real-time and answer these questions. Likewise, click chemistry could be utilized to study the pathogenic changes in the nodes of Ranvier directly. In that regard, it would be interesting to examine how $Na_V1.6$ redistributes upon oxidative injury in co-cultured neurons. These future experiments could help to reveal the mechanism of neurodegenerative diseases such as multiple sclerosis (e.g., it has been shown that the nodes of Ranvier are particularly vulnerable in the previously described reversible form of axonal injury[275]). For such studies, the recombinant proteins should be specifically expressed in neurons but not glial cells. A specific expression could be achieved with neuron-specific promoters for the amber mutant and orthogonal translational machinery.

In addition to the studies of $Na_V1.6$, new minimally invasive approaches for live labeling of the other Na_V isoforms would be necessary for further discoveries in the field since such approaches are currently lacking. Considering that the structure of the Na_V is highly conserved, the labeling approach developed for one isoform can be easily adapted for other isoforms. The example is a BAD domain that was originally used for live labeling Nav1.6 and later transferred to $Na_V1.7$. [84,121]. Similarly, the click chemistry could be easily adapted for live labeling of other Na_V isoforms. Selecting potential click labeling sites will be even easier with the development of the

abovementioned AlphaFold Protein Structure Database[263]. Neuronal $Na_V1.1$ and $Na_V1.2$, implicated in different neurodevelopmental and neurodegenerative diseases, are particularly interesting[12,14,50,276]. However, labeling these, even with conventional immunostaining in fixed cells/tissue, is challenging[277]. Live labeling of $Na_V1.2$ is limited to relatively large FPs that can potentially introduce artefacts[65,123]. To my knowledge, there are no reports on the $Na_V1.1$ live labeling in cultured neurons. Click chemistry can be used for localization and trafficking studies of WT and pathogenic variants of these two Na_V isoforms. Live labeling approaches for the $Na_V1.7$, which is highly expressed in the PNS and included in the regulation of pain sensation, are also limited[121]. Click labeling of the $Na_V1.7$ could help reveal mechanisms of pain sensation in the sensory neurons. Moreover, click labeling could find applications beyond neuroscience for labeling of cardiac $Na_V1.5$ isoform that had been implicated in Brugada syndrome[50,276]. With detailed protocols and optimizations described in this thesis and accompanying paper[75] and the highly efficient AAVs, other large and spatially-confined ion channels and neuronal proteins for which labeling approaches are lacking can be easily labeled with click chemistry.

Highly efficient genetic code expansion and click labeling of neuronal proteins in neuronal cell lines and primary neurons

The main limiting factor for successful GCE in mammalian cells, including neurons, is the expression of orthogonal tRNA imported from other domains of life[159,160,222]. Likewise, the ratio between aaRS and tRNA can influence GCE efficiency[227]. I designed a new plasmid that increased the GCE efficiency in mammalian cell lines and primary neurons, as shown by the widefield microscopy. The novelty introduced in this plasmid was an improved (codon-optimized) NES $PylRS^{AF}$ gene for expression in eukaryotic cells combined with a single copy of U6-$tRNA^{Pyl}$. It was not surprising that codon optimization of the gene encoding NES $PylRS^{AF}$ improved the efficiency of the GCE compared to the non-optimized version[150]. The optimized codons are used more optimally in mammalian cells, resulting in a more efficient translation and improved expression of the aaRS. These findings were supported by a recent publication from our laboratory in which NFL^{TAG} amber mutant was labeled in neurons with click chemistry[97]. This study showed by quantitative western blot that the codon-optimized NES $PylRS^{AF}$/U6-$tRNA^{Pyl}$ plasmid was more efficient than the corresponding plasmid that bore a non-optimized NES $PylRS^{AF}$ version. Furthermore, Arsić et al. showed that codon-optimized NES $PylRS^{AF}$ was more efficient in combination with $tRNA^{Pyl}$ than when combined with four copies of the improved $tRNA^{M15}$ described by Serfling et al[151]. These results were somehow surprising since Serfling et al. reported that the 4xU6-$tRNA^{M15}$ cassette was more efficient than the U6-$tRNA^{Pyl}$. The discrepancy between

these two publications was most likely due to the difference in NES PylRS^{AF} that was used (codon-optimized Arsić et al. vs. codon non-optimized in Serfling et al.). The widefield microscopy results described in my thesis are in agreement with the results published in Arsić et al[97]. However, quantitative analysis (microscopy, fluorescence-activated cell sorting—FACS, and western blot) will be needed to estimate the exact differences in the efficiency of 4xU6-tRNA^{M15} and U6-tRNA^{Pyl} as well as codon-optimized and non-optimized NES PylRS^{AF}.

To boost the GCE efficiency, I also attempted to increase the efficiency of the orthogonal tRNA^{Pyl} expression by improving its stability. To this aim, I removed the variable polyT tail from tRNA^{Pyl} using a self-cleaving HDV ribozyme[278]. Previously, HDV ribozyme had been inserted between the 3' end of the CRISPR (cr)RNA, a part of the CRISPR/Cpf1 (CRISPR-associated endonuclease in prevotella and francisella 1) system, used for genome editing[279] and the polyT to release free crRNA and increased its activity[216]. However, in the same study inserting HDV ribozyme at the 3' end of gRNA (a part of the CRISPR/Cas9 genome editing technology) did not increase its activity[216]. As I showed by widefield microscopy, HDV did not seem to improve the GCE efficiency. However, quantification and further experiments are needed to determine the exact effect of HDV on the tRNA stability and GCE efficiency. Since the activity of the HDV ribozyme depends on the surrounding sequences, engineering those might improve its effectiveness and, subsequently, stability of the orthogonal tRNA[216,217]. The GCE efficiency could also be improved by engineering 5' and 3' sequences surrounding orthogonal tRNA^{Pyl}. Alternatively, directed evolution or further engineering the tRNA^{Pyl} could help[151,220].

For efficient GCE and click labeling of endogenous proteins in primary neurons or recombinant proteins in slice cultures, organoids, and animal models, delivering one copy of the orthogonal tRNA might not be enough[173,180,227]. The quantitative analysis of the intensity of fluorescent reporters in neurons transduced with AAVs showed no significant difference between one and four copies of tRNA^{Pyl}, as described in the Results section. Therefore, it might be necessary to deliver more than four U6-tRNA^{Pyl} copies, e.g., 16 copies, as reported previously[227]. However, such a high number of U6-tRNA^{Pyl} copies increases the probability of recombination between repetitive sequences. I attempted to overcome this issue by probing additional type 3 pol III promoters (Y3, MRP/7-2, 7SK) that could be combined with the commonly used strong U6 promoters[226,244]. Although widefield microscopy implied that none of the tested promoters proved more efficient than the U6, an additional characterization and quantitative analysis with FACS might help identify the promoter with similar or higher efficiency. Based on widefield microscopy results from this thesis and the previously published literature[180], 7SK might be promising in this

regard. Alternative promoters would also allow fine-tuning tRNA expression depending on the target protein, host cell line, and experimental design.

Alternatively, a 5' self-cleaving Hammerhead ribozyme (HH) and the 3' self-cleaving HDV[278] could be combined to express multiple tRNA^{Pyl} from a single promoter. The combination of these two has been used to simultaneously express multiple gRNA from U6 or CMV promoters[280]. The same strategy could be used to express multiple tRNA^{Pyl} from a single U6 promoter or to express tRNA^{Pyl} together with aaRS from a single CMV promoter. As suggested in[280], this approach could also help pack multiple tRNA^{Pyl} in the AAVs.

As discussed above, the GCE of proteins expressed in mammalian cells, and in particular primary neurons, is generally low to moderate due to inefficient expression of orthogonal tRNA[160,222]. The transfection efficiency of non-dividing primary neurons is also low[163], especially when multiple and large plasmids, such as those encoding *SCN8A* and GCE components, need to be delivered. Low transfection combined with low GCE efficiency results in the poor expression of amber mutants of protein of interest in a few neurons. I partially overcame these problems and successfully established click labeling of the AIS in living primary neurons[75] by using conventional transfections for GCE based on the existing work from our laboratory[97]. However, further improvements in the GCE efficiency, resulting in a high number of neurons expressing amber mutant, would allow more reliable quantitative, SRM, and live-imaging studies. It would also allow efficient click labeling of neuronal proteins in more complex model systems such as slice cultures, organoids, and living animals. Although the endogenous NFL has been tagged with clickable UAAs in neurons[97], site-specific click labeling of NFL and other proteins might not be possible with conventional transfection due to the low GCE efficiency. Hence, the highly efficient GCE would enable site-specific labeling of endogenous proteins at their native level of expression. For these reasons, I probed viral vectors for the delivery of the GCE components.

Baculoviruses with a stable genome that tolerates repetitive sequences and can accept large cargo[231,232] have been previously used to deliver simultaneously five different proteins to primary neurons[233]. Baculoviral-based vectors, such as pACBac, have also been utilized for the GCE of fluorescent reporters in neurons and mouse brains[226,227]. The MultiBacTAG system was used for UAA incorporation and click labeling of recombinant eukaryotic proteins produced in Sf21 insect cells[281]. Therefore, baculoviruses are promising vectors for the delivery of all GCE components to primary neurons, including multiple tRNA copies and genes encoding large AIS components. However, in my hands, MultiBacMam production was tedious, time-consuming, with high variability between experiments. I noticed inconsistent virus quality and differences in virus

titers collected from the V2 generations. The same happened even when multiple V2 were generated from the same V1 generation. I did not achieve a high MOI even when I (ultra)concentrated V2. Therefore, I had to use large amounts of virus to transduce mammalian cells successfully. In order to improve transduction efficiency, it will be necessary to increase the MOI of the baculoviruses. To this end, different protocols for virus production and purification need to be tested.

An additional issue with baculoviruses was the low transduction efficiency of ND7/23 cells. According to the manufacturer of the MultiBacMam™ system (Geneva Biotech), some neuronal cell lines might be less susceptible to transduction with baculoviruses. Therefore, other neuronal cell lines could be used for experiments involving baculoviruses. Although baculoviruses allowed the successful transduction of a high number of HEK293T cells, the efficiency of the amber codon suppression was low due to the insufficient expression of the orthogonal $tRNA^{Pyl}$. Creating a baculovirus that bears multiple tRNA copies and combining it with one that carries amber mutant and NES $PylRS^{AF}$ might solve the problem of insufficient $tRNA^{Pyl227}$ even at lower MOIs. Alternatively, previously published pAcBac vectors[227] could be tested instead of the MultiBacMam system.

When testing baculoviruses, I observed that the expression level of NF186 amber mutant in HEK293T cells was low even when cells were transfected with additional $tRNA^{Pyl}$. Generating fresh baculoviruses might solve this problem since I observed differences between various V2 batches. Regarding $Na_V1.6$ baculoviruses generation, special conditions might be required. For example, it might be necessary to propagate viruses at less than 30 °C since there is no available information on the mutation rate of $Na_V1.6$ in Sf21 cells and to sequence the whole bacmid genome to determine that the *SCN8A* gene is intact[236].

Due to the variability of the titers and quality of the baculoviral stocks, I started, in parallel, to optimize an alternative approach that involved the use of AAV-based viral vectors for the delivery of GCE components. Since this approach allowed efficient and reliable GCE in neurons, I did not further optimize MultiBacMam.

As expected, the initial test experiments showed that AAVs improved the GCE efficiency of a dual fluorescent reporter compared to conventional transfection, resulting in many neurons expressing $mCherry\text{-}GFP^{TAG}$. However, due to the low cargo capacity[231], large AIS components could not be packed into AAVs. Nevertheless, by combining transfections and transductions, I increased the number of neurons expressing $Na_V1.6$ by ~3.5 times. For the AVVs generation, a

codon non-optimized NES PylRS^{AF} was used. Generating AAV with codon-optimized NES PylRS^{AF} might further improve $Na_V1.6$ GCE and click labeling efficiency. Such a virus might also help improve the dSTORM quality of click-labeled $Na_V1.6$. However, combining transduction and transfection for experiments involving GCE and click labeling of $Na_V1.6$ in living animals or mouse brains might be challenging. That is why optimizing baculoviruses for amber mutant and orthogonal translational machinery delivery is still worth considering.

It has previously been reported that the co-expression of the eRF1^{E55D} with orthogonal translational machinery and amber mutant of a target protein improved the efficiency of the GCE[222]. Hence, as expected, adding AAVs that bore eRF1^{E55D} mutant further improved the efficiency of GCE in neurons. These results agreed with the previously published report[97] in which eRF1^{E55D} combined with codon-optimized NES PylRS^{AF}/U6-tRNA^{Pyl} boosted NFL^{TAG} GCE efficiency from 48.6% to 97.4% and even allowed labeling of the endogenous NFL. However, due to the high GCE efficiency, eRF1^{E55D}, in some instances, led to the overexpression of the $Na_V1.6^{TAG}$. Hence, I did not use the recombinant eRF1^{E55D} mutant for click labeling of recombinant AIS components. Nevertheless, eRF1^{E55D} might be helpful for click labeling of other neuronal proteins that are not spatially confined. In addition to overexpression, I observed higher background in the click channel in neurons transduced with eRF1^{E55D} in the presence of the UAA. I did not investigate this further due to time constraints. However, one explanation could be that eRF1^{E55D} increased the expression of AIS components too much, resulting in a higher number of dead cells that accumulated ATTO488-tz. Another explanation could be a potential effect of the eRF1^{E55D} mutant on the translation termination of endogenous proteins. The latter explanation is less likely since the previous experiments from our laboratory with the eRF1^{E55D} mutant implied that its overexpression did not seem to significantly increase unspecific amber codon suppression in primary neurons[97]. Thus, further optimization of transduction conditions with AAVs carrying eRF1^{E55D} will be highly beneficial for site-specific click labeling of endogenous AIS components and other neuronal targets.

Establishing labeling of the endogenous proteins in living neurons is essential since it would allow studying them under physiological conditions. Labeling endogenous AIS components is particularly important since it will solve the mislocalization problem associated with the overexpression of recombinant constructs. At present, there is some progress toward labeling endogenous AIS components. Using CRISPR/Cas9 technology, I and other members of the laboratory labeled endogenous NF186 with a GFP tag (unpublished data). Also, the endogenous Na_V was labeled with GFP, V5, or HA tags[65,123]. However, similarly to recombinant proteins,

tagging endogenous proteins with relatively large tags could affect their localization or function. Recently, CRISPR/Cas9 has been combined with click chemistry for proof-of principle labeling of the endogenous NFL with minimally invasive UAA tags[97]. To achieve labeling of the endogenous NFL, the linker that bore TAG amber mutation followed by a 3xFLAG tag was added to its C terminus. The introduction of the UAAs into the C-terminal linker prevented the knockdown of the NFL, which would be caused by low amber codon suppression efficiency. Although promising, the disadvantage of this approach, apart from the low GCE efficiency, was click labeling in a few neurons and the absence of site-specificity. Therefore, GCE efficiency would need to be increased to achieve site-specific labeling of endogenous proteins.

The site-specific labeling could be achieved with the AAVs carrying 4xU6-tRNA^{Pyl} and eRF1^{E55D}. The other laboratory members and I are currently testing this strategy for site-specific UAA incorporation and click labeling of endogenous NF186. The NF186 was chosen because it was highly expressed and click labeled even with conventional transfections. Although it might appear challenging, the AAVs and further optimization of the method could allow the click labeling of the endogenous $Na_V1.6$. To this end, iPSCs might be more suitable since they would enable the generation of clones that stably express orthogonal translational machinery[180]. In this regard, the inducible GCE technology[282] or inducible promoters[98] can be used to switch on the expression of the specific orthogonal components. High expression of the endogenous amber mutant could be achieved with the expression of the eRF1^{E55D} and multiple tRNA copies (16 or more).

Super-resolution imaging of click-labeled AIS and node of Ranvier components

One of the advantages of click labeling is its compatibility with advanced super-resolution microscopy techniques, such as GSDM[148], dSTORM[98], STED[97], MINFLUX[204], and click-PAINT[150]. However, most of the previous studies have been carried out in cell lines[148,150,204]. Recent studies have reported the application of click labeling for STED and dSTORM imaging of small membrane and cytosolic proteins in primary neurons[97,98]. Combining UAA-based minimal tags with SRM microscopy would allow studying the AIS compartment at the single-molecule level. However, SRM imaging of the large, spatially confined AIS components, organized in a complex way, brings additional challenges compared to imaging of small and highly abundant proteins (e.g., TARPs, NFL). The AIS components are periodically arranged with a spacing of 190 nm[16,28]. Capturing the periodic organization of NF186 and Na_V is not straightforward due to their less regular periodicity and lack of highly-specific antibodies and other labeling tags. That is why only a few proof-of-principle reports on dSTORM and DNA-PAINT imaging of immunolabeled NF186 and Na_V have been published[16,28]. The nanoscale organization of the $Na_V1.6$ at the AIS is unclear

since most of the abovementioned studies used an anti-panNa_V antibody that recognizes all sodium channel isoforms. By combining conventional immunostaining and dSTORM, I obtained SRM images showing the periodic distribution of the NF186 and Na_V, as previously reported[16,28]. However, not every imaged AIS immunostained with the panNa_V antibody exhibited periodic organization. In addition, as previously suggested[28], I observed that Na_V periodicity was less regular, i.e., ring-like patterns were observed only in some regions of the immunostained axon initial segments. The published literature also suggests that at the nodes of Ranvier, NF186 and Na_V are not distributed homogenously[45]. Since the AIS and the nodes of Ranvier share structural organization, that could explain the lack of periodicity in some regions of the AIS. Another reason for the lack of periodicity could be the Na_V sensitivity to strong fixatives, such as PFA, that can mask the epitopes recognized by panNa_V antibodies[277]. This is supported by the ongoing experiments that are not included in the thesis, in which optimization of fixation protocols resulted in better preservation of the Na_V periodicity.

The dSTORM imaging of the neurons immunostained with anti-Na_V1.6 antibody did not reveal apparent periodicity, most likely due to the poor quality of the immunostaining with this antibody. On the contrary, the results presented in this thesis, which involved dSTORM imaging of a large number of neurons expressing recombinant Na_V1.6-HA immunostained with an anti-HA antibody, showed that the ring-like distribution of the recombinant Na_V1.6, confirming that the 1.6 isoform is at least partially periodically arranged at the AIS. Currently, I am conducting additional experiments involving immunostaining with an anti-HA antibody to quantify the periodicity of recombinant Na_V1.6 at the AIS.

After confirming with the immunostaining that Na_V1.6-HA was periodically arranged, I attempted to establish dSTORM imaging of click-labeled AIS components. With the immunostaining approach, primary antibodies specific to the protein of interest are recognized by multiple secondary antibodies conjugated to a fluorescent dye, resulting in the amplification of the fluorescent signal. With click labeling, the fluorescent dye is directly attached to a protein of interest. Since there is no signal amplification, the intensity of click labeling is usually weaker than the conventional immunostaining. Since the main requirement for a successful dSTORM is bright labeling of a target protein, the background must be minimal to acquire high-quality SRM images of click-labeled proteins. When I attempted to establish dSTORM of click-labeled AIS components in primary neurons, one of the main issues was the lower quality of labeling with photoswitchable far-red dyes (AF647-tz and Cy5-tz) compared to the ATTO488-tz. In addition, click labeling of primary neurons with far-red dyes resulted in numerous dye accumulations that contributed to the

low signal-to-noise ratio. The high background can be explained by the tendency of certain dyes (e.g., Cy5) to form aggregates in aqueous solution at higher concentrations, such as those used for click labeling (5 µM) [269,270]. That would also explain why such aggregates were not observed for ATTO488-tz (5 µM) or lower Cy5-tz dye concentrations used for dSTORM of click-labeled TARPs (0.5 µM or 1 µM)[98]. The click labeling quality could also depend on the dye size. The higher quality of $Na_V1.6$ click labeling with ATTO488-tz (Mw = 758.78 g/mol) than the AF647-tz or Cy5-tz (Mw > 1100 g/mol) was most likely caused by the inaccessibility of larger dyes to the incorporated TCO*A-Lys[80]. However, increasing the concentration of larger tetrazine dyes improved click labeling. As I showed, AF647-Pyr-tz used at high concentrations (12.5 µM) allowed SRM of the click-labeled AIS. I chose this dye since it formed fewer aggregates compared to the AF647-tz or Cy5-tz. With such optimized conditions, I successfully imaged click-labeled NF186 with dSTORM microscopy. In addition, by using AAVs to increase GCE efficiency, I obtained dSTORM images of click-labeled neurons expressing recombinant $Na_V1.6$. However, due to the lower signal-to-noise ratio and slightly worse click labeling signal, the quality of dSTORM images of the $Na_V1.6$ was lower compared to NF186. Further optimization will be necessary to improve the dSTORM quality of click-labeled $Na_V1.6$. I am currently trying to improve the click labeling by probing new AVVs carrying codon-optimized NES $PylRS^{AF}$. In addition, the other colleagues from the laboratory and I are attempting to establish click-PAINT, which has been used for SRM imaging of low-abundance and difficult-to-label proteins[150]. These experiments are ongoing and therefore are not included in the thesis.

Establishing click-PAINT of the AIS would have additional advantages compared to (d)STORM. For example, combining DNA- and click-PAINT would allow high-quality multi-color SRM imaging of the AIS components[16,46]. Although multi-color STORM of AIS components[16,28] and dSTORM of highly-abundant proteins[136,137] have been achieved, both approaches have limitations. The fluorescent antibodies compatible with STORM are not commercially available; hence, this approach is not easy to implement in the laboratory. Regarding dSTORM, the number of suitable combinations of photoswitchable dyes is limited. Besides commonly used AF647, AF555 or AF568 can be used for dSTORM in combination with GLOX MEA imaging buffer[135]. However, the blinking properties of orange dyes are inferior compared to the AF647[135], resulting in lower quality of dSTORM images in the second channel. This could be especially problematic when fine structures, such as the periodic skeleton at the AIS, need to be resolved. In addition, establishing click-PAINT would also allow studying different populations of the AIS components, labeled with different dyes, during development or injury, with high precision. Alternatively, to

study different populations of the AIS components with high precision, click-PAINT could be combined with click labeling.

Regarding the dSTORM imaging of immunostained or click-labeled proteins, the additional disadvantage is the requirement for a unique GLOX imaging buffer that induces photoswitching of the fluorophores[135]. After the samples are placed in GLOX, they cannot be reused and are discarded upon imaging. Furthermore, immunostained or click-labeled samples are usually stored in PBS before imaging. Since the fluorescence in PBS fades with time, samples cannot be stored for more than a few days. A possible solution would be to store and image samples in 25% VS[136,246]. Alternatively, another SRM imaging approach (e.g., STED) can be explored[97] since, for this approach, buffers that allow long-term storage could be used.

In conclusion, I successfully incorporated UAA-based minimal tags into two AIS and node of Ranvier components (NF186 and $Na_V1.6$) by taking advantage of the GCE technology. Using a bioorthogonal click reaction, I subsequently labeled incorporated UAAs with small organic dyes in living neurons. I expanded the application of click chemistry for labeling of large and spatially-confined proteins with a complex organization, including voltage-gated ion channels. Apart from proof-of-principle labeling and imaging of the wild-type AIS constituents, I demonstrated that click labeling could be used for localization studies of the pathogenic AIS components and dSTORM imaging of the AIS. A new minimally invasive tool that allows studying AIS and nodes of Ranvier components with advanced microscopy will help answer many questions regarding ion channels and AIS and the node of Ranvier biology. The significance of my Ph.D. work goes beyond AIS and the nodes of Ranvier components since I found a way to improve GCE and click labeling efficiency. To do so, I engineered GCE components and utilized AAVs to deliver orthogonal translational elements to primary neurons more efficiently than conventional transfections. With more efficient GCE and click labeling, it will be possible to study various recombinant and endogenous proteins in primary neurons and more complex model systems (brain organoids or slice cultures) and at the level of living animals. This novel and efficient approach for live labeling of ion channels and other neuronal proteins in living neurons will open new avenues of research in the neurobiology field.

6. Appendix

6.1. Appendix Tables

Appendix Table 1. *Primers used for cloning and mutagenesis.*

Aim	**Primer name**	**Primer sequence 5'→ 3'**
Deletion of HA tag from the N terminus of NF186	HA(del)-NF186fw	GCCATTGAGATTCCGATGGATCCAAG CATTCAGAATGAG
	HA(del)-NF186rv	CTCATTCTGAATGCTTGGATCCATCG GAATCTCAATGGC
Introduction of TAG. amber mutation into *Nfasc*	$NF186^{K519TAG}$fw	GAGGTCTAGGACCCCACCAGGATCTA CAGGATG
	$NF186^{K519TAG}$rv	GGGGTCCTAGACCTCCAGGCGGACTT GATTTTCA
	$NF186^{K534TAG}$fw	GTGGCCTAGAGGGGCACCACAGTGC AG
	$NF186^{K534TAG}$rv	GCCCCTCTAGGCCACCTGGTCTTCAG GC
	$NF186^{K571TAG}$fw	AGGATGTAGAAGGAAGATGACTCCCT GACCATCTTCG
	$NF186^{K571TAG}$rv	TTCCTTCTACATCCTGTTTCCAATGTA GAGTGGCTC
	$NF186^{K604TAG}$fw	CTGGCATAGGCCTACCTCACTGTTCT AGCTGATCAG
	$NF186^{K604TAG}$rv	GTAGGCCTATGCCAGGTCCTGGTCCA G
	$NF186^{K680TAG}$fw	CACTCCTAGTTCCCAGGCAGTGTCAA CTCAG
	$NF186^{K680TAG}$rv	TGGGAACTAGGAGTGGTCATGCCAGA CTCCT
	$NF186^{K809TAG}$fw	TTTGGGTAGGGCCCGGAGCCTGAAAC
	$NF186^{K809TAG}$rv	CGGGCCCTACCCAAAGTCATTTTCAG CCTGGACTC

Addition of HA tag to the C terminus of NF186	NF186-HAfw	GGTGGTGGGCCCTGAAGACCCCAAAGAAG
	NF186-HArv	ACCACCGCGGCCGCTCAAGCGTAGTCTGGGACGTCGTATGGGTAGGCCAGGGAATAGATGGCATTGACTG
hNSE cloning into NF186	hNSE(AseI)fw	GGTGGTATTAATTGTATGCAGCTGGACCTAGGAGAG AAG
	hNSE(BglII)rv	ACCACCAGATCTCGGTGGTAGTGGCGG
Cloning of *mSCN1B* into pACEMam2 to make multigene plasmid	*mSCN1B*(KpnI) rv	GGTGGTGCTAGCCACCATGGGGACGCTGCTGGCTCT
	mSCN1B(NheI)fw	ACCACCGGTACCTTATTCAGCCACCTGGACGCCT
Cloning of *mSCN1B* into pMDS to make multigene plasmid	*mSCN2B*(NheI)fw	GGTGGTGCTAGCCACCATGGAAGTCACAGCGCCCACC A
	mSCN2B(KpnI)rv	ACCACCGGTACCTTACTTGGTGCCATCTTCCGCGTTG
Cloning of mEGFP into pMDC to make multigene plasmid	mGFP(BamHI)fw	GGTGGTGGATCCCACCATGGTGAGCAAGGGCG
	mGFP(XbaII)rv	ACCACCTCTAGATTACTTGTACAGCTCGTCCATGCCGA
Cloning of *mSCN1B* and *mSCN2B* for PiggyBAC expression vector for generation of neuronal stable cells	*mSCN1B*(NheI)fw	GGTGGTGCTAGCCACCATGGGGACGCTGCTGGCTCT
	mSCN1B(NotI)rv	CCGTCCGCGGCCGCCTATTCAGCCACCTGGACGCC
	mSCN2B(NheI)fw	GGTGGTGCTAGCCACCATGCACAGGGATGCCTGGCTACC
	mSCN2B(NotI)rv	CCGTCCGCGGCCGCTTACTTGGTGCCATCTTCCGCGT
Amplification of *mSCN1B* and *mSCN2B* from gDNA of neuronal cells	*mSCN1B*rv	CTATTCAGCCACCTGGACGCCTG
	*mSCN2B*rv	TTACTTGGTGCCATCTTCCGCGTTG
	PiggyBACfw	ATGTAATTACGTCCCTCCCCCGCTAG

Loss-of-function *SCN8A* mutagenesis	*mSCN8A*^{I652N}rv	CAGCAGGCCGTTATTGAACAGGGCTGGCAG
	mSCN8A^{I652N}fw	CTGCCAGCCCTGTTCAATAACGGCCTGCTG
	mSCN8A^{T1785P}rv	CCAGATCTCATAGAAGGGCTCGAAGTCATCCTCAG
	mSCN8A^{T1785P}fw	CTGAGGATGACTTCGAGCCCTTCTATGAGATCTGG
Introduction of TTXr (Y371C) mutation into *mSCN8A*	*mSCN8A*^{Y371C}fw	GTACAGGTTCTCCCAGCAGTCCTGGGTCATCAG
	mSCN8A^{Y371C}rv	CTGATGACCCAGGACTGCTGGGAGAACCTGTAC
Addition of HA tag on the C terminus of $Na_V1.6$	*mSCN8A*-HAfw	(Phos)CTAGATACCCATACGACGTCCCAGACTACGCTTAAGGGCC
	mSCN8A-HArv	(Phos)CTTAAGCGTAGTCTGGGACGTCGTATGGGTAT
Cloning of $Na_V1.6$ into mGFP	*mSCN8A*(HindIII)fw	GCTGATAAGCTTCACCATGGCTGCACGGC
	mSCN8A(ApaI)rv	CGGCGAGGGCCCCGCACTTTGACTCTCTCACTTCTTTCTGTCTCTTAG
Cloning of U6-tRNA^{Pyl} into NES PylRS^{AF}	rvU6-tRNA^{Pyl}(BglII)fw	GGTGGTAGATCTAAAAAACGGAAACCCCGGGAATCTAACC
	rvU6-tRNA^{Pyl} (MfeI)rv	CAAATATGAAGGAATCATGGGAAATAGGCCCTCCAATTGAAAGGG
Cloning of U6-tRNA^{Pyl}-HDV into NES PylRS^{AF}	rvU6-tRNA^{Pyl}-HDV(BglII)fw	GGTGGT AGATCTAAAAAAGTCCCATTCGCCATG CCG
Cloning of 4xU6-tRNA^{M15} into NES PylRS^{AF}	4x(rvU6-tRNA^{M15}) BglII fw	GGTGGTAGATCTGAAAAGTGCCACCTGACGTCGAC
	4x(rvU6-tRNA^{M15}) MfeI rv	CGGCGACAATTGTCGGTCAAGCCTTGCCTTG

Cloning of NLS into mCherry	NLS-mCherry (NheI)fw	GCTGGCGCTAGCACCATGCCGCCGAAAAAAAAACGCAAAGTGGAAGATAGCGTGAGCAAGGGCGAGGAGG
	mCherry(NotI)rv	CGCGCAGCGGCCGCTCACTTGTACAGCTCGTCCATGCCG
Removing NLS from iRFP	iRFP(NheI)fw	GGAGGAGCTAGCCACCATGGCGGAAGGATCCGTCGCC
	iRFP(NotI)rv	GCTGTACAAGCATCACCATCACCATCACTGAGCGGCCGCAAAGGG
Cloning NES PylRS^{AF}/U6-tRNA^{Pyl} into pACMam1	CMV-NES PylRS^{AF}/U6-tRNA^{Pyl}(PvuI)fw	GGTGGTCGATCGAAAAAACGGAAACCCCGGGAA TCTAACC
	CMV-NES PylRS^{AF}/U6-tRNA^{Pyl}(BstZ17I)rv	ACCACCGTATACCCATAGAGCCACCGCATCC
Cloning CMV-NF186^{K680TAG}-HA into pMDC	NF186-HA(Sal)	GGTGGTGTCGACATGGCCAGGCAGCAGGC
	NF186-HA(Xbal)rv	ACCACCTCTAGATCAAGCGTAGTCTGGGACGTCGTATG
Cloning iRFP-GFP^{Y39TAG} into pMDC	iRFP-GFP^{Y39TAG}(SalI)fw	GGTGGTGTCGACCACCATGGCGGAAGGATCCG
	iRFP-GFP^{Y39TAG}(Xbal)rv	ACCACCTCTAGATCAGTGATGGTGATGGTGATG CTTGTAC

Appendix Table 2. *Biophysical properties of $Na_V1.6^{WT,\ Y371C}$-HA and $Na_V1.6^{K1546TAG,Y371C}$-P2A-EGFP, or $Na_V1.6^{WT,Y371C}$-P2A-EGFP and $Na_V1.6^{K1425TAG,Y371C}$-P2A-EGFP recorded in neuronal N1E-115-1$^{\beta1\beta2}$ cells. The analysis of the patch-clamp recordings of WT vs. K1425TAG was previously published[75].*

	Steady-state activation			Steady-state inactivation			τ_h at 0 mV	n	τ_{rec} at -100 mV (ms)	n	Current density (pA/pF)	n
	$V_{1/2}$ (mV)	k	n	$V_{1/2}$ (mV)	k	n	(ms)					
$Na_V1.6^{WT}$	-17.4±0.9	-5.9±0.3	14	-62.3±0.6	4.9±0.1	14	0.52±0.02	14	3.8±0.2	14	-252.4±32.0	14
$Na_V1.6^{K1546TAG}$	-15.6±1.2	-5.5±0.3	13	-56.6±0.4***	4.7±0.1*	13	0.60±0.02*	13	3.0±0.1**	13	-196.4±22.8	13
$Na_V1.6^{WT}$	-9.9±1.1	-7.3±0.3	18	-58.8±0.5	4.9±0.1	18	0.59±0.02	18	3.6±0.2	17	-124.6±15.5	18
$Na_V1.6^{K1425TAG}$	-11.4±0.6	-7.4±0.2	20	-60.2±0.5	4.8±0.1	20	0.60±0.03	20	3.6±0.2	20	-89.0±5.5* (p=0.0426)	20

*Note. Data are presented as means ± S.E.M.s; number of recorded cells (n); * p < 0.05, ** p < 0.01. Student's t-test or Mann-Whitney U test.*

Appendix Table 3. *Pairwise comparisons of the AIS length (measured in ankG channel) between NF186 transfected (HA+) and surrounding untransfected (HA-) neurons using the nonparametric Kruskal-Wallis test. These results were previously published[75].*

Categories: 1. WT HA+; 2. WT HA-; 3. K519TAG HA+; 4. K519TAG HA-; 5. K604TAG HA+; 6. K604TAG HA-; 7. K680TAG HA+; and 8. K680TAG HA-. Pairwise comparisons of transfected (HA+ ankG+) and surrounding untransfected (HA- ankG+) neurons for WT and three amber mutants (1-2, 3-4, 5-6, and 7-8) are highlighted in grey.

Pairwise comparisons					
Comparisons	**Test statistic**	**Standard error**	**Standard test statistic**	**Significance**	**Adjusted significance [a]**
4.00-2.00	6.433	11.390	0.565	0.572	1.000
4.00-8.00	-9.382	12.969	-0.723	0.469	1.000
4.00-6.00	-23.138	17.448	-1.326	0.185	1.000
4.00-1.00	40.443	13.875	2.915	0.004	0.100
4.00-7.00	-41.832	13.875	-3.015	0.003	0.072
4.00-3.00	42.133	16.240	2.594	0.009	0.265
4.00-5.00	-52.360	16.795	-3.118	0.002	0.051
2.00-8.00	-2.949	11.693	-0.252	0.801	1.000
2.00-6.00	-16.705	16.523	-1.011	0.312	1.000
2.00-1.00	34.010	12.691	2.680	0.007	0.206
2.00-7.00	-35.399	12.691	-2.789	0.005	0.148
2.00-3.00	-35.700	15.241	-2.342	0.019	0.537
2.00-5.00	-45.927	15.831	-2.901	0.004	0.104
8.00-6.00	13.756	17.648	0.779	0.436	1.000
8.00-1.00	31.062	14.125	2.199	0.028	0.781
8.00-7.00	32.450	14.125	2.297	0.022	0.605
8.00-3.00	32.751	16.455	1.990	0.047	1.000
8.00-5.00	42.978	17.002	2.528	0.011	0.321
6.00-1.00	17.306	18.325	0.944	0.345	1.000
6.00-7.00	-18.694	18.325	-1.020	0.308	1.000
6.00-3.00	18.995	20.175	0.942	0.346	1.000
6.00-5.00	29.222	20.624	1.417	0.157	1.000
1.00-7.00	-1.389	14.962	-0.093	0.926	1.000
1.00-3.00	-1.689	17.178	-0.098	0.922	1.000
1.00-5.00	-11.917	17.703	-0.673	0.501	1.000
7.00-3.00	0.301	17.178	0.017	0.986	1.000
7.00-5.00	10.528	17.703	0.595	0.552	1.000
3.00-5.00	-10.227	19.612	-0.521	0.602	1.000

Note. Each row tests the null hypothesis that the Sample 1 and Sample 2 distributions are the same. Asymptotic significances (two-sided tests) are displayed. The significance level is 0.05.

[a.] Significance values have been adjusted by the Bonferroni correction for multiple tests.

Appendix Table 4. *Multiple comparisons of the AIS length (measured in ankG channel) between $Na_V1.6^{TAG}$-HA transfected (HA+) and surrounding untransfected (HA-) cells using one-way ANOVA with the Tukey posthoc. These results were previously published[75].*

Categories: 1. K1425TAG HA+; 2. K1425TAG HA-; 3. K1546TAG HA+; and 4. K1546TAG HA-. Multiple comparisons of transfected (HA+ ankG+) and surrounding untransfected (HA- ankG+) neurons for two amber mutants (1-2, 3-4) are highlighted in grey.

Multiple comparisons						
Tukey HSD						
(I) Category	(J) Category	Mean difference (I-J)	Standard error	Significance	95% Confidence interval	
					Lower bound	Upper bound
1.00	2.00	3.66061	1.64177	0.124	-0.6418	7.9630
	3.00	0.78047	1.96907	0.979	-4.3797	5.9406
	4.00	4.90039*	1.79007	0.037	0.2094	9.5914
2.00	1.00	-3.66061	1.64177	0.124	-7.9630	0.6418
	3.00	-2.88014	1.74582	0.357	-7.4552	1.6949
	4.00	1.23979	1.54110	0.852	-2.7988	5.2784
3.00	1.00	-0.78047	1.96907	0.979	-5.9406	4.3797
	2.00	2.88014	1.74582	0.357	-1.6949	7.4552
	4.00	4.11993	1.88595	0.136	-0.8224	9.0622
4.00	1.00	-4.90039*	1.79007	0.037	-9.5914	-0.2094
	2.00	-1.23979	1.54110	0.852	-5.2784	2.7988
	3.00	-4.11993	1.88595	0.136	-9.0622	0.8224

*Note. *The mean difference is significant at the 0.05 level.*

Appendix Table 5. *Biophysical properties of $Na_V1.6^{WT,\ Y371C}$-HA, and $Na_V1.6^{K1546TAG,\ Y371C}$-HA recorded in neuronal N1E-115-1 neuroblastoma cell line. These results were previously published[75].*

	Steady-state activation			Steady-state inactivation			τ_h at 0 mV (ms)	n	τ_{rec} at -100 mV (ms)	n	Current density (pA/pF)	n
	$V_{1/2}$ (mV)	k	n	$V_{1/2}$ (mV)	k	n						
$Na_V1.6^{WT}$	-11.8±1.0	-6.8±0.3	20	-58.6±0.5	4.8±0.1	20	0.47±0.02	20	2.8±0.1	20	-149.4±17.5	20
$Na_V1.6^{K1546TAG}$	-11.5±0.8	-6.6±0.3	18	-55.8±0.6** (p=0.0025)	4.9±0.1	17	0.57±0.03** (p=0.0026)	18	2.4±0.2* (p=0.0173)	18	-105.5±12.5	18

*Note. Data are presented as means ± SEMs; a number of recorded cells (n); * p < 0.05, ** p < 0.01, Student's t-test or Mann-Whitney U test*.

Appendix Table 6. *Mean AIS fluorescence intensities (measured in click—ATTO488-tz or HA channel) between control ($Na_V1.6^{K1546TAG,\ Y371C}$-HA) and LOF pathogenic variants ($Na_V1.6^{K1546TAG,\ Y371C,I1652N}$-HA and $Na_V1.6^{K1546TAG,\ Y371C,T1785P}$-HA) using the nonparametric Kruskal-Wallis test. The results shown in the upper table were previously published[75].*

Independent-samples Kruskal-Wallis test: summary (ATTO488-tz channel)	
Total number of cells (n)	79
Test statistic	2.244[a]
Degree of freedom	2
Asymptotic significance (2-sided test)	0.326

[a] *The test statistic is adjusted for ties.*

Independent-samples Kruskal-Wallis test: summary (HA channel)	
Total number of cells (n)	79
Test statistic	3.326[a]
Degree of freedom	2
Asymptotic significance (2-sided test)	0.190

[a] *The test statistic is adjusted for ties.*

Appendix Table 7. *The quantification of the GFP^{Y39TAG}/mCherry ratio in neurons transduced with different combinations of the AAVs. Pairwise comparisons of the GFP/mCherry ratio of neurons transduced with AAVs that bore a dual fluorescent reporter (NLS-mCherry-GFP^{Y39TAG}) and different combinations of the genetic code expansion elements by using the independent-samples Kruskal-Wallis test.*

Categories: 1. AAV#1, 2 and 6; 2. AAV#4 and 6; 3. AAV#3, 4, and 6; 4. AAV#4, 5 and 6; 5. AAV#1, 5 and 6; 6. AAV#1, 2, 4, and 6. Pairwise comparisons of neurons transduced with different combinations of the AAVs that are significantly different are highlighted in grey.

Pairwise Comparisons of groups					
Comparisons	**Test Statistic**	**Standard error**	**Standard test statistic**	**Significance**	**Adjusted significance[a]**
1.00-2.00	-19.733	27.105	-0.728	0.467	1.000
1.00-5.00	-320.972	28.300	-11.342	0.000	0.000
1.00-4.00	-326.673	28.057	-11.643	0.000	0.000
1.00-3.00	-387.980	28.300	-13.710	0.000	0.000
1.00-6.00	-405.657	28.426	-14.271	0.000	0.000
2.00-5.00	-301.239	29.021	-10.380	0.000	0.000
2.00-4.00	-306.939	28.784	-10.663	0.000	0.000
2.00-3.00	-368.247	29.021	-12.689	0.000	0.000
2.00-6.00	-385.923	29.144	-13.242	0.000	0.000
5.00-4.00	5.701	29.912	0.191	0.849	1.000
5.00-3.00	67.008	30.139	2.223	0.026	0.393
5.00-6.00	-84.684	30.258	-2.799	0.005	0.077
4.00-3.00	61.307	29.912	2.050	0.040	0.606
4.00-6.00	-78.984	30.031	-2.630	0.009	0.128
3.00-6.00	-17.677	30.258	-0.584	0.559	1.000

Note. Each row tests the null hypothesis that the Sample 1 and Sample 2 distributions are the same. Asymptotic significances (2-sided tests) are displayed. The significance level is 0.05.

[a.] *Significance values have been adjusted by the Bonferroni correction for multiple tests*

6.2. The sequences of the genes, promoters, and different cassettes used in the thesis

mSCN8A^{WT}-P2A-GFP:

atggctgcacggctgctggcacctcctggccccgattcctttaagcctttcacacctgagagcctggctaacatcgagagaa
gaattgccgagtccaagctgaagaagcctcccaaggccgatggctctcacagagaggacgacgaggattctaagcctaagccca
atagcgatctggaggccggcaagtccctgcctttcatctacggcgacatcccacagggcctggtggccgtgccactggaggactttga
cccctattacctgacccagaagacatttgtggtgctgaatcggggcaagacactgttccgcttctctgccacccccgccctgtatatcctg
tccccttttcaacctgatccgcagaatcgccatcaagatcctgatccactccgtgttctctatgatcatcatgtgcacaatcctgaccaattg
cgtgttcatgaccttctccaatccaccagagtggagcaagaatgtggagtacaccttcacaggcatctacacctttgagtctctggtgaa
gatcatcgcccggggcttttgcatcgacggcttcacctttctgagagacccatggaactggctggactttagcgtgatcatgatggcctac
atcaccgagtttgtgaatctgggcaacgtgagcgccctgcggacattccgggtgctgcgcgccctgaagaccatctctgtgatccctgg
cctgaagacaatcgtgggcgccctgatccagtccgtgaagaagctgtccgacgtgatgatcctgaccgtgttctgcctgtccgtgtttgc
cctgatcggcctgcagctgttcatgggcaacctgaggaacaagtgcgtggtgtggccaatcaactttaatgagagctatctggagaac
ggcaccagaggcttcgattgggaggagtacatcaacaacaagaccaatttctatatggtgcctggcatgctggagccactgctgtgcg
gcaactcctctgatgccggccagtgccccgagggctttcagtgcatgaaggccggcagaaatcctaattatggctacacctcttttgac
acctttcctgggcctttctggccctgttcagactgatgacccaggactactgggagaacctgtaccagctgaccctgagagccgccgg
caagacctacatgatcttctttgtgctggtaatcttcgtgggctccttctacctggtgaacctgatcctggccgtggtggccatggcctacga
ggagcagaaccaggccaccctggaggaggccgagcagaaggaggccgagttcaaggccatgctggagcagctgaagaagca
gcaggaggaggcccaggccgccgccatggccacatccgccggcaccgtgagcgaggacgccatcgaggaggagggcgagga
tggcgtgggctccccccggtcttctagcgagctgtccaagctgtcctctaagtccgccaaggagaggcggaatcggagaaagaagc
ggaagcagaaggagctgtccgagggcgaggagaagggcgatccagagaaggtgttcaagagcgagtccgaggatggcatgag
acggaaggcctttcgcctgcctgacaatagaatcggcaggaagttttccatcatgaatcagagcctgctgtccatccctggcagcccttt
cctgtcccggcacaattccaagtccagcatcttctcttttcgcggccctggcagattccgcgatccaggctccgagaacgagtttgccga
tgacgagcacagcaccgtggaggagtccgagggccggagagactccctgtttatccctatccgcgcccgggagcgcagatcctctt
actccggctactccggctattctcagtgctccagatcttctcggatctttccatctctgcggagatccgtgaagagaaactccaccgtgga
ctgtaatggcgtggtgagcctgatcggccccggctcccacatcggcagactgctgccagaggccaccaccgaggtggagatcaag
aagaaggggcctggcagcctgctggtgtctatggagcagctggccagctatggcagaaaggaccggatcaattctatcatgtccgtg
gtgacaaacaccctggtggaggagctggaggagtcccagaggaagtgtcccccatgttggtacaagtttgccaatacatttctgatctg
ggagtgtcacccatattggatcaagctgaaggagatcgtgaatctgatcgtgatggacccattcgtggatctggccatcacaatctgcat
cgtgctgaacaccctgtttatggccatggagcaccaccccatgacaccacagtttgagcacgtgctggccgtgggcaatctggtgttca
ccggcatctttaccgccgagatgttcctgaagctgatcgccatggacccatactactattttcaggagggctggaatatcttcgatggcttt
atcgtgagcctgtccctgatggagctgggcctggccgatgtggagggcctgtctgtgctgcgcagctttcggctgctgcgcgtgttcaag
ctggccaagagctggccaaccctgaatatgctgatcaagatcatcggcaactccgtgggcgccctgggcaatctgaccctggtgctg

gccatcatcgtgttcatctttgccgtggtgggcatgcagctgttcggcaagtcctacaaggagtgcgtgtgcaagatctcccaggagtgt
aagctgccacggtggcacatgaacgatttctttcactctttcctgatcgtgttccgggtgctgtgcggcgagtggatcgagaccatgtggg
actgcatggaggtggccggccaggccatgtgcctgatcgtgttcatgatggtaatggtaatcggcaatctggtggtgctgaatctgttcct
ggccctgctgctgtcttcttttagcgccgacaacctggccgccacagacgatgacggcgagatgaataacctgcagatctccgtgatc
agaatcaagaagggcgtggcctgggccaaggtgaaggtgcacgcctttatgcaggcccactttaagcagagggaggccgatgag
gtgaagccactggacgagctgtacgagaagaaggccaattgtatcgccaaccacacaggcgtggatatacaccgcaatggcgattt
ccagaagaacggcaatggcaccacctccggcatcggctcctctgtggagaagtacatcatcgacgaggaccacatgtccttcatca
ataatccaaatctgaccgtgcgggtgcctatcgccgtgggcgagtctgactttgagaatctgaacaccgaggacgtgtccagcgagtc
cgacccagagggctccaaggacaagctggatgatacatcctctagcgagggctctaccatcgacatcaagcctgaggtggaggag
gtgcctgtggagcagccagaggagtacctggaccctgatgcctgtttcaccgagggctgcgtgcagagattcaagtgctgtcaggtga
acatcgaggagggcctgggcaagtcttggtggatactgcggaagacatgcttcctgatcgtggagcacaactggtttgagacctttatc
atcttcatgatcctgctgtcctccggcgccctggcctttgaggacatctatatcgagcagagaaagaccatcagaaccatcctggagta
cgccgacaaggtgttcacatatatctttatcctggagatgctgctgaagtggaccgcctacggctttgtgaagttctttaccaatgcctggt
gctggctggactttctgatcgtggccgtgtctctggtgtccctgatcgccaacgccctgggctattctgagctgggcgccatcaagtctctg
agaaccctgagagccctgcgccccctgagagccctgagcagatttgagggcatgagggtggtggtgaatgccctggtgggcgccat
ccctagcatcatgaacgtgctgctggtgtgcctgatcttttggctgatcttttctatcatgggcgtgaatctgttcgccggcaagtaccactac
tgctttaatgagacctccgagatccggttcgagatcgatgaggtgaacaacaagacagactgtgagaagctgatggagggcaacaa
tacagagatccggtggaagaatgtgaagatcaatttcgataacgtgggcgccggctacctggccctgctgcaggtggccacctttaag
ggctggatggatataatgtacgccgccgtggattcccgcaagcccgatgagcagccagactatgagggcaacatctacatgtacatc
tatttcgtgatcttcatcatcttcggcagctttttcaccctgaatctgtttatcggcgtgatcatcgataacttcaaccagcagaagaagaagt
tcggcggccaggacatcttcatgacagaggagcagaagaagtactataacgccatgaagaagctgggctccaagaagcctcaga
agccaatccctagaccactgaataagatccagggcatcgtgttcgacttcgtgacccagcaggcctttgacatcgtgatcatgatgctg
atctgtctgaacatggtgaccatgatggtggagacagatacccagtccaagcagatggagaatatcctgtattggatcaacctggtgttt
gtgatctttttcacatgtgagtgcgtgctgaagatgttcgccctgcgccactattatttcacaatcggctggaacatctttgacttcgtggtggt
aatcctgtctatcgtgggcatgtttctggccgacatcatcgagaagtacttcgtgagcccaacactgttcagagtgatccggctggccag
gatcggcagaatcctgcggctgatcaagggcgccaagggcatcagaaccctgctgttcgccctgatgatgtctctgccagccctgttc
aatatcggcctgctgctgtttctggtaatgttcatcttttccatctttggcatgtccaacttcgcctatgtgaagcacgaggccggcatcgatg
atatgtttaacttcgagacattcggcaactccatgatctgtctgttccagatcaccacctctgccggctgggatggcctgctgctgcctatc
ctgaatagaccaccagattgtagcctggataaggagcaccctggcagcggcttcaagggcgattgtggcaatccttccgtgggcatct
tcttcttcgtgtcctacatcatcatctctttcctgatcgtggtgaacatgtacatcgccatcatcctggagaatttctctgtggccaccgagga
gtctgccgacccactgtctgaggatgacttcgagaccttctatgagatctgggagaagtttgaccctgatgccacccagtttatcgagtat
tgcaagctggccgactttgccgacgccctggagcacccactgagagtgccaaagccaaataccatcgagctgatcgccatggatct
gcccatggtgagcggcgatagaatccactgcctggacatcctgtttgccttcacaaagagagtgctgggcgatagcggcgagctgga
catcctgaggcagcagatggaggagaggttcgtggcctctaaccccagcaaggtgtcctacgagcctatcaccacaaccctgcgga

gaaagcaggaggaggtgtccgccgtggtgctgcagagagcctacagaggccacctggcccggagaggctttatctgcagaaagat
cacctccaacaagctggagaatggcggcacccaccgcgagaagaaggagtctacccccctctaccgccagcctgccttcctacgac
tccgtgaccaagccagataaggagaagcagcagcgcgcagaggagggacggagagaaagagctaagagacagaaagaagt
gagagagtcaaagtgctctagaggaagcggagctactaacttcagcctgctgaagcaggctggagacgtggaggagaaccctgg
acctatgagcaagggcgaggagctgttcaccggggtggtgcccatcctggtcgagctggacggcgacgtaaacggccacaagttc
agcgtgtccggcgagggcgagggcgatgccacctacggcaagctgaccctgaagttcatctgcaccaccggcaagctgcccgtgc
cctggcccaccctcgtgaccaccctgacctacggcgtgcagtgcttcagccgctaccccgaccacatgaagcagcacgacttcttca
agtccgccatgcccgaaggctacgtccaggagcgcaccatcttcttcaaggacgacggcaactacaagacccgcgccgaggtga
agttcgagggcgacaccctggtgaaccgcatcgagctgaagggcatcgacttcaaggaggacggcaacatcctggggcacaagc
tggagtacaactacaacagccacaacgtctatatcatggccgacaagcagaagaacggcatcaaggtgaacttcaagatccgcca
caacatcgaggacggcagcgtgcagctcgccgaccactaccagcagaacaccccatcggcgacggccccgtgctgctgcccga
caaccactacctgagcacccagtccgccctgagcaaagaccccaacgagaagcgcgatcacatggtcctgctggagttcgtgacc
gccgccgggatcactcacggcatggacgagctgtacaagtaa

- *SCN8A*^{WT}
- XbaI restriction site
- P2A self-cleaving sequence
- EGFP-TAA stop codon

***mSCN8A*^{WT}*-EGFP*:**

atggctgcacggctgctggcacctcctggccccgattcctttaagcctttcacacctgagagcctggctaacatcgagagaa
gaattgccgagtccaagctgaagaagcctcccaaggccgatggctctcacagagaggacgacgaggattctaagcctaagccca
atagcgatctggaggccggcaagtccctgcctttcatctacggcgacatcccacagggcctggtggccgtgccactggaggactttga
cccctattacctgacccagaagacatttgtggtgctgaatcggggcaagacactgttccgcttctctgccacccccgccctgtatatcctg
tccccttcaacctgatccgcagaatcgccatcaagatcctgatccactccgtgttctctatgatcatcatgtgcacaatcctgaccaattg
cgtgttcatgaccttctccaatccaccagagtggagcaagaatgtggagtacaccttcacaggcatctacaccttgagtctctggtgaa
gatcatcgcccggggcttttgcatcgacggcttcacctttctgagagacccatggaactggctggactttagcgtgatcatgatggcctac
atcaccgagtttgtgaatctgggcaacgtgagcgccctgcggacattccgggtgctgcgcgccctgaagaccatctctgtgatccctgg
cctgaagacaatcgtgggcgccctgatccagtccgtgaagaagctgtccgacgtgatgatcctgaccgtgttctgcctgtccgtgtttgc
cctgatcggcctgcagctgttcatgggcaacctgaggaacaagtgcgtggtgtggccaatcaactttaatgagagctatctggagaac
ggcaccagaggcttcgattgggaggagtacatcaacaacaagaccaatttctatatggtgcctggcatgctggagccactgctgtgcg
gcaactcctctgatgccggccagtgccccgagggctttcagtgcatgaaggccggcagaaatcctaattatggctacacctcttttgac
acctttttcctgggcctttctggccctgttcagactgatgacccaggactactgggagaacctgtaccagctgaccctgagagccgccgg
caagacctacatgatcttctttgtgctggtaatcttcgtgggctccttctacctggtgaacctgatcctggccgtggtggccatggcctacga
ggagcagaaccaggccaccctggaggaggccgagcagaaggaggccgagttcaaggccatgctggagcagctgaagaagca

gcaggaggaggcccaggccgccgccatggccacatccgccggcaccgtgagcgaggacgccatcgaggaggagggcgagga
tggcgtgggctccccccggtcttctagcgagctgtccaagctgtcctctaagtccgccaaggagaggcggaatcggagaaagaagc
ggaagcagaaggagctgtccgagggcgaggagaagggcgatccagagaaggtgttcaagagcgagtccgaggatggcatgag
acggaaggcctttcgcctgcctgacaatagaatcggcaggaagttttccatcatgaatcagagcctgctgtccatccctggcagcccttt
cctgtcccggcacaattccaagtccagcatcttctcttttcgcggccctggcagattccgcgatccaggctccgagaacgagtttgccga
tgacgagcacagcaccgtggaggagtccgagggccggagagactccctgtttatccctatccgcgcccgggagcgcagatcctctt
actccggctactccggctattctcagtgctccagatcttctcggatctttccatctctgcggagatccgtgaagagaaactccaccgtgga
ctgtaatggcgtggtgagcctgatcggccccggctcccacatcggcagactgctgccagaggccaccaccgaggtggagatcaag
aagaaggggcctggcagcctgctggtgtctatggagcagctggccagctatggcagaaaggaccggatcaattctatcatgtccgtg
gtgacaaacaccctggtggaggagctggaggagtcccagaggaagtgtcccccatgttggtacaagtttgccaatacatttctgatctg
ggagtgtcacccatattggatcaagctgaaggagatcgtgaatctgatcgtgatggacccattcgtggatctggccatcacaatctgcat
cgtgctgaacaccctgtttatggccatggagcaccaccccatgacaccacagtttgagcacgtgctggccgtgggcaatctggtgttca
ccggcatctttaccgccgagatgttcctgaagctgatcgccatggacccatactactattttcaggagggctggaatatcttcgatggcttt
atcgtgagcctgtccctgatggagctgggcctggccgatgtggagggcctgtctgtgctgcgcagctttcggctgctgcgcgtgttcaag
ctggccaagagctggccaaccctgaatatgctgatcaagatcatcggcaactccgtgggcgccctgggcaatctgaccctggtgctg
gccatcatcgtgttcatctttgccgtggtgggcatgcagctgttcggcaagtcctacaaggagtgcgtgtgcaagatctcccaggagtgt
aagctgccacggtggcacatgaacgatttctttcactctttcctgatcgtgttccgggtgctgtgcggcgagtggatcgagaccatgtggg
actgcatggaggtggccggccaggccatgtgcctgatcgtgttcatgatggtaatggtaatcggcaatctggtggtgctgaatctgttcct
ggccctgctgctgtcttcttttagcgccgacaacctggccgccacagacgatgacggcgagatgaataacctgcagatctccgtgatc
agaatcaagaagggcgtggcctgggccaaggtgaaggtgcacgcctttatgcaggcccactttaagcagagggaggccgatgag
gtgaagccactggacgagctgtacgagaagaaggccaattgtatcgccaaccacacaggcgtggatatacaccgcaatggcgattt
ccagaagaacggcaatggcaccacctccggcatcggctcctctgtggagaagtacatcatcgacgaggaccacatgtccttcatca
ataatccaaatctgaccgtgcgggtgcctatcgccgtgggcgagtctgactttgagaatctgaacaccgaggacgtgtccagcgagtc
cgacccagagggctccaaggacaagctggatgatacatcctctagcgagggctctaccatcgacatcaagcctgaggtggaggag
gtgcctgtggagcagccagaggagtacctggaccctgatgcctgtttcaccgagggctgcgtgcagagattcaagtgctgtcaggtga
acatcgaggagggcctgggcaagtcttggtggatactgcggaagacatgcttcctgatcgtggagcacaactggtttgagacctttatc
atcttcatgatcctgctgtcctccggcgccctggcctttgaggacatctatatcgagcagagaaagaccatcagaaccatcctggagta
cgccgacaaggtgttcacatatatctttatcctggagatgctgctgaagtggaccgcctacggctttgtgaagttctttaccaatgcctggt
gctggctggactttctgatcgtggccgtgtctctggtgtccctgatcgccaacgccctgggctattctgagctgggcgccatcaagtctctg
agaaccctgagagccctgcgccccctgagagccctgagcagatttgagggcatgagggtggtggtgaatgccctggtgggcgccat
ccctagcatcatgaacgtgctgctggtgtgcctgatcttttggctgatcttttctatcatgggcgtgaatctgttcgccggcaagtaccactac
tgctttaatgagacctccgagatccggttcgagatcgatgaggtgaacaacaagacagactgtgagaagctgatggagggcaacaa
tacagagatccggtggaagaatgtgaagatcaatttcgataacgtgggcgccggctacctggccctgctgcaggtggccacctttaag
ggctggatggatataatgtacgccgccgtggattcccgcaagcccgatgagcagccagactatgagggcaacatctacatgtacatc

tatttcgtgatcttcatcatcttcggcagctttttcaccctgaatctgtttatcggcgtgatcatcgataacttcaaccagcagaagaagaagt
tcggcggccaggacatcttcatgacagaggagcagaagaagtactataacgccatgaagaagctgggctccaagaagcctcaga
agccaatccctagaccactgaataagatccagggcatcgtgttcgacttcgtgacccagcaggcctttgacatcgtgatcatgatgctg
atctgtctgaacatggtgaccatgatggtggagacagatacccagtccaagcagatggagaatatcctgtattggatcaacctggtgttt
gtgatctttttcacatgtgagtgcgtgctgaagatgttcgccctgcgccactattatttcacaatcggctggaacatctttgacttcgtggtggt
aatcctgtctatcgtgggcatgtttctggccgacatcatcgagaagtacttcgtgagcccaacactgttcagagtgatccggctggccag
gatcggcagaatcctgcggctgatcaagggcgccaagggcatcagaaccctgctgttcgccctgatgatgtctctgccagccctgttc
aatatcggcctgctgctgtttctggtaatgttcatcttttccatctttggcatgtccaacttcgcctatgtgaagcacgaggccggcatcgatg
atatgtttaacttcgagacattcggcaactccatgatctgtctgttccagatcaccacctctgccggctgggatggcctgctgctgcctatc
ctgaatagaccaccagattgtagcctggataaggagcaccctggcagcggcttcaagggcgattgtggcaatccttccgtgggcatct
tcttcttcgtgtcctacatcatcatctctttcctgatcgtggtgaacatgtacatcgccatcatcctggagaatttctctgtggccaccgagga
gtctgccgacccactgtctgaggatgacttcgagaccttctatgagatctgggagaagtttgaccctgatgccacccagtttatcgagtat
tgcaagctggccgactttgccgacgccctggagcacccactgagagtgccaaagccaaataccatcgagctgatcgccatggatct
gcccatggtgagcggcgatagaatccactgcctggacatcctgtttgccttcacaaagagagtgctgggcgatagcggcgagctgga
catcctgaggcagcagatggaggagaggttcgtggcctctaaccccagcaaggtgtcctacgagcctatcaccacaaccctgcgga
gaaagcaggaggaggtgtccgccgtggtgctgcagagagcctacagaggccacctggcccggagaggctttatctgcagaaagat
cacctccaacaagctggagaatggcggcacccaccgcgagaagaaggagtctacccccctctaccgccagcctgccttcctacgac
tccgtgaccaagccagataaggagaagcagcagcgcgcagaggagggacggagagaaagagctaagagacagaaagaagt
gagagagtcaaagtgctctagaggcacccgcattctgcagagcaccgtgggcaccgcgccgggcggcagcattgcgaccatgag
caagggcgaggagctgttcaccggggtggtgcccatcctggtcgagctggacggcgacgtaaacggccacaagttcagcgtgtcc
ggcgagggcgagggcgatgccacctacggcaagctgaccctgaagttcatctgcaccaccggcaagctgcccgtgccctggccca
ccctcgtgaccaccctgacctacggcgtgcagtgcttcagccgctaccccgaccacatgaagcagcacgacttcttcaagtccgccat
gcccgaaggctacgtccaggagcgcaccatcttcttcaaggacgacggcaactacaagacccgcgccgaggtgaagttcgaggg
cgacaccctggtgaaccgcatcgagctgaagggcatcgacttcaaggaggacggcaacatcctggggcacaagctggagtacaa
ctacaacagccacaacgtctatatcatggccgacaagcagaagaacggcatcaaggtgaacttcaagatccgccacaacatcgag
gacggcagcgtgcagctcgccgaccactaccagcagaacaccccccatcggcgacggccccgtgctgctgcccgacaaccactac
ctgagcacccagtccgccctgagcaaagaccccaacgagaagcgcgatcacatggtcctgctggagttcgtgaccgccgccgggga
tcactcacggcatggacgagctgtacaagtaa

- *SCN8A*^{WT}
- Linker
- EGFP-STOP codon

mSCN8A^{WT}-HA:

atggctgcacggctgctggcacctcctggccccgattcctttaagcctttcacacctgagagcctggctaacatcgagagaa
gaattgccgagtccaagctgaagaagcctcccaaggccgatggctctcacagagaggacgacgaggattctaagcctaagccca
atagcgatctggaggccggcaagtccctgcctttcatctacggcgacatcccacagggcctggtggccgtgccactggaggactttga
cccctattacctgacccagaagacatttgtggtgctgaatcggggcaagacactgttccgcttctctgccacccccgccctgtatatcctg
tccccttcaacctgatccgcagaatcgccatcaagatcctgatccactccgtgttctctatgatcatcatgtgcacaatcctgaccaattg
cgtgttcatgaccttctccaatccaccagagtggagcaagaatgtggagtacaccttcacaggcatctacacctttgagtctctggtgaa
gatcatcgcccggggcttttgcatcgacggcttcacctttctgagagacccatggaactggctggactttagcgtgatcatgatggcctac
atcaccgagtttgtgaatctgggcaacgtgagcgccctgcggacattccgggtgctgcgcgccctgaagaccatctctgtgatccctgg
cctgaagacaatcgtgggcgccctgatccagtccgtgaagaagctgtccgacgtgatgatcctgaccgtgttctgcctgtccgtgtttgc
cctgatcggcctgcagctgttcatgggcaacctgaggaacaagtgcgtggtgtggccaatcaactttaatgagagctatctggagaac
ggcaccagaggcttcgattgggaggagtacatcaacaacaagaccaatttctatatggtgcctggcatgctggagccactgctgtgcg
gcaactcctctgatgccggccagtgccccgagggctttcagtgcatgaaggccggcagaaatcctaattatggctacacctcttttgac
acctttttcctgggcctttctggccctgttcagactgatgacccaggactactgggagaacctgtaccagctgaccctgagagccgccgg
caagacctacatgatcttctttgtgctggtaatcttcgtgggctccttctacctggtgaacctgatcctggccgtggtggccatggcctacga
ggagcagaaccaggccaccctggaggaggccgagcagaaggaggccgagttcaaggccatgctggagcagctgaagaagca
gcaggaggaggcccaggccgccgccatggccacatccgccggcaccgtgagcgaggacgccatcgaggaggagggcgagga
tggcgtgggctccccccggtcttctagcgagctgtccaagctgtcctctaagtccgccaaggagaggcggaatcggagaaagaagc
ggaagcagaaggagctgtccgagggcgaggagaagggcgatccagagaaggtgttcaagagcgagtccgaggatggcatgag
acggaaggcctttcgcctgcctgacaatagaatcggcaggaagttttccatcatgaatcagagcctgctgtccatccctggcagcccttt
cctgtcccggcacaattccaagtccagcatcttctcttttcgcggccctggcagattccgcgatccaggctccgagaacgagtttgccga
tgacgagcacagcaccgtggaggagtccgagggccggagagactccctgtttatccctatccgcgcccgggagcgcagatcctctt
actccggctactccggctattctcagtgctccagatcttctcggatctttccatctctgcggagatccgtgaagagaaactccaccgtgga
ctgtaatggcgtggtgagcctgatcggccccggctcccacatcggcagactgctgccagaggccaccaccgaggtggagatcaag
aagaaggggcctggcagcctgctggtgtctatggagcagctggccagctatggcagaaaggaccggatcaattctatcatgtccgtg
gtgacaaacaccctggtggaggagctggaggagtcccagaggaagtgtcccccatgttggtacaagtttgccaatacatttctgatctg
ggagtgtcacccatattggatcaagctgaaggagatcgtgaatctgatcgtgatggacccattcgtggatctggccatcacaatctgcat
cgtgctgaacaccctgtttatggccatggagcaccaccccatgacaccacagtttgagcacgtgctggccgtgggcaatctggtgttca
ccggcatctttaccgccgagatgttcctgaagctgatcgccatggacccatactactattttcaggagggctggaatatcttcgatggcttt
atcgtgagcctgtccctgatggagctgggcctggccgatgtggagggcctgtctgtgctgcgcagctttcggctgctgcgcgtgttcaag
ctggccaagagctggccaaccctgaatatgctgatcaagatcatcggcaactccgtgggcgccctgggcaatctgaccctggtgctg
gccatcatcgtgttcatctttgccgtggtgggcatgcagctgttcggcaagtcctacaaggagtgcgtgtgcaagatctcccaggagtgt
aagctgccacggtggcacatgaacgatttctttcactctttcctgatcgtgttccgggtgctgtgcggcgagtggatcgagaccatgtggg
actgcatggaggtggccggccaggccatgtgcctgatcgtgttcatgatggtaatggtaatcggcaatctggtggtgctgaatctgttcct

ggccctgctgctgtcttcttttagcgccgacaacctggccgccacagacgatgacggcgagatgaataacctgcagatctccgtgatc
agaatcaagaagggcgtggcctgggccaaggtgaaggtgcacgcctttatgcaggcccactttaagcagagggaggccgatgag
gtgaagccactggacgagctgtacgagaagaaggccaattgtatcgccaaccacacaggcgtggatatacaccgcaatggcgattt
ccagaagaacggcaatggcaccacctccggcatcggctcctctgtggagaagtacatcatcgacgaggaccacatgtccttcatca
ataatccaaatctgaccgtgcgggtgcctatcgccgtgggcgagtctgactttgagaatctgaacaccgaggacgtgtccagcgagtc
cgacccagagggctccaaggacaagctggatgatacatcctctagcgagggctctaccatcgacatcaagcctgaggtggaggag
gtgcctgtggagcagccagaggagtacctggaccctgatgcctgtttcaccgagggctgcgtgcagagattcaagtgctgtcaggtga
acatcgaggagggcctgggcaagtcttggtggatactgcggaagacatgcttcctgatcgtggagcacaactggtttgagacctttatc
atcttcatgatcctgctgtcctccggcgccctggcctttgaggacatctatatcgagcagagaaagaccatcagaaccatcctggagta
cgccgacaaggtgttcacatatatctttatcctggagatgctgctgaagtggaccgcctacggctttgtgaagttctttaccaatgcctggt
gctggctggactttctgatcgtggccgtgtctctggtgtccctgatcgccaacgccctgggctattctgagctgggcgccatcaagtctctg
agaaccctgagagccctgcgccccctgagagccctgagcagatttgagggcatgagggtggtggtgaatgccctggtgggcgccat
ccctagcatcatgaacgtgctgctggtgtgcctgatcttttggctgatcttttctatcatgggcgtgaatctgttcgccggcaagtaccactac
tgctttaatgagacctccgagatccggttcgagatcgatgaggtgaacaacaagacagactgtgagaagctgatggagggcaacaa
tacagagatccggtggaagaatgtgaagatcaatttcgataacgtgggcgccggctacctggccctgctgcaggtggccacctttaag
ggctggatggatataatgtacgccgccgtggattcccgcaagcccgatgagcagccagactatgagggcaacatctacatgtacatc
tatttcgtgatcttcatcatcttcggcagctttttcaccctgaatctgtttatcggcgtgatcatcgataacttcaaccagcagaagaagaagt
tcggcggccaggacatcttcatgacagaggagcagaagaagtactataacgccatgaagaagctgggctccaagaagcctcaga
agccaatccctagaccactgaataagatccagggcatcgtgttcgacttcgtgacccagcaggcctttgacatcgtgatcatgatgctg
atctgtctgaacatggtgaccatgatggtggagacagatacccagtccaagcagatggagaatatcctgtattggatcaacctggtgttt
gtgatctttttcacatgtgagtgcgtgctgaagatgttcgccctgcgccactattatttcacaatcggctggaacatctttgacttcgtggtggt
aatcctgtctatcgtgggcatgtttctggccgacatcatcgagaagtacttcgtgagcccaacactgttcagagtgatccggctggccag
gatcggcagaatcctgcggctgatcaagggcgccaagggcatcagaaccctgctgttcgccctgatgatgtctctgccagccctgttc
aatatcggcctgctgctgtttctggtaatgttcatcttttccatctttggcatgtccaacttcgcctatgtgaagcacgaggccggcatcgatg
atatgtttaacttcgagacattcggcaactccatgatctgtctgttccagatcaccacctctgccggctgggatggcctgctgctgcctatc
ctgaatagaccaccagattgtagcctggataaggagcaccctggcagcggcttcaagggcgattgtggcaatccttccgtgggcatct
tcttcttcgtgtcctacatcatcatctctttcctgatcgtggtgaacatgtacatcgccatcatcctggagaatttctctgtggccaccgagga
gtctgccgacccactgtctgaggatgacttcgagaccttctatgagatctgggagaagtttgaccctgatgccacccagtttatcgagtat
tgcaagctggccgactttgccgacgccctggagcacccactgagagtgccaaagccaaataccatcgagctgatcgccatggatct
gcccatggtgagcggcgatagaatccactgcctggacatcctgtttgccttcacaaagagagtgctgggcgatagcggcgagctgga
catcctgaggcagcagatggaggagaggttcgtggcctctaaccccagcaaggtgtcctacgagcctatcaccacaaccctgcgga
gaaagcaggaggaggtgtccgccgtggtgctgcagagagcctacagaggccacctggcccggagaggctttatctgcagaaagat
cacctccaacaagctggagaatggcggcacccaccgcgagaagaaggagtctacccccctctaccgccagcctgccttcctacgac

tccgtgaccaagccagataaggagaagcagcagcgcgcagaggagggacggagagaaagagctaagagacagaaagaagt
gagagagtcaaagtgctctagaacccatacgacgtcccagactacgcttaa

- *SCN8A*^{WT}
- XbaI restriction site
- HA tag-STOP codon

mSCN1B:

atggggacgctgctggctctcgtggtgggcgcggcgctggtatcctcagcctgggggggctgcgtggaggtggattccgat
accgaggctgtgtatgggatgaccttcaaaatcctgtgcatctcctgtaagcgtcgtagtgagaccaccgccgaaaccttcacggagt
ggaccttccgccagaaggggacagaggaatttgtcaagatcctacgctatgagaatgaggtgctgcagctggaggaagatgagcg
ctttgagggccgagtggtgtggaacggtagtcggggcaccaaggacctgcaggacctgtccatcttcatcaccaacgtcacctacaa
ccactctggcgactacgaatgtcacgtctaccgtctcctcttctttgataattatgagcacaacaccagcgtcgtcaagaagatccacct
ggaggtggtggacaaggccaacagagatatggcatccatcgtgtcagagatcatgatgtacgtgctcattgtggtgttgaccatatggc
ttgtggcagagatggtgtactgctacaagaagattgctgctgctacggaggctgctgcacaagagaacgcctcagaatacctggccat
tacatccgagagcaaagaaaactgtacaggcgtccaggtggctgaatag

mSCN2B:

atggaagtcacagcgcccaccactcttagtgtcctcaatgggtccgatacccgcctgccctgtaccttcaactcctgctacac
cgtgaaccacaagcagttctctcttaactggacttaccaggagtgtaacaattgcacagaggagatgttcctccagttccgaatgaaga
tcattaacctgaagctggagcggtttggagaccgcgtggagttctcagggaaccccagtaagtacgacgtgtcagtgactctaaaga
acgtgcagctagaagacgaaggcatttacaactgctacattaccaaccctccagaccgccaccgcggccacggcaagatttacctg
caggtccttctagaagtacccccagagcgggactccacggtggcggtcatcgtgggtgcctcagtgggggtttcctggctgtggtcat
cttggtgctgatggtggtcaaatgtgtgaggaggaaaaaagagcagaagctgagcacggatgacctgaagactgaagaggaagg
caagatggatggtgagggcaacgcggaagatggcaccaagtaa

Nfasc^{WT}-HA:

atggccaggcagcaggcgccaccctgggtccacgtagccctcatcctcttcctcctcagcctcggaggggccattgagatt
ccgatggatccaagcattcagaatgagctgacccaacccccaacgatcaccaagcagtcggtgaaggaccacatcgtggaccccc
gagataacatcctgattgaatgtgaagctaaagggaaccccgccccccagtttccactggactcgcaacagcaggttcttcaacattgc
caaggacccacgggtgtccatgaggaggaggtctgggaccttggtgatcgacttccgcagtggtgggcggcctgaggagtacgaa
ggggagtaccagtgctttgcccggaacaaattcggcacagctcttagcaaccgcatccgcctgcaggtgtccaaatctcccctgtggc
ccaaggaaaacctagaccccgtcgtggttcaagagggtgccccttaaccctgcagtgcaacccccacctggcctcccatccccc
gtcatcttctggatgagcagctccatggagcccatcacccaggacaagcgtgtctcccagggtcacaacggggacctgtacttctcca
acgtcatgctgcaggacatgcagaccgactacagctgcaatgcacgcttccacttcacccacaccattcagcagaagaatcccttca

ccctcaaagtcctcaccacccgaggagttgcggaaagaacacctagcttcatgtatccccagggcacgtcaagcagtcagatggta
ctgcgcggcatggacctgctgctggagtgcattgcctctggggtcccaacaccagatattgcatggtacaagaaaggtggggacctc
ccatctgacaaggccaagttcgagaattttaacaaggctctgcgcatcaccaatgtctctgaagaggactctggggagtatttctgcctg
gcctccaacaagatgggcagcatccggcacacgatctcggtgagagtaaaggctgccccatactggctggatgagcccaagaactt
gatcctggctcctggtgaagatgggaggctggtgtgtcgagccaatgggaacccgaagccgaccgtccagtggctggtgaatggag
acccctttgcaatcggcaccacccaaccccaaccgtgaggtggccggagacactatcatcttccgggacactcagatcagcagcagg
gcagtgtaccagtgtaacacatccaacgaacatggctacctgctggccaatgccttcgtcagcgtattagatgtacccccctcggatgct
gtctccccggaaccagctcatcagggtgatcctttacaaccggacgcgactggactgtccgttctttgggtctcccattccaacactccg
atggtttaagaatgggcaaggaagcaacctggatggtggtaactaccacgtctacgaaaatggcagcctggaaatcaagatgattcg
caaagaggaccaaggcatctacacctgtgtggccaccaacatcctgggaaaagctgaaaatcaagtccgcctggaggtcaaaga
ccccaccaggatctacaggatgcctgaagaccaggtggccaagaggggcaccacagtgcagctggagtgccgtgtgaagcatga
cccctccttgaaactcacagtctcctggctgaaggatgacgagccactctacattggaaacaggatgaaaaaggaagatgactccct
gaccatcttcggagtggcagagcgggaccaaggcagttacacgtgcatggccagcaccgagctggaccaggacctggcaaagg
cctacctcactgttctagctgatcaggccactccgactaaccgtttggctgccctgcccaaagggcggccagaccgacccagggacc
tggagctcactgacctggcggaaaggagtgtgaggctgacctggatcccgggggatgataacaacagtcccatcacagactacgtt
gtccagtttgaagaggaccagttccagccaggagtctggcatgaccactccaagttcccaggcagtgtcaactcagccgtcctccatc
tgtccccgtatgtcaactatcagttccgagtcatcgctgtcaacgaggttgggagcagccaccccagccttccatccgagcggtaccga
acaagcggggcacccccctgaatccaaccccagtgatgtgaagggcgaagggacacgaaaaaacaatatggagatcacatggac
gcctatgaatgctacctccgcctttggccccaacctgcgctacattgtcaagtggcgacggagagaaacccgagagacttggaacaa
tgtcaccgtgtggggctctcgctatgtggtggggcagacccctgtctacgtaccctatgagatccgagtccaggctgaaaatgactttgg
gaaaggcccggagcctgaaaccgtcattgggtactcgggggaagatttacccagtgcccccaggcgtttcagagtccgacagccca
acctggagaccatcaacctggaatgggatcacccagagcaccccaacgggatcctgattggatacacgctcagatacgtgcccttta
atggaaccaaactgggaaagcagatggtggaaaacttctctcccaatcagaccaagttctcggtgcagagagcagaccccgtgtcc
cgttaccgcttctccctcagtgccaggacgcaggtgggctctggagaagcagccacggaggagtccccaacacctccaaatgaag
ctactccaactgcagctcctcccacattgcccccgactaccgtgggtaccacaggccttgtgagcagtactgatgctactgcccttgctg
ccaccagtgaagccacaacagttcccatcatcccaaccgtcgtacctaccaccgtcgccaccaccattgccacaactactacaacc
actgccgccgccaccaccactaccaccacggagagtcctcccactaccaccactgggactaagattcacgaaaccgccccgac
gagcagtccatttggaacgtcacggtgctccccaacagtaaatgggccaacatcacctggaagcacaatttcaggcctggaactgac
tttgtggttgagtacatcgacagcaaccatacgaaaaaaactgtccctgttaaggcccaagcccagcccatacagctgacagacctct
ttcccgggatgacgtacacgttgcgggtgtattcccgggacaacgagggcatcagcagtaccgtcatcacctttatgaccagtacagct
tacaccaacaaccagactgacatcgccacccagggctggttcatcgggctcatgtgtgccattgcccttctggtgctgatcctgcttatcg
tctgcttcatcaagaggagtcgtggcggcaagtacccagtgcgagaaaagaaggatgtccccttgggccctgaagaccccaaaga
agaagatggttcatttgactacagtgacgaggacaacaagcccctgcagggcagccagacatctctggacggcaccatcaagcag
caggagagtgacgacagcctagtggactacggcgagggtggcgagggccagttcaacgaagatggctcctttattggccagtacac

tgtcagaaaggacaaggaggagaccgagggcaatgagagctcagaggccacatctccagtcaatgccatctattccctggcctac
ccatacgacgtcccagactacgcttga

- HA tag-TGA stop codon

hNES promoter

tgtatgcagctggacctaggagagaagcaggagaggaagatccagcacaaaaaatccgaagctaaaaacaggacac
agagatgggggaagaaaagagggcagagtgaggcaaaaagagactgaagagatgagggtggccgccaggcactttagatag
gggagaggctttatttacctctgtttgtttttttttttttttttttttttgcgaggtagtcttgcttagtctccaggctggagtgcagtggcacaatctc
agctcactgcaacttccacctcctgggttcaagcaattctcctgcctcagcctcccgagtagctgggactacaggcgcatgcaaccgc
gcctggctaatttttgtatttttagtagaaacggggtttcaccacgttagccaggatggtctggatctcctgacctcgtgatctgcccgcctcc
gccttccaaagtgctgggattacaggggtgagccacagcgcctggtccctatttacttctgtcttctacctccaggagatcaaagacgct
ggccttcagacctgatcagactcccaggggcagccaccacatgtatgacagagaacagaggatgcctgtttttgccccaaagctgga
aattcatcacaacctgaggcccaggatctgctctgtgccggtcctctgggcagtgtggggtgcagaatggggtgcctaggcctgagcg
ttgcctggagcctaggccgggggccgccctcgggcaggcgtgggtgagagccaagaccgcgtgggccgcggggtgctggtagga
gtggttggagagacttgcgaaggcggctggggtgttcggatttccaataaagaaacagagtgatgctcctgtgtctgaccgggtttgtg
agacattgaggctgtcttgggcttcactggcagtgtgggccttcgtacccgggctacaggggtgcggctctgcctgttactgtcgagtgg
gtcgggccgtgggtatgagcgcttgtgtgcgctggggccaggtcgtgggtgcccccacccttcccccatcctcctcccttccccactcca
ccctcgtcggtcccccacccgcgctcgtacgtgcgcctccgccggcagctcctgactcatcgggggctccgggtcacatgcgcccgc
gcggccctataggcgcctcctccgcccgccgcccgggagccgcagccgccgccgccactgccactcccgctctctcagcgccgcc
gtcgccaccgccaccgccaccgccactaccaccg

Codon-optimized NES PylRS^{AF}:

atggcttgccctgtgcctctgcagctgcctcccctggaacgcctgaccctggacgataagaaaccactgaacaccctgatta
gcgccaccggcctgtggatgtccaggaccggcacaatccacaagatcaagcaccacgaggtgagcagatccaaaatctacatcg
agatggcctgcggcgaccacctggtggtgaacaacagcaggagcagcaggaccgcccgggccctgaggcaccacaagtatcgc
aagacatgcaagcggtgtcgcgtgtccgacgaggatctgaacaagttcctgaccaaggccaatgaggatcagacatccgtgaaggt
gaaggtggtgtctgccccaacccggacaaagaaggcaatgccaaagagcgtggccagggcccccaagcctctggagaacaccg
aggcagcacaggcacagccatctggcagcaagtttagcccagcaatccccgtgagcacccaggagtccgtgtctgtgcctgccagc
gtgtccacatctatctctagcatctctaccggagcaacagccagcgccctggtgaagggcaacaccaatcctatcacaagcatgtccg
ccccagtgcaggccagcgcccctgccctgaccaagtcccagacagaccgcctggaggtgctgctgaaccctaaggatgagatcag
cctgaacagcggcaagccattcagggagctggagtccgagctgctgtctaggagaaagaaggacctgcagcaaatctacgccga
ggagagggagaactatctgggcaagctggagagggagatcaccagattctttgtggatagaggctttctggagatcaagtccccaat
cctgatccccctggagtacatcgagcggatgggcatcgacaacgatacagagctgtctaagcagattttcagggtggacaagaatttt
gcctgaggcccatgctggccccaaacctggccaattacctgaggaagctggaccgcgccctgcccgaccccatcaagattttcgag

atcggcccatgttatagaaaggagtctgatggcaaggagcacctggaggagtttaccatgctgaatttttgccagatgggctctggctgt
acccgggagaacctggagagcatcatcacagacttcctgaatcacctgggcatcgactttaagatcgtgggcgatagctgtatggtgtt
tggcgacacactggatgtgatgcacggcgatctggagctgtcctctgccgtggtgggacctatcccactggacagggagtggggcat
cgataagccctggatcggagcaggattcggcctggagcgcctgctgaaggtgaagcacgactttaagaacatcaagcgggctgcc
agaagcgaaagttattacaatgggattagcacaaacctgtga

U6-tRNA^{Pyl}-HDV(rv):

aaaaaagtcccattcgccatgccgaagcatgttgcccagccggcgccagcgaggaggctgggaccatgccggcccgg
aaaccccgggaatctaacccggctgaacggatttagagtccattcgatctacatgatcaggtttccggtgtttcgtcctttccacaagata
tataaagccaagaaatcgaaatactttcaagttacggtaagcatatgatagtccattttaaaacataatttttaaaactgcaaactaccca
agaaattattactttctacgtcacgtattttgtactaatatctttgtgtttacagtcaaattaattccaattatctctctaacagccttgtatcgtata
tgcaaatatgaaggaatcatgggaaataggccctc

- **PolyA**
- HDV self-cleaving ribozyme
- tRNA^{Pyl}
- U6 promoter

7SK-tRNA^{Pyl}-HDV(rv):

aaaaaagtcccattcgccatgccgaagcatgttgcccagccggcgccagcgaggaggctgggaccatgccggcccgg
aaaccccgggaatctaacccggctgaacggatttagagtccattcgatctacatgatcaggtttccgaggtacccaggcggcgcaca
agctatataaacctgaaggaaatctcaactttacacttaggtcaagttacttatcgtactagagcttcagcaggaaatttaactaaaatct
aatttaaccagcatagcaaatatcatttattcccaaaatgctaaagtttgagataaacggacttgatttccggctgttttgacactatccag
aatgccttgcagatgggtggggcatgctaaatactgcag

- **PolyA**
- HDV self-cleaving ribozyme
- tRNA^{Pyl}
- 7SK promoter

Y3-tRNA^{Pyl}-HDV(rv):

aaaaaagtcccattcgccatgccgaagcatgttgcccagccggcgccagcgaggaggctgggaccatgccggcccgg
aaaccccgggaatctaacccggctgaacggatttagagtccattcgatctacatgatcaggtttccgaaagttaggcctgtagttgtaga
tatataaggtttataatattcacccttacaagtcatggtggattatgagcataaactgttaaaaatatgtttgtgtattccaaatacatacctc

atacgtaataataaaaccacagaaaagtatttaatttagaagaaaaatctatttacatttcaacgaccttacagggcttccggataacgt
ctggttcaaagcatgctgggtaatcg

- **PolyA**
- HDV self-cleaving ribozyme
- tRNA^{Pyl}

- Y3 promoter

MRP/7/2-tRNA^{Pyl}-HDV(rv):

aaaaaagtcccattcgccatgccgaagcatgttgcccagccggcgccagcgaggaggctgggaccatgccggcccgg
aaaccccgggaatctaacccggctgaacggatttagagtccattcgatctacatgatcaggtttccCACGTCCTCAGCTTCACAGAGTA
GTATTTTATAGCCCTAAAGAAATTGTGTTTTATGATTAGGGTGAGAAAGTTGGTGGCGTGAGATTAAAAAAACCGTTTTCGGGCATAACTTTCT
AAGACTATAGGCTTTCAGAGGCATTGTGGCTAGCAGAATAGCTAATAGACACGAAATGAACAAATACAGGAAAGCTAGAATGACA
CTATCTTATGCAAATATGGTCTGGCCCCGCCCTACGGGGAGTGGGCGTGGCCTCCCCGGAGCCGGCCGGCCTGCTCGCGTGCGCGTGC
GCGTTGGGGCGGCCGGCCAATGCCGGACCGCTTCGGCACCGCCCGCCCGATCCCTCCACCCGTGGGCCGGCAATGGCGGGCGCA
GTTTCGCTCTTGGGTGTGGTGGGGCTGCTGCTTGTGTCTGCGCTGTCCGGGGTCCTAGGAGACCGCGCCAATCCCGACCTCCGGGCACAC
CCAGGTACCAGCTAGGGCTGCTGGAGGAGGGCTGGGACTGCGCACGGGTCCCAGGCCCCAGCTCGGCTGACTCGCCTGTATCCTCC
CTCCGCAGGGAACGCAGCCCACCCCGGCTCTGGAGCCACGGAACCCCGGCGGCGACCACCGCTCAAGGATCAACGCGAGCGG
ACCCGGGCCGGGTCGCTGCCTCTGGGGGCGCTGTACACCGCGGCCGTCGCGGCTTTTGTGCTGTACAAGTGTTTGCAGGTACG

- **PolyA**
- HDV self-cleaving ribozyme
- tRNA^{Pyl}

- MRP/7-2 promoter

4xU6-tRNA^{M15}(rv):

AAAAAACGGAAACCCCGGGAATCGAACCCGGCTGAACGGATTTAGAGTCCGTTCGGTCTCCCTGACCAGGTTTCCGGTGTT
TCGTCCTTTCCACAAGATATATAAAGCCAAGAAATCGAAATACTTTCAAGTTACGGTAAGCATATGATAGTCCATTTTAAAACATAATTTTA
AAACTGCAAACTACCCAAGAAATTATTACTTTCTACGTCACGTATTTTGTACTAATATCTTTGTGTTTACAGTCAAATTAATTCTAATTATCTCTCT
AACAGCCTTGTATCGTATATGCAAATATGAAGGAATCATGGGAAATAGGCCCTC**TTCCTGCCCCTCGAC**AAAAAACGGAAACCCC
GGGAATCGAACCCGGCTGAACGGATTTAGAGTCCGTTCGGTCTCCCTGACCAGGTTTCCGGTGTTTCGTCCTTTCCACAAGATATATAAAG
CCAAGAAATCGAAATACTTTCAAGTTACGGTAAGCATATGATAGTCCATTTTAAAACATAATTTTAAAACTGCAAACTACCCAAGAAATT
ATTACTTTCTACGTCACGTATTTTGTACTAATATCTTTGTGTTTACAGTCAAATTAATTCTAATTATCTCTCTAACAGCCTTGTATCGTATATGCAAAT
ATGAAGGAATCATGGGAAATAGGCCCTC**TTCCTGCCCCTCGAC**AAAAAACGGAAACCCCGGGAATCGAACCCGGCTGAACGGA

tttagagtccgttcggtctccctgaccaggtttccggtgtttcgtcctttccacaagatatataaagccaagaaatcgaaatactttcaagtt
acggtaagcatatgatagtccattttaaaacataatttttaaaactgcaaactacccaagaaattattactttctacgtcacgtattttgtacta
atatctttgtgtttacagtcaaattaattctaattatctctctaacagccttgtatcgtatatgcaaatatgaaggaatcatgggaaataggcc
ctc**ttcctgcccctcgac**aaaaaacggaaaccccgggaatcgaacccggctgaacggatttagagtccgttcggtctccctgacca
ggtttccggtgtttcgtcctttccacaagatatataaagccaagaaatcgaaatactttcaagttacggtaagcatatgatagtccattttaa
aacataatttttaaaactgcaaactacccaagaaattattactttctacgtcacgtattttgtactaatatctttgtgtttacagtcaaattaattct
aattatctctctaacagccttgtatcgtatatgcaaatatgaaggaatcatgggaaataggccctc

- **Linker**
- tRNA^{M15}
- U6 promoters

NLS:

cgaaaaaaaaacgcaaagtggaagatagc

mEGFP:

atggtgagcaagggcgaggagctgttcaccggggtggtgcccatcctggtcgagctggacggcgacgtaaacggccac
aagttcagcgtgtccggcgagggcgagggcgatgccacctacggcaagctgaccctgaagttcatctgcaccaccggcaagctgc
ccgtgccctggcccaccctcgtgaccaccctgacctacggcgtgcagtgcttcagccgctaccccgaccacatgaagcagcacgac
ttcttcaagtccgccatgcccgaaggctacgtccaggagcgcaccatcttcttcaaggacgacggcaactacaagacccgcgccga
ggtgaagttcgagggcgacaccctggtgaaccgcatcgagctgaagggcatcgacttcaaggaggacggcaacatcctggggca
caagctggagtacaactacaacagccacaacgtctatatcatggccgacaagcagaagaacggcatcaaggtgaacttcaagatc
cgccacaacatcgaggacggcagcgtgcagctcgccgaccactaccagcagaacaccccatcggcgacggccccgtgctgctg
cccgacaaccactacctgagcacccagtccaagctgagcaaagaccccaacgagaagcgcgatcacatggtcctgctggagttcg
tgaccgccgccgggatcactctcggcatggacgagctgtacaagtaa

iRFP:

atggcggaaggatccgtcgccaggcagcctgacctcttgacctgcgacgatgagccgatccatatccccggtgccatcca
accgcatggactgctgctcgccctcgccgccgacatgacgatcgttgccggcagcgacaaccttcccgaactcaccggactggcga
tcggcgccctgatcggccgctctgcggccgatgtcttcgactcggagacgcacaaccgtctgacgatcgccttggccgagcccgggg
cggccgtcggagcaccgatcactgtcggcttcacgatgcgaaaggacgcaggcttcatcggctcctggcatcgccatgatcagctca
tcttcctcgagctcgagcctccccagcgggacgtcgccgagccgcaggcgttcttccgccgcaccaacagcgccatccgccgcctgc
aggccgccgaaaccttggaaagcgcctgcgccgccgcggcgcaagaggtgcggaagattaccggcttcgatcgggtgatgatcta
tcgcttcgcctccgacttcagcggcgaagtgatcgcagaggatcggtgcgccgaggtcgagtcaaaactaggcctgcactatcctgc
ctcaaccgtgccggcgcaggcccgtcggctctataccatcaacccggtacggatcattcccgatatcaattatcggccggtgccggtc

accccagacctcaatccggtcaccgggcggccgattgatcttagcttcgccatcctgcgcagcgtctcgcccgtccatctggaattcat
gcgcaacataggcatgcacggcacgatgtcgatctcgattttgcgcggcgagcgactgtggggattgatcgtttgccatcaccgaacg
ccgtactacgtcgatctcgatggccgccaagcctgcgagctagtcgcccaggttctggcctggcagatcggcgtgatggaagag

mCherry:

atgccggtgagcaagggcgaggaggataacatggccatcatcaaggagttcatgcgcttcaaggtgcacatggagggct
ccgtgaacggccacgagttcgagatcgagggcgagggcgagggccgcccctacgagggcacccagaccgccaagctgaaggt
gaccaagggtggcccccctgcccttcgcctgggacatcctgtcccctcagttcatgtacggctccaaggcctacgtgaagcaccccgcc
gacatccccgactacttgaagctgtccttccccgagggcttcaagtgggagcgcgtgatgaacttcgaggacggcggcgtggtgacc
gtgacccaggactcctccctgcaggacggcgagttcatctacaaggtgaagctgcgcggcaccaacttcccctccgacggccccgt
aatgcagaagaagaccatgggctgggaggcctcctccgagcggatgtaccccgaggacggcgccctgaagggcgagatcaagc
agaggctgaagctgaaggacggcggccactacgacgctgaggtcaagaccacctacaaggccaagaagcccgtgcagctgccc
ggcgcctacaacgtcaacatcaagttggacatcacctcccacaacgaggactacaccatcgtggaacagtacgaacgcgccgag
ggccgccactccaccggcggcatggacgagctgtacaagtga

6.3. The appendix lists of the cell culture mediums/supplements, chemicals, kits, cells, antibodies, dyes, and other materials used in this dissertation

Cell culture mediums and supplements:

- B27 (Thermo Fisher Scientific, cat. no. 17504044)
- B-27™ Plus Neuronal Culture System (Thermo Fisher Scientific, cat. no. A3653401)
- DPBS, no calcium, no magnesium (Thermo Fisher Scientific, cat. no. 14190169)
- Fetal Bovine Serum, qualified, EU-approved, South America origin (Thermo Fisher Scientific, cat. no. 10270106)
- HEPES, 1 M (Thermo Fisher Scientific, cat. no. 15630056)
- Hibernate E - Low Fluorescence (Brain Bits, cat. no. HELFF)
- High-glucose Dulbecco's Modified Eagle Medium (Thermo Fisher Scientific, cat. no. 41965062)
- L-glutamine (Thermo Fisher Scientific, cat. no. 25030024)
- Neurobasal culture medium (Thermo Fisher Scientific, cat. no. 21103049)
- Opti-MEM Reduced serum media unless stated otherwise (Thermo Fisher, cat. no. 31985062)
- Penicillin-streptomycin (Sigma Aldrich, cat. no. P0781)
- Penicillin-streptomycin (Thermo Fisher Scientific, cat. no. 15140122)
- Poly-D-lysine (Sigma Aldrich, cat. no. P6407)
- Poly-L-lysine (Sigma Aldrich, cat. no. P1524)
- Puromycin dihydrochloride (Sigma Aldrich, cat. no. P8833)
- Sf-900™ III SFM complete 1x liquid medium (Thermo Fisher Scientific, cat. no. 12658019)
- Sodium pyruvate, 100 mM (Thermo Fisher Scientific, cat. no. 11360039)
- Trypsin-EDTA (0.05%), phenol red (Thermo Fisher Scientific, cat. no. 25300054)

Chemicals:

- 16% Paraformaldehyde EM Grade (Electron Microscopy Sciences, cat. no. E15710)
- 2-Mercaptoethanol (Sigma Aldrich, cat. no. M3148)
- 2-Propanol (Honeywell research, cat. no. 33539)
- Bovine Serum Albumin (Sigma Aldrich, cat. no. A9647)
- Catalase (Sigma Aldrich, cat. no. C3155)

- DMSO, sterile, filtered (Sigma Aldrich, cat. no. D2438)
- Glucose (Sigma Aldrich, cat. no. D9559)
- Goat serum (Thermo Fisher, cat. no. 16210072)
- Paraformaldehyde (Sigma –Aldrich, cat. no. 158127)
- Phenylmethanesulfonyl fluoride (Sigma Aldrich, cat. no. P7626)
- Protease inhibitor cocktail (PIC., Sigma Aldrich, cat. no. P8340)
- Skim milk (Carl Roth, cat. no. T145.1)
- Sodium borohydride (Sigma Aldrich, cat. no. 71320)
- Sodium chloride (Sigma Aldrich, cat. no. S7653)
- Sodium deoxycholate (Sigma Aldrich, cat. no. D6750)
- Sodium butyrate (Sigma Aldrich, cat. no. B5887)
- Sodium fluoride (Sigma Aldrich, cat.no. S7920).
- TetraSpeck Microspheres (Thermo Fisher, cat. no. T7279)
- The glucose oxidase (Sigma Aldrich, cat. no. G2133)
- Triton X-100 (Sigma-Aldrich, cat. no. X100)
- Trizma hydrochloride (Sigma Aldrich, cat. no. T5941)
- Trizma® base, BioPerformance Certified (Sigma Aldrich, cat. no. T6066)
- TWEEN® 20 BioXtra, viscous liquid (Sigma Aldrich, cat. no. P7949)
- Vectashield (Biozol, cat. no. VEC-H-1000)

Kits:

- BacPAK™ baculovirus rapid titer kit (Takara Bio/Clontech, cat. no. 631406)
- E.Z.N.A. Plasmid mini kit I (V-spin column; VWR, cat no. D6943-02)
- EndoFree Plasmid Maxi Kit (10; Qiagen, cat no. 12362)
- MultiBacMam™ kit (Geneva Biotech)
- PCR Purification Kit (Thermo Fisher Scientific, cat no. K310001)
- PiggyBAC Transposon system (BioCat)
- PureLink gDNA kit (Thermo Fisher, cat. no. K1820-01)
- PureLink® Quick Gel Extraction Kit (Thermo Fisher Scientific, cat no. K210012)
- PureLink® Quick Plasmid Miniprep Kit (Thermo Fisher Scientific, cat no. K210011)
- PureLink™ HiPure Plasmid Maxiprep Kit (Thermo Fisher Scientific, cat no. K210007)
- Quick Change II XL site-directed mutagenesis kit (Agilent Technologies, cat. no. 200522)

Bacteria, insect, and mammalian cell lines:

- Gibco primary cortical neurons isolated from embryonic day 17 C57BL/6 mice (Thermo Fisher Scientific, cat. no. A15586)
- Gibco primary cortical neurons isolated from Sprague Dawley embryonic day 18 rats (Thermo Fisher, scientific, cat. no. A365512)
- Gibco Sf21 cells in Sf-900™ III serum-free medium (Thermo Fisher Scientific, cat. no. 12682019)
- MAX Efficiency Stbl2™ cells (Thermo Fisher Scientific, cat. no. 10268019)
- One Shot™ TOP10 Electrocompetent™ E. coli (Thermo Fisher Scientific, cat. no. C40452)
- XL 10-Gold Ultracompetent *E.coli* (Agilent, cat. no. 200315)
- Mouse neuroblastoma N1E-115-1 cell line (Sigma Aldrich; ECACC 08062511)
- Mouse neuroblastoma x rat neuron hybrid ND7/23 cell line (Sigma Aldrich; ECACC 92090903)

Primary antibodies:

- Mouse anti-ankyrin G antibody (Santa Cruz, cat. no. 12719)
- Mouse anti-HA tag (Thermo Fisher Scientific, cat. no. 26183)
- Mouse anti-panNa_V (Sigma Aldrich, cat. no. S8809)
- Mouse anti-β3-tubulin antibody (BioLegend, cat. no. 801202)
- Mouse Na_V1.6 Na+ channel (Neuromab, cat. no. 75-026)
- Rabbit anti-HA tag (C29F4) monoclonal antibody (Cell Signaling, cat. no. 3724)
- Rabbit anti-HA tag (SG77) polyclonal antibody (Thermo Fisher Scientific, cat. no. 71-5500)
- Rabbit anti-panNF (Abcam, cat.no. ab31457)

Secondary antibodies:

- Goat anti-rabbit AF647 (Thermo Fisher Scientific, cat. no. A21245)
- Goat anti-mouse AF633 (Thermo Fisher Scientific, cat. no. A-21052)
- Goat anti-mouse AF647 (Thermo Fisher Scientific, cat. no. A21236)
- Goat anti-mouse AF647 Plus (Thermo Fisher Scientific, cat. no. A32728)
- Goat anti-mouse horseradish peroxidase (Thermo Fisher Scientific, cat. no. A16072)
- Goat anti-rabbit AF555 (Thermo Fisher Scientific, cat. no. A21429)

- Goat anti-rabbit AF647 Plus (Thermo Fisher Scientific, cat. no. A32733)
- Goat-anti-rabbit horseradish peroxidase (Thermo Fisher Scientific, cat. no. A16104)

Tetrazine dyes:

- AF647-Pyr-tz (Jena Bioscience, cat. no. CLK-102)
- ATTO488-tz (Jena Bioscience, cat. no. CLK-010-02)
- Cy5-H-tz (Jena Bioscience)

Transfection reagents:

- Cellfectin™ II (Thermo Fisher Scientific, cat. no. 10362100)
- FuGene HD (Promega, cat. no E2311)
- JetPrime transfection reagent (Polyplus-transfection, cat. no. 114-15)
- Lipofectamine 2000 (Thermo Fisher Scientific, cat. no. 11668027)
- Lipofectamine 3000 (Thermo Fisher Scientific, cat. no. L3000015)

Unnatural amino acids:

- BOC-Lys (Iris Biotech GMBH, cat. no. HAA1096)
- Endo-BCN-Lys (SICHEM cat. no. SC-8014)
- TCO*A-Lys (Sirius Fine Chemicals, SICHEM, cat. no. SC-8008)
- TCO4en/eq-Lys (a gift from Prof. Dr. Edward Lemke; can be obtained from SICHEM, cat. no. SC-8060)

Cell culture dishes:

- 35 mm Petri dishes (Greiner Bio-one, cat. no. 627160)
- Amicon® Ultra-15 centrifugal filter units (100 kDa MWCO, 15 ml sample volume; Sigma Aldrich, cat.no. UFC910008)
- Eight-well Lab-Tek II chambered cover glasses (German #1.5 borosilicate glass; Thermo Fisher Scientific, cat. no. 155409)
- Four-well Lab-Tek II chambered cover glasses (German #1.5 borosilicate glass; Thermo Fisher Scientific, cat. no. 155382)
- P10 Petri dishes (Greiner Bio-one, cat. no. 664160)
- P20 Petri dishes (Greiner Bio-one, cat. no. 639160)

Western blot materials:

- 0.2 µm nitrocellulose membrane (BioRad, 1704158)
- 1xNuPAGE™ MOPS SDS running buffer (Thermo Fisher, NP0001)
- 4x Leammlie buffer (BioRad, 1610747)
- Bradford assay (Sigma-Aldrich, cat. no. B6916)
- Clarity Western ECL substrate (Bio Rad, 1705060)
- NuPAGE™ 4-12% Bis-Tris Protein Gels (Thermo Fisher, NP0329)
- Precision Plus Protein™ WesternC™ ladder (BioRad, 610376)
- Trans-Blot® Turbo™ Transfer System

6.4. List of abbreviations

aaRS – aminoacyl-tRNA synthetase

AAV – adeno-associated virus

ab – antibody

ABD – ankyrin binding domain

AcNPV – *Autographa californica* nuclear polyhedrosis virus

AF488 – Alexa Fluor 488

AF(+)647 – Alexa Fluor 647 Plus

AF555 – Alexa Fluor 555

AF633 – Alexa Fluor 633

AF647 – Alexa Fluor 647

AF647-Pyr-tz – Alexa Fluor 647-Pyrimidyl-tetrazine

AF647-tz – Alexa Fluor 647-tetrazine

AIS – axon initial segment

AMPA – α-amino-3-hydroxy-5-methyl-4-isoxazole propionic acid

ankB – ankyrin B

ankG – ankyrin G

APP - amyloid precursor protein

ATTO488-tz – ATTO488-tetrazine

BAD – biotin acceptor domain

BOC-Lys – N-ε-t-butyloxycarbonyl-L-lysine

BSA – bovine serum albumin

CAG – chicken β-actin promoter

CAM – cell adhesion molecule

Cas9 – CRISPR-associated protein 9

Caspr – contactin-associated protein

CAT – catalase

Ca_V – voltage-gated calcium channels

CiVSP – *Ciona intestinalis* voltage-sensitive phosphates

CK2 – casein kinase 2

CMV - cytomegalovirus

CNS – central nervous system

CNTN – contactin

Cpf1 – CRISPR-associated endonuclease in prevotella and francisella 1

CpK – cyclopropene – L – lysine

CRISPR – clustered regularly interspaced short palindromic repeats

crRNA – CRISPR RNA

CuACC – Cu(I)-catalyzed azide–alkyne cycloaddition

Cy5 – Cyanine 5

Cy5-tz – tetrazine-Cyanine 5

DIV – day *in vitro*

DNA – deoxyribonucleic acid

DNA-PAINT – DNA-points accumulation for imaging in nanoscale topography

dSTORM - direct stochastic optical reconstruction microscopy

E. coli - Escherichia coli

ECM – extracellular matrix molecules

EGFP – enhanced GFP

EGFR – epidermal growth factor receptor

endo-BCN-Lys – bicyclo [6.1.0] nonyne – L – lysine

eRF1 – eukaryotic release factor 1

FACS – fluorescence-activated cell sorting

FBS – fetal bovine serum

FN III domain – fibronectin type III repeats (domains)

FPALM – fluorescence photoactivation localization microscopy

FPs – fluorescent proteins

GABA – gamma-amino butyric acid

GCE – genetic code expansion

gDNA – genomic DNA

GFP – green fluorescent protein

GO – glucose oxidase

GOI – gene of interest

GPCR – G-protein-coupled receptor

gRNA – guide RNA

GS – goat serum

GSDM – ground state depletion microscopy

HA tag – hemagglutinin tag

HDV ribozyme – hepatitis delta virus ribozyme

HEK293T – highly transfectable derivative of human embryonic kidney 293 cells

HH ribozyme – hammerhead ribozyme

HILO – highly inclined and laminated optical sheet

hiPSCs – human induced pluripotent stem cells

HIV-1 – human immunodeficiency virus-1

hNSE – human neuron-specific enolase 2 promoter

HRP – horseradish peroxidase

ICC – immunocytochemistry

IFITM3 – interferon-induced transmembrane protein 3

Ig-like domain – immunoglobulin-like domain

iPASS – identification of permissive amber suppression sites

iPSCs – induced pluripotent stem cells

IR – insulin receptor

iRFP – near-infrared fluorescent protein

ITR – inverted terminal repeat

Kir2.1 – potassium inwardly rectifying 2.1 channel

K_V – voltage-gated potassium channels

LeuRS – leucil tRNA synthetase

LOF – loss-of-function

LUT – look-up table

MAP1B – microtubule-associated protein 1B

mCMV – minimal CMV

MCN – mouse cortical neurons

MEA – monoethanolamine

mGFP – monomeric GFP

MHN – mouse hippocampal neurons

MINFLUX – minimal photon fluxes

MOI – multiplicity of infection

mPOI – membrane protein of interest

mRNA – messenger RNA

MRP – mitochondrial RNA processing

MS – multiple sclerosis

Na_V – voltage-gated sodium channels

ND7/23 – mouse neuroblastoma (N18 tg 2) x rat dorsal root ganglion neuron hybrid cell

NES – nuclear export signal

NES $PylRS^{AF}$ – Y306A/Y384F (AF) double mutant of the *Methanosarcina mazei*-derived orthogonal $tRNA^{Pyl}$ synthetase fused to a nuclear export signal (NES)

NF – neurofascin

NF140 – neurofascin 140 kDa isoform

NF155 – neurofascin 155 kDa isoform

NF180 – neurofascin 180 kDa isoform

NF186 – neurofascin 186 kDa isoform

NFL – neurofilament light chain

NLS – nuclear localization signal

NMD – nonsense-mediated decay

NMDA – N-Methyl-D-aspartate

NPC – nuclear pore complex

NrCAM – neuronal cell adhesion molecule

Nup153 – nucleoporin 153

ORF – open reading frame

OxEA buffer – oxyrase/βME buffer

PALM – photo-activated localization *microscopy*

PB – phosphate buffer

PBS – phosphate-buffered saline

PCR – polymerase chain reaction

PFA – paraformaldehyde

PGK-1 – phosphoglycerate kinase

PNS – peripheral nervous system

POI – protein of interest

pol – polymerase

PylRS – pyrrolysyl tRNA synthetase

RCN – rat cortical neurons

RNA – ribonucleic acid

RPM – revolutions per minute

RT – room temperature

SA – streptavidin

SCO-Lys – cyclooctyne – L – lysine

SDS-PAGE – sodium dodecyl-sulfate polyacrylamide gel electrophoresis

seSPIEDAC – selectivity enhanced SPIEDAC

Sf21 – *Spodoptera frugiperda* 21 cells

shRNA – short hairpin RNA

siRNA – small interfering RNA

SiR-tz – silicon rhodamine-tetrazine

SMLM – single-molecule localization microscopy

snRNA – small noncoding RNA

SPAAC – strain-promoted azide-alkyne cycloaddition

SPIEDAC – strain-promoted inverse electron-demand diels-alder cycloaddition

SRM – super-resolution microscopy

STED – stimulated emission depletion microscopy

TAG-1 – transiently expressed axonal glycoprotein-1

TARP – transmembrane AMPAR regulatory protein

TBS – tris-buffered saline

TBST – tris-buffered saline with 0.1% Tween® 20

TCO*A-Lys – trans-cyclooct-2-en – L – lysine axial isomer

TCO*-Lys – trans-cyclooct-2-en – L – lysine

TCO4en/eq-Lys – trans-cyclooct-4-en – L – lysine equatorial isomer

TCO4en-Lys – trans-cyclooct-4-en – L – lysine

TIRF – total internal reflection fluorescence

TNFR1 – tumor necrosis factor 1 receptor

tRNA – transfer RNA

$tRNA^{Pyl}$ – pyrrolysyl suppressor tRNA

TTX – tetrodotoxin

TTXr – tetrodotoxin-resistant

TTXs – tetrodotoxin-sensitive

TyrRS – Tyrosil tRNA synthetase

tz – tetrazine

UAA – unnatural amino acid

UbiC – ubiquitin C

UV – ultra-violet

VS – Vectashield

VSV – vesicular stomatitis virus

WT – Wild-Type

βME – β-mercaptoethanol

7. References

1 Brodal, P. *The central nervous system: structure and function*. (oxford university Press, 2004).

2 Kole, M. H. *et al.* Action potential generation requires a high sodium channel density in the axon initial segment. *Nat Neurosci* **11**, 178-186, doi:10.1038/nn2040 (2008).

3 Kole, M. H. & Stuart, G. J. Signal processing in the axon initial segment. *Neuron* **73**, 235-247, doi:10.1016/j.neuron.2012.01.007 (2012).

4 Leterrier, C. The Axon Initial Segment: An Updated Viewpoint. *J Neurosci* **38**, 2135-2145, doi:10.1523/JNEUROSCI.1922-17.2018 (2018).

5 Lubetzki, C., Sol-Foulon, N. & Desmazières, A. Nodes of Ranvier during development and repair in the CNS. *Nature Reviews Neurology* **16**, 426-439, doi:10.1038/s41582-020-0375-x (2020).

6 Rasband, M. N. & Peles, E. The Nodes of Ranvier: Molecular Assembly and Maintenance. *Cold Spring Harb Perspect Biol* **8**, a020495, doi:10.1101/cshperspect.a020495 (2015).

7 Rasband, M. N. & Peles, E. Mechanisms of node of Ranvier assembly. *Nat Rev Neurosci* **22**, 7-20, doi:10.1038/s41583-020-00406-8 (2021).

8 Sole, L. & Tamkun, M. M. Trafficking mechanisms underlying Nav channel subcellular localization in neurons. *Channels (Austin)* **14**, 1-17, doi:10.1080/19336950.2019.1700082 (2020).

9 Sherman, D. L. *et al.* Neurofascins Are Required to Establish Axonal Domains for Saltatory Conduction. *Neuron* **48**, 737-742, doi:https://doi.org/10.1016/j.neuron.2005.10.019 (2005).

10 Zonta, B. *et al.* A Critical Role for Neurofascin in Regulating Action Potential Initiation through Maintenance of the Axon Initial Segment. *Neuron* **69**, 945-956, doi:https://doi.org/10.1016/j.neuron.2011.02.021 (2011).

11 Zonta, B. *et al.* Glial and neuronal isoforms of Neurofascin have distinct roles in the assembly of nodes of Ranvier in the central nervous system. *Journal of Cell Biology* **181**, 1169-1177, doi:10.1083/jcb.200712154 (2008).

12 Craner, M. J. *et al.* Molecular changes in neurons in multiple sclerosis: altered axonal expression of Nav1.2 and Nav1.6 sodium channels and Na+/Ca2+ exchanger. *Proc Natl Acad Sci U S A* **101**, 8168-8173, doi:10.1073/pnas.0402765101 (2004).

13 Johannesen, K. M. *et al.* Genotype-phenotype correlations in SCN8A-related disorders reveal prognostic and therapeutic implications. *Brain*, doi:10.1093/brain/awab321 (2021).

14 Meisler, M. H., Hill, S. F. & Yu, W. Sodium channelopathies in neurodevelopmental disorders. *Nat Rev Neurosci* **22**, 152-166, doi:10.1038/s41583-020-00418-4 (2021).

15 Kira, J.-i., Yamasaki, R. & Ogata, H. Anti-neurofascin autoantibody and demyelination. *Neurochemistry International* **130**, 104360, doi:https://doi.org/10.1016/j.neuint.2018.12.011 (2019).

16 Leterrier, C. *et al.* Nanoscale Architecture of the Axon Initial Segment Reveals an Organized and Robust Scaffold. *Cell Rep* **13**, 2781-2793, doi:10.1016/j.celrep.2015.11.051 (2015).

17 Song, A.-h. *et al.* A Selective Filter for Cytoplasmic Transport at the Axon Initial Segment. *Cell* **136**, 1148-1160, doi:https://doi.org/10.1016/j.cell.2009.01.016 (2009).

18 Huang, C. Y. & Rasband, M. N. Axon initial segments: structure, function, and disease. *Ann N Y Acad Sci* **1420**, 46-61, doi:10.1111/nyas.13718 (2018).

19 Hedstrom, K. L., Ogawa, Y. & Rasband, M. N. AnkyrinG is required for maintenance of the axon initial segment and neuronal polarity. *J Cell Biol* **183**, 635-640, doi:10.1083/jcb.200806112 (2008).

20 Sobotzik, J.-M. *et al.* AnkyrinG is required to maintain axo-dendritic polarity in vivo. *Proceedings of the National Academy of Sciences* **106**, 17564-17569, doi:doi:10.1073/pnas.0909267106 (2009).
21 Hu, W. *et al.* Distinct contributions of Na(v)1.6 and Na(v)1.2 in action potential initiation and backpropagation. *Nat Neurosci* **12**, 996-1002, doi:10.1038/nn.2359 (2009).
22 Lorincz, A. & Nusser, Z. Cell-Type-Dependent Molecular Composition of the Axon Initial Segment. *The Journal of Neuroscience* **28**, 14329-14340, doi:10.1523/jneurosci.4833-08.2008 (2008).
23 Van Wart, A., Trimmer, J. S. & Matthews, G. Polarized distribution of ion channels within microdomains of the axon initial segment. *J Comp Neurol* **500**, 339-352, doi:10.1002/cne.21173 (2007).
24 Duflocq, A., Le Bras, B., Bullier, E., Couraud, F. & Davenne, M. Nav1.1 is predominantly expressed in nodes of Ranvier and axon initial segments. *Mol Cell Neurosci* **39**, 180-192, doi:10.1016/j.mcn.2008.06.008 (2008).
25 Petersen, A. V., Cotel, F. & Perrier, J.-F. Plasticity of the Axon Initial Segment: Fast and Slow Processes with Multiple Functional Roles. *The Neuroscientist* **23**, 364-373, doi:10.1177/1073858416648311 (2017).
26 Jenkins, P. M. *et al.* Giant ankyrin-G: a critical innovation in vertebrate evolution of fast and integrated neuronal signaling. *Proc Natl Acad Sci U S A* **112**, 957-964, doi:10.1073/pnas.1416544112 (2015).
27 Fréal, A. *et al.* Cooperative Interactions between 480 kDa Ankyrin-G and EB Proteins Assemble the Axon Initial Segment. *The Journal of Neuroscience* **36**, 4421-4433, doi:10.1523/jneurosci.3219-15.2016 (2016).
28 Xu, K., Zhong, G. & Zhuang, X. Actin, spectrin, and associated proteins form a periodic cytoskeletal structure in axons. *Science* **339**, 452-456, doi:10.1126/science.1232251 (2013).
29 Zhong, G. *et al.* Developmental mechanism of the periodic membrane skeleton in axons. *Elife* **3**, doi:10.7554/eLife.04581 (2014).
30 D'Este, E., Kamin, D., Gottfert, F., El-Hady, A. & Hell, S. W. STED nanoscopy reveals the ubiquity of subcortical cytoskeleton periodicity in living neurons. *Cell Rep* **10**, 1246-1251, doi:10.1016/j.celrep.2015.02.007 (2015).
31 Huang, C. Y., Zhang, C., Zollinger, D. R., Leterrier, C. & Rasband, M. N. An alphaII Spectrin-Based Cytoskeleton Protects Large-Diameter Myelinated Axons from Degeneration. *J Neurosci* **37**, 11323-11334, doi:10.1523/JNEUROSCI.2113-17.2017 (2017).
32 Yamada, R. & Kuba, H. Structural and Functional Plasticity at the Axon Initial Segment. *Frontiers in Cellular Neuroscience* **10**, doi:10.3389/fncel.2016.00250 (2016).
33 Evans, M. D., Dumitrescu, A. S., Kruijssen, D. L. H., Taylor, S. E. & Grubb, M. S. Rapid Modulation of Axon Initial Segment Length Influences Repetitive Spike Firing. *Cell Rep* **13**, 1233-1245, doi:10.1016/j.celrep.2015.09.066 (2015).
34 Grubb, M. S. & Burrone, J. Activity-dependent relocation of the axon initial segment fine-tunes neuronal excitability. *Nature* **465**, 1070-1074, doi:10.1038/nature09160 (2010).
35 Evans, M. D. *et al.* Calcineurin Signaling Mediates Activity-Dependent Relocation of the Axon Initial Segment. *The Journal of Neuroscience* **33**, 6950-6963, doi:10.1523/jneurosci.0277-13.2013 (2013).
36 Kuba, H., Oichi, Y. & Ohmori, H. Presynaptic activity regulates Na+ channel distribution at the axon initial segment. *Nature* **465**, 1075-1078, doi:10.1038/nature09087 (2010).
37 Arancibia-Carcamo, I. L. & Attwell, D. The node of Ranvier in CNS pathology. *Acta Neuropathol* **128**, 161-175, doi:10.1007/s00401-014-1305-z (2014).

38 Boiko, T. *et al.* Compact myelin dictates the differential targeting of two sodium channel isoforms in the same axon. *Neuron* **30**, 91-104, doi:10.1016/s0896-6273(01)00265-3 (2001).
39 Caldwell, J. H., Schaller, K. L., Lasher, R. S., Peles, E. & Levinson, S. R. Sodium channel Na(v)1.6 is localized at nodes of ranvier, dendrites, and synapses. *Proc Natl Acad Sci U S A* **97**, 5616-5620, doi:10.1073/pnas.090034797 (2000).
40 Tait, S. *et al.* An Oligodendrocyte Cell Adhesion Molecule at the Site of Assembly of the Paranodal Axo-Glial Junction. *Journal of Cell Biology* **150**, 657-666, doi:10.1083/jcb.150.3.657 (2000).
41 Devaux, J. J., Kleopa, K. A., Cooper, E. C. & Scherer, S. S. KCNQ2 Is a Nodal K⁺ Channel. *The Journal of Neuroscience* **24**, 1236-1244, doi:10.1523/jneurosci.4512-03.2004 (2004).
42 Susuki, K. *et al.* Three mechanisms assemble central nervous system nodes of Ranvier. *Neuron* **78**, 469-482, doi:10.1016/j.neuron.2013.03.005 (2013).
43 Ghosh, A., Sherman, D. L. & Brophy, P. J. The Axonal Cytoskeleton and the Assembly of Nodes of Ranvier. *Neuroscientist* **24**, 104-110, doi:10.1177/1073858417710897 (2018).
44 Amor, V. *et al.* The paranodal cytoskeleton clusters Na(+) channels at nodes of Ranvier. *Elife* **6**, doi:10.7554/eLife.21392 (2017).
45 D'Este, E., Kamin, D., Balzarotti, F. & Hell, S. W. Ultrastructural anatomy of nodes of Ranvier in the peripheral nervous system as revealed by STED microscopy. *Proceedings of the National Academy of Sciences* **114**, E191-E199, doi:doi:10.1073/pnas.1619553114 (2017).
46 Huang, C. Y. *et al.* alphaII Spectrin Forms a Periodic Cytoskeleton at the Axon Initial Segment and Is Required for Nervous System Function. *J Neurosci* **37**, 11311-11322, doi:10.1523/JNEUROSCI.2112-17.2017 (2017).
47 D'Este, E. *et al.* Subcortical cytoskeleton periodicity throughout the nervous system. *Scientific Reports* **6**, 22741, doi:10.1038/srep22741 (2016).
48 Catterall, W. A., Lenaeus, M. J. & El-Din, T. M. G. Structure and Pharmacology of Voltage-Gated Sodium and Calcium Channels. *Annual Review of Pharmacology and Toxicology* **60**, 133-154, doi:10.1146/annurev-pharmtox-010818-021757 (2020).
49 Hille, B. *Ionic Channels of Excitable Membranes*. (Sinauer, 2001).
50 Catterall, W. A. Voltage-gated sodium channels at 60: structure, function and pathophysiology. *The Journal of Physiology* **590**, 2577-2589, doi:https://doi.org/10.1113/jphysiol.2011.224204 (2012).
51 Goldin, A. L. *et al.* Nomenclature of voltage-gated sodium channels. *Neuron* **28**, 365-368, doi:10.1016/s0896-6273(00)00116-1 (2000).
52 de Lera Ruiz, M. & Kraus, R. L. Voltage-Gated Sodium Channels: Structure, Function, Pharmacology, and Clinical Indications. *Journal of Medicinal Chemistry* **58**, 7093-7118, doi:10.1021/jm501981g (2015).
53 Zubovic, L., Baralle, M. & Baralle, F. E. Mutually exclusive splicing regulates the Nav 1.6 sodium channel function through a combinatorial mechanism that involves three distinct splicing regulatory elements and their ligands. *Nucleic Acids Res* **40**, 6255-6269, doi:10.1093/nar/gks249 (2012).
54 Gazina, E. V. *et al.* Differential expression of exon 5 splice variants of sodium channel alpha subunit mRNAs in the developing mouse brain. *Neuroscience* **166**, 195-200, doi:10.1016/j.neuroscience.2009.12.011 (2010).
55 Plummer, N. W., McBurney, M. W. & Meisler, M. H. Alternative splicing of the sodium channel SCN8A predicts a truncated two-domain protein in fetal brain and non-neuronal cells. *J Biol Chem* **272**, 24008-24015, doi:10.1074/jbc.272.38.24008 (1997).
56 Yu, F. H. & Catterall, W. A. Overview of the voltage-gated sodium channel family. *Genome Biol* **4**, 207, doi:10.1186/gb-2003-4-3-207 (2003).

57 Rohl, C. A. *et al.* Solution structure of the sodium channel inactivation gate. *Biochemistry* **38**, 855-861, doi:10.1021/bi9823380 (1999).
58 Mantegazza, M., Yu, F. H., Catterall, W. A. & Scheuer, T. Role of the C-terminal domain in inactivation of brain and cardiac sodium channels. *Proc Natl Acad Sci U S A* **98**, 15348-15353, doi:10.1073/pnas.211563298 (2001).
59 Fotia, A. B. *et al.* Regulation of neuronal voltage-gated sodium channels by the ubiquitin-protein ligases Nedd4 and Nedd4-2. *J Biol Chem* **279**, 28930-28935, doi:10.1074/jbc.M402820200 (2004).
60 Herzog, R. I., Liu, C., Waxman, S. G. & Cummins, T. R. Calmodulin binds to the C terminus of sodium channels Nav1.4 and Nav1.6 and differentially modulates their functional properties. *J Neurosci* **23**, 8261-8270 (2003).
61 Zybura, A., Hudmon, A. & Cummins, T. R. Distinctive Properties and Powerful Neuromodulation of Nav1.6 Sodium Channels Regulates Neuronal Excitability. *Cells* **10**, 1595 (2021).
62 Pan, Y., Xiao, Y., Pei, Z. & Cummins, T. R. S-Palmitoylation of the sodium channel Nav1.6 regulates its activity and neuronal excitability. *J Biol Chem* **295**, 6151-6164, doi:10.1074/jbc.RA119.012423 (2020).
63 Gasser, A. *et al.* Two Nedd4-binding Motifs Underlie Modulation of Sodium Channel Nav1.6 by p38 MAPK*. *Journal of Biological Chemistry* **285**, 26149-26161, doi:https://doi.org/10.1074/jbc.M109.098681 (2010).
64 Zybura, A. S., Baucum, A. J., 2nd, Rush, A. M., Cummins, T. R. & Hudmon, A. CaMKII enhances voltage-gated sodium channel Nav1.6 activity and neuronal excitability. *J Biol Chem* **295**, 11845-11865, doi:10.1074/jbc.RA120.014062 (2020).
65 Liu, H., Wang, H.-G., Pitt, G. S. & Liu, Z. J. Nanometer-Scale Imaging of Compartment-Specific Localization and Dynamics of Voltage-Gated Sodium Channels. *bioRxiv*, 2021.2009.2028.462114, doi:10.1101/2021.09.28.462114 (2021).
66 O'Malley, H. A. & Isom, L. L. Sodium channel beta subunits: emerging targets in channelopathies. *Annu Rev Physiol* **77**, 481-504, doi:10.1146/annurev-physiol-021014-071846 (2015).
67 Isom, L. L. *et al.* Primary structure and functional expression of the beta 1 subunit of the rat brain sodium channel. *Science* **256**, 839-842, doi:10.1126/science.1375395 (1992).
68 Isom, L. L. *et al.* Structure and function of the beta 2 subunit of brain sodium channels, a transmembrane glycoprotein with a CAM motif. *Cell* **83**, 433-442, doi:10.1016/0092-8674(95)90121-3 (1995).
69 Wong, H.-K. *et al.* β Subunits of Voltage-gated Sodium Channels Are Novel Substrates of β-Site Amyloid Precursor Protein-cleaving Enzyme (BACE1) and γ-Secretase*. *Journal of Biological Chemistry* **280**, 23009-23017, doi:https://doi.org/10.1074/jbc.M414648200 (2005).
70 Morgan, K. *et al.* beta 3: an additional auxiliary subunit of the voltage-sensitive sodium channel that modulates channel gating with distinct kinetics. *Proc Natl Acad Sci U S A* **97**, 2308-2313, doi:10.1073/pnas.030362197 (2000).
71 Qin, N. *et al.* Molecular cloning and functional expression of the human sodium channel β1B subunit, a novel splicing variant of the β1 subunit. *European Journal of Biochemistry* **270**, 4762-4770, doi:https://doi.org/10.1046/j.1432-1033.2003.03878.x (2003).
72 Yu, F. H. *et al.* Sodium channel beta4, a new disulfide-linked auxiliary subunit with similarity to beta2. *J Neurosci* **23**, 7577-7585 (2003).
73 Kazen-Gillespie, K. A. *et al.* Cloning, Localization, and Functional Expression of Sodium Channel β1A Subunits*. *Journal of Biological Chemistry* **275**, 1079-1088, doi:https://doi.org/10.1074/jbc.275.2.1079 (2000).

74 Patino, G. A. *et al.* Voltage-Gated Na_V Channel β1B: A Secreted Cell Adhesion Molecule Involved in Human Epilepsy. *The Journal of Neuroscience* **31**, 14577-14591, doi:10.1523/jneurosci.0361-11.2011 (2011).
75 Stajković, N. *et al.* Direct fluorescent labeling of NF186 and $Na_V1.6$ in living primary neurons using bioorthogonal click chemistry. *bioRxiv*, 2022.2003.2001.480798, doi:10.1101/2022.03.01.480798 (2022).
76 Burgess, D. L. *et al.* Mutation of a new sodium channel gene, Scn8a, in the mouse mutant 'motor endplate disease'. *Nat Genet* **10**, 461-465, doi:10.1038/ng0895-461 (1995).
77 Schaller, K. L., Krzemien, D. M., Yarowsky, P. J., Krueger, B. K. & Caldwell, J. H. A novel, abundant sodium channel expressed in neurons and glia. *J Neurosci* **15**, 3231-3242 (1995).
78 Jenkins, S. M. & Bennett, V. Ankyrin-G coordinates assembly of the spectrin-based membrane skeleton, voltage-gated sodium channels, and L1 CAMs at Purkinje neuron initial segments. *J Cell Biol* **155**, 739-746, doi:10.1083/jcb.200109026 (2001).
79 Boiko, T. *et al.* Functional Specialization of the Axon Initial Segment by Isoform-Specific Sodium Channel Targeting. *The Journal of Neuroscience* **23**, 2306-2313, doi:10.1523/jneurosci.23-06-02306.2003 (2003).
80 Akin, E. J. *et al.* Single-Molecule Imaging of Nav1.6 on the Surface of Hippocampal Neurons Reveals Somatic Nanoclusters. *Biophys J* **111**, 1235-1247, doi:10.1016/j.bpj.2016.08.016 (2016).
81 Garrido, J. J. *et al.* A targeting motif involved in sodium channel clustering at the axonal initial segment. *Science* **300**, 2091-2094, doi:10.1126/science.1085167 (2003).
82 Lemaillet, G., Walker, B. & Lambert, S. Identification of a conserved ankyrin-binding motif in the family of sodium channel alpha subunits. *J Biol Chem* **278**, 27333-27339, doi:10.1074/jbc.M303327200 (2003).
83 Gasser, A. *et al.* An ankyrinG-binding motif is necessary and sufficient for targeting Nav1.6 sodium channels to axon initial segments and nodes of Ranvier. *J Neurosci* **32**, 7232-7243, doi:10.1523/JNEUROSCI.5434-11.2012 (2012).
84 Akin, E. J., Sole, L., Dib-Hajj, S. D., Waxman, S. G. & Tamkun, M. M. Preferential targeting of Nav1.6 voltage-gated Na+ Channels to the axon initial segment during development. *PLoS One* **10**, e0124397, doi:10.1371/journal.pone.0124397 (2015).
85 Hien, Y. E. *et al.* CK2 accumulation at the axon initial segment depends on sodium channel Nav1. *FEBS Letters* **588**, 3403-3408, doi:https://doi.org/10.1016/j.febslet.2014.07.032 (2014).
86 Brechet, A. *et al.* Protein kinase CK2 contributes to the organization of sodium channels in axonal membranes by regulating their interactions with ankyrin G. *J Cell Biol* **183**, 1101-1114, doi:10.1083/jcb.200805169 (2008).
87 Sole, L., Wagnon, J. L., Akin, E. J., Meisler, M. H. & Tamkun, M. M. The MAP1B Binding Domain of Nav1.6 Is Required for Stable Expression at the Axon Initial Segment. *J Neurosci* **39**, 4238-4251, doi:10.1523/JNEUROSCI.2771-18.2019 (2019).
88 Davis, J. Q., McLaughlin, T. & Bennett, V. Ankyrin-binding proteins related to nervous system cell adhesion molecules: candidates to provide transmembrane and intercellular connections in adult brain. *Journal of Cell Biology* **121**, 121-133, doi:10.1083/jcb.121.1.121 (1993).
89 Kriebel, M., Wuchter, J., Trinks, S. & Volkmer, H. Neurofascin: A switch between neuronal plasticity and stability. *The International Journal of Biochemistry & Cell Biology* **44**, 694-697, doi:https://doi.org/10.1016/j.biocel.2012.01.012 (2012).
90 Kriebel, M. *et al.* The Cell Adhesion Molecule Neurofascin Stabilizes Axo-axonic GABAergic Terminals at the Axon Initial Segment*. *Journal of Biological Chemistry* **286**, 24385-24393, doi:https://doi.org/10.1074/jbc.M110.212191 (2011).

91 Koticha, D. *et al.* Cell adhesion and neurite outgrowth are promoted by neurofascin NF155 and inhibited by NF186. *Molecular and Cellular Neuroscience* **30**, 137-148, doi:https://doi.org/10.1016/j.mcn.2005.06.007 (2005).
92 Suzuki, S. *et al.* Spatio-temporal and dynamic regulation of neurofascin alternative splicing in mouse cerebellar neurons. *Scientific Reports* **7**, 11405, doi:10.1038/s41598-017-11319-5 (2017).
93 Zhang, A. *et al.* Neurofascin 140 Is an Embryonic Neuronal Neurofascin Isoform That Promotes the Assembly of the Node of Ranvier. *The Journal of Neuroscience* **35**, 2246-2254, doi:10.1523/jneurosci.3552-14.2015 (2015).
94 Schafer, D. P. *et al.* Disruption of the axon initial segment cytoskeleton is a new mechanism for neuronal injury. *J Neurosci* **29**, 13242-13254, doi:10.1523/JNEUROSCI.3376-09.2009 (2009).
95 Dzhashiashvili, Y. *et al.* Nodes of Ranvier and axon initial segments are ankyrin G-dependent domains that assemble by distinct mechanisms. *J Cell Biol* **177**, 857-870, doi:10.1083/jcb.200612012 (2007).
96 Dumitrescu, A. S., Evans, M. D. & Grubb, M. S. Evaluating Tools for Live Imaging of Structural Plasticity at the Axon Initial Segment. *Front Cell Neurosci* **10**, 268, doi:10.3389/fncel.2016.00268 (2016).
97 Arsić, A., Hagemann, C., Stajković, N., Schubert, T. & Nikić-Spiegel, I. Minimal genetically encoded tags for fluorescent protein labeling in living neurons. *Nature Communications* **13**, 314, doi:10.1038/s41467-022-27956-y (2022).
98 Bessa-Neto, D. *et al.* Bioorthogonal labeling of transmembrane proteins with non-canonical amino acids unveils masked epitopes in live neurons. *Nat Commun* **12**, 6715, doi:10.1038/s41467-021-27025-w (2021).
99 Tuvia, S., Garver, T. D. & Bennett, V. The phosphorylation state of the FIGQY tyrosine of neurofascin determines ankyrin-binding activity and patterns of cell segregation. *Proceedings of the National Academy of Sciences* **94**, 12957-12962, doi:doi:10.1073/pnas.94.24.12957 (1997).
100 Garver, T. D., Ren, Q., Tuvia, S. & Bennett, V. Tyrosine Phosphorylation at a Site Highly Conserved in the L1 Family of Cell Adhesion Molecules Abolishes Ankyrin Binding and Increases Lateral Mobility of Neurofascin. *Journal of Cell Biology* **137**, 703-714, doi:10.1083/jcb.137.3.703 (1997).
101 Zhang, X., Davis, J. Q., Carpenter, S. & Bennett, V. Structural requirements for association of neurofascin with ankyrin. *J Biol Chem* **273**, 30785-30794, doi:10.1074/jbc.273.46.30785 (1998).
102 Hedstrom , K. L. *et al.* Neurofascin assembles a specialized extracellular matrix at the axon initial segment. *Journal of Cell Biology* **178**, 875-886, doi:10.1083/jcb.200705119 (2007).
103 Howell, O. W. *et al.* Disruption of neurofascin localization reveals early changes preceding demyelination and remyelination in multiple sclerosis. *Brain* **129**, 3173-3185, doi:10.1093/brain/awl290 (2006).
104 Hamada, M. S. & Kole, M. H. P. Myelin Loss and Axonal Ion Channel Adaptations Associated with Gray Matter Neuronal Hyperexcitability. *The Journal of Neuroscience* **35**, 7272-7286, doi:10.1523/jneurosci.4747-14.2015 (2015).
105 Coman, I. *et al.* Nodal, paranodal and juxtaparanodal axonal proteins during demyelination and remyelination in multiple sclerosis. *Brain* **129**, 3186-3195, doi:10.1093/brain/awl144 (2006).
106 Ma, F. *et al.* The amyloid precursor protein modulates the position and length of the axon initial segment offering a new perspective on Alzheimer's disease genetics. *bioRxiv*, 2022.2001.2023.477413, doi:10.1101/2022.01.23.477413 (2022).

107 Senol, A. D. *et al.* Alterations of the axon initial segment in multiple sclerosis. *bioRxiv*, 2022.2003.2007.483302, doi:10.1101/2022.03.07.483302 (2022).
108 Harty, R. C. *et al.* Axon initial segment structural plasticity in animal models of genetic and acquired epilepsy. *Epilepsy Research* **105**, 272-279, doi:https://doi.org/10.1016/j.eplepsyres.2013.03.004 (2013).
109 Liu, Y. *et al.* Neuronal mechanisms of mutations in SCN8A causing epilepsy or intellectual disability. *Brain* **142**, 376-390, doi:10.1093/brain/awy326 (2019).
110 Lin, S. *et al.* Over-expression of Nav1.6 channels is associated with lymph node metastases in colorectal cancer. *World Journal of Surgical Oncology* **17**, 175, doi:10.1186/s12957-019-1715-4 (2019).
111 Mao, W., Zhang, J., Körner, H., Jiang, Y. & Ying, S. The Emerging Role of Voltage-Gated Sodium Channels in Tumor Biology. *Frontiers in Oncology* **9**, doi:10.3389/fonc.2019.00124 (2019).
112 Devaux, J. J., Odaka, M. & Yuki, N. Nodal proteins are target antigens in Guillain-Barré syndrome. *Journal of the Peripheral Nervous System* **17**, 62-71, doi:https://doi.org/10.1111/j.1529-8027.2012.00372.x (2012).
113 Mathey , E. K. *et al.* Neurofascin as a novel target for autoantibody-mediated axonal injury. *Journal of Experimental Medicine* **204**, 2363-2372, doi:10.1084/jem.20071053 (2007).
114 Delmont, E. *et al.* Autoantibodies to nodal isoforms of neurofascin in chronic inflammatory demyelinating polyneuropathy. *Brain* **140**, 1851-1858, doi:10.1093/brain/awx124 (2017).
115 Torii, T. *et al.* NuMA1 promotes axon initial segment assembly through inhibition of endocytosis. *J Cell Biol* **219**, doi:10.1083/jcb.201907048 (2020).
116 Freal, A. *et al.* Feedback-Driven Assembly of the Axon Initial Segment. *Neuron* **104**, 305-321 e308, doi:10.1016/j.neuron.2019.07.029 (2019).
117 Hamdan, H. *et al.* Mapping axon initial segment structure and function by multiplexed proximity biotinylation. *Nat Commun* **11**, 100, doi:10.1038/s41467-019-13658-5 (2020).
118 Ghosh, A., Malavasi, E. L., Sherman, D. L. & Brophy, P. J. Neurofascin and Kv7.3 are delivered to somatic and axon terminal surface membranes en route to the axon initial segment. *Elife* **9**, doi:10.7554/eLife.60619 (2020).
119 Thetiot, M. *et al.* An alternative mechanism of early nodal clustering and myelination onset in GABAergic neurons of the central nervous system. *Glia* **68**, 1891-1909, doi:10.1002/glia.23812 (2020).
120 Bekku, Y. & Salzer, J. L. Independent anterograde transport and retrograde cotransport of domain components of myelinated axons. *Journal of Cell Biology* **219**, doi:10.1083/jcb.201906071 (2020).
121 Akin, E. J. *et al.* Building sensory axons: Delivery and distribution of NaV1.7 channels and effects of inflammatory mediators. *Sci Adv* **5**, eaax4755, doi:10.1126/sciadv.aax4755 (2019).
122 Sizova, D. V. *et al.* A 49-residue sequence motif in the C terminus of Nav1.9 regulates trafficking of the channel to the plasma membrane. *J Biol Chem* **295**, 1077-1090, doi:10.1074/jbc.RA119.011424 (2020).
123 Fréal, A. *et al.* Sodium channel endocytosis drives axon initial segment plasticity. *bioRxiv*, 2022.2011.2009.515770, doi:10.1101/2022.11.09.515770 (2022).
124 Schermelleh, L. *et al.* Super-resolution microscopy demystified. *Nature Cell Biology* **21**, 72-84, doi:10.1038/s41556-018-0251-8 (2019).
125 Sigal, Y. M., Zhou, R. & Zhuang, X. Visualizing and discovering cellular structures with super-resolution microscopy. *Science* **361**, 880-887, doi:doi:10.1126/science.aau1044 (2018).
126 Sahl, S. J., Hell, S. W. & Jakobs, S. Fluorescence nanoscopy in cell biology. *Nature Reviews Molecular Cell Biology* **18**, 685-701, doi:10.1038/nrm.2017.71 (2017).

127 Hell, S. W. & Wichmann, J. Breaking the diffraction resolution limit by stimulated emission: stimulated-emission-depletion fluorescence microscopy. *Opt. Lett.* **19**, 780-782, doi:10.1364/OL.19.000780 (1994).
128 Klar, T. A., Jakobs, S., Dyba, M., Egner, A. & Hell, S. W. Fluorescence microscopy with diffraction resolution barrier broken by stimulated emission. *Proceedings of the National Academy of Sciences* **97**, 8206-8210, doi:doi:10.1073/pnas.97.15.8206 (2000).
129 Donnert, G. *et al.* Macromolecular-scale resolution in biological fluorescence microscopy. *Proceedings of the National Academy of Sciences* **103**, 11440-11445, doi:doi:10.1073/pnas.0604965103 (2006).
130 Betzig, E. *et al.* Imaging intracellular fluorescent proteins at nanometer resolution. *Science* **313**, 1642-1645, doi:10.1126/science.1127344 (2006).
131 Hess, S. T., Girirajan, T. P. K. & Mason, M. D. Ultra-High Resolution Imaging by Fluorescence Photoactivation Localization Microscopy. *Biophysical Journal* **91**, 4258-4272, doi:https://doi.org/10.1529/biophysj.106.091116 (2006).
132 Rust, M. J., Bates, M. & Zhuang, X. Sub-diffraction-limit imaging by stochastic optical reconstruction microscopy (STORM). *Nature Methods* **3**, 793-796, doi:10.1038/nmeth929 (2006).
133 Heilemann, M., van de Linde, S., Mukherjee, A. & Sauer, M. Super-Resolution Imaging with Small Organic Fluorophores. *Angewandte Chemie International Edition* **48**, 6903-6908, doi:https://doi.org/10.1002/anie.200902073 (2009).
134 Balzarotti, F. *et al.* Nanometer resolution imaging and tracking of fluorescent molecules with minimal photon fluxes. *Science* **355**, 606-612, doi:doi:10.1126/science.aak9913 (2017).
135 Dempsey, G. T., Vaughan, J. C., Chen, K. H., Bates, M. & Zhuang, X. Evaluation of fluorophores for optimal performance in localization-based super-resolution imaging. *Nat Methods* **8**, 1027-1036, doi:10.1038/nmeth.1768 (2011).
136 Olivier, N., Keller, D., Rajan, V. S., Gönczy, P. & Manley, S. Simple buffers for 3D STORM microscopy. *Biomed. Opt. Express* **4**, 885-899, doi:10.1364/BOE.4.000885 (2013).
137 Nahidiazar, L., Agronskaia, A. V., Broertjes, J., van den Broek, B. & Jalink, K. Optimizing Imaging Conditions for Demanding Multi-Color Super Resolution Localization Microscopy. *PLoS One* **11**, e0158884, doi:10.1371/journal.pone.0158884 (2016).
138 He, J. *et al.* Prevalent presence of periodic actin-spectrin-based membrane skeleton in a broad range of neuronal cell types and animal species. *Proc Natl Acad Sci U S A* **113**, 6029-6034, doi:10.1073/pnas.1605707113 (2016).
139 Watson, J. D. *Molecular Biology of the Gene*. (Pearson, 2014).
140 Böck, A. *et al.* Selenocysteine: the 21st amino acid. *Molecular Microbiology* **5**, 515-520, doi:https://doi.org/10.1111/j.1365-2958.1991.tb00722.x (1991).
141 Srinivasan, G., James, C. M. & Krzycki, J. A. Pyrrolysine encoded by UAG in Archaea: charging of a UAG-decoding specialized tRNA. *Science* **296**, 1459-1462, doi:10.1126/science.1069588 (2002).
142 Wang, L. & Schultz, P. G. Expanding the Genetic Code. *Angewandte Chemie International Edition* **44**, 34-66, doi:https://doi.org/10.1002/anie.200460627 (2005).
143 Shandell, M. A., Tan, Z. & Cornish, V. W. Genetic Code Expansion: A Brief History and Perspective. *Biochemistry* **60**, 3455-3469, doi:10.1021/acs.biochem.1c00286 (2021).
144 Johnson, J. A., Lu, Y. Y., Van Deventer, J. A. & Tirrell, D. A. Residue-specific incorporation of non-canonical amino acids into proteins: recent developments and applications. *Current Opinion in Chemical Biology* **14**, 774-780, doi:https://doi.org/10.1016/j.cbpa.2010.09.013 (2010).
145 Lang, K. *et al.* Genetically encoded norbornene directs site-specific cellular protein labelling via a rapid bioorthogonal reaction. *Nat Chem* **4**, 298-304, doi:10.1038/nchem.1250 (2012).

146 Plass, T. *et al.* Amino acids for Diels-Alder reactions in living cells. *Angew Chem Int Ed Engl* **51**, 4166-4170, doi:10.1002/anie.201108231 (2012).
147 Lang, K. *et al.* Genetic Encoding of bicyclononynes and trans-cyclooctenes for site-specific protein labeling in vitro and in live mammalian cells via rapid fluorogenic Diels-Alder reactions. *J Am Chem Soc* **134**, 10317-10320, doi:10.1021/ja302832g (2012).
148 Nikic, I. *et al.* Minimal tags for rapid dual-color live-cell labeling and super-resolution microscopy. *Angew Chem Int Ed Engl* **53**, 2245-2249, doi:10.1002/anie.201309847 (2014).
149 Borrmann, A. *et al.* Genetic Encoding of a Bicyclo[6.1.0]nonyne-Charged Amino Acid Enables Fast Cellular Protein Imaging by Metal-Free Ligation. *ChemBioChem* **13**, 2094-2099, doi:https://doi.org/10.1002/cbic.201200407 (2012).
150 Nikic, I. *et al.* Debugging Eukaryotic Genetic Code Expansion for Site-Specific Click-PAINT Super-Resolution Microscopy. *Angew Chem Int Ed Engl* **55**, 16172-16176, doi:10.1002/anie.201608284 (2016).
151 Serfling, R. *et al.* Designer tRNAs for efficient incorporation of non-canonical amino acids by the pyrrolysine system in mammalian cells. *Nucleic Acids Res* **46**, 1-10, doi:10.1093/nar/gkx1156 (2018).
152 Beliu, G. *et al.* Bioorthogonal labeling with tetrazine-dyes for super-resolution microscopy. *Communications Biology* **2**, 261, doi:10.1038/s42003-019-0518-z (2019).
153 Neubert, F. *et al.* Bioorthogonal Click Chemistry Enables Site-specific Fluorescence Labeling of Functional NMDA Receptors for Super-Resolution Imaging. *Angew Chem Int Ed Engl* **57**, 16364-16369, doi:10.1002/anie.201808951 (2018).
154 Sappakhaw, K., Jantarug, K., Slavoff, S. A., Israsena, N. & Uttamapinant, C. A Genetic Code Expansion-Derived Molecular Beacon for the Detection of Intracellular Amyloid-beta Peptide Generation. *Angew Chem Int Ed Engl* **60**, 3934-3939, doi:10.1002/anie.202010703 (2021).
155 van Husen, L. S. *et al.* Dual Bioorthogonal Labeling of the Amyloid-beta Protein Precursor Facilitates Simultaneous Visualization of the Protein and Its Cleavage Products. *J Alzheimers Dis* **72**, 537-548, doi:10.3233/JAD-190898 (2019).
156 Peng, T. & Hang, H. C. Site-Specific Bioorthogonal Labeling for Fluorescence Imaging of Intracellular Proteins in Living Cells. *Journal of the American Chemical Society* **138**, 14423-14433, doi:10.1021/jacs.6b08733 (2016).
157 Schvartz, T. *et al.* Direct fluorescent-dye labeling of α-tubulin in mammalian cells for live cell and superresolution imaging. *Molecular Biology of the Cell* **28**, 2747-2756, doi:10.1091/mbc.e17-03-0161 (2017).
158 Uttamapinant, C. *et al.* Genetic code expansion enables live-cell and super-resolution imaging of site-specifically labeled cellular proteins. *J Am Chem Soc* **137**, 4602-4605, doi:10.1021/ja512838z (2015).
159 Wang, L. Engineering the Genetic Code in Cells and Animals: Biological Considerations and Impacts. *Acc Chem Res* **50**, 2767-2775, doi:10.1021/acs.accounts.7b00376 (2017).
160 Nikic-Spiegel, I. Expanding the Genetic Code for Neuronal Studies. *Chembiochem* **21**, 3169-3179, doi:10.1002/cbic.202000300 (2020).
161 Chin, J. W. Expanding and reprogramming the genetic code of cells and animals. *Annu Rev Biochem* **83**, 379-408, doi:10.1146/annurev-biochem-060713-035737 (2014).
162 Cervettini, D. *et al.* Rapid discovery and evolution of orthogonal aminoacyl-tRNA synthetase–tRNA pairs. *Nature Biotechnology* **38**, 989-999, doi:10.1038/s41587-020-0479-2 (2020).
163 Wang, W. *et al.* Genetically encoding unnatural amino acids for cellular and neuronal studies. *Nat Neurosci* **10**, 1063-1072, doi:10.1038/nn1932 (2007).

164 Chen, P. R. *et al.* A Facile System for Encoding Unnatural Amino Acids in Mammalian Cells. *Angewandte Chemie International Edition* **48**, 4052-4055, doi:https://doi.org/10.1002/anie.200900683 (2009).
165 Neumann, H., Peak-Chew, S. Y. & Chin, J. W. Genetically encoding Nε-acetyllysine in recombinant proteins. *Nature Chemical Biology* **4**, 232-234, doi:10.1038/nchembio.73 (2008).
166 Gautier, A. *et al.* Genetically Encoded Photocontrol of Protein Localization in Mammalian Cells. *Journal of the American Chemical Society* **132**, 4086-4088, doi:10.1021/ja910688s (2010).
167 Yanagisawa, T. *et al.* Multistep Engineering of Pyrrolysyl-tRNA Synthetase to Genetically Encode Nε-(o-Azidobenzyloxycarbonyl) lysine for Site-Specific Protein Modification. *Chemistry & Biology* **15**, 1187-1197, doi:https://doi.org/10.1016/j.chembiol.2008.10.004 (2008).
168 Mukai, T. *et al.* Adding l-lysine derivatives to the genetic code of mammalian cells with engineered pyrrolysyl-tRNA synthetases. *Biochem Biophys Res Commun* **371**, 818-822, doi:10.1016/j.bbrc.2008.04.164 (2008).
169 Plass, T., Milles, S., Koehler, C., Schultz, C. & Lemke, E. A. Genetically Encoded Copper-Free Click Chemistry. *Angewandte Chemie International Edition* **50**, 3878-3881, doi:https://doi.org/10.1002/anie.201008178 (2011).
170 Nikic, I., Kang, J. H., Girona, G. E., Aramburu, I. V. & Lemke, E. A. Labeling proteins on live mammalian cells using click chemistry. *Nat Protoc* **10**, 780-791, doi:10.1038/nprot.2015.045 (2015).
171 Belin, D. & Puigbò, P. Why Is the UAG (Amber) Stop Codon Almost Absent in Highly Expressed Bacterial Genes? *Life (Basel, Switzerland)* **12**, doi:10.3390/life12030431 (2022).
172 Sun, J., Chen, M., Xu, J. & Luo, J. Relationships Among Stop Codon Usage Bias, Its Context, Isochores, and Gene Expression Level in Various Eukaryotes. *Journal of Molecular Evolution* **61**, 437-444, doi:10.1007/s00239-004-0277-3 (2005).
173 Ernst, R. J. *et al.* Genetic code expansion in the mouse brain. *Nat Chem Biol* **12**, 776-778, doi:10.1038/nchembio.2160 (2016).
174 Chen, Y. *et al.* Heritable expansion of the genetic code in mouse and zebrafish. *Cell Research* **27**, 294-297, doi:10.1038/cr.2016.145 (2017).
175 Kang, J. Y. *et al.* In vivo expression of a light-activatable potassium channel using unnatural amino acids. *Neuron* **80**, 358-370, doi:10.1016/j.neuron.2013.08.016 (2013).
176 Wang, L., Brock, A., Herberich, B. & Schultz, P. G. Expanding the genetic code of Escherichia coli. *Science* **292**, 498-500, doi:10.1126/science.1060077 (2001).
177 Chin, J. W. *et al.* An expanded eukaryotic genetic code. *Science* **301**, 964-967, doi:10.1126/science.1084772 (2003).
178 Wang, Q. & Wang, L. New methods enabling efficient incorporation of unnatural amino acids in yeast. *J Am Chem Soc* **130**, 6066-6067, doi:10.1021/ja800894n (2008).
179 Shen, B. *et al.* Genetically encoding unnatural amino acids in neural stem cells and optically reporting voltage-sensitive domain changes in differentiated neurons. *Stem Cells* **29**, 1231-1240, doi:10.1002/stem.679 (2011).
180 van Husen, L. S. *et al.* Engineered Human Induced Pluripotent Cells Enable Genetic Code Expansion in Brain Organoids. *Chembiochem* **22**, 3208-3213, doi:10.1002/cbic.202100399 (2021).
181 Bianco, A., Townsley, F. M., Greiss, S., Lang, K. & Chin, J. W. Expanding the genetic code of Drosophila melanogaster. *Nat Chem Biol* **8**, 748-750, doi:10.1038/nchembio.1043 (2012).
182 Greiss, S. & Chin, J. W. Expanding the Genetic Code of an Animal. *Journal of the American Chemical Society* **133**, 14196-14199, doi:10.1021/ja2054034 (2011).

183 Parrish, A. R. *et al.* Expanding the genetic code of Caenorhabditis elegans using bacterial aminoacyl-tRNA synthetase/tRNA pairs. *ACS Chem Biol* **7**, 1292-1302, doi:10.1021/cb200542j (2012).
184 Xi, Z. *et al.* Using a quadruplet codon to expand the genetic code of an animal. *Nucleic Acids Research* **50**, 4801-4812, doi:10.1093/nar/gkab1168 (2022).
185 Han, S. *et al.* Expanding the genetic code of Mus musculus. *Nature Communications* **8**, 14568, doi:10.1038/ncomms14568 (2017).
186 Xiao, H. & Schultz, P. G. At the Interface of Chemical and Biological Synthesis: An Expanded Genetic Code. *Cold Spring Harb Perspect Biol* **8**, doi:10.1101/cshperspect.a023945 (2016).
187 Chin, J. W. Expanding and reprogramming the genetic code. *Nature* **550**, 53-60, doi:10.1038/nature24031 (2017).
188 Elia, N. Using unnatural amino acids to selectively label proteins for cellular imaging: a cell biologist viewpoint. *The FEBS Journal* **288**, 1107-1117, doi:https://doi.org/10.1111/febs.15477 (2021).
189 Kim, E. & Koo, H. Biomedical applications of copper-free click chemistry: in vitro, in vivo, and ex vivo. *Chemical Science* **10**, 7835-7851, doi:10.1039/C9SC03368H (2019).
190 Kolb, H. C., Finn, M. G. & Sharpless, K. B. Click Chemistry: Diverse Chemical Function from a Few Good Reactions. *Angewandte Chemie International Edition* **40**, 2004-2021, doi:https://doi.org/10.1002/1521-3773(20010601)40:11<2004::AID-ANIE2004>3.0.CO;2-5 (2001).
191 Sletten, E. M. & Bertozzi, C. R. Bioorthogonal Chemistry: Fishing for Selectivity in a Sea of Functionality. *Angewandte Chemie International Edition* **48**, 6974-6998, doi:https://doi.org/10.1002/anie.200900942 (2009).
192 Lang, K. & Chin, J. W. Cellular Incorporation of Unnatural Amino Acids and Bioorthogonal Labeling of Proteins. *Chemical Reviews* **114**, 4764-4806, doi:10.1021/cr400355w (2014).
193 Lee, K. J., Kang, D. & Park, H.-S. Site-Specific Labeling of Proteins Using Unnatural Amino Acids. *Molecules and cells* **42**, 386-396, doi:10.14348/molcells.2019.0078 (2019).
194 Beatty, K. E. *et al.* Live-cell imaging of cellular proteins by a strain-promoted azide-alkyne cycloaddition. *Chembiochem* **11**, 2092-2095, doi:10.1002/cbic.201000419 (2010).
195 Yu, Z., Pan, Y., Wang, Z., Wang, J. & Lin, Q. Genetically encoded cyclopropene directs rapid, photoclick-chemistry-mediated protein labeling in mammalian cells. *Angew Chem Int Ed Engl* **51**, 10600-10604, doi:10.1002/anie.201205352 (2012).
196 Blackman, M. L., Royzen, M. & Fox, J. M. Tetrazine Ligation: Fast Bioconjugation Based on Inverse-Electron-Demand Diels−Alder Reactivity. *Journal of the American Chemical Society* **130**, 13518-13519, doi:10.1021/ja8053805 (2008).
197 Hoffmann, J.-E. *et al.* Highly Stable trans-Cyclooctene Amino Acids for Live-Cell Labeling. *Chemistry – A European Journal* **21**, 12266-12270, doi:https://doi.org/10.1002/chem.201501647 (2015).
198 Reinkemeier, C. D. *et al.* Synthesis and Evaluation of Novel Ring-Strained Noncanonical Amino Acids for Residue-Specific Bioorthogonal Reactions in Living Cells. *Chemistry – A European Journal* **27**, 6094-6099, doi:https://doi.org/10.1002/chem.202100322 (2021).
199 Yang, J., Šečkutė, J., Cole, C. M. & Devaraj, N. K. Live-Cell Imaging of Cyclopropene Tags with Fluorogenic Tetrazine Cycloadditions. *Angewandte Chemie International Edition* **51**, 7476-7479, doi:https://doi.org/10.1002/anie.201202122 (2012).
200 Kozma, E. & Kele, P. Fluorogenic probes for super-resolution microscopy. *Organic & Biomolecular Chemistry* **17**, 215-233, doi:10.1039/C8OB02711K (2019).
201 Sakin, V. *et al.* A Versatile Tool for Live-Cell Imaging and Super-Resolution Nanoscopy Studies of HIV-1 Env Distribution and Mobility. *Cell Chemical Biology* **24**, 635-645.e635, doi:https://doi.org/10.1016/j.chembiol.2017.04.007 (2017).

202 Meineke, B., Heimgärtner, J., Eirich, J., Landreh, M. & Elsässer, S. J. Site-Specific Incorporation of Two ncAAs for Two-Color Bioorthogonal Labeling and Crosslinking of Proteins on Live Mammalian Cells. *Cell Reports* **31**, 107811, doi:https://doi.org/10.1016/j.celrep.2020.107811 (2020).
203 Bednar, R. M. *et al.* Genetic Incorporation of Two Mutually Orthogonal Bioorthogonal Amino Acids That Enable Efficient Protein Dual-Labeling in Cells. *ACS Chemical Biology* **16**, 2612-2622, doi:10.1021/acschembio.1c00649 (2021).
204 Mihaila, T. S. *et al.* Enhanced incorporation of subnanometer tags into cellular proteins for fluorescence nanoscopy via optimized genetic code expansion. *Proceedings of the National Academy of Sciences* **119**, e2201861119, doi:doi:10.1073/pnas.2201861119 (2022).
205 Sauer, M. Localization microscopy coming of age: from concepts to biological impact. *Journal of Cell Science* **126**, 3505-3513, doi:10.1242/jcs.123612 (2013).
206 Zhu, S. *et al.* Genetically encoding a light switch in an ionotropic glutamate receptor reveals subunit-specific interfaces. *Proceedings of the National Academy of Sciences* **111**, 6081-6086, doi:doi:10.1073/pnas.1318808111 (2014).
207 Klippenstein, V., Ghisi, V., Wietstruk, M. & Plested, A. J. R. Photoinactivation of Glutamate Receptors by Genetically Encoded Unnatural Amino Acids. *The Journal of Neuroscience* **34**, 980-991, doi:10.1523/jneurosci.3725-13.2014 (2014).
208 Poulsen, M. H., Poshtiban, A., Klippenstein, V., Ghisi, V. & Plested, A. J. R. Gating modules of the AMPA receptor pore domain revealed by unnatural amino acid mutagenesis. *Proceedings of the National Academy of Sciences* **116**, 13358-13367, doi:doi:10.1073/pnas.1818845116 (2019).
209 Kuhlemann, A. *et al.* Genetic Code Expansion and Click-Chemistry Labeling to Visualize GABA-A Receptors by Super-Resolution Microscopy. *Frontiers in Synaptic Neuroscience* **13**, doi:10.3389/fnsyn.2021.727406 (2021).
210 Konig, A. I. *et al.* Live cell single molecule tracking and localization microscopy of bioorthogonally labeled plasma membrane proteins. *Nanoscale* **12**, 3236-3248, doi:10.1039/c9nr08594g (2020).
211 Alvarez-Castelao, B. *et al.* Cell-type-specific metabolic labeling of nascent proteomes in vivo. *Nat Biotechnol* **35**, 1196-1201, doi:10.1038/nbt.4016 (2017).
212 Evans, H. T., Bodea, L. G. & Gotz, J. Cell-specific non-canonical amino acid labelling identifies changes in the de novo proteome during memory formation. *Elife* **9**, doi:10.7554/eLife.52990 (2020).
213 Evans, H. T., Benetatos, J., van Roijen, M., Bodea, L.-G. & Götz, J. Decreased synthesis of ribosomal proteins in tauopathy revealed by non-canonical amino acid labelling. *The EMBO Journal* **38**, e101174, doi:https://doi.org/10.15252/embj.2018101174 (2019).
214 Paule, M. R. & White, R. J. Survey and summary: transcription by RNA polymerases I and III. *Nucleic Acids Res* **28**, 1283-1298, doi:10.1093/nar/28.6.1283 (2000).
215 Nielsen, S., Yuzenkova, Y. & Zenkin, N. Mechanism of eukaryotic RNA polymerase III transcription termination. *Science* **340**, 1577-1580, doi:10.1126/science.1237934 (2013).
216 Gao, Z. L., Herrera-Carrillo, E. & Berkhout, B. Delineation of the Exact Transcription Termination Signal for Type 3 Polymerase III. *Mol Ther-Nucl Acids* **10**, 36-44, doi:10.1016/j.omtn.2017.11.006 (2018).
217 Gao, Z., Herrera-Carrillo, E. & Berkhout, B. Improvement of the CRISPR-Cpf1 system with ribozyme-processed crRNA. *RNA Biology* **15**, 1458-1467, doi:10.1080/15476286.2018.1551703 (2018).
218 Niu, W., Schultz, P. G. & Guo, J. An Expanded Genetic Code in Mammalian Cells with a Functional Quadruplet Codon. *ACS Chemical Biology* **8**, 1640-1645, doi:10.1021/cb4001662 (2013).

219 DeBenedictis, E. A., Carver, G. D., Chung, C. Z., Söll, D. & Badran, A. H. Multiplex suppression of four quadruplet codons via tRNA directed evolution. *Nature Communications* **12**, 5706, doi:10.1038/s41467-021-25948-y (2021).
220 Kelemen, R. E. *et al.* Virus-assisted directed evolution of enhanced suppressor tRNAs in mammalian cells. *bioRxiv*, 2022.2001.2021.477302, doi:10.1101/2022.01.21.477302 (2022).
221 Ding, W. *et al.* Chimeric design of pyrrolysyl-tRNA synthetase/tRNA pairs and canonical synthetase/tRNA pairs for genetic code expansion. *Nature Communications* **11**, 3154, doi:10.1038/s41467-020-16898-y (2020).
222 Schmied, W. H., Elsässer, S. J., Uttamapinant, C. & Chin, J. W. Efficient Multisite Unnatural Amino Acid Incorporation in Mammalian Cells via Optimized Pyrrolysyl tRNA Synthetase/tRNA Expression and Engineered eRF1. *Journal of the American Chemical Society* **136**, 15577-15583, doi:10.1021/ja5069728 (2014).
223 Brogna, S. & Wen, J. Nonsense-mediated mRNA decay (NMD) mechanisms. *Nature Structural & Molecular Biology* **16**, 107-113, doi:10.1038/nsmb.1550 (2009).
224 Bartoschek, M. D. *et al.* Identification of permissive amber suppression sites for efficient non-canonical amino acid incorporation in mammalian cells. *Nucleic Acids Res*, doi:10.1093/nar/gkab132 (2021).
225 Mansouri, M. & Berger, P. Strategies for multigene expression in eukaryotic cells. *Plasmid* **75**, 12-17, doi:https://doi.org/10.1016/j.plasmid.2014.07.001 (2014).
226 Chatterjee, A., Xiao, H., Bollong, M., Ai, H. W. & Schultz, P. G. Efficient viral delivery system for unnatural amino acid mutagenesis in mammalian cells. *Proc Natl Acad Sci U S A* **110**, 11803-11808, doi:10.1073/pnas.1309584110 (2013).
227 Zheng, Y., Lewis, T. L., Jr., Igo, P., Polleux, F. & Chatterjee, A. Virus-Enabled Optimization and Delivery of the Genetic Machinery for Efficient Unnatural Amino Acid Mutagenesis in Mammalian Cells and Tissues. *ACS Synth Biol* **6**, 13-18, doi:10.1021/acssynbio.6b00092 (2017).
228 Elsasser, S. J., Ernst, R. J., Walker, O. S. & Chin, J. W. Genetic code expansion in stable cell lines enables encoded chromatin modification. *Nat Methods* **13**, 158-164, doi:10.1038/nmeth.3701 (2016).
229 Brake, O. t. *et al.* Lentiviral Vector Design for Multiple shRNA Expression and Durable HIV-1 Inhibition. *Molecular Therapy* **16**, 557-564, doi:https://doi.org/10.1038/sj.mt.6300382 (2008).
230 Haggerty, D. L., Grecco, G. G., Reeves, K. C. & Atwood, B. Adeno-Associated Viral Vectors in Neuroscience Research. *Molecular therapy. Methods & clinical development* **17**, 69-82, doi:10.1016/j.omtm.2019.11.012 (2020).
231 Warnock, J. N., Daigre, C. & Al-Rubeai, M. in *Viral Vectors for Gene Therapy: Methods and Protocols* (eds Otto-Wilhelm Merten & Mohamed Al-Rubeai) 1-25 (Humana Press, 2011).
232 Chambers, A. C. *et al.* Overview of the Baculovirus Expression System. *Current Protocols in Protein Science* **91**, 5.4.1-5.4.6, doi:https://doi.org/10.1002/cpps.47 (2018).
233 Mansouri, M. *et al.* Highly efficient baculovirus-mediated multigene delivery in primary cells. *Nat Commun* **7**, 11529, doi:10.1038/ncomms11529 (2016).
234 Leffler, A., Herzog, R. I., Dib-Hajj, S. D., Waxman, S. G. & Cummins, T. R. Pharmacological properties of neuronal TTX-resistant sodium channels and the role of a critical serine pore residue. *Pflugers Arch* **451**, 454-463, doi:10.1007/s00424-005-1463-x (2005).
235 O'Brien, J. E. Regulation and Mutation of Voltage-Gated Sodium Channel SCN8A (Nav1.6). (2013).
236 Feldman, D. H. & Lossin, C. The Nav channel bench series: Plasmid preparation. *MethodsX* **1**, 6-11, doi:10.1016/j.mex.2014.01.002 (2014).

237 Kim, J., Adam, R. M., Solomon, K. R. & Freeman, M. R. Involvement of cholesterol-rich lipid rafts in interleukin-6-induced neuroendocrine differentiation of LNCaP prostate cancer cells. *Endocrinology* **145**, 613-619, doi:10.1210/en.2003-0772 (2004).
238 Yuan, Y. & Reddy, R. 5' flanking sequences of human MRP/7-2 RNA gene are required and sufficient for the transcription by RNA polymerase III. *Biochim Biophys Acta* **1089**, 33-39, doi:10.1016/0167-4781(91)90081-v (1991).
239 Gao, Z., Harwig, A., Berkhout, B. & Herrera-Carrillo, E. Mutation of nucleotides around the +1 position of type 3 polymerase III promoters: The effect on transcriptional activity and start site usage. *Transcription* **8**, 275-287, doi:10.1080/21541264.2017.1322170 (2017).
240 Farris, A. D., Gross, J. K., Hanas, J. S. & Harley, J. B. Genes for murine Y1 and Y3 Ro RNAs have class 3 RNA polymerase III promoter structures and are unlinked on mouse chromosome 6. *Gene* **174**, 35-42, doi:10.1016/0378-1119(96)00279-x (1996).
241 Arsić, A. & Nikić-Spiegel, I. Bioorthogonal click chemistry-based labelling of proteins in living neuronal cell lines and primary neurons. *Protocol Exchange*, doi:10.21203/rs.3.pex-1727/v1 (2022).
242 Sharkey, L. M. *et al.* The ataxia3 mutation in the N-terminal cytoplasmic domain of sodium channel Na(v)1.6 disrupts intracellular trafficking. *J Neurosci* **29**, 2733-2741, doi:10.1523/JNEUROSCI.6026-08.2009 (2009).
243 Fitzgerald, D. J. *et al.* Protein complex expression by using multigene baculoviral vectors. *Nature Methods* **3**, 1021-1032, doi:10.1038/nmeth983 (2006).
244 Xiao, H. *et al.* Genetic incorporation of multiple unnatural amino acids into proteins in mammalian cells. *Angew Chem Int Ed Engl* **52**, 14080-14083, doi:10.1002/anie.201308137 (2013).
245 Schindelin, J. *et al.* Fiji: an open-source platform for biological-image analysis. *Nat Methods* **9**, 676-682, doi:10.1038/nmeth.2019 (2012).
246 Arsić, A., Stajković, N., Spiegel, R. & Nikić-Spiegel, I. Effect of Vectashield-induced fluorescence quenching on conventional and super-resolution microscopy. *Scientific Reports* **10**, 6441, doi:10.1038/s41598-020-63418-5 (2020).
247 Huang, B., Wang, W., Bates, M. & Zhuang, X. Three-dimensional super-resolution imaging by stochastic optical reconstruction microscopy. *Science* **319**, 810-813, doi:10.1126/science.1153529 (2008).
248 Grubb, M. S. AIS quantification (https://www.mathworks.com/matlabcentral/fileexchange/28181-ais-quantification), MATLAB Central File Exchange. Retrieved December 22, 2021. . (2021).
249 Meijering, E. *et al.* Design and validation of a tool for neurite tracing and analysis in fluorescence microscopy images. *Cytometry A* **58**, 167-176, doi:10.1002/cyto.a.20022 (2004).
250 Arsić, A. & Nikić-Spiegel, I. The tail domain of neurofilament light chain accumulates in neuronal nuclei during oxidative injury. *bioRxiv*, 2022.2003.2003.481279, doi:10.1101/2022.03.03.481279 (2022).
251 DeKeyser, J.-M., Thompson, C. H. & George, A. L. Cryptic prokaryotic promoters explain instability of recombinant neuronal sodium channels in bacteria. *Journal of Biological Chemistry* **296**, 100298, doi:https://doi.org/10.1016/j.jbc.2021.100298 (2021).
252 Szymczak, A. L. & Vignali, D. A. A. Development of 2A peptide-based strategies in the design of multicistronic vectors. *Expert Opinion on Biological Therapy* **5**, 627-638, doi:10.1517/14712598.5.5.627 (2005).
253 Herzog, R. I., Cummins, T. R., Ghassemi, F., Dib-Hajj, S. D. & Waxman, S. G. Distinct repriming and closed-state inactivation kinetics of Nav1.6 and Nav1.7 sodium channels in mouse spinal sensory neurons. *J Physiol* **551**, 741-750, doi:10.1113/jphysiol.2003.047357 (2003).

254 Haberberger, R. V., Barry, C. & Matusica, D. Immortalized Dorsal Root Ganglion Neuron Cell Lines. *Front Cell Neurosci* **14**, 184, doi:10.3389/fncel.2020.00184 (2020).
255 Yin, K., Baillie, G. J. & Vetter, I. Neuronal cell lines as model dorsal root ganglion neurons: A transcriptomic comparison. *Molecular pain* **12**, doi:10.1177/1744806916646111 (2016).
256 Baroni, D. & Moran, O. Molecular differential expression of voltage-gated sodium channel α and β subunit mRNAs in five different mammalian cell lines. *Journal of Bioenergetics and Biomembranes* **43**, 729-738, doi:10.1007/s10863-011-9399-7 (2011).
257 Vega, A. V., Avila, G. & Matthews, G. Interaction between the transcriptional corepressor Sin3B and voltage-gated sodium channels modulates functional channel expression. *Scientific Reports* **3**, 2809, doi:10.1038/srep02809 (2013).
258 Hirsh, J. K. & Quandt, F. N. Down-regulation of Na channel expression by A23187 in NlE-115 neuroblastoma cells. *Brain Research* **706**, 343-346, doi:https://doi.org/10.1016/0006-8993(95)01340-7 (1996).
259 Bienert, S. *et al.* The SWISS-MODEL Repository-new features and functionality. *Nucleic Acids Res* **45**, D313-D319, doi:10.1093/nar/gkw1132 (2017).
260 von Castelmur, E. *et al.* A regular pattern of Ig super-motifs defines segmental flexibility as the elastic mechanism of the titin chain. *Proc Natl Acad Sci U S A* **105**, 1186-1191, doi:10.1073/pnas.0707163105 (2008).
261 Galiano, M. R. *et al.* A distal axonal cytoskeleton forms an intra-axonal boundary that controls axon initial segment assembly. *Cell* **149**, 1125-1139, doi:10.1016/j.cell.2012.03.039 (2012).
262 Jumper, J. *et al.* Highly accurate protein structure prediction with AlphaFold. *Nature* **596**, 583-589, doi:10.1038/s41586-021-03819-2 (2021).
263 Varadi, M. *et al.* AlphaFold Protein Structure Database: massively expanding the structural coverage of protein-sequence space with high-accuracy models. *Nucleic Acids Research* **50**, D439-D444, doi:10.1093/nar/gkab1061 (2021).
264 Wang, T., Larcher, L. M., Ma, L. & Veedu, R. N. Systematic Screening of Commonly Used Commercial Transfection Reagents towards Efficient Transfection of Single-Stranded Oligonucleotides. *Molecules* **23**, 2564 (2018).
265 Dommerholt, J. *et al.* Readily Accessible Bicyclononynes for Bioorthogonal Labeling and Three-Dimensional Imaging of Living Cells. *Angewandte Chemie International Edition* **49**, 9422-9425, doi:https://doi.org/10.1002/anie.201003761 (2010).
266 Borner, K. *et al.* Pre-arrayed Pan-AAV Peptide Display Libraries for Rapid Single-Round Screening. *Mol Ther* **28**, 1016-1032, doi:10.1016/j.ymthe.2020.02.009 (2020).
267 Lelek, M. *et al.* Single-molecule localization microscopy. *Nature Reviews Methods Primers* **1**, 39, doi:10.1038/s43586-021-00038-x (2021).
268 Klippenstein, V., Hoppmann, C., Ye, S., Wang, L. & Paoletti, P. Optocontrol of glutamate receptor activity by single side-chain photoisomerization. *eLife* **6**, e25808, doi:10.7554/eLife.25808 (2017).
269 v. Berlepsch, H. & Böttcher, C. H-Aggregates of an Indocyanine Cy5 Dye: Transition from Strong to Weak Molecular Coupling. *The Journal of Physical Chemistry B* **119**, 11900-11909, doi:10.1021/acs.jpcb.5b05576 (2015).
270 Mishra, A., Behera, R. K., Behera, P. K., Mishra, B. K. & Behera, G. B. Cyanines during the 1990s: A Review. *Chemical Reviews* **100**, 1973-2012, doi:10.1021/cr990402t (2000).
271 Shibata, N. *et al.* Degradation of Stop Codon Read-through Mutant Proteins via the Ubiquitin-Proteasome System Causes Hereditary Disorders*. *Journal of Biological Chemistry* **290**, 28428-28437, doi:https://doi.org/10.1074/jbc.M115.670901 (2015).
272 Kramarski, L. & Arbely, E. Translational read-through promotes aggregation and shapes stop codon identity. *Nucleic Acids Research* **48**, 3747-3760, doi:10.1093/nar/gkaa136 (2020).

273 Basak, S. *et al.* Differential expression and functions of neuronal and glial neurofascin isoforms and splice variants during PNS development. *Developmental Biology* **311**, 408-422, doi:https://doi.org/10.1016/j.ydbio.2007.08.045 (2007).
274 Schwarz, N. *et al.* Long-term adult human brain slice cultures as a model system to study human CNS circuitry and disease. *eLife* **8**, e48417, doi:10.7554/eLife.48417 (2019).
275 Nikic, I. *et al.* A reversible form of axon damage in experimental autoimmune encephalomyelitis and multiple sclerosis. *Nat Med* **17**, 495-499, doi:10.1038/nm.2324 (2011).
276 Wang, J., Ou, S. W. & Wang, Y. J. Distribution and function of voltage-gated sodium channels in the nervous system. *Channels (Austin)* **11**, 534-554, doi:10.1080/19336950.2017.1380758 (2017).
277 Tian, C., Wang, K., Ke, W., Guo, H. & Shu, Y. Molecular identity of axonal sodium channels in human cortical pyramidal cells. *Frontiers in Cellular Neuroscience* **8**, doi:10.3389/fncel.2014.00297 (2014).
278 Doherty, E. A. & Doudna, J. A. Ribozyme structures and mechanisms. *Annu Rev Biochem* **69**, 597-615, doi:10.1146/annurev.biochem.69.1.597 (2000).
279 Zetsche, B. *et al.* Cpf1 Is a Single RNA-Guided Endonuclease of a Class 2 CRISPR-Cas System. *Cell* **163**, 759-771, doi:https://doi.org/10.1016/j.cell.2015.09.038 (2015).
280 Xu, L., Zhao, L., Gao, Y., Xu, J. & Han, R. Empower multiplex cell and tissue-specific CRISPR-mediated gene manipulation with self-cleaving ribozymes and tRNA. *Nucleic Acids Res* **45**, e28, doi:10.1093/nar/gkw1048 (2017).
281 Koehler, C. *et al.* Genetic code expansion for multiprotein complex engineering. *Nature Methods* **13**, 997-1000, doi:10.1038/nmeth.4032 (2016).
282 Koehler, C., Estrada Girona, G., Reinkemeier, C. D. & Lemke, E. A. Inducible Genetic Code Expansion in Eukaryotes. *ChemBioChem* **21**, 3216-3219, doi:https://doi.org/10.1002/cbic.202000338 (2020).

Statement of contributions

All experiments and the data collection and analysis described in this Ph.D. dissertation titled: *"Novel minimally invasive labeling tools for advanced microscopy studies of voltage-gated sodium channels and associated proteins in health and disease"* were conducted by myself. The exceptions are listed in the paragraphs below. Briefly, I optimized the genetic code expansion and click labeling in ND7/23 cell line, optimized Lipofectamine 2000 and Lipofectamine 3000 transfection, and genetic code expansion of $Na_V1.6$ plasmids in the N1E-115-1 neuronal cell line, and generated stable neuronal cell lines. I performed all experiments involving mutagenesis, cloning, and amplification of the plasmids, with the exceptions described in the Materials and Methods section. I carried out all experiments involving transfection or transduction of insect and mammalian cell lines and primary neurons, genetic code expansion, and click labeling of mammalian cell lines and primary neurons. I prepared neuronal cell lines for the whole-cell patch clamp recordings of recombinant Na^+ current. I also set up insect cell culture in the laboratory, optimized the production of baculoviruses in the Sf21 cell line, and transduction of mammalian cells with baculoviruses. I performed widefield, fixed- and live-cell confocal imaging, and dSTORM super-resolution imaging. I analyzed the AIS length and AIS fluorescence intensity of primary neurons. I produced the codon-optimized NES $PylRS^{AF}$/U6-$tRNA^{Pyl}$ and NES $PylRS^{AF}$/4xU6-$tRNA^{M15}$ plasmids used in the following publication: *Arsić, A., Hagemann, C., Stajković, N., Schubert, T. and Nikić-Spiegel, I., 2022. Minimal genetically encoded tags for fluorescent protein labeling in living neurons. Nature communications, 13(1), pp.1-18.*

My Ph.D. supervisor, Dr. Ivana Nikić-Spiegel, helped me to design the experiments, select initial TAG sites for click labeling of the $Na_V1.6$, generate a stable ND7/23 cell line, and perform statistical analysis. Dr. Ivana Nikić-Spiegel and George Philippos carried out TAG site-directed mutagenesis of the NF186-HA plasmids.

Aleksandra Arsić optimized protocol for Lipofectamine 2000 transfection and genetic code expansion in primary neurons, and wrote a macro for the analysis of the GFP^{Y39TAG}/mCherry ratio (this macro was modified based on the one published in *Arsić, A. and Nikić-Spiegel, I., 2022. The tail domain of neurofilament light chain accumulates in neuronal nuclei during oxidative injury. bioRxiv*), and performed quantitative analysis of the GFP^{Y39TAG}/mCherry ratio in primary neurons transduced with AAVs (**Fig. 31c**). Aleksandra Arsić and I cultured mouse cortical neurons for the experiments described in this Ph.D. dissertation, including the ones involving widefield and dSTORM imaging of neurons immunostained with anti-panNa_V primary and AF647 and AF(+)647-conjugated secondary antibodies in different imaging mediums (**Fig. 40–42**). I

performed immunostaining, widefield, and dSTORM imaging of neurons shown in **Fig. 40–42**. The widefield and dSTORM imaging of neurons is different imaging medium is part of Aleksandra's and mine published work: *Arsić, A., Stajković, N., Spiegel, R. and Nikić-Spiegel, I., 2020. Effect of Vectashield-induced fluorescence quenching on conventional and super-resolution microscopy. Scientific reports, 10(1), pp.1-13*. The figures shown in this dissertation (**Fig. 40–42**) are included in the same publication. I modified figures for presentation purposes in this thesis.

The electrophysiological recordings of recombinant Na^+ currents and analysis of loss-of-function pathogenic $Na_V1.6$ variants were performed in collaboration with the laboratory of Prof. Dr. Holger Lerche. These results are shown in **Fig. 3b, 4b–h, 24, and 26** and published in *Stajković, N., Liu, Y., Arsić, A., Meng, N., Lyu, H., Zhang, N., Grimm, D., Lerche, H. and Nikić-Spiegel, I., 2022. Direct fluorescent labeling of NF186 and $Na_V1.6$ in living primary neurons using bioorthogonal click chemistry. bioRxiv*. Dr. Yunyuan Liu performed whole-cell patch clamp recordings of recombinant Na^+ currents in WT or stable ND7/23 and N1E-115-1 cell lines (**Fig. 3b, 4b–h, 24**). Hang Lyu and Nan Zhang performed whole-cell patch clamp recordings of recombinant Na^+ currents in N1E-115-1 cells transfected with loss-of-function $Na_V1.6$-HA variants (**Fig. 26a and b**). Dr. Yunyuan Liu analyzed all the data and generated graphs (**Fig. 26a and b**), which I further modified and incorporated into figures. For the analysis of the AIS fluorescence in neurons expressing WT or loss-of-function $Na_V1.6$-HA variants, Dr. Yunyuan Liu cultured mouse hippocampal neurons. Experiments involving whole-cell patch clamp and loss-of-function pathogenic variants were designed with the help of Dr. Ivana Nikić-Spiegel, Prof. Dr. Holger Lerche, and Dr. Yuanyuan Liu. They also helped in the interpretation of the results.

The AAVs described in this dissertation were generated as a part of a collaboration with the laboratory of Prof. Dr. Dirk Grimm. These data are shown in **Fig.31–33 26** and published in *Stajković, N., Liu, Y., Arsić, A., Meng, N., Lyu, H., Zhang, N., Grimm, D., Lerche, H. and Nikić-Spiegel, I., 2022. Direct fluorescent labeling of NF186 and $Na_V1.6$ in living primary neurons using bioorthogonal click chemistry. bioRxiv*. Prof. Dr. Dirk Grimm and Ning Meng designed AAVs. Ning Meng generated AAVs.

Christine Koehler and Dr. Daniel Fitzgerald (Geneva Biotech) advised me on how to culture Sf21 cells, produce viruses, and transduce mammalian cells. They also provided me with protocols for Sf21 cell propagation and transduction of mammalian cells.

Cathleen Hagemann and I established protocols for generation of stable neuronal cell line.

Acknowledgments

I am very grateful to my supervisor, Dr. Ivana Nikić-Spiegel, for giving me the opportunity to pursue a Ph.D. in her laboratory. I would also like to thank her for supporting me, encouraging me to keep going even in the most challenging moments and teaching me how to become a better scientist. I would like to thank members of my advisory board, Prof. Dr. Mathias Jucker and Prof. Dr. Michela Deleidi, for their support and the time they invested in monitoring my Ph.D. progress. I would like to extend my sincere thanks to Prof. Dr. Holger Lerche for reading my dissertation and helping with a challenging research project that involved $Na_V1.6$ channels. Special thanks to members of Dr. Nikić-Spiegel's laboratory and collaborators. Working and collaborating with such great scientists has been a pleasure. In particular, I would like to thank Katja Widmaier and Dr. Friederike Pfeiffer for their help during our time in the lab. I am incredibly grateful to Aleksandra Arsić for reading my dissertation and for valuable advice, support, and exciting discussions regarding science.

I would also like to thank Aleksandra for encouraging me in the most challenging moments during my Ph.D. journey. I am also very grateful for the fun time out of the lab and for being such a good colleague and friend. Special thanks to my dear friend Dr. Julien Genty for reading my dissertation, listening to numerous troubles related (and unrelated) to my Ph.D. project (and that is quite a long list), and making funny jokes that kept my serotonin levels up. I would also like to thank my flatmates, who have become my second family, Dr. Andrea Corna and Stan Petre, for their support and the beautiful and fun moments we spent together. I am also grateful to Dr. Melina Matthiesen, one of the first and dearest friends I met in Tuebingen, for her support and encouragement. I am also thankful to all the other lovely people I have met in Tuebingen, Sonja, Jelena, Aura, Stefano, Ivan, Anna, Laura, Sarrah, Luka, Ale, Flavia, GuoDa, Guiseppe, Cathleen, and Theresa. I am also incredibly grateful for my Serbian friends that were there for me (although not always in person). Likewise, I could not have undertaken this journey without my master's thesis supervisors, Prof. Dr. Sanja Dacić and Dr. Sanja Peković, and my dear friend and English teacher, Marija Milovanović.

I am incredibly grateful to my family for always being there for me, supporting me, and teaching me how to become a better person. Special thanks to my dad, who inspired me to become a scientist, taught me that knowledge is power, encouraged me to be curious, and that everything is possible with determination and hard work.